NETWORK BIOLOGY APPROACHES REVEAL A LINK BETWEEN RIBOSOME BIOGENESIS AND METABOLIC REPROGRAMMING IN AGEING SKELETAL MUSCLES

by

KIM CLARKE

A thesis submitted to
The University of Birmingham
for the degree of
Doctor of Philosophy

Supervisor: Francesco Falciani

School of Biosciences
College of Life and Environmental Science
University of Birmingham
September 2013

ABSTRACT

Human ageing is characterised by reduced skeletal muscle function and increased incidence of a wide range of pathologies. The prevalence of muscle dysfunction in elderly populations represents a significant burden on healthcare due to the increased risk of injury, and difficulty in maintaining activities of daily living. Skeletal muscle dysfunction is also an important factor in age related diseases such as chronic obstructive pulmonary disease (COPD) and diabetes. Revealing the molecular alterations that occur in skeletal muscle of the elderly is therefore clearly an important step towards understanding an important aspect of the ageing process.

This thesis describes the application of advanced computational techniques designed to "learn" the structure of molecular networks to understanding human skeletal muscle ageing. Using this approach we have been able to discover a link between protein translation and age-dependent metabolic reprogramming. Experimental validation using the haploinsufficient eukaryotic initiation factor 6 (eIF6) mouse confirmed this important hypothesis and revealed a substantial molecular reprogramming. The role of eIF6 in skeletal muscle and myoblasts was further investigated, revealing potential up and down-stream signalling mechanisms.

The process of angiogenesis is an important step in morphogenesis including systems as diverse as muscle regeneration and tumour growth. This thesis presents the first temporal model of transcriptional alterations in tumour and the surrounding stroma during vascularisation. The application of reverse engineering approaches that are able to integrate perturbation data lead to the hypothesis that modulation of the proinflammatory cytokine IL1α may be an important upstream event in angiogenesis

This thesis supports the effectiveness of systems biology approaches in the study of human health and ageing.

ACKNOWLEDGEMENTS

This thesis would not be possible without the large network of friends and collaborators who have worked with me and offered support and friendly guidance along the way.

In no particular order, I would like to thank the following for their help and advice: Dan Tennant for isolating mitochondria from skeletal muscle and regularly working 12 hour days to do so, Stuart Egginton for performing countless sample collections for us and providing excellent expert advice, Dada Pisconti for help with the analysis of satellite cells and Stefano Biffo and his lab. I would like to thank Andreas Bikfalvi and Roy Bicknell for their advice and support towards the glioblastoma project, and Sarah Durant for the huge number of hours she spent in the lab producing the samples we needed.

I would like to extend my heartfelt thanks to everyone in our lab, past and present, for teaching and putting up with my stubborn questions over the 4 years of my PhD: Phil, Wazeer, Nil, Rita, Jaanika, Peter, John H, John A, Danilo and Michela.

I would like to thank Francesco Falciani for being a fantastic, supportive supervisor and not giving up hope that I would finish my PhD even in the face of stubborn apathy. A lesser supervisor would certainly not have led me to pass my doctorate.

Finally, I would like to thank Emily, who put up with my months of anxiety, anguish and anti-social behaviour, as well as providing a proofreading service second to none.

Thank you all.

COMMON ABBREVIATIONS USED IN THIS THESIS

AMPK	AMP-activated protein kinase
ANOVA	Analysis of variance
BP	Gene ontology - biological process
CC	Gene ontology - cellular compartment
CM	Connectivity map (Broad Institute)
COPD	Chronic obstructive pulmonary disease
Cy3	Cyanine 3 dye
Cy5	Cyanine 5 dye
DAVID	DAVID Bioinformatics Resources 6.7
EDTA	Ethylenediaminetetraacetic acid
EIF	Eukaryotic initiation factor
FDR	False discovery rate
GC-RMA	Robust multi-array average with non-specific binding estimates
GSEA	Gene set enrichment analysis
H_2O_2	Hydrogen peroxide
HDAC	Histone deacetylase
HIF	Hypoxia inducible factor (HIF1α)
HOPACH	Hierarchical Ordered Partitioning and Collapsing Hybrid algorithm
INSR	Insulin receptor
IPA	Ingenuity Pathway Analysis
KEGG	Kyoto Encyclopedia of Genes and Genomes
LDA	Linear discriminant analysis
LOESS	Regression based microarray normalisation procedure
MAS5	Microarray suit 5 (Affymetrix) normalisation algorithm
MF	Gene ontology - molecular function
MI	Mutual information
Myod	Myogenic differentiation 1
ox. phos.	Oxidative phosphorylation
PBS	phosphate buffered saline
PCA	Principle component analysis
PGC-1α	Peroxisome proliferator-activated receptor gamma coactivator 1-alpha
RMA	Robust multi-array average microarray normalisation
ROS	Reactive oxygen species
SAM	Significance Analysis of Microarrays
TCA	Tricarboxylic acid cycle
VEGF	Vascular endothelial growth factor (VEGF-A)
VL	*vastus lateralis* muscle
DXA	Dual-energy X-ray absorptiometry
CT	X-ray computed tomography

CONTENTS

LIST OF FIGURES

LIST OF TABLES

CHAPTER 1

INTRODUCTION

1.2 Mammalian Skeletal muscle

Humans have evolved a complex musculoskeletal system which provides structural support and motor control. Movement is coordinated by the motor cortex via the central nervous system which stimulates contraction in voluntary skeletal muscles. Muscle contraction provides the force needed to move and support the body during all of its normal activities of daily living. Skeletal muscle function is impaired in ageing, a condition known as sarcopenia. This has recently been precisely defined according to physiological measurements of walking speed and muscle mass compared to young people in order to aid medical diagnosis [1]. Impairment of skeletal muscle function is also a contributing factor to diseases such as COPD [2], as well as being a key player in the development of insulin resistance and type 2 diabetes [3]. At the epidemiological level, muscle weakness is a strong and independent predictor of all-cause mortality in older adults [4][5][6].

In the following sections, the structure and function of skeletal muscle will be described. The effects of ageing and age-related diseases on skeletal muscle function will be reviewed, including popular intervention strategies that target muscle dysfunction such as hormone replacement therapy and physical training. The use of functional genomics and systems biology approaches has led to a greater understanding of skeletal muscle function in recent years. These approaches and key findings will also be reviewed.

1.1.1 The structure and function of mammalian skeletal muscle

Skeletal muscles which can be controlled at will, termed voluntary muscles, are stimulated through the propagation of action potentials from the source, typically a neuronal cell, to a neuromuscular junction (NMJ) which is directly connected to muscle fibres [7] (**Figure 1.1A**). By releasing the neurotransmitter acetylcholine the NMJ stimulates contraction of muscle fibres. Each skeletal muscle is connected to multiple NMJs. This allows for the great range of precision and scale of movement many mammals are capable of.

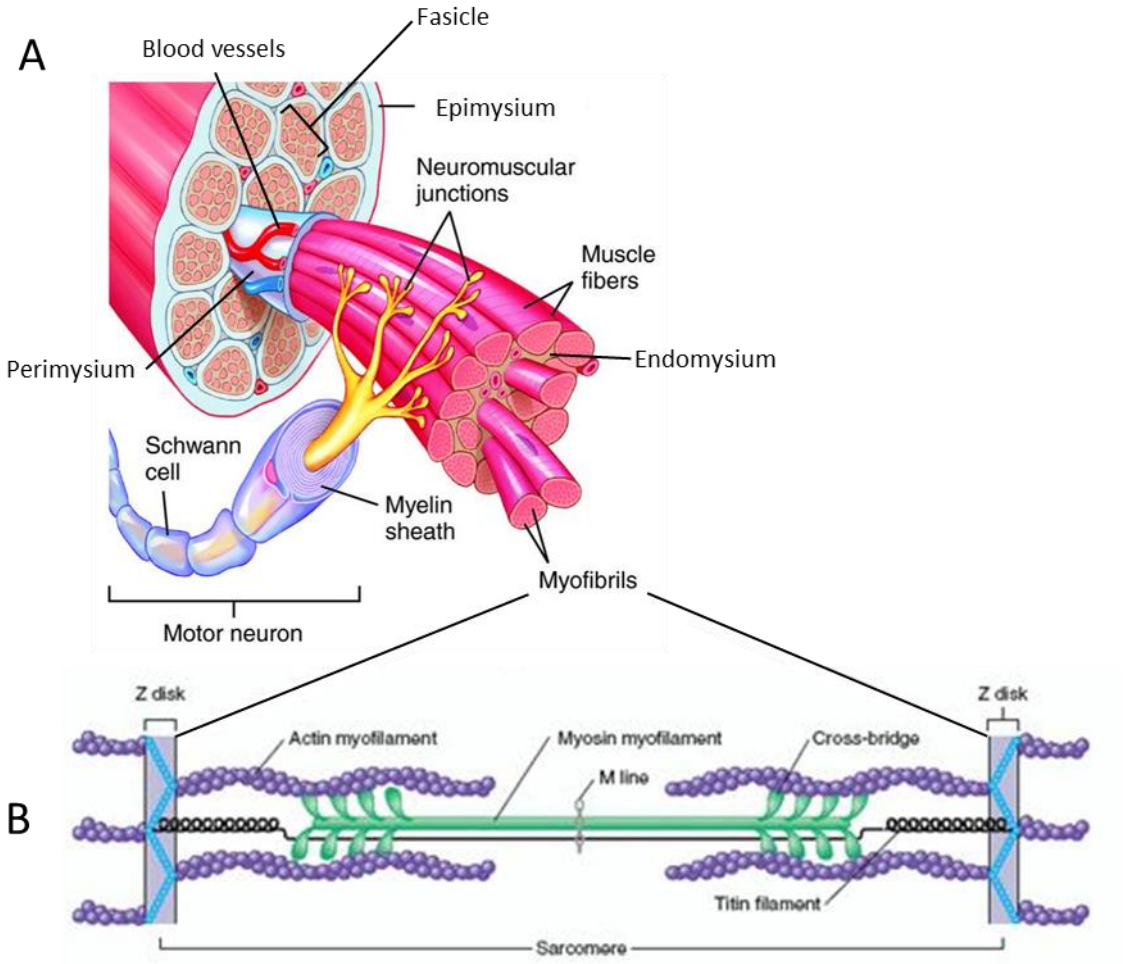

Figure 1.1 – The structure of mammalian skeletal muscle

Panel A shows the arrangement of skeletal muscle fibres into bundles or fascicles, surrounded by support components such as blood vessels. Panel B shows the arrangement of actin and myosin filaments within the sarcomere. The myosin filaments move along the actin filaments away from the M line towards the Z disks, causing contraction of the sarcomere. Image source: en.wikipedia.net

Skeletal muscles are composed of bundles or fascicles of parallel muscle fibres (**Figure 1.1A**). Each muscle fibre is a multi-nucleated cell formed from the fusion of multiple myoblasts during development. A population of myoblast precursor cells or satellite cells remain into adulthood and can be found within the endomysium. Here they lie in a quiescent state until injury or anabolic stimuli cause them to activate and re-enter the cell cycle [8]. Satellite cells repair existing fibres or form new muscle fibres [9]. The muscle is provided with oxygen and nutrients by blood vessels within the perimysium, which also contains the nerves.

Within muscle fibres are many chains of fibrous proteins known as myofibrils which contain a thin filament, actin, and a thick filament, myosin (**Figure 1.1B**). These filaments are arranged into units called sarcomeres. Stimulation of the neuromuscular junction causes the propagation of an action potential across the skeletal muscle fibres. Excitation-contraction coupling then causes myosin filaments to move along the actin filaments by repeated mechanical movements powered by ATP hydrolysis [10] [11] [12] [13]. The actin filaments are fixed to the end structures of the sarcomere, the Z discs. The movement of myosin along the actin filaments towards the Z discs pulls the Z discs closer together and subsequently shortens the overall length of the muscle. The simultaneous stimulation of many sarcomeres provides the contraction force of the muscle.

1.1.2 Skeletal muscle fibre types

Skeletal muscle fibres can be classified as type I or type II fibres. These have a different performance, and are characterised by different myosin isoforms [14] and metabolic capacity [15].

Type I skeletal muscle fibres are responsible for postural support of the body and endurance exercise and are required to be highly resistant to fatigue. They have a very high density of mitochondria in order to maintain ATP production by oxidative phosphorylation and express a “slow” isoform of myosin which hydrolyses ATP at a slower rate, thereby decreasing both the speed of contraction and

the maximum amount of force that can be generated (**Table 1.1**). On the other hand, type II skeletal muscles fibres are used during periods of high activity such as resistance training and are less resistant to fatigue. They rely more heavily on generation of ATP by glycolysis. These fibres express a "fast" isoform of myosin which hydrolyses ATP quickly allowing for a greater speed of contraction and increased force generation (**Table 1.1**).

	Type I	Type IIa	Type IIx/b
Contractile Speed	Slow	Fast	Fast
Resistance to fatigue	High	Moderate-High	Low
Maximum power	Low	High	High
Capillary Density	Dense	Dense	Sparse
Oxidative Capacity	High	Moderate-High	Low
Glycolytic Capacity	Low	High	High

Table 1.1- Characteristics of different skeletal muscle fibre types

Skeletal muscles are made up of different proportions of fibre types dependent on the role of the muscle. In humans this ranges from more glycolytic muscles such as the *vastus lateralis* which has an average of 50% type I fibres to the predominantly oxidative *soleus*, which has an average of 80% type I fibres [16].

1.1.3 Skeletal muscle regeneration and repair

Skeletal muscle fibres are inevitably damaged during exercise and injury, and old fibres need to be replaced throughout life. When a muscle fibre is damaged and becomes necrotic, phagocytic inflammatory cells remove the debris prior to regeneration. Regeneration is the task of a population

of progenitor cells, called satellite cells, which reside under the basal lamina of muscle fibres in a quiescent state [17]. Satellite cells possess the ability to respond to skeletal muscle damage by activating a program of expansion, proliferation, differentiation and finally fusion with existing fibres. After each period of muscle regeneration, a proportion of the expanded satellite cell population remains undifferentiated and replenishes the pool of quiescent satellite cells [18].

There are a number of key regulators of satellite cell function. The activation of satellite cells involves the up-regulation of myogenic factors such as Myf5 and MyoD [19], followed by the up-regulation of myogenin during differentiation. Together these factors dynamically control the transition of satellite cells from re-entry into the cell cycle (MyoD) to terminal differentiation (myogenin). Mice lacking both Myf5 and MyoD are lacking myoblasts, myofibres and in fact expression of any muscle specific mRNAs, highlighting the requirement of these genes for the development of skeletal muscle [20]. Notch signalling is important in maintenance of satellite cell quiescence. When Notch signalling is disrupted satellite cells prematurely differentiate and undergo fusion [21]. The activation of satellite cells is mediated by nitric oxide production by nitric oxide synthase (NOS) in response to mechanical stimulation of muscle. NO stimulates the release of hepatocyte growth factor (HGF) by activating metalloproteinases (MMPs). HGF then binds to the receptor c-Met which induces activation of the satellite cell [22]. Other growth factors and inflammatory cytokines also play important roles in skeletal muscle regeneration such as IL-4, IL-6, LIF, TGF-β and TNF-α, IGFs and FGFs [23]. For example, IGF-1 activates Myf5 and the myogenic program [24] and FGF2 promotes proliferation of satellite cells which is controlled by sprouty1 (Spry1) in old age [25].

1.2 Skeletal muscle in elderly populations

The skeletal muscles of elderly individuals begin to show differences to young muscles as early as the 4th decade of life. These include a decrease in fibre cross sectional area, muscle strength and muscle quality (measured as muscle strength normalised for fat free mass) and an accumulation of

intramuscular lipids [26] [27] [28] [29] [30] [31] [32] [33]. The decline in skeletal muscle area accelerates during the later stages of life, with studies reporting an average reduction in muscle area of 40% between 20 and 80 year old healthy men [29] [34]. The loss of muscle area is mainly due to a decrease in muscle fibre number; however a decrease in type II fibre size has been observed relative to type I fibres in mixed fibre type muscles [29]. Studies utilising standard force measurements, DXA and CT scanning have shown that the rate of decline of muscle strength is not proportional to the loss of muscle mass, indicating that muscle quality (force per unit of muscle mass) is reduced [32] [33]. Another key aspect of muscle ageing is an age dependent decline in exercise capacity. This is coupled to a decline in VO_2 max (the capacity of the body to deliver and utilise oxygen during exercise) of approximately 30% between 20-29 year olds and those over 70 [35]. These findings suggest additional alterations in elderly muscle other than a reduction in muscle mass that affect muscle function. This question has been intensely studied in recent years and benefitted greatly from modern analytical techniques.

1.2.1 The balance between protein synthesis and proteolysis

Skeletal muscle is a highly plastic tissue which responds to anabolic stimuli such as physical training by increasing metabolic capacity [36] and fibre area, regardless of fibre type [37]. Conversely, elderly populations tend to expend less energy and do less physical exercise and show a loss of fibre area. This has been linked to a decrease in the rate of protein synthesis in elderly individuals [35]. This includes synthesis of specific muscle proteins such as myofibrillar proteins [38] [39], myosin heavy chain (MHC) [40] and mitochondrial proteins [41]. This decrease is linked to a relative reduction in gene expression of myosin 2a and 2x/b isoforms [42]. However, it should be noted that more recent measures of protein synthesis have reported no difference in baseline protein synthesis in healthy physically active elderly individuals, suggesting that lifestyle is a determining factor [43] [44]. The research community appears to support the hypothesis that basal protein synthesis and breakdown

are not significantly different in elderly individuals without accompanying factors such as a sedentary lifestyle; however the limits of current technology and the large inter-subject variance make coordinate but small differences difficult to measure [45]. The ingestion of amino acids in amounts similar to a daily meal stimulates muscle protein synthesis. This has been shown to be attenuated in the elderly and is thought to be a significant contributor to the age-dependent decline in muscle mass [45] [44]. Relatively little attention has been paid to the impact of muscle protein breakdown to the overall decline in muscle mass in the elderly. It is a well-established concept that muscle atrophy occurs when basal protein breakdown overtakes protein synthesis, such as during limb immobilisation or periods of extended disuse [46]. Genes such as TGF-β [47] and myostatin [48] have been shown to regulate the ubiquitin ligases Murf1 and MAFbx (atrogin-1) which control ubiquitination mediated proteolysis and thus skeletal muscle atrophy, however there exact roles in ageing remain contradictory [49] [50] [51]. Myostatin has been shown to inhibit the IGF1 pathway [48]. IGF1 is one of the key factors inducing hypertrophy and thus preventing skeletal muscle atrophy. Induction of IGF1 expression in mouse skeletal muscle reversed the age related loss of fibres and reduction in muscle strength [52]. IGF1 has been shown to limit fibrosis, accelerate muscle regeneration and modulate the inflammatory response to muscle injury by decreasing the expression of tumour necrosis factor alpha (TNFα) and interleukin 1 beta (IL1β) [53]. Studies have shown that insulin availability decreases the rate of muscle protein breakdown [54] [54]; however the exact dynamics and mechanism of action of insulin on muscle protein turnover are still unclear [55].

1.2.2 Mitochondrial dysfunction

Research aiming to understand the role of mitochondria in skeletal muscle ageing has grown substantially in recent years. In 1956 Harman proposed the “free-radical theory of ageing”, outlining the theory that oxygen free radicals cause cellular damage which accumulates during the lifetime of an organism [56]. This research was supported by work showing how anti-oxidant compounds extend

the average lifespan of multiple animal models including mice [57]. In 1972, Harman proposed that mitochondria were the main component of the free-radical theory of ageing, based on the observations that anti-oxidants that were not able to penetrate mitochondria failed to extend maximum lifespan [58]. Reactive oxygen species (ROS) are predominantly produced in the mitochondria as a by-product of oxidative phosphorylation and can damage proteins, RNA and DNA. Mice constitutively expressing the free radical scavenging enzyme catalase in mitochondria of muscle have been shown to have an increased average lifespan, produce less ROS, obtain less oxidative damage and accumulate less mitochondrial DNA abnormalities with ageing [59]. Mitochondria have been the focus of research investigating the various facets of ROS mediated signalling and damage in skeletal muscle during ageing, and pathologies effecting skeletal muscle functions such as COPD. ROS induced damage includes irreversible carbonylation of amino acid side chains of proteins and lipid peroxidation [60]. Protein carbonylation has been linked to decreases in creatine kinase activity in *vastus lateralis* of COPD patients, potentially impacting on skeletal muscle metabolic capacity [61].

Mitochondrial function declines with age in human skeletal muscle [62]. This includes a decrease in the rate of mitochondrial protein synthesis occurring by middle age [41], decreased activity of mitochondrial enzymes such as cytochrome C and citrate synthase [41], an accumulation of mtDNA damage linked to a decrease in ATP production rate [63] and an overall decrease in oxidative capacity coupled with a decrease in mitochondrial content volume [64].

It is thought that due to their proximity to the source of ROS release mitochondrial DNA and proteins accumulate oxidative damage at an accelerated rate. Mitochondrial proteins with oxidative damage are degraded by Lon protease, which is expressed at lower levels in elderly muscle of mice [65]. It has recently been shown that Lon protease regulates mitochondrial transcription through the degradation of the mitochondrial transcription factor A (TFAM) [66]. However, if oxidative damage becomes extreme, the damaged proteins have a destabilising effect on the mitochondrial membrane potential and cause fission of the damaged region which is then degraded by lysosomes [67]. Mouse models expressing the lysosome associated protein LAMP2A showed improved mitochondrial

function in old age compared to wild types due an increased rate of removing damaged proteins [68]. Mitochondrial DNA damage has been linked to sarcopenia. Wanagat et al revealed that within skeletal muscles of rats the fibres harbouring greater amounts of mtDNA damage were co-localised with electron transport chain abnormalities, increased ROS release and fibre atrophy [69].

Several key proteins have emerged as regulators of mitochondrial function in skeletal muscle. Chief amongst them is the transcriptional factor PGC-1α (peroxisome proliferator-activated receptor gamma co-activator 1-alpha), which stimulates mitochondrial biogenesis by activating down-stream factors such as nuclear respiratory factor 1 (NRF1) and TFAM [70]. PGC-1α mRNA levels are decreased in muscles of elderly individuals [71]. Mice with constitutive PGC-1α expression in skeletal muscles show impressive improvements in whole body health including improved mitochondrial function, increased insulin sensitivity, decreased sarcopenia, decreased chronic inflammation and preserved neuromuscular junctions in old age [72]. Further studies have shown that PGC-1α drives the formation of slow-twitch muscle fibres in mice [73], controls the expression of the insulin sensitive glucose transporter GLUT4 by co-activation of MEF2C [74] and controls oxidative function in response to nutrient sensing by mTOR through a YY1-PGC-1α complex [75].

Another important regulator of energy production is AMP-activated protein kinase (AMPK). Activation of AMPK increases fatty acid oxidation and activity of mitochondrial enzymes in skeletal muscle [76]. It regulates mitochondrial biogenesis by activation of NRF-1 [77] and is required for mitochondrial biogenesis in skeletal muscle in response to energy stress [78]. In muscles of rats and mice, the activity of AMPK is blunted in old age leading to a reduction in AMPK mediated mitochondrial biogenesis [79] and an accompanying decrease in PGC-1α expression [80].

Protein acetylation is emerging as a key regulatory mechanism of both activity and abundance of metabolic enzymes including those in the mitochondria [81] [82] (**Table 1.2**). Exciting recent work has linked together activity of AMPK to NAD-dependent deacetylase sirtuin-1 (SIRT1) mediated protein deacetylation, including PGC-1α [83]. Canto et al describe a mechanism by which AMPK acts as an

energy sensor, which regulates NAD+ levels, this in turn modulates SIRT1 activity which activates PGC-1α in times of energy deprivation [83].

Name	Organism	Effect on enzyme	Mechanism	Nutrient signal
Acyl-Coenzyme A dehydrogenase, long-chain (Acadl)	Mouse	Down-regulation	Unknown	Inhibited by fasting
Aldehyde dehydrogenase 2 (Aldh2)	Mouse	Up-regulation	Deacetylation increases acetaminophen toxic-metabolite binding	Inhibited by fasting
Acyl-CoA synthetase short-chain family member 1 (ACSS1)	Human	Down-regulation	Unknown	Unknown
Acyl-CoA synthetase short-chain family member 1 (ACSS2)	Human	Down-regulation	Active site interference	Unknown
Carbamoyl phosphate synthetase 1(CPS1)	Human	Down-regulation	Unknown	Inhibited by starvation, high protein diet and calorie restriction
Enoyl-CoA, hydratase/3-hydroxyacyl CoA dehydrogenase (EHHADH)	Human	Up-regulation	Unknown	Stimulated by high fatty acid
Isocitrate dehydrogenase 2 (IDH2)	Mouse	Down-regulation	Unknown	Inhibited by caloric restriction
Malate dehydrogenase (MDH)	Human	Up-regulation	Unknown	Stimulated by high glucose
Phosphoenolpyruvate carboxykinase 1 (PCK1)	Human	Down-regulation	Promoting degradation via proteasome	Stimulated by high glucose
Phosphoglycerate mutase 1 (PGAM1)	Human	Up-regulation	Allowing efficient phosphotransfer	Stimulated by high glucose
PK, muscle (PKM2)	Human	Down-regulation	Targeting to lysosomal degradation	Stimulated by high glucose
Succinate dehydrogenase complex, subunit A (Sdha)	Mouse	Down-regulation	Acetylation controls the substrate entry	Unknown
Superoxide dismutase 2 (SOD2)	Human	Down-regulation	Unknown	Inhibited by nutrient starvation
Sphingosine kinase 1 (SPHK1)	Human	Up-regulation	Inhibiting degradation via proteasome	Unknown

Table 1.2 – The effect of acetylation on metabolic enzymes

This table is adapted from a review by Yue Xiong and shows the effect of acetylation on well-known metabolic enzymes and superoxide dismutase 2 (SOD2). For the full table see [84].

1.2.3 The role of insulin resistance

The majority of dietary glucose is transported to peripheral tissues such as skeletal muscles. This is dependent on insulin which is released in response to increased concentrations of blood glucose and stimulates the transport of glucose into muscle cells through insulin responsive transporters such as GLUT4 [85]. Glucose can then be stored for later use as glycogen or utilised for ATP production. Indeed, insulin stimulation of *vastus lateralis* muscle in healthy humans causes an increase in ATP production capacity of up to 42% accompanied by an increase in mRNA levels of mitochondrial proteins and an increase in mitochondrial protein synthesis [86]. Skeletal muscle represents a major site of insulin resistance in obese, diabetic, and to a lesser extent elderly individuals [87]. Type 2 diabetes is an increasing problem in elderly populations and is associated with increased prevalence of obesity. In elderly individuals the levels of plasma glucose and insulin response was higher

compared to young people after a glucose tolerance test, although the changes were modest [88]. In many elderly individuals the build-up of both intra and extra-cellular adipose deposits occurs in skeletal muscle. In obese individuals adiposity is a major contributor to insulin resistance and incidence of type 2 diabetes. Yu et al have shown that increased concentration of free fatty acids in the muscle leads to the activation of protein kinase C (PKC-θ). This in turn triggers a signalling cascade resulting in decreased insulin receptor 1 (IRS1) signalling and lower glucose transport [89]. Petersen et al revealed that insulin resistance in elderly muscle is related to increases in intramyocellular fatty acids, which may be due to decreased mitochondrial oxidative metabolic activity. They propose that this is consistent with an age-related decline in mitochondrial DNA quality and mitochondrial density [90].

1.3 Interventions to prevent skeletal muscle dysfunction

1.3.1 Hormone Replacement Therapy

A decrease in levels of testosterone is associated with old age [91]. In elderly men, treatment with relatively high doses of testosterone does increase muscle mass and strength [92]. However the risks of prolonged testosterone treatment are many and most likely overshadow the benefits.

Another potential hormone replacement therapy which has become extremely common is growth hormone (GH) supplementation. GH levels drop with age [93], and supplementation does appear to improve muscle mass and exercise capacity marginally [94], however the incidence of side effects makes it an inappropriate strategy for the general elderly population [95].

1.3.2 Physical exercise training

There is an outstanding body of research supporting the role of physical exercise in improving skeletal muscle function and in fact, whole body function and health. Physical exercise has been shown to have a beneficial effect on patients with a wide range of conditions including type 2 diabetes [96], COPD [97], pulmonary hypertension [98], asthma [99] and heart failure [100]. Many different avenues of research have been considered including type of exercise (resistance training or endurance training), exercise intensity, impact on ageing and age related diseases such as COPD and type 2 diabetes.

The effects of physical exercise training can go some way towards reversing the age related decline in muscle function. Endurance exercise can increase overall muscle protein synthesis and mRNA levels of mitochondrial proteins [35] [36], induces PGC-1α expression [35] [101] [102] and increases metabolic enzyme activity and aerobic capacity in both young and elderly individuals [35]. It has been shown in mice that the population of satellite cells in elderly muscle is reduced, as well as their proliferative potential [103]. Endurance exercise in rats increased the myogenic capacity and number of satellite cells residing on myofibres compared to young rats [104]. Resistance exercise is routinely used as an intervention to combat sarcopenia. A sixteen week resistance exercise program is sufficient to significantly improve muscle strength, increase muscle cross sectional area and increase the proportion of type IIa fibres in both young and elderly men and women [105]. Resistance exercise increases muscle protein synthesis of MHC and mixed muscle protein [106]. However, it is important to note that the response to physical exercise training is highly heterogeneous between individuals, with increases in VO_2 max ranging from 0-100% [107] and gains in muscle strength ranging from 3-28% [108]. Analysis of molecular networks of skeletal muscle ageing and response to exercise have recently been generated from databases of existing knowledge, and suggest that age-related processes are distinct from the adaptation to physical exercise [108].

1.4 The regulation of angiogenesis

Angiogenesis is the process by which the existing vasculature is extended by the growth of new blood vessels. In physiological conditions the activation of angiogenesis depends on a fall in oxygen tension (hypoxia) due to either an increase in oxygen demand by the surrounding tissue, or a decrease in the oxygen concentration in the blood. Hypoxia leads to stabilisation of the HIF-1α subunit of the hypoxia inducible factor (HIF-1) transcription factor which is degraded in normoxic conditions [109]. HIF-1 then activates an extensive transcriptional program including key pro-angiogenic factors such as vascular endothelial growth factor (VEGF) [110], VEGF receptor-1 (Flt-1) [111], nitric oxide synthase 2 (NOS2) [112] and others [113]. Many of the factors involved in angiogenesis are responsible for the recruitment and proliferation of endothelial cells which form the new blood vessels.

Hypoxia, HIF-1, growth factor and cytokine signalling plays a key role in both physiological and pathological angiogenesis. In human skeletal muscle PGC-1α and VEGF [114] are up-regulated in response to exercise. Up-regulation of PGC-1α leads to increased oxygen consumption in the muscle due to a shift towards oxidative metabolism and a subsequent stabilisation of HIF-1α and activation of pro-angiogenic HIF-1 transcriptional targets [115].

Angiogenesis is perhaps most well studied in the context of tumour progression. As tumours develop and grow larger they have a greater oxygen demand. Without an adequate supply of oxygen and metabolites a tumour cannot grow larger than a few mm's in diameter [116]. One of the most aggressive human tumours, glioblastoma, up-regulates VEGF in response to hypoxia [117] [118]. VEGF signalling through the receptor KDR activates pathways controlling endothelial cell migration, proliferation and survival. However, many other growth factors and cytokines such as IL8, IL1, FGF2, GCSF, IGF1, ANGPT2, CXCR4 and CXCL12 also play a role in tumour angiogenesis [119]. Counteracting the pro-angiogenic factors are a number of anti-angiogenesis factors such thrombospondin 1 (THBS1), endostatin, canstatin, tumstatin, interferon-α and interferon-β [120]. The onset of angiogenesis relies on the balance between pro and anti-angiogenesis factors, termed the

"angiogenic switch". When the activity of pro-angiogenic factors outweighs the anti-angiogenesis factors the angiogenic program is initiated and tumour growth occurs [120].

1.5 The application of systems biology approaches to human health

The advent of functional genomics has made it possible to measure gene, protein and metabolite concentration in single experiments at a genome wide scale. The goal of researchers employing systems biology approaches is to develop and utilise analysis pipelines able to effectively generate novel hypothesis from this data. These hypotheses should be both relevant and testable given our current knowledge of the physiology of the experimental system.

The first commercially available systems for measuring genome wide gene expression using microarray technology appeared over a decade ago. Using precise probe spotting or photolithographic synthesis, oligonucleotides complimentary to all known mRNAs in an organism can be printed to microarray slides. These oligos will hybridise to complimentary mRNAs from cells or tissues. Precise measurement of relative gene expression is achieved by incorporation of a fluorescent dye into the mRNA sample prior to hybridisation. After washing off unbound mRNAs, a high-resolution laser scanning device captures the fluorescence signal from labelled mRNA bound to each microarray probe. The signal intensity is proportional to the amount of bound mRNA, which is dependent on the abundance of transcript within the cells. Modern microarrays allow the transcriptional profiling of over 30,000 unique genes in 8 samples simultaneously.

The use of protein mass spectrometry (MS) allows the measurement of thousands of proteins in a single experiment. Multiple platforms are widely used, with the more common methods such as Matrix-assisted laser desorption/ionization – time of flight (MALDI-TOF) able to generate peptide mass fingerprints at a rapid rate. In a MALDI-TOF analysis, proteins are first digested to create proteolytic fragments (peptides), which are then analysed by MS. The mass fingerprint of the

peptides can then be matched to known proteins by comparison to a database of mass fingerprints generated by virtual digestion of each protein in the sequence database. Any unmatched peptides can be sequenced using a further round of MS if necessary, followed by protein identification by sequence homology.

At the final step of the "omics" cascade is metabolomics, or the systems level analysis of metabolite concentrations in biological samples. Similar to MS proteomics, the aim of MS metabolomics is to generate metabolite fingerprints (whole metabolome, hypothesis generating) or metabolite profiles (targeted pathways, hypothesis driven). Unlike proteins and nucleotides which have well defined sequence databases, metabolite identification relies on mass spectra alone. Some large libraries of spectra are currently available, however metabolite identification remains as a bottleneck in metabolomics analysis [121].

The analysis of transcriptional data generated using whole genome microarray profiling is amongst the better developed areas of omics data analysis. This thesis utilises multiple large-scale transcriptomics datasets to study muscle ageing and a dynamical model of angiogenesis. In this section an overview of microarray data generation and analysis will be described. Many of these approaches are applicable to large datasets generated using different functional genomics approaches, however as we have focussed on gene expression the methodology is described in that context. The recent advances in our understanding of skeletal muscle biology and angiogenesis that have originated from studies utilising systems biology approaches will be outlined in the following section.

1.5.1 From raw data to processed expression data

Raw microarray data covering the entire genome consists of fluorescence intensity values representative of the relative concentration of mRNAs from the starting tissue or cell culture. Firstly,

the range of intensity values, which exist on a multiplicative scale, is normally log2 transformed in order to represent the highly asymmetric signal distribution as a symmetrical normal distribution. In practice, this allows the representation of gene repression and induction on a comparable scale. This data is subject to experimental, biological and technical variation, which must be corrected before the data can be analysed. Therefore, the first step in microarray data analysis consists of a normalisation procedure aimed to remove the experimental and technical variance and ensure the data is comparable across multiple arrays.

There are a number of popular methods used for microarray data normalisation depending on the microarray technology. So called “one colour” microarrays are hybridised to a single mRNA sample labelled with a fluorescent dye, typically Cy3. “Two colour” microarray analysis involves competitive hybridisation of two mRNA samples, normally a control and a treatment, labelled with different dyes, typically Cy3 and Cy5. The fluorescent signal of each dye for each gene can be converted into a ratio, allowing the comparison of two samples with a single microarray. Both approaches have strengths and weaknesses. One colour hybridisations generate relative abundances for each gene and data that is comparable between multiple experimental conditions. Two colour hybridisations reduce the experimental cost at the risk of low data precision in the case of a low quality sample. One-colour Affymetrix microarrays are designed with 11-20 probes that match different locations across gene transcripts. Methods such as RMA [122], MAS5 [123]and GC-RMA [124] that have been developed to take advantage of this feature allow the unsupervised normalisation and probe set averaging of Affymetrix data. While these normalisation methods are conceptually very similar, GC-RMA has been found to introduce artificial correlations into transcriptional data while MAS5 introduced the least [125]. Therefore use of GC-RMA could have a detrimental impact on many statistical procedures. Data produced using other microarray platforms such as Agilent is most commonly normalised using quantile normalisation [126]. This method assumes that the distribution of signal intensities is almost equal in all samples. For each value on the microarray, the quantile is calculated and matched to the corresponding quantile of the reference distribution of probe intensities across all arrays. The original value is then transformed to the corresponding value from the reference distribution. This

brings the distribution of all the microarrays in line with each other. Two-colour microarray data can be normalised using the popular LOESS algorithm, which effectively generates expression ratios between control and treatment samples while removing technical variation [127].

1.5.2 Detecting gene expression patterns

Gene expression is a dynamic process in which stimuli such as hypoxia or exercise induce a transient production and repression of a set of mRNAs. Patterns of expression over time and across multiple stimuli can be captured using data analysis techniques. Several techniques can be used for this

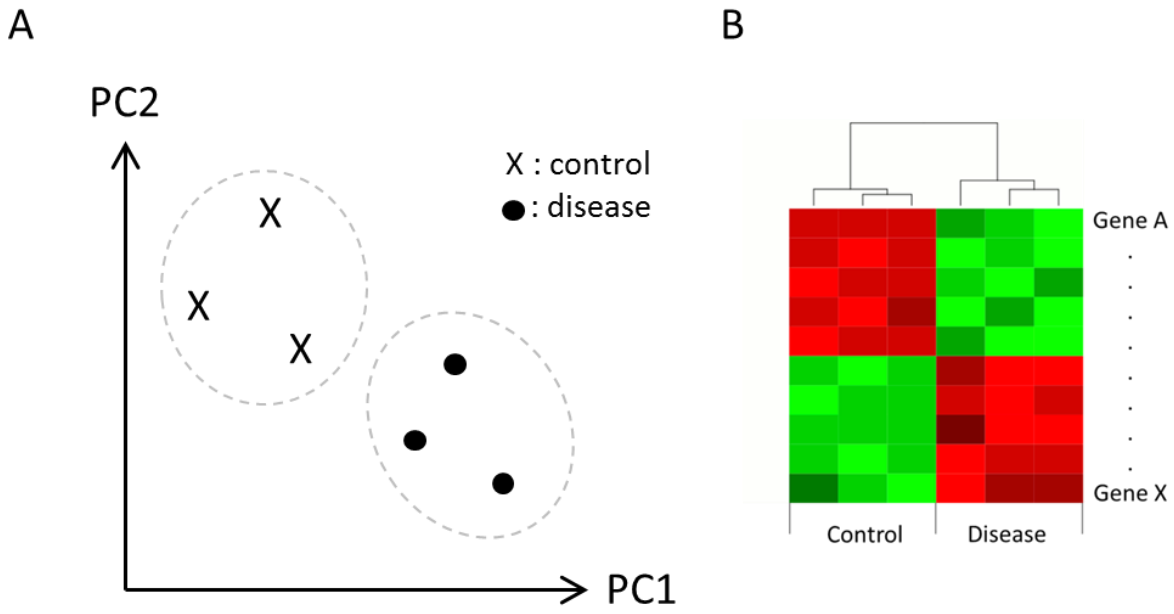

Figure 1.2 – Example of Principle Component Analysis and hierarchical clustering

Panel A shows the separation of two groups of samples based on the projection of the first two principle components (PCs) onto a 2D plot. Principle components are uncorrelated variables derived from the original data which are representative of variation within the data. The first principle component (PC1) represents the largest amount of variance, and each successive component represents variance that is uncorrelated to all those preceding it. In the example in panel A, the first principle component separates both sample groups, suggesting that disease status is responsible for the largest source of variation. Panel B shows an example of hierarchical clustering applied to gene expression. A similarity metric is calculated between all samples, such as correlation or Euclidian distance, and this is used to organise the samples in a dendrogram such that highly correlated samples are clustered close together.

purpose, they allow data exploration to identify gene or sample clusters on the basis of their molecular state. Principal Component Analysis (PCA) is one such technique that reduces the dimensionality of large datasets while retaining the majority of the information. Very often, PCA is used as a data visualization technique in the form of 2D or 3D plots [128] (**Figure 1.2A**).

Cluster analysis is a different technique that can achieve similar results. It aims at identifying groups of genes or samples with similar expression profiles. By using a measure of cluster homogeneity some of these procedures (e.g. HOPACH [129]) are able to objectively distinguish the number of true clusters in the data. In the case of cluster analysis the relationship between samples and/or genes is often visualised using a dendrogram (**Figure 1.2B**).

1.5.3 Defining transcriptional signatures of perturbations

Large-scale transcriptomics experiments can be complex and cover multiple time points and treatments or they can be as simple as a single treatment. In either case identification of the genes differentially expressed between the sample groups is a key step.

Several statistical techniques and software packages have been developed for this purpose. The choice of methodology depends on the experimental design. A t-test, analysis of variance (ANOVA) or Significance Analysis for Microarrays (SAM) [130] can be used to identify genes, proteins or metabolites that are differentially expressed between two groups of paired or unpaired samples. On the other hand, Analysis of variance (ANOVA) and SAM can be applied to compare multiple groups of samples. Two-way ANOVA can be applied to designs integrating multiple experimental factors within groups. SAM and Bayesian Estimation of Temporal Regulation (BETR) [131] can identify differentially expressed genes in time-course experiments. SAM allows the user to control the false discovery rate (FDR), however when using a t-test or ANOVA it is important to control for multiple comparisons. This can be done using a method to estimate the FDR such as that proposed by Benjamini and

Hochberg [132]. An FDR threshold of less than 10% is commonly used to define the upper limits of statistical significance.

Modern whole genome microarrays routinely provide expression measurements for 20,000-30,000 unique genes. Thousands of these genes may be differentially expressed, making interpretation of the results a serious challenge. One way to reduce the complexity of the analysis is to define groups of genes that perform similar biological functions such as a class of enzymes, membrane bound proteins, transcription factors and many others. The Gene Ontology database [133] contains many thousands of these gene sets. Using software tools such as DAVID [134] it is possible to statistically determine whether a particular gene set is overrepresented in a list of differentially expressed genes, taking into account the overall abundance of that gene set in the genome. Alternatively, GSEA [135] detects enrichment of functional groups within lists of genes ranked by a metric such as the t-statistic or logged fold change and allows the specification of many custom gene sets which can be tested simultaneously. For this reason GSEA can be used to identify coordinate changes in expression of functional groups in data that may only present a few differentially expressed genes.

The Gene Ontology database contains both well-defined and predicted functional annotation of genes. Other database tools such as KEGG and Ingenuity Pathway Systems (IPA) contain only curated information. KEGG is a set of experimentally validated pathways across many organisms which can be queried through DAVID. IPA is a powerful tool containing relationships described in the literature between genes, proteins, metabolites and drugs. The suite of analysis tools offered by IPA includes prediction of up-stream effector molecules of a particular set of genes and identification of interaction networks enriched with genes of interest.

Using these tools it is possible to build up a “functional profile” of a given treatment which can be used to generate testable hypotheses.

1.5.4 Constructing biological networks

A difficult challenge in the analysis of gene expression data is to formulate hypotheses from the analysis of very large datasets. Unfortunately this is a difficult task and the relatively simple data exploration techniques I have outlined above are not sufficient to achieve this task.

Network inference methodologies are able to capture statistical dependencies between variables and "learn" the structure of underlying biological networks from observational data. The decision of which method to use is dependent on the biological question and the design of the experiments. Networks can be generated containing many thousands of nodes by using a pairwise score of dependency such as correlation or mutual information. The nodes are connected by connections, called arcs or edges, which represent the statistical dependency between the two genes, proteins or other entities. In this context, one of the most popular tools for inferring large networks, ARACNE [136], infers large networks based on mutual information (MI). Mutual information provide a measure of how much variation in one variable (for example, a gene) is explainable by the variation in a second variable. Therefore it is able to detect non-linear relationships such as those present in biological systems. ARACNE allows simple thresholding of the network through the input of a desired p-value or MI threshold [137]. Unlike other network inference frameworks such as Bayesian networks which are suitable for small networks usually consisting of less than 100 nodes, ARACNE has been designed specifically to utilise microarray expression profiles to reconstruct networks with sufficient levels of complexity to represent eukaryotic systems. ARACNE also makes use of the data processing inequality (DPI), which provides a framework to remove indirect relationships within networks. This is an important step when reconstructing precise networks such as the first neighbours of transcription factors, which are very likely to produce a large number of indirect downstream effects.

Large mutual information based networks need to be represented in an organised manner in order to be interpreted. Adjusting the position of each node in the network in accordance with its

connectivity to surrounding nodes is an effective way of visualising large networks so that highly interconnected clusters of nodes become spatially distinct. Objective network community detection algorithms such as those available within the GLay [138] or MCODE [139] packages can be applied which will identify distinct sub-networks. MCODE is suitable for identifying small intra-connected clusters with very high modularity scores within large networks; however this can be hard to interpret in a biological setting due to the large number of clusters and the number of unclustered genes. GLay has a higher sensitivity than MCODE with a slightly lower specificity, leading to a smaller number of larger clusters at the cost of a slightly reduced modularity score. The fast-greedy algorithm within GLay (implemented by Wakita et al [140]) improves the community detection by controlling the merging of smaller clusters using a cluster size and density parameter, leading to a more balanced distribution of cluster sizes. In practice, analysis pipelines designed to functionally annotate large networks such as those presented in this thesis are facilitated by the use of GLay. Both of these approaches are available in the open-source Cytoscape software [141].

Mutual information and correlation based networks do not infer the directionality of network connections. By using ordinary differential equation (ODE)-based network inference techniques the directionality of network connections can be identified [142] [143]. Due to the computational power needed to infer ODE networks it is limited to a small number of nodes, generally 50 or less. ODE networks can be useful when applied to a smaller, targeted set of genes such as transcription factors that are regulated in response to a perturbation.

1.6 Application of systems biology to skeletal muscle function and angiogenesis

1.6.1 Skeletal muscle

The application of transcriptional profiling and systems biology techniques has revealed alterations in gene expression underlying many issues affecting human health. In this section the approaches and findings of several key studies focusing on skeletal muscle function and angiogenesis will be described.

Welle et al identified a comprehensive set of over 1000 probes differentially expressed between muscle of young and elderly people including over 100 genes involved in energy metabolism which were down-regulated in elderly muscle [144]. The transcriptional profiling of young and elderly muscle performed by Melov et al. [145] and Zahn et al. [146] was consistent with a decrease in expression of energy metabolism genes with age. The Melov study also identified up-regulation of genes related to DNA repair and cell death in elderly muscle. In contrast, a recent study by Phillips et al. compared the transcriptional signature of 3 independent studies [145] [147] [108] of ageing muscle and concluded that no common signature of ageing could be detected. By using a relatively large clinical dataset (n=52) they identified 580 genes correlated significantly with age which were enriched with genes related to muscle disorders but not mitochondrial metabolism. Phillips et al suggest that the inconsistency between the transcriptional signatures is due to the substantial differences in physical fitness between the study groups and that mitochondrial dysfunction is unlikely to be attributed to ageing *per se*.

Giresi et al. generated a predictive model of sarcopenia in *vastus lateralis* muscle using a supervised classification technique that identified 45 genes which achieved 75% classification accuracy when distinguishing young and elderly muscle in an independent dataset [148]. Amongst the gene signature was Forkhead Box O3 (FOXO3A) and CCAAT/Enhancer Binding Protein Beta (CEBPβ), which were recently shown to play a key role in AMPK mediated control of muscle autophagy in mice [149] and up-regulation of the ubiquitin ligase MAFbx respectively [150]. Abadi et al identified a transcriptional signature of muscle disuse and atrophy including down-regulation of mitochondrial metabolism genes and up-regulation of protein degradation related genes (including Murf1 and MAFbx) in response to muscle immobilisation [151]. This was linked to decreased protein content of

cytochrome C oxidase, decreased mTOR phosphorylation and increased protein ubiquitination. Reich et al. found similar transcriptional changes in response to muscle immobilisation (increased expression of protein ubiquitination genes, decreased expression of mitochondrial metabolism genes) as well as identifying an increase in genes related to oxidative stress [152]. Furthermore, reloading of the muscle did not fully reverse these expression changes.

Several studies have used transcriptional profiling to investigate the effects of physical training on gene expression. Radom-Aizik et al. reported up-regulation of genes related to mitochondrial metabolism and down-regulation of genes linked to protein catabolism in response to 3 months of training [153]. Melov et al. showed that the transcriptional profiles of a subset of genes in skeletal muscle of elderly individuals after 6 months of training resembled that of younger individuals [145].

Molecular networks underlying normal healthy skeletal muscle function regardless of age or gender have previously been defined by combining a meta-analysis approach with canonical pathway databases (KEGG) and existing literature [154]. The authors make use of existing microarray data from over 250 healthy muscle biopsies as well as a range of other tissues (fat, liver, kidney, brain, skin and hair) to identify mRNAs under or over-expressed in skeletal muscle. This information was combined with existing pathway information to create networks. These networks, which represent excitation, mechanical transmission, energy metabolism and signalling cascades, are a comprehensive snapshot of our current knowledge of normal muscle function.

1.6.2 Angiogenesis

The process of angiogenesis involves the coordination of endothelial cell proliferation, migration and extracellular matrix remodelling. Abdollahi et al. analysed the transcriptional profiles of microvasculature endothelial cells treated with pro and anti-angiogenesis factors (VEGF, FGF2, endostatin) and identified 600 unique genes that responded inversely to pro and anti-angiogenic factors [155]. By using data mining of the current literature and online databases they identified

interactions between these genes and constructed an “angiogenesis network”. One of the pro-angiogenic hubs, PPAR-δ, was confirmed to be an important regulator of tumour vascularisation that correlated with tumour progression in clinical samples. Anders et al. performed a meta-analysis of 15 cancer microarray studies (979 samples) aiming to identify a signature of angiogenesis related genes common to human cancers [156]. They identified 25 genes able to classify cancer and healthy tissues with a high accuracy. These genes were related to angiogenesis such as CXCL12, TGFBR3, CCL2, PDGFRA and SPARC-1. However, genes previously reported as pro-angiogenic such as VEGF, IL8 and MMP2 were not identified as part of the signature, suggesting that additional post-transcriptional regulation and the contribution of the tumour microenvironment could be important factors in the role of these genes. This finding was consistent with a second study by Liang-Hui et al. which used machine-learning techniques to construct a network of protein-protein interactions in the neighbourhood of a set of 84 well known angiogenesis related factors [157]. None of the VEGF proteins or receptors were hub genes in the network, however all of them were present. This lends weight to the argument that angiogenesis is controlled by the interactions of a large network of factors.

In conclusion, systems biology approaches have revealed novel insights that are key to our understanding of skeletal muscle ageing, exercise and angiogenesis. As the availability of functional genomics data increases, there is a need to understand the underlying structure of relationships between genes, proteins and metabolites in order to interpret and integrate data from multiple domains. The use of network inference methods can provide the underlying networks at a genome wide scale if sufficient observational data is available. The use of network inference methods has so far not been applied to skeletal muscle ageing and angiogenesis despite representing attractive targets for study, due to the availability of functional genomics data and significant impacts on human health. This thesis has developed network models of muscle ageing and angiogenesis in order to delineate the transcriptional reprogramming that characterises these processes. A number of hypotheses are revealed which are validated using an animal model and *in vitro* experiments.

CHAPTER 2

INFERENCE AND ANALYSIS OF TRANSCRIPTIONAL NETWORKS REPRESENTING AGEING HUMAN SKELETAL MUSCLES

2.1 Introduction

Sarcopenia, described as age related skeletal muscle dysfunction and atrophy, is a condition intrinsic to human health and has a substantial impact on conditions such as cancer cachexia [158], COPD [159] and other movement impairing disabilities [160] [161]. Muscle weakness can significantly impact on quality of life and life expectancy [162] [163] [164]. Management of sarcopenia is therefore an important factor in disease management. Interventions to combat the loss of muscle function in various clinical populations have been reported including hormone supplementation, pharmacological treatment and exercise training [165] [166]. Physical exercise is recognised as one of the best options for improving skeletal muscle function, regardless of age. It has been shown to improve inflammatory status [167], strength [105], and metabolic capacity [36].

Some of the molecular events underlying skeletal muscle ageing, such as an increase in nitric oxide synthase expression [168], a disruption in the hypoxia response pathways (e.g. loss of PGC-1α target activation) [169], and a decrease in protein synthesis following anabolic stimuli [44] have been intensively studied for their potential involvement in muscle wasting in humans and animal models. Recently, the role of mitochondrial dysfunction in ageing muscle has been highlighted. Mitochondrial respiratory efficiency is an important determinant of activities of daily living in elderly people such as walking speed [170]. There is a decline in respiratory chain function and accumulation of mtDNA mutations with age in skeletal muscle [63], accompanied by a decrease in expression of proteins and mRNAs related to mitochondrial function [145]. An accumulation of mitochondrial DNA mutations has been shown to induce mitochondrial dysfunction and increase apoptosis and sarcopenia [171]. The generation of reactive oxygen species (ROS) within mitochondria has been found to induce mitochondrial dysfunction, leading to age dependent muscle atrophy [172] and insulin resistance

[173]. A recent study in which the antioxidant enzyme catalase was stably expressed in mitochondria of elderly mice resulted in decreased mitochondrial dysfunction, suggesting that mitochondrial ROS scavenging can prevent age-related mitochondrial dysfunction [80].

However, despite intense efforts it is not yet clear what molecular mechanisms control muscle wasting and in particular mitochondrial dysfunction. A number of groups have applied omics-based approaches to characterise the molecular state of muscles in COPD [174], diabetes [175] and ageing [145]. With a few isolated exceptions, such as the role of PGC-1α in diabetes [176] and the contribution of histone deacetylases (HDACs) to muscle wasting in COPD [174], this approach has failed to provide a framework for developing robust hypotheses on the mechanisms underlying muscle dysfunction. The main reason for this is the difficulty in integrating genome-wide descriptive data into an interpretative model that allows the identification of the driving factors of the degeneration process.

Here we address this issue by using a network biology approach designed to infer age specific gene regulatory networks from expression-profiling data derived from multiple independent studies. Our analysis revealed that networks representing young and elderly muscles are characterised by several distinct functional modules. Further analysis revealed a link between the expression of ribosomal proteins and age-dependent, transcriptional uncoupling of genes encoding for oxidative phosphorylation enzymes. This specific finding allowed us to formulate the hypothesis that the uncoupling of translation and energy related gene expression might be at the heart of mitochondrial dysfunction, a process that is recognised as one of the landmarks of muscle wasting.

2.2 Methods

2.2.1 Selection of public domain microarray datasets

Publically available microarray studies used in this work were either downloaded from the online microarray database Gene Expression Omnibus (GEO) (www.ncbi.nlm.nih.gov/geo) as raw data or obtained directly from the author.

To select potential microarray datasets to integrate as part of the skeletal muscle meta-analysis we searched GEO using the terms “skeletal muscle” and filtered the results to include only human data. We further refined the selection by outlining a set of specific biological and technological criteria (**Table 2.1**). These are:

- Biopsy from v*astus lateralis* muscle using a standard needle technique
- Use of the Affymetrix microarray platform

By using these strict criteria we can improve the likelihood that the data integration method will correctly preserve the true transcriptional state of each muscle biopsy by decreasing the number of confounding factors that need to be considered. From these datasets we selected only those that used the Affymetrix U133A or U133 Plus 2 platform in order to maximise the number of shared probes between all studies in the meta-analysis, resulting in a 22,215 probes representing 13,116 unique genes. Some of the samples within these studies originate from volunteers who are undergoing interventions such as training or treatment for significant pathologies, as we are interested in the baseline transcriptional state of healthy muscle in young and elderly people these samples were removed. We defined young (N = 55, 18-30 years) and elderly (N = 78, 60-80 years) age groups (**Figure 2.1**) in order to subset the data.

Ref No.	GEO Accession	GEO Title	Author	Year	Platform	Sex	Integrated
[148]	GSE1428	Skeletal muscle sarcopenia	Giresi PG, et al	2004	U133A	Male	Yes
[151]	GSE14901	Limb immobilization induces a coordinate down-regulation of mitochondrial and other metabolic pathways in men and women	Abadi A, et al	2009	Plus 2.0	Mixed	Yes
[153]	GSE1786	Vastus lateralis biopsies from healthy trained and sedentary males	Radom-Aizik S, et al	2004	U133A	Male	Yes
[177]	GSE19420	Skeletal muscle mitochondrial dysfunction is secondary to T2DM	van Tienen FH, et al	2009	Plus 2.0	Mixed	Yes
[152]	GSE21496	Effects of 48h Lower Limb Unloading in Human Skeletal Muscle	Reich KA, et al	2010	Plus 2.0	Male	Yes
[178]	GSE9419	The skeletal muscle transcript profile reflects responses to inadequate protein intake in younger and older males	Thalacker-Mercer AE, et al	2007	Plus 2.0	Male	Yes
[179]	GSE9676	Effects of sex and age on skeletal muscle gene expression in normal men and women	Welle S, et al	2007	U133A	Mixed	Yes
[174]	Un-released	Effects of training on COPD patients with varying BMI	Turan N, et al	2009	Plus 2.0	Mixed	Yes
[180]	GSE1832	Time and Exercise effects on Human Skeletal Muscle	Zambon AC, et al	2003	U95A	Male	No
[181]	GSE18583	Baseline skeletal muscle gene expression	Keller P, et al	2009	Plus 2.0	Male	No
[182]	GSE18732	mRNA expression data from skeletal muscle of type 2 diabetes	Gallagher IJ, et al	2010	Plus2.0	Mixed	No
[183]	GSE9105	Effect of Acute Physiologic Hyperinsulinemia on Gene Expression in Human Skeletal Muscle in vivo	Coletta DK, et al	2008	U133A	Mixed	No
[184]	GSE22309	Expression data from human skeletal muscle	Wu X, et al	2007	U95A	Mixed	No
[185]	GSE7146	Effect of insulin infusion on human skeletal muscle	Parikh H, et al	2007	HuGeneFL	Mixed	No
[186]	GSE13070	Human Insulin Resistance and Thiazolidinedione-Mediated Insulin Sensitization	Sears DD, et al	2009	Plus 2.0	Mixed	No

Table 2.1 – Microarray datasets identified in the GEO search

Microarray studies within the NCBI Gene Expression Omnibus (GEO) database matching the initial search criteria. Studies that were integrated into the meta-analysis contained young and/or elderly samples and used U133A or Plus 2.0 Affymetrix platforms.

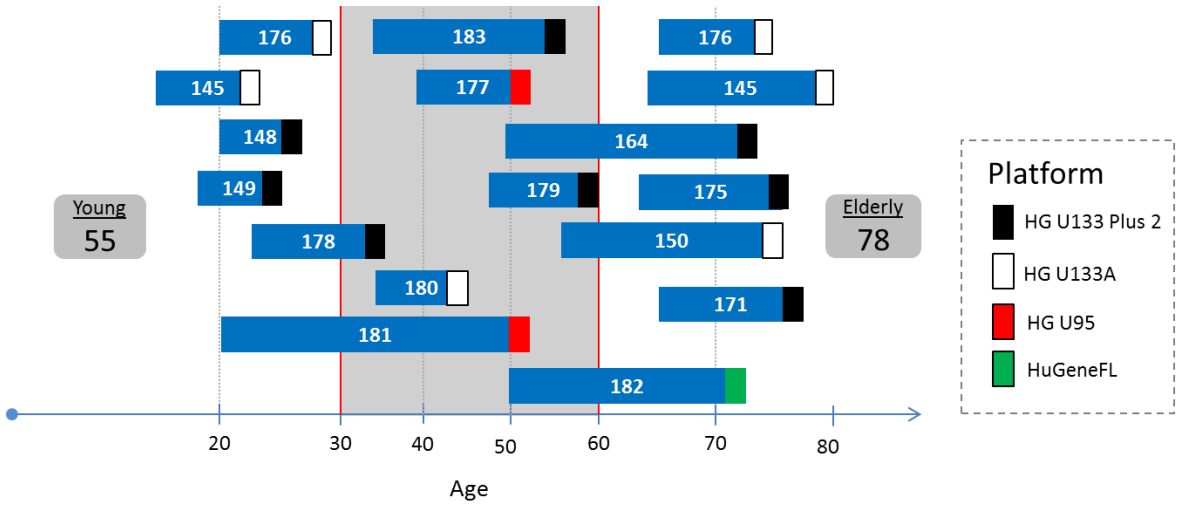

Figure 2.1 – The distribution of samples according to age for each study identified in the GEO search (from Table 2.1).

The age groups used in the meta-analysis correspond to the area either side of the grey section. Studies containing samples within both the acceptable age range and the grey section were removed unless they provided the age of each sample, in which case only the unsuitable samples were removed. Numeric labels indicate reference numbers.

We used an independent dataset produced by Melov et al (GEO accession GSE8479) to identify genes differentially expressed in young and elderly human skeletal muscle and between elderly untrained and trained muscle. The training regime and generation of the transcriptomics data is described in ref [145]. Briefly, they selected healthy elderly (N = 25) and young (N = 26) men and women and obtained a resting muscle biopsy from the *vastus lateralis*. 14 elderly volunteers underwent 26 weeks of resistance exercise training and a muscle biopsy was obtained after completion of the program with a 48hr recovery period following the final session. Transcriptional profiles were generated using Illumina Human Ref-8 microarrays.

We used a dataset produced by Edwards et al (GEO accession GSE6323) [187] to identify genes differentially expressed in skeletal muscle of young (5 month) and elderly mice (25 month) C57BL/6NHsd mice. Gastrocnemius muscle was extracted from each mouse and snap frozen before RNA extraction. Transcriptional profiles were generated using Affymetrix Mouse MOE430A microarrays.

2.2.2 Affymetrix microarray processing

Affymetrix microarray datasets were individually summarised and normalised using either the MAS5 or RMA algorithm. MAS5 has been applied to studies integrated into the meta-analysis. MAS5 has been shown to perform well when assessing normalisation methods for their effects on downstream network inference applications [125]. For other microarray studies used in this analysis such as the comparison between young and elderly mice, the data was summarised and normalised using the popular RMA algorithm with quantile normalisation.

2.2.3 Illumina microarray processing

The study of Melov et al is hybridised to Illumina Human Ref-8 microarrays. The Illumina microarray methodology includes the generation of confidence values (p value) comparing the signal of each probe to the background signal. All probes with a non-significant detection p value ($p > 0.05$) across more than 50% of samples were removed. The data was then quantile normalised resulting in a final dataset of 11,339 genes.

2.2.4 Integration of microarray data from multiple studies

We have integrated samples from studies hybridised to Affymetrix microarrays. The data integration strategy is outlined in **Figure 2.2**. There are a number of standard approaches for processing Affymetrix data, such as MAS5 normalisation. However these do not account for batch-to-batch variation between microarrays. Microarray signal intensity is sensitive to factors such as environmental conditions, reagents and small differences in procedures by research staff. These can cause small but coordinate differences between studies, even if the underlying biological finding is very similar. We used ComBat [188], a Bayesian approach to remove these batch effects from the data.

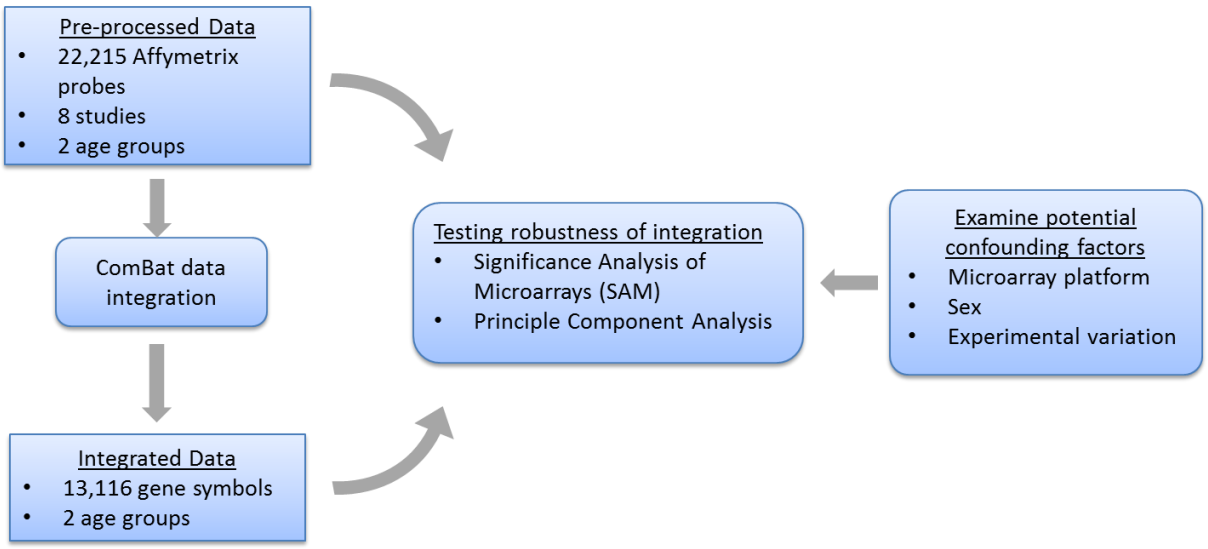

Figure 2.2 – The data integration strategy using ComBat.

This figure shows the tests using SAM and PCA that were applied to both the pre-processed and integrated data to identify the effects of confounding factors such as microarray platform, sex and experimental variation on the integration process.

ComBat was run using the recommended settings with age defined as a covariate, in order to preserve the variation due to age. We used PCA and SAM before and after the batch correction process to assess the variation between the samples, and thus the effectiveness of the integration. PCA analysis was performed using the *prcomp* command in the R software package. Using PCA we can gain a visual measure of the batch effects between the samples in terms of their laboratory of origin, microarray platform and age group. We found that prior to the batch correction the PCA revealed systematic batch effects within the data relating to dataset and microarray platform, and that these effects were not present after integration using ComBat (**section 2.3.1 - Figure 2.4**).

2.2.5 Detecting and comparing differentially expressed genes

Differentially expressed genes were detected using the Significance Analysis of Microarrays (SAM) [130] method. Unless stated, a significance threshold of 1% FDR was applied. Where sets of differentially expressed genes were tested for their level of overlap a resampling procedure was used to generate a statistical likelihood (p-value) of obtaining that level of overlap by chance. This was

done by generating a large null distribution, taking as a background the full potential overlap between the two experimental platforms in terms of gene names or probe IDs. Human and mouse homologs were identified using the Mouse Genome Informatics database (www.informatics.jax.org/). Functional annotation of gene lists was performed using the online gene ontology analysis tool DAVID [134] and applying a 10% FDR threshold.

2.2.6 Constructing and visualising transcriptional networks

In order to infer gene-to-gene connections in young and elderly muscles we used the well-validated network inference methodology ARACNE [137]. An ARACNE mutual information (MI) matrix has been generated for both young and elderly age groups, independently. In order to ensure that the inference of gene connections was not affected by sample size, we have used a resampling procedure to direct the choice of a statistical threshold at which the number of significant connections in both young and elderly individuals is independent from any differences in the number of samples (**Figure 2.3**). Two sparse networks representing the two age groups were then generated using a mutual information cut off of 0.25, which corresponds to a p value < 10^{-9} for both age groups (**Table 2.2**). This corresponds to an average of less than 1 false positive connection within the network. Networks were visualised using a force driven layout as implemented in the network visualization software Cytoscape [141].

2.2.7 Identification of network modules

Modules of highly connected genes within the network were identified using the network community detection algorithm GLay [138] using the recommended settings. The GLay algorithm is implemented in the Cytoscape plugin ClusterMaker [189]. Enrichment of gene sets corresponding to GLay modules and other custom gene lists within transcriptional signatures such as ageing was tested using the Gene Set Enrichment Analysis (GSEA) tool [135]. Transcriptional signatures were ranked according to the fold change or t-statistic, and a q-value (FDR) was calculated by GSEA for enrichment of gene sets

within the top or bottom of the ranked list. A q-value (FDR) of 10% or lower (unless stated) was used to define statistically significant enrichment.

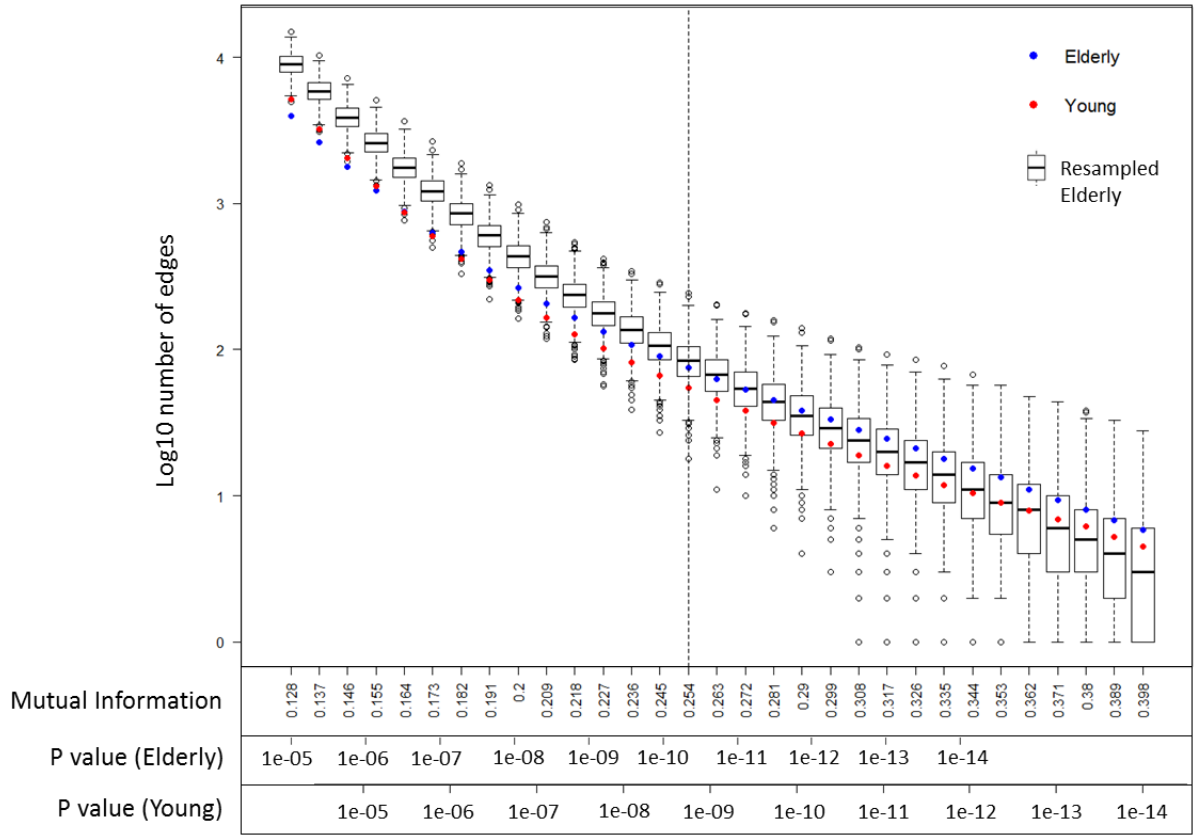

Figure 2.3 – The application of a resampling procedure to empirically define an MI threshold

This figure shows the mutual information threshold at which the average number of edges in the elderly network is comparable to the number of edges in networks generated from resampled elderly data. The number of samples chosen during resampling was identical to the number of young samples available (N = 55).

	Elderly			Young		
P Value	MI	Nodes	Edges	MI	Nodes	Edges
0.05	0.041341	13116	25419000	0.048555	13116	21561000
0.01	0.057739	13116	8962000	0.067813	13116	7050700
0.001	0.081198	13116	2068500	0.095366	13116	1382100
0.0001	0.10466	13114	547520	0.12292	13116	293320
1.00E-05	0.12812	11913	170170	0.15047	12542	71075
1.00E-06	0.15158	7753	60971	0.17802	7404	21079
1.00E-07	0.17504	4342	25337	0.20558	2929	7889
1.00E-08	0.1985	2488	11976	0.23313	1207	3732
1.00E-09	0.22195	1464	6458	0.26068	588	2042
1.00E-10	0.24541	930	3816	0.28824	335	1188
1.00E-11	0.26887	602	2407	0.31579	201	695
1.00E-12	0.29233	398	1577	0.34334	146	451
1.00E-13	0.31579	284	1067	0.37089	110	295
1.00E-14	0.33925	208	715	0.39845	71	191

Table 2.2 – The properties of sparse networks generated from the young and elderly data at a range of MI thresholds

2.3 Results

2.3.1 Integration of expression profiling datasets representing human healthy skeletal muscles

In order to develop a sufficiently large dataset to allow network inference, we first searched the public domain database gene expression omnibus (GEO) for expression profiling datasets representing skeletal muscle biopsy samples. We focused on *vastus lateralis* as this muscle was the most represented in the database.

We could identify 8 datasets (**Table 2.1**) covering a broad age range (18-80 years old) and representing over 300 biopsies (see **Figure 2.1** for a schematic overview of the relationship between samples, age and study). Two subsets of samples were then defined to represent young (55 samples representing the 18-30 age range) and elderly (78 samples representing the 60-80 age range) healthy individuals. Datasets were then integrated using the Bayesian data normalisation method ComBat, a procedure designed to minimise batch effects while retaining variation associated to a given biological signal (age).

ComBat successfully removed differences related to non-biological factors while maximising age related gene expression signatures. We found that prior to correction 45%, 52.6% and 99.99% of probes within the dataset were detected as significantly different between age, microarray platform and clinical study respectively. This was reduced to 26.5%, 0% and 1.4% respectively after processing the data with ComBat (**Table 2.3**). The small number of genes that were significant between studies had 100% overlap with genes differentially expressed between age groups. These results were consistent with visualisation of the samples using PCA (**Figure 2.4**), proving that from a statistical perspective, the integration procedure removed 99% of non-biological effects while maintaining most of the information associated to age.

Before ComBat

Factor	Significant Probes	% Dataset
Age	10,005	45.04%
Study	22214	99.99%
Microarray Platform	11,695	52.64%

After ComBat

Factor	Significant Genes	% Dataset
Age	3479	26.52%
Study	182	1.39%
Microarray Platform	0	0%

Table 2.3 – The number of differentially expressed probes and genes before and after the ComBat procedure

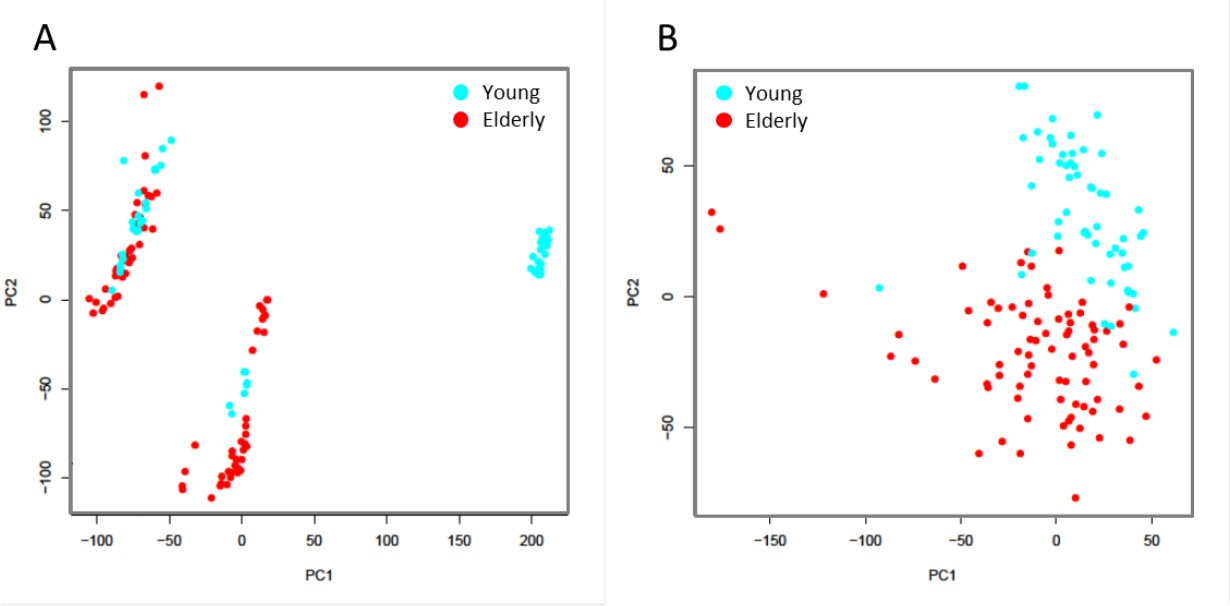

Figure 2.4 – Principle component analysis reveals systemic batch effects related to both microarray platform and dataset

PCA was applied to the young and elderly data combined. Panel A - PCA before ComBat correction shows no separation by age. Panel B - PCA after ComBat correction shows separation of young and elderly samples.

Further evidence of the effectiveness of our data integration strategy came from the analysis of the expression of genes located on the X and Y-chromosomes. We reasoned that if the data integration procedure truly removed non-biological variation without creating artefacts we should be able to identify gender specific gene expression by comparing male and female biopsies. A previous study by Welle et al has identified differentially expressed genes between male and female skeletal muscle [179]. Unsurprisingly, these included genes located on the X and Y chromosome. We used GSEA to test whether the transcriptional differences between skeletal muscle from male and females in the meta-analysis dataset was similar to a that published by Welle et al. We downloaded the differentially expressed genes identified by the Welle study. In the meta-analysis, the differences between male and females were highly similar to those identified in the Welle study (FDR < 0.001%). This was true for differentially expressed genes detected in the Welle study at multiple significance thresholds (1%, 5%, 10% FDR). We also found that genes relating to sex-specific differences such as those located on the X and Y chromosomes were significantly different between young males and females in the meta-analysis dataset (**Table 2.4**). Genes up-regulated in female muscle include XIST which is responsible for inactivation of one copy of the X-chromosome in females [190] and GRB10 and oestrogen receptor 1 (ESR1) which are involved in hormone signalling [191]. Down-regulated genes include 8 Y-linked genes such as RPS4Y1, EIF1AY, and DDX3Y.

2.3.2 Differential gene expression in elderly human skeletal muscles

Having developed a high-quality integrated dataset we set to identify and functionally characterise differentially expressed genes between the two age groups. We reasoned that, because of the larger number of samples in the integrated dataset, our analysis would be more effective than others previously reported based on the individual studies.

We identified 1549 genes up-regulated and 1930 genes down-regulated in old human muscles at a high degree of confidence (FDR < 1%). Functional analysis of the differentially expressed genes

A

Chr.	Genes
Y	8
X	4
1	4
10	4
8	3
15	2
17	2
6	2
7	2
9	2
11	1
12	1
2	1
21	1
4	1

B

Higher in young female	
Gene	Chromosome
EIF1AX	X
KDM6A	X
XIST	X
MMD	17
HTRA1	10
PDLIM1	10
C1QA	1
EIF1AXP1	1
LPL	8
HMGCS2	1
GRB10	7

C

Lower in young female	
Gene	Chromosome
RPS4Y1	Y
EIF1AY	Y
DDX3Y	Y
KDM5D	Y
USP9Y	Y
NCRNA00185	Y
CYorf15B	Y
CD24	Y
TPD52	8
DAAM2	6
ALDH1A1	9
CDC37L1	9
MAPK6	15
WWP1	8
GPD1	12
ZBED1	X
IPW	15
CTNNBIP1	1
NRIP1	21
PTPN20A	10
PTPN20B	10
ARSJ	4
RCAN2	6
MMADHC	2
FDXR	17
LMO2	11
PGAM2	7

Table 2.4 – Differentially expressed genes between young males and females in the meta-analysis data

38 genes were detected as differentially expressed between young male and female muscle at 1% FDR. Table A shows the sum of genes from each chromosome shows X and Y linked genes are the most prevalent. Table B shows genes highly expressed in female muscle. Table C shows genes under expressed in female muscle.

revealed significantly enriched functional terms (**Table 2.5**). Briefly, the down-regulated genes were enriched in functions related to oxidative metabolism and mitochondrial biogenesis such as *oxidative phosphorylation*, *TCA cycle*, *mitochondrial ribosome*, *pyruvate metabolic process* and *protein targeting in mitochondrion*. The up-regulated genes were enriched in terms such as *RNA Splicing*, *cytoskeleton organisation*, *contractile fibre*, *chromatin modification* and *response to DNA damage stimulus*.

Down-regulated in elderly muscle

Annotation	Term	Count	FDR
CC	Mitochondrion	314	3.35E-63
KEGG	Oxidative Phosphorylation	63	5.30E-19
KEGG	TCA Cycle	22	3.3E-10
CC	Mitochondrial Ribosome	23	3.92E-08
BP	Pyruvate metabolic process	19	2.5E-05
BP	Glucose metabolic process	39	1.56E-04
BP	Protein targeting in mitochondrion	13	1.9E-02

Up-regulated in elderly muscle

Annotation	Term	Count	FDR
BP	RNA Processing	122	3.01E-17
BP	RNA Splicing	75	3.32E-14
CC	Contractile Fibre	28	8.43E-05
BP	Intracellular transport	102	7.06E-05
MF	Cytoskeletal protein binding	80	1.81E-04
BP	Ribonucleoprotein complex biogenesis	39	3.44E-04
BP	Cytoskeleton organization	68	3.9E-03
BP	Response to DNA damage stimulus	59	7.0E-03
BP	Chomatin modification	44	2.7E-02

Table 2.5 – Functional analysis of genes differentially expressed in skeletal muscle of elderly individuals

Gene Ontology categories: CC – cellular compartment, BP – biological process, MF – molecular function, KEGG – pathway within the KEGG database.

In order to test whether our approach could detect novel age related functional processes, we compared the meta-analysis with a re-analysis of the independent Melov study performed by Melov et al. The analysis of the Melov dataset identified a similar number of differentially expressed genes between skeletal muscle of young and elderly people (1470 genes up-regulated and 1454 genes down-regulated, FDR < 1%). There was a highly significant overlap between the genes identified in the meta-analysis dataset (32% of up-regulated genes and 43% of down-regulated genes in the Melov dataset, **Figure 2.5**).

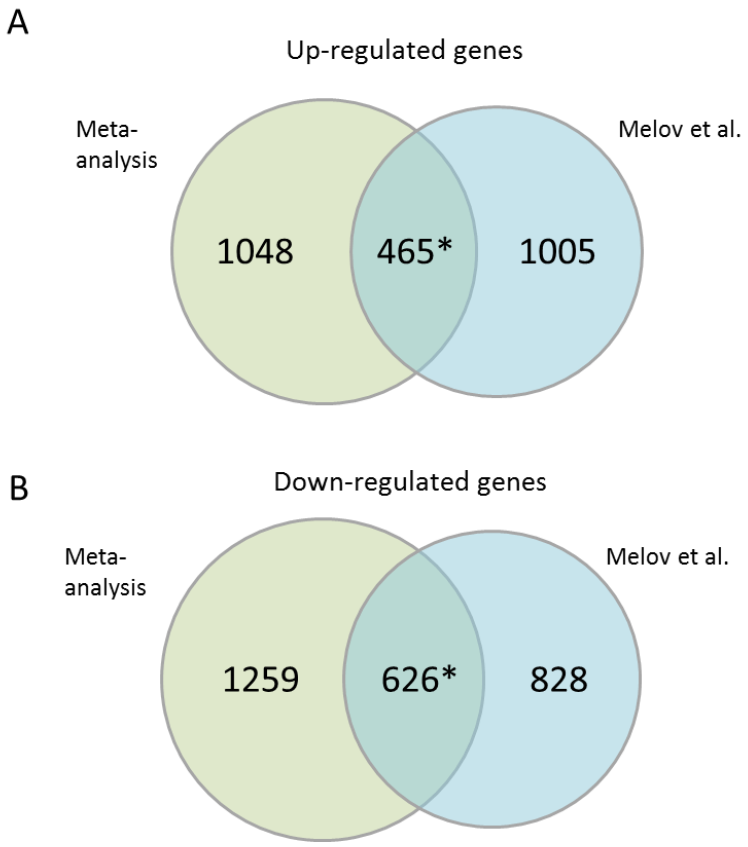

Figure 2.5 – The gene level overlaps between the differentially expressed genes identified by the Melov study and the meta-analysis.

*The overlap in both cases is highly significant. Panel A – p value: $3.26e^{-110}$. Panel B - p-value $5.79e^{-188}$

We then performed a more detailed functional analysis of the shared and unique differentially expressed genes in each dataset (**Table 2.6, Table 2.7**). This comparison revealed that both analyses were characterised by an age related down-regulation of genes involved in energy metabolism and general mitochondrial function. This includes genes involved in *oxidative phosphorylation*, carbohydrate metabolism such as the *TCA cycle* and *glycolysis*, components of the *mitochondrial ribosome* and genes involved in *mitochondrial transport*, *fatty acid oxidation* and *cell redox homeostasis*. Functional terms enriched in the common up-regulated genes include *contractile fibre*, *regulators of apoptosis*, components of *RNA processing* and *RNA splicing* pathways, components of the *extracellular matrix* and *ribonucleoprotein complex biogenesis*.

Intersection			
category	**term**	**count**	**Fdr**
CC	mitochondrion	214	3.38E-102
KEGG	Oxidative phosphorylation	54	8.03E-33
KEGG	TCA cycle	18	5.58E-13
CC	mitochondrial ribosome	19	9.76E-13
BP	cofactor biosynthetic process	17	3.21E-05
BP	mitochondrial transport	13	3.94E-04
KEGG	Glycolysis / Gluconeogenesis	12	0.0051096
CC	peroxisome	14	0.0014425
BP	Cell redox homeostasis	9	0.055711
BP	Fatty acid oxidation	7	0.072411
Meta-analysis only			
category	**term**	**count**	**Fdr**
CC	plasma membrane part	210	0.002169
BP	ubiquitin-dependent protein catabolic process	38	0.016612
BP	positive regulation of lipase activity	16	0.072418
Melov only			
category	**term**	**count**	**Fdr**
CC	mitochondrion	147	1.21E-35
CC	mitochondrial ribosome	11	8.69E-04
KEGG	Oxidative phosphorylation	17	0.023771

Table 2.6 – Down-regulated functional terms in common between the meta-analysis and the Melov study

At the threshold used to define differentially expressed genes in our analysis, several functions were enriched in either the meta-analysis or Melov data only. In the meta-analysis, this included up-regulation of genes related to RNA processing (*RNA binding*, *RNA splicing*), *intracellular transport* and *negative regulation of gene expression*. Terms enriched in down-regulated genes specific to the meta-analysis were related to ubiquitin-mediated proteolysis and lipase activity. Functional terms specific to the genes up-regulated in the Melov data include *regulation of transcription*, *cytoskeletal protein binding* and *telomere maintenance*. The functions specific to genes down-regulated in the Melov dataset represent a further set of mitochondria related functions. We conclude that despite less than a 50% overlap in the genes detected by both studies, the functional profiles of elderly muscle in both studies is remarkably similar. In addition, the meta-analysis was able to capture

Intersection			
category	**term**	**count**	**Fdr**
CC	nuclear lumen	92	7.57E-13
BP	RNA processing	45	1.15E-06
BP	RNA splicing	29	1.05E-05
CC	contractile fiber	15	1.60E-04
BP	cytoskeleton organization	31	0.003562
BP	regulation of apoptosis	43	0.027034
CC	extracellular matrix	20	0.031666
BP	ribonucleoprotein complex biogenesis	15	0.071484
BP	negative regulation of gene expression	29	0.072633
MF	helicase activity	13	0.093197
Meta-analysis only			
category	**term**	**count**	**Fdr**
CC	nuclear lumen	173	6.02E-19
MF	RNA binding	102	6.18E-13
BP	RNA splicing	46	6.75E-06
BP	intracellular transport	70	0.006925
BP	negative regulation of gene expression	54	0.048531
Melov only			
category	**term**	**count**	**Fdr**
BP	regulation of transcription	208	5.10E-05
MF	cytoskeletal protein binding	51	0.019876
BP	telomere maintenance	9	0.096935

Table 2.7 – Up-regulated functional terms in common between the meta-analysis and the Melov study.

additional functional enrichment not identified by analysis of the Melov data at an identical statistical threshold.

2.3.3 Inference of gene regulatory networks representing young and elderly skeletal muscles

Using our meta-analysis dataset and the well-validated network inference platform ARACNE, we constructed mutual information based transcriptional networks for both young and elderly human skeletal muscle. This allowed us to investigate the hypothesis that core molecular networks underlying skeletal muscle physiology change their structure as age progresses, potentially leading to

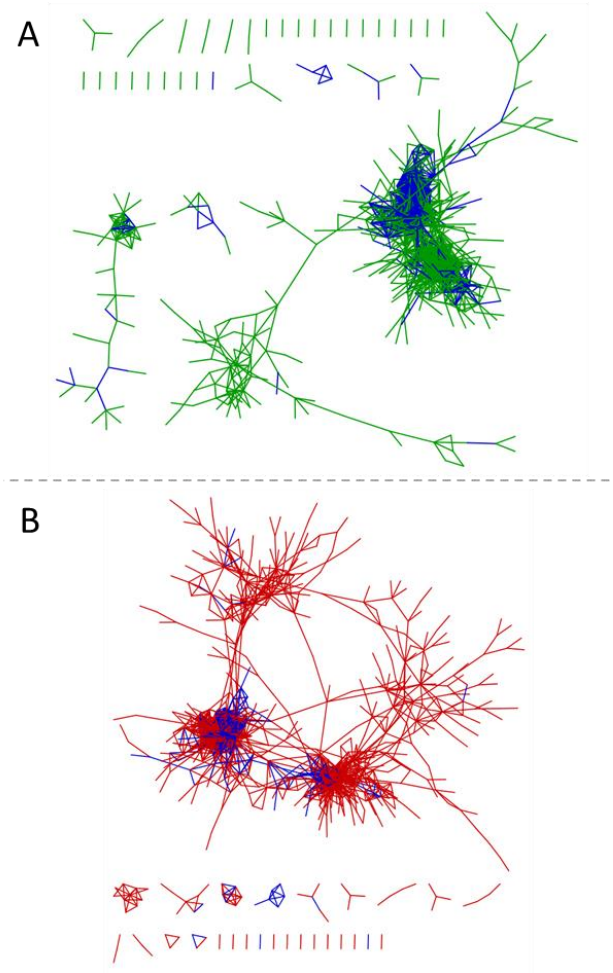

Figure 2.6 – Graphical representation of the young and elderly muscle networks.

Panel A and B show the young and elderly networks respectively organised using a force directed layout. The edges have been colour coded for visual accuracy (red = edge in elderly network, green = edge in young network, blue = edge common to both networks).

age related muscle dysfunction. The networks representing young and elderly muscle contain 505 and 674 nodes and 2203 and 3107 edges respectively (**Figure 2.6**). These networks, which represent only highly significant interactions, were significantly different with only 312 nodes and 1064 edges shared between the two age groups.

In order to visualise and compare the two networks we generated the union of the young and elderly muscle networks and visualised the resulting network using a force driven layout (**Figure 2.7A**). The union of the two networks consists of 867 nodes (genes) and 4246 edges.

2.3.4 Community analysis of muscle transcriptional networks reveals functionally enriched age-specific modules

Visual inspection of the integrated network led us to formulate the hypothesis that there were very distinct age specific network modules. We tested this hypothesis by applying the network community detection algorithm GLay [138], a procedure that automatically identifies clusters of nodes (modules) with a high interconnectivity. GLay identified 30 distinct network modules, seven of which consisted of more than 30 genes, representing 73% of the total number of nodes (**Figure 2.7B** and **Table 2.8**). We found that with the exception of module M1 that contained the largest number of age independent edges, all modules were characterised by a high frequency of age specific edges (up to 90%, modules M2 - M7) (**Figure 2.8B**, **Table 2.8**). We found that the connectivity between the modules was low, with the exception of the 3 centrally positioned modules M1, M2 and M3 (**Figure 2.8A**). We then tested the hypothesis that network modules, defined on the basis of connectivity, may also represent specific biological functions. Functional analysis of genes in each module indeed confirmed that this hypothesis was correct (**Table 2.9**).

Module M1 represents a large number of ribosome related genes such as large and small cytosolic ribosomal subunits and eukaryotic initiation factors (EIF3F, EIFG, EIF3H, EIF3L, EIF1), as well as a number of muscle fibre constituents (such as TNNC1, TNNC2, ACTA1, MYH2) and glycolysis/gluconeogenesis related genes (PFKM, ENO3, ALDOA, GAPDH, PGM1). The age-specific properties of this module suggest that both age groups possess many of these connections. **Module M2** is composed of connections predominantly present in young muscle only (74%) and contains 66% (39/59) of the oxidative phosphorylation genes present in the network as well as components of the mitochondrial ribosome. Module M2 is highly connected to module M1 (**Figure 2.8A**). The 112 connections between module M1 and M2 are characterised by two distinct subsets of connections

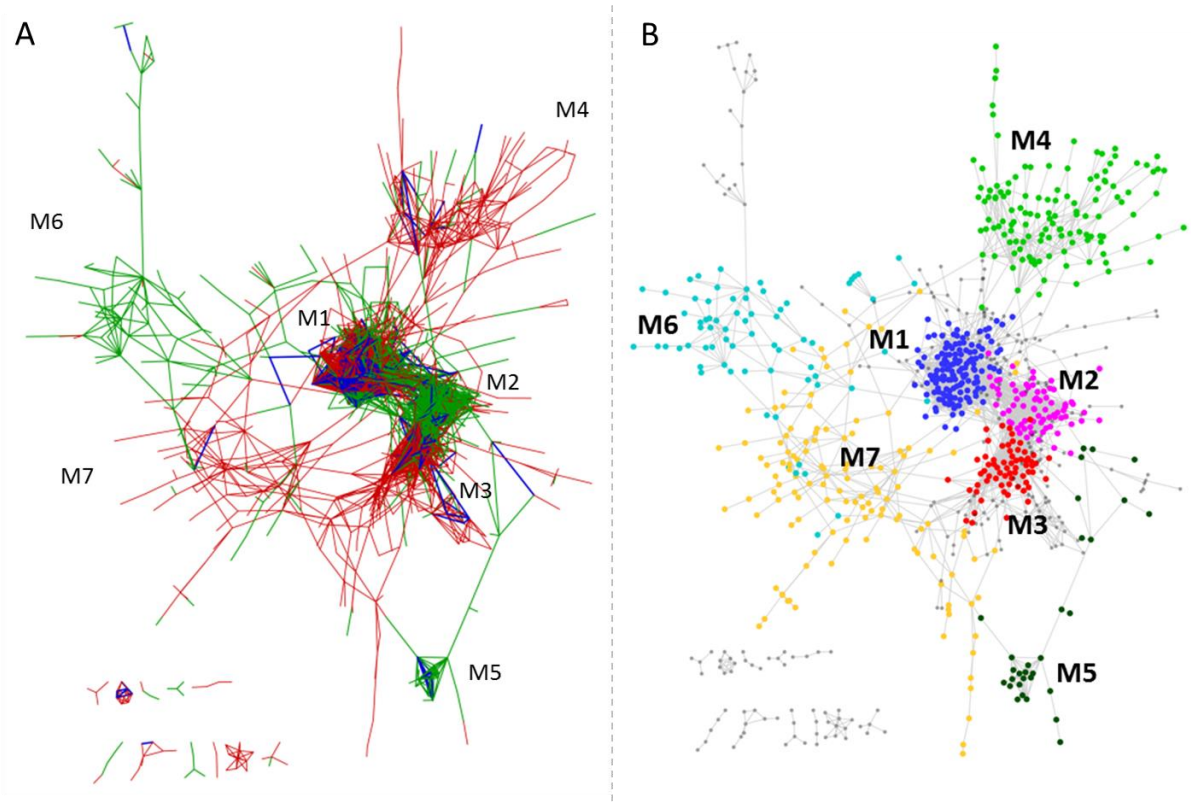

Figure 2.7 – The union of the young and elderly networks

Panel A shows the union of the young and elderly networks, revealing age specific sub-networks. Network edges have been colour coded according to the age group of origin as in Figure 2.6. Panel B shows that the results of the GLay modularisation closely match the visually identifiable sub-networks within panel A. Modules are labelled M1-M7 and labels have been mapped to Panel A. The modules in panel B are colour coded for visual effect only. Panel A and B have been organised using a force-driven layout.

		Edges – Age Groups		
Cluster	**Nodes**	**Young**	**Shared**	**Elderly**
M1	137	343 (15%)	896 (40%)	996 (45%)
M2	74	266 (74%)	32 (9%)	61 (17%)
M3	66	39 (11%)	48 (14%	264 (75%)
M4	128	20 (8%)	8 (3%)	211 (89%)
M5	31	52 (78%)	11 (16%)	4 (6%)
M6	69	89 (90%)	10 (10%)	0 (0%)
M7	126	18 (11%)	1 (<1%)	149 (89%)
M1 ↔ M2	-	48 (43%)	10 (16%)	46 (41%)
M2 ↔ M3	-	73 (71%)	10 (10%)	19 (19%)

Table 2.8 – Properties of the GLay modules

The age group of origin of the edges connecting the 3 central network modules (M1-3) is shown in the last 3 rows of the table.

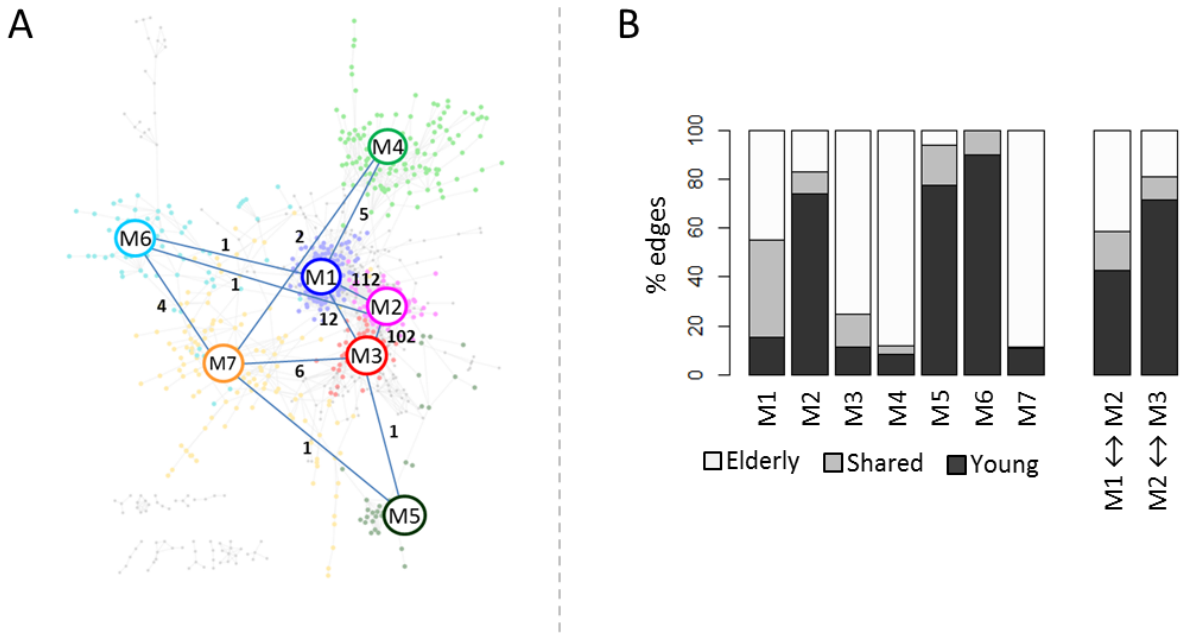

Figure 2.8 – Modules are characterised by age specific edges and inter-module connections

Panel A shows the number of network edges connecting the modules. This shows the low connectivity between modules with the exception of M1 & M2 (112 edges) and M2 & M3 (102 edges). Panel B shows the disparity of age-specific and shared edges in each GLay module and the inter-module connections

present in young and elderly respectively, with a smaller number of shared connections (**Table 2.8, Figure 2.8B**). The 102 connections between M2 and M3 are mostly found in young muscle (71%). **Module M3** consists of connections present primarily in elderly muscle (75%) and contains TCA cycle, oxidative phosphorylation, and pyruvate metabolism related genes. 12/14 (85.7%) of the TCA cycle genes present in the network are found in module M3, and the enrichment is highly significant (FDR < 2.0e-15). The connectivity between module M3 and module M2 is highly specific for young muscle, thus we have identified module M3 as a component of energy metabolism that is disconnected to other components of oxidative phosphorylation, translation and muscle fibre structural components

Module M1

Term	Count	FDR
Ribosome	70	1.5E-114
ribosome biogenesis	15	1.3E-9
striated muscle contraction	11	1.6E-9
translational initiation	7	1.7E-4
generation of precursor metabolites and energy	10	5.5E-2

Module M2

Term	Count	FDR
Mitochondrion	61	1.6E-53
Oxidative phosphorylation	39	2.5E-50
NADH dehydrogenase activity	17	3.6E-27
Proton-transporting ATP synthase complex	8	7.4E-11
Cytochrome c oxidase activity	8	2.2E-9
Ubiquinol-cytochrome-c reductase activity	6	4.3E-9
Mitochondrial ribosome	5	9.2E-3

Module M3

Term	Count	FDR
Mitochondrion	46	2.7E-32
TCA Cycle	12	2.0E-15
Oxidative phosphorylation	15	1.0E-12
NADH dehydrogenase activity	5	7.1E-4
Pyruvate metabolism	5	1.3E-3
Proton-transporting ATP synthase complex	3	3.7E-2

Module M4

Term	Count	FDR
Extracellular matrix	34	2.8E-23
Collagen	11	9.8E-12
Cell adhesion	23	4.4E-6
Calcium ion binding	26	1.7E-6
Blood vessel development	13	6.2E-5
Inflammatory response	12	3.0E-3
Glycosaminoglycan binding	8	3.6E-3
Plasma membrane	51	6.7E-3
Wound healing	9	6.8E-3
Adherens junction	7	2.6E-2

Module M5

Term	Count	FDR
Oxidoreductases	6	4.4E-2
Aldehyde dehydrogenase	3	2.1E-2

Module M6

Term	Count	FDR
Proteolysis	12	8.8E-2

Module M7

Term	Count	FDR
Glycogen metabolic process	6	4.7E-3
GTPase activity	9	7.0E-2

Table 2.9 – Functional analysis of each network module reveals distinct functional profiles

in elderly individuals. The other modules are enriched in other important pathways within skeletal muscle. **Module M7** is enriched with genes related to glycogen metabolism (such as AGL, PHKB, PPP1R2, PPP1R3A, PPP1R3C) and GTPase activity (such as RHOA, ARF1) two processes which have recently been linked in human cells [192]. **Module M4** is enriched with inflammatory components

(such as CD46, C1R, C1S, and FN1), extracellular matrix remodelling (such as TIMP1, DCN, and MMP2), collagens, cell adhesion and blood vessel development (such as EPAS1, NRP1). **Module M6** is enriched with genes related to proteolysis. **Module M5** is enriched with oxidoreductases and aldehyde dehydrogenases.

Analysis of networks created at a lower threshold (MI = 0.2, p-value < 10e-7) was consistent with the finding that the union of the young and elderly networks contains distinct network modules. At this threshold the union of the young and elderly networks contained 4638 nodes and 17950 edges. GLay clustering identified 567 modules within this network, of which 14 had more than 30 genes. We mapped the GLay clusters from the high-threshold network onto the modules generated from the low-threshold network, and found that each module remained clearly identifiable (**Figure 2.9**).

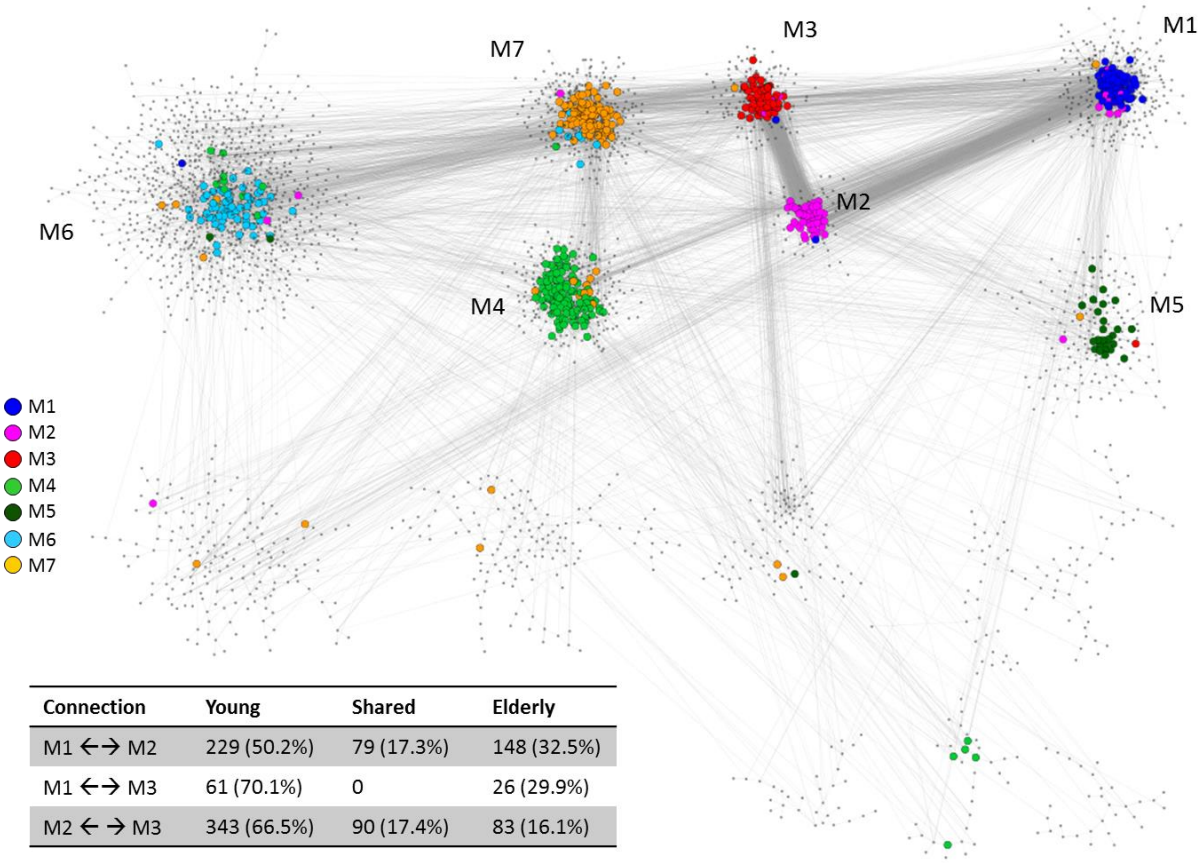

Connection	Young	Shared	Elderly
M1 ←→ M2	229 (50.2%)	79 (17.3%)	148 (32.5%)
M1 ←→ M3	61 (70.1%)	0	26 (29.9%)
M2 ← → M3	343 (66.5%)	90 (17.4%)	83 (16.1%)

Figure 2.9 – GLay modularisation of a lower threshold network recapitulates the network modules.

This figure shows the results of GLay clustering on a lower threshold network. Each GLay cluster has been separated and represented as a sub-network. Network module labels correspond to the modules in the high threshold network and the nodes are colour coded to match. The connections shown in the inset table are between genes in modules M1-3 at the lower threshold

The connections between genes comprising the network modules were consistent with the high-threshold network. Inter module connectivity between genes within module M1 and module M2 was split between edges significant in young (50.2%), shared (17.3%) and elderly (32.5%), this does represents a small shift towards connections in young between these modules. The connectivity between genes in M2 and M3 remained predominantly significant in young muscle (66.5%). There was an increase in the number of connections between module M1 and M3, and these connections were also specific to the young networks (70.1%). This shows that at a lower threshold the age-specific properties of connections between network modules containing translation and energy metabolism genes are conserved.

2.3.5 Mapping age dependent differential gene expression on the integrated transcriptional network

Having shown that co-expression networks representing young and elderly skeletal muscle are very divergent with age we set to assess the relationship between co-transcription and levels of mRNA expression. We therefore mapped on to the network modules genes differentially expressed between young and elderly muscle (**Figure 2.10A**). Strikingly, 51.6% (306) of the total network nodes mapped to the 3479 genes differentially regulated in the two age groups. Using Gene Set Enrichment Analysis, we found that modules M2, M3 and M7 were enriched with down-regulated genes while modules M1, M4 and M6 were enriched with up-regulated genes (FDR < 0.1%). This shows us that the changes in gene-gene associations with age that have been identified by the network are accompanied by coordinated changes in gene expression between young and elderly muscle relating to specific molecular functions. More in depth functional analysis of the correspondence between changes in the mRNA levels and gene co-expression in the network modules revealed that genes up-regulated in elderly muscle in **module M1** include 12 ribosomal subunits, 5 components of muscle structure (TCAP, MYBPC1, TNNT1, TNNC2, MYL2), 2 translation

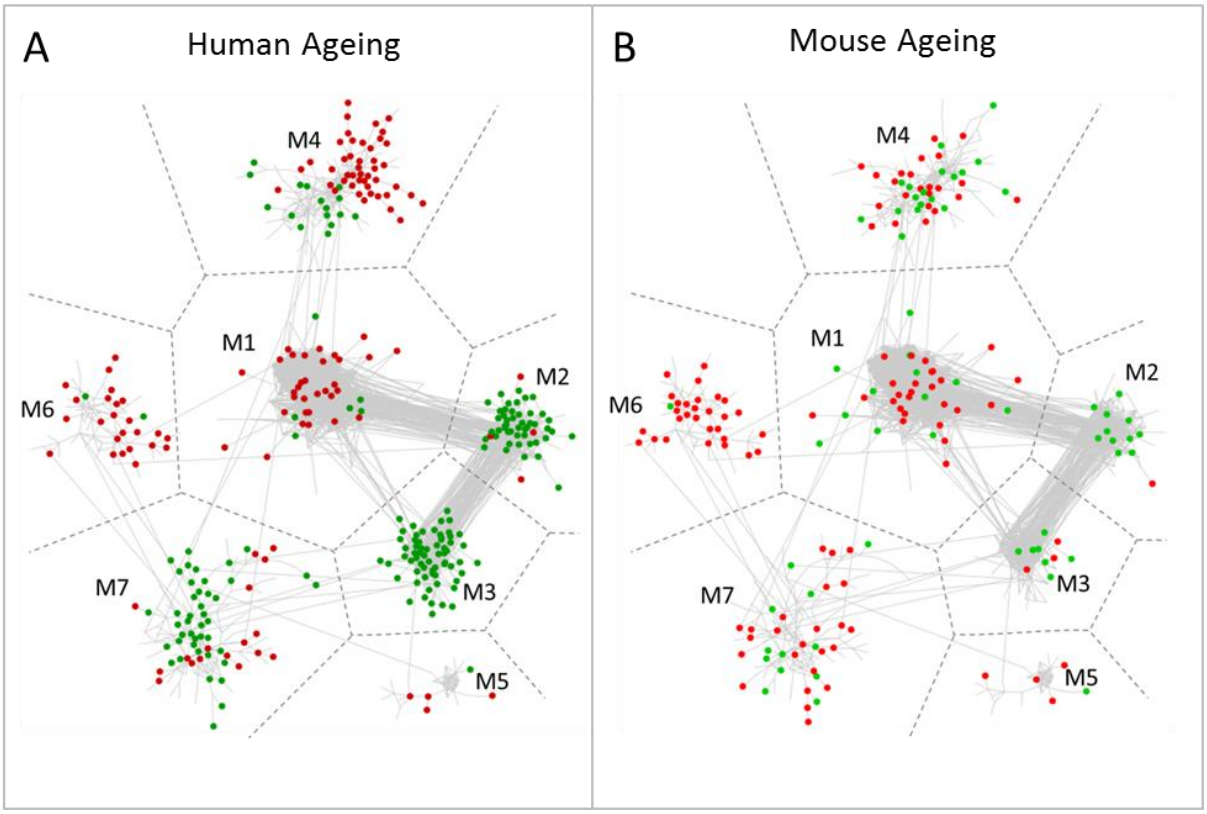

Figure 2.10 – Network modules are enriched with genes differentially expressed with age

Panel A and B shows the up (red) and down (green) regulated genes in elderly human and mouse muscle respectively mapped to the network modules. The network modules have been represented as distinct sub-networks to aid distinction of enriched clusters.

initiation factors (EIF3C, EIF3G), 3 genes related to proteolysis including proteasome subunits (PSMB1, PSMD4) and MYOZ1. Down-regulated genes in **module M1** include 4 ribosomal subunits, the translation initiation factor EIF1, and PARK7 which has been shown to be part of the oxidative stress response in various cell types [193]. In **module M2** the up-regulated genes include 2 mitochondrial ribosomal subunits and the mitochondrial small molecule transporter VDAC 3. The down-regulated genes include 31 subunits of oxidative phosphorylation enzymes, 2 TCA cycle enzymes and 2 mitochondrial ribosomal subunits. There are no up-regulated genes in **module M3**. The down-regulated genes include 12 enzymes in the TCA cycle, 15 subunits of oxidative phosphorylation enzymes, 3 glycolysis enzymes, mitochondrial protein import (MTX2), lipid transport (APOO) and small molecule transporters SLC25A4 (ATP), SLC25A3 (phosphate) and VDAC2. In **module**

M7 the up-regulated genes include 2 cell adhesion molecules (CLDN5, PECAM1) and 3 genes related to protein transport (GDI1, USO1, ACTN4). The down-regulated genes in **module M7** include 4 enzymes involved in glycogen metabolism (PHKA1, PHKB, PPP1R3A, PPP1R3C), 3 genes related to regulation of translation (PAIP1, SELT, EIF4A2), skeletal muscle differentiation (RHOA, NOTCH3), genes related to mitochondrial functions such as VDAC1 (transport), HSPA9 (stress response), COX11 (enzyme assembly), UCP3 (fatty acid export) and MFF (mitochondrial fission). The genes differentially expressed between young and elderly muscle that can be found in **module M4** represent tissue remodelling and immune processes. Up-regulated genes include 3 genes related to blood vessel development (EPAS1, NRP1, IGF1). Down-regulated genes in **module M4** include 14 genes related to extracellular matrix processes (including TIMP1, NOTCH2), 4 genes related to the activation of immune response and 6 genes related to cell adhesion. The up-regulated genes in **module M6** include 4 genes involved in RNA splicing (YTHDC1, LUC7L3, HNRNPA3, RBM39) and 3 cytoskeleton related genes (AKAP9, CBX1, DMD).

Interestingly, the analysis of a gene expression dataset representing ageing in mice revealed a common transcriptional signature of ageing in mice and humans (**Figure 2.11**). We identified 1641 genes down-regulated and 1431 genes up-regulated in elderly (25 months) versus young (5 months) mice (FDR < 5%). The overlap between genes up-regulated in elderly humans and mice was significant ($p < 0.05$, 15% of genes differentially expressed in aged mice). Functional analysis of the common up-regulated genes revealed enrichment of genes related to *cytoskeleton, transcriptional regulation, cell death, RNA processing, GTPase signalling* and *cell cycle*. The overlap between the genes down-regulated in elderly humans and mice was not significant (12% of genes differentially expressed in mice). However functional analysis reveals a common signature related to mitochondrial function that is down-regulated in both humans and mice. This includes

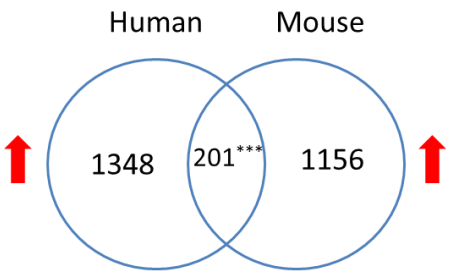

Category	Term	Count	FDR
CC	GO:0005856~cytoskeleton	38	6.65E-05
CC	GO:0031981~nuclear lumen	44	1.28E-06
BP	GO:0045449~regulation of transcription	54	0.033453
CC	GO:0015630~microtubule cytoskeleton	22	7.90E-05
BP	GO:0008219~cell death	23	0.039622
BP	GO:0000122~negative regulation of transcription from RNA polymerase II promoter	11	0.094944
BP	GO:0006396~RNA processing	17	0.084689
KEGG	hsa04540:Gap junction	7	0.074587
BP	GO:0007264~small GTPase mediated signal transduction	13	0.042386
CC	GO:0043005~neuron projection	13	0.020248
BP	GO:0007265~Ras protein signal transduction	7	0.089028
BP	GO:0000086~G2/M transition of mitotic cell cycle	4	0.088896

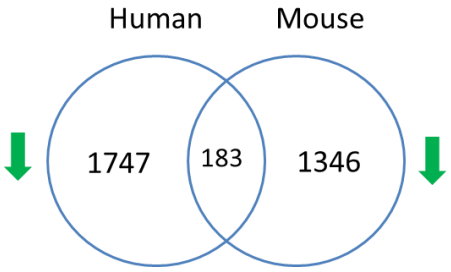

Category	Term	Count	FDR
CC	GO:0005739~mitochondrion	40	1.36E-08
BP	GO:0006091~generation of precursor metabolites and energy	21	1.00E-06
KEGG	hsa00190:Oxidative phosphorylation	12	2.66E-04
BP	GO:0006006~glucose metabolic process	9	0.05999
BP	GO:0006090~pyruvate metabolic process	6	0.02154

Figure 2.11 – Common transcriptional signature of age in humans and mice

This figure shows the gene level overlap between a transcriptional signature of mouse ageing and the human ageing signature from the meta-analysis. The functional analysis was done using only the overlapping genes. A comparison was performed for up-regulated genes (red arrows) and down-regulated genes (green arrows).

components of *oxidative phosphorylation, pyruvate metabolism* and *glucose metabolism*. This shows that despite a low statistical power in the aged mice study (n = 4) compared to the human meta-analysis, a common transcriptional signature of ageing muscle can be detected. We mapped the differentially expressed genes in elderly mice to the network modules, then using GSEA we tested if the genes from the modules in the human muscle network are enriched within the differentially expressed genes in elderly skeletal muscle of mice in the same way they are for human (**Figure 2.10B**). We found that **module M2** is significantly enriched with down-regulated genes in mouse and human. **Module M1 and M6** are enriched in genes up-regulated in mouse and human, however **Module M7** is enriched in genes up-regulated in the mouse and down-regulated in human. This shows that the functional modules within the network representing energy metabolism, translation, muscle fibre constituents and proteolysis contain genes that are differentially expressed in both

human and mouse skeletal muscle. However the modules relating to glycogen metabolism, GTPase signalling and extracellular matrix components are divergent between mice and human in terms of the changes in expression with ageing.

2.3.6 Transcriptional response to physical exercise affects specific network modules

We have shown that the transcriptional effects of ageing affect both the level of mRNA and the ability to co-ordinately regulate groups of functionally linked genes. Here we perform a similar analysis to test the hypothesis that response to exercise will also affect specific modules in the integrated network.

We have used the publically available Melov et al microarray dataset [145] created from *vastus lateralis* skeletal muscle biopsies from elderly individuals who undertook a 6 month endurance training program. Melov et al. chose to control the family-wise error rate (FWER) to correct for multiple comparisons, a method that was appropriate for their study. This provides a low probability of any false positives amongst results at the expense of statistical power [194]. By using SAM, which controls the FDR, we were able to identify a larger selection of differentially expressed genes while maintaining only a 1% false positive selection. There were 1248 genes up-regulated in the trained individuals and 1507 genes down-regulated. We have used a gene ontology analysis to identify functional terms significantly enriched within the up and down-regulated genes (FDR < 10%) (**Table 2.10**). Briefly, the up-regulated genes are enriched with terms such as *localisation to mitochondria*, *mitochondrial and cytosolic ribosomal components*, *oxidative phosphorylation*, *RNA splicing*, *protein*

Up-regulated in response to training

Annotation	Term	Count	FDR
CC	Mitochondrion	136	2.8E-25
BP	Translation (mitochondrial + cytosolic)	64	1.3E-18
KEGG	Oxidative Phosphorylation	41	5.0E-15
BP	RNA Splicing	33	9.2E-4
BP	Protein complex assembly	45	8.4E-3
BP	RNA elongation	12	3.3E-3
BP	Pyruvate metabolic process	9	6.2E-2

Down-regulated in response to training

Annotation	Term	Count	FDR
BP	Protein transport	81	3.6E-5
CC	Contractile Fibre	23	7.3E-6
MF	Protein serine/threonine kinase activity	48	5.1E-3
BP	Ubiquitin-dependant protein catabolic process	33	7.2E-4
BP	Response to hormone stimulus	36	5.3E-2
BP	Cell cycle	70	5.6E-3
BP	G1/S Phase Transition	13	3.7E-3
BP	Muscle cell differentiation	23	2.7E-4
BP	Cellular response to stress	58	1.3E-3

Table 2.10 – Functional analysis of genes responding to endurance training in skeletal muscle

complex assembly, *RNA elongation* and *pyruvate metabolism*. The down-regulated terms in response to training include *protein transport*, *contractile fibres*, *protein kinase activity*, *protein catabolism*, *response to hormone stimulus*, *cell cycle*, *muscle cell differentiation* and *cellular response to stress*. We have mapped the differentially expressed genes in response to training on to the human muscle network (**Figure 2.12**). There is a striking difference between the transcriptional signature of elderly muscle and that of exercise training.

Whereas module M2 (oxidative phosphorylation) and M3 (TCA cycle) contain many genes that are down-regulated in elderly muscle, only module M2 was significantly enriched in genes up-regulated in response to training (FDR < 0.1%) while module M3 contained few genes. Module M6 (proteolysis) is significantly enriched in genes up-regulated in elderly muscle and down-regulated in response to

training (FDR < 0.1%). These results suggest that endurance training targets networks of genes that are more correlated in young muscle, and that a sub-network of energy metabolism genes in module M3 is refractory to induction by training despite being highly correlated in elderly muscle.

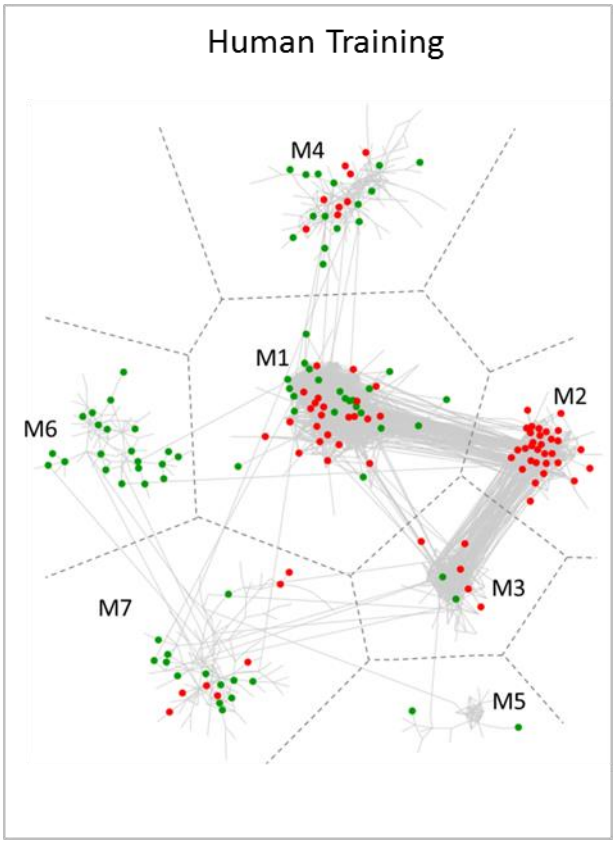

Figure 2.12- Specific network modules are enriched with genes responsive to training

Up (red) and down (green) regulated genes in response to training are colour coded.

2.4 Discussion

2.4.1 The transcriptional signature of ageing skeletal muscle

We have conducted the first meta-analysis of the transcriptional state of human skeletal muscle using a data integration approach. We show that there is a strong functional overlap between the transcriptional changes in ageing muscle in the meta-analysis and an independent study.

Our results are consistent with previous studies analysing transcriptional differences between young and elderly muscle, and suggest a broad range of mitochondrial dysfunction in ageing muscle, suggested to be a driving force of ageing by the mitochondrial theory of ageing [58]. We see a down-regulation of electron transport chain enzymes and transcription factors controlling mitochondrial biogenesis such as PGC-1α and TFAM. Interestingly, the intermediate step in the PGC-1α-TFAM pathway, nuclear respiratory factor 1 (NRF1), is up-regulated in elderly muscle. The increase in NRF1 expression could be linked to the increased inflammatory status of elderly muscle [195] [196], as NRF1 overexpression has been shown to increase expression of cytokines [197]. We see a down-regulation of genes related to anti-oxidant pathways such as glutaredoxin 2 (GLRX2), thioredoxin reductase (TXNRD1) and superoxide dismutase (SOD1), suggesting a decrease in the ability to respond to ROS via redox signalling and conversion of superoxides to oxygen and H_2O_2. SOD1 deficient mice have recently been shown to have high levels of oxidative damage and accelerated sarcopenia [198]. The meta-analysis identified 38 genes related to ubiquitin-mediated protein catabolism that were down-regulated in elderly muscle. These include 11 ubiquitin specific peptidases and 7 proteasomal components (5 subunits of the 26S proteasome). This supports previous findings that the rate of protein turnover is decreased with age [199] and suggests that lower expression of these genes could play a role.

Recent work by Timmons et al has shown that when levels of physical activity are normalized, the transcriptional signatures of ageing muscle are not consistent between their data and existing studies. They show that the overlap between the Melov ageing study [145] and their own (and very

likely our own data) is negligible. They suggest that the decline in expression of mitochondrial genes is a result of reduced physical activity and not the ageing process specifically. Interestingly, inhibition of MYC was predicted to be upstream of the age-related changes in expression. MYC mRNA is up-regulated in elderly muscle of our meta-analysis. MYC is a known oncogene involved in control of transcription and cellular senescence through regulation of p16 [200] and CDK2 [201]. Further work utilizing large clinical studies are required to validate these findings and investigate the different role of transcription factors in ageing and muscle disuse atrophy.

Skeletal muscle mass declines with age in humans, due to an increase in skeletal muscle atrophy. Atrophy related genes such as Atrogin-1 and Murf1 are thought to be controlled at the transcriptional level during ageing, however their exact role remains unclear [49] [50]. Modulation of Atrogin 1 in cardiomyocytes has recently been shown to alter the expression of genes related to cell death and inflammation, providing an interesting new hint to additional roles of atrophy related genes [202]. Neither Atrogin 1 (FBXO32) nor Murf1 (TRIM63) were differentially expressed between young and elderly muscle in our meta-analysis. However, no data was available for the meta-analysis regarding muscle mass or basal protein turnover, making it difficult to draw any conclusions. The functional profile of the genes up-regulated in elderly muscle did contain a large number of genes linked to protein catabolism. This included 95 genes linked to proteolysis such as 10 ubiquitin specific peptidases, 7 components of the proteasome, Calpain 3 and the mitochondrial protease Lonp1. The detailed transcriptional changes in proteolytic pathways during ageing have not been elucidated. Our data suggests that a large number of genes involved in proteolysis are up-regulated in a heterogenous elderly population. The factors controlling these genes can be revealed with further study.

2.4.2 The construction of gene co-expression networks in young and elderly skeletal muscle

We have used the skeletal muscle meta-analysis dataset to generate gene expression networks for young and elderly skeletal muscle. We chose a high statistical threshold to define the connections

within in the network in order to achieve a very low probability of false positive connections. Using a network community detection method we have identified distinct sub-networks which are enriched with genes relating to key molecular functions in skeletal muscle. The network analysis reveals a link between expression of energy metabolism related genes and the translational machinery. The analysis shows that the expression of a core sub-network of ribosomal genes and muscle fibre constituents is linked to distinct modules of genes related to energy metabolism via a set of age dependent connections that are either altered or uncoupled in elderly muscle.

Our network analysis pipeline focused on the union of both the young and elderly muscle networks. However, it is important to note that the observation that elderly networks show a decoupling of a subset of metabolic genes is recapitulated in network modules generated from young and elderly muscle separately (**Figure 2.13**). These networks support the analysis of the union network. They show a decoupling of the translational machinery from a module comprised of oxidative metabolism genes in the elderly.

Interestingly, we found that the network modules related to energy metabolism are highly enriched in genes that are down-regulated with age. Thus the coordinate down-regulation of energy metabolism genes is associated with a shift in correlation from one subset of genes in the young which are highly correlated to the translational machinery to another subset in the elderly that are decoupled from the translational machinery. The young subset is highly enriched with electron transport chain components only, while the elderly subset is highly enriched in TCA cycle components. This suggests a change in regulatory mechanisms controlling expression of energy metabolism genes with age.

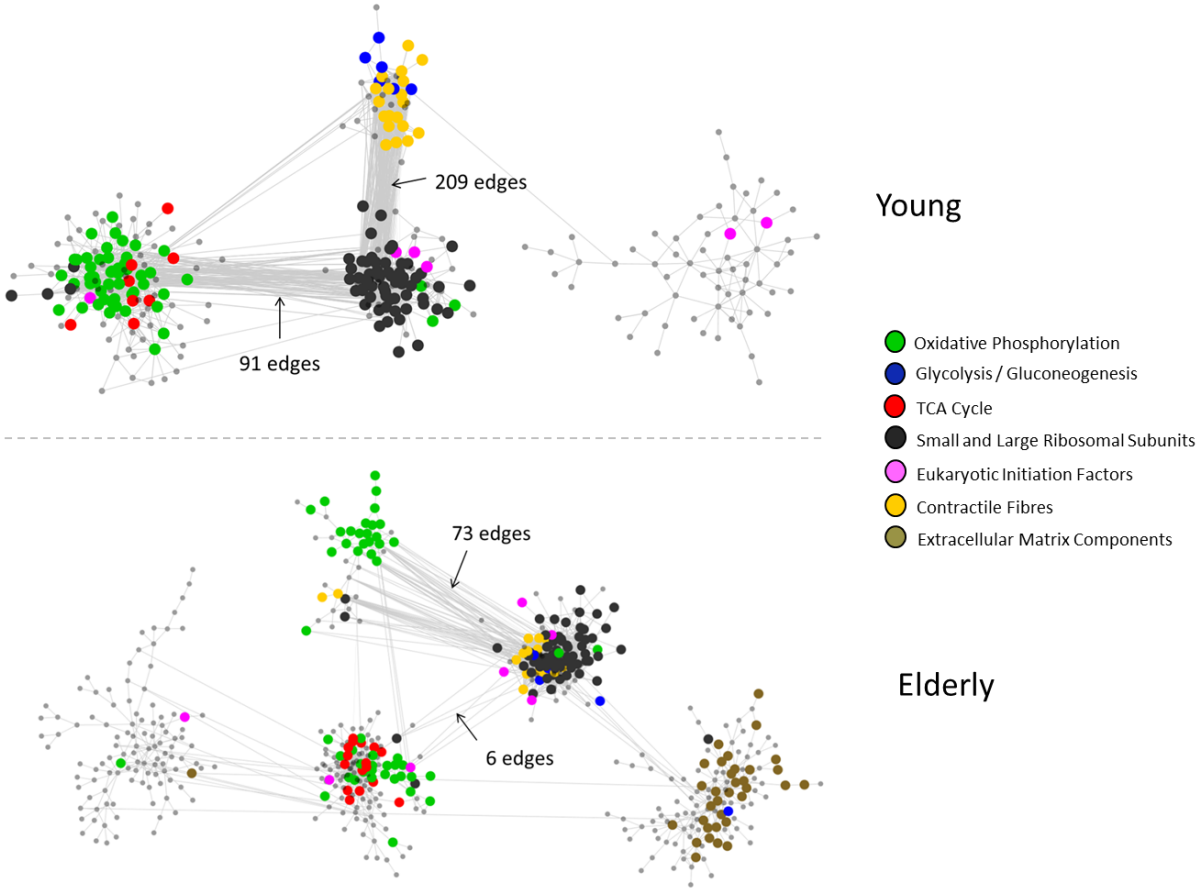

Figure 2.13 – Modularisation of separate young and elderly networks recapitulates the findings of the union network

GLay modules were identified in the young and elderly networks and represented as distinct sub-networks. Functional annotation of the genes within the networks has been colour coded. These networks show a clear separation of energy metabolism genes in the elderly networks, and a striking uncoupling of many oxidative phosphorylation and TCA cycle genes from ribosomal genes.

2.4.3 The expression of genes in distinct network modules responds to physical exercise

A key question surrounding skeletal muscle ageing is the relative contribution of muscle disuse to the ageing muscle phenotype. Skeletal muscle is sensitive to physical activity, with just one bout of exercise sufficient to induce adaptations [203] [204], albeit short-lived ones. Most studies do not control specifically for long term physical activity levels in subjects, and thus reported differences in young and elderly muscle could be attributed to a decrease in physical activity and not ageing *per se*. In muscles subjected to 5 weeks of unloading, there is a coordinate down-regulation of genes related to oxidative metabolism [205]. In contrast, exercise training induces the expression of mitochondrial

genes [145], increases mitochondrial biogenesis [206] and increases neuromuscular junction hypertrophy in animal models [207].

Level of physical activity was not a factor when selecting studies for inclusion into the meta-analysis, although we did not include recently trained individuals. Many of the samples integrated into the meta-analysis were therefore sedentary. The functional profile of elderly muscle we have identified could be attributed to the decrease in physical activity more likely to be seen in elderly individuals. We identified the genes that respond to six months of training in elderly individuals in the network. The most significant enrichment was in the electron transport chain components that are found in module M2, which are up-regulated in response to training. This leads to the interesting observation that resistance exercise in elderly people increases the expression of metabolic genes that are highly correlated in young muscle, and suggests the subset of metabolic genes in module M3 are more refractory to physical training. It could be potentially valuable to analyse in detail the networks surrounding these subsets of genes at a lower threshold, to identify potential regulatory mechanisms controlling their expression.

2.4.4 Control of translation and metabolism in response to cellular signaling

A key regulator of ribosome biogenesis and protein synthesis in response to multiple cellular signals such as nutrient availability [208], oxidative stress [209] and hypoxia [210] is the mTOR pathway. The mTOR pathway is also known to control mitochondrial oxidative metabolism through a PGC-1α dependent mechanism [75]. mTOR is a key regulator of ageing and age related diseases [211], however the many signaling pathways of mTOR are not completely understood. Further analysis of the skeletal muscle networks is needed, as they may allow us to identify potential regulatory mechanisms, either mTOR dependent or independent, that could explain the age related changes we have observed.

CHAPTER 3

EUKARYOTIC INITIATION FACTORS ARE POTENTIAL REGULATORS OF MUSCLE BIOENERGETICS AND REMODELLING

3.1 Introduction

In the previous chapter we have described how a meta-analysis approach to study transcriptional profiling in skeletal muscle can allow us to determine the underlying networks in young and elderly skeletal muscle. Ageing is known to be a highly heterogeneous process, with many genetic and environmental factors influencing the progressive decline in functionality of many cellular processes. By analysing networks at a very stringent statistical threshold we have revealed a network with distinct age-dependent modules. Functional analysis of these modules revealed a decoupling of energy metabolism and translation related genes accompanied by a coordinate down-regulation of energy metabolism genes in elderly muscle. The mechanisms of coupling metabolism and translation such as the mTOR pathway have been increasingly studied in recent years due to its potential role in age-related diseases such as diabetes [212], COPD [213] [214] and obesity [215].

In this chapter we focus on the link between genes that form the translation machinery and energy metabolism pathways. We analyse the network modules in greater detail and identify key genes that could play a regulatory role linking these two functions. This analysis reveals that eukaryotic initiation factors (EIFs), which control translation at the step of ribosomal assembly and recycling, are found within the core network modules and are differentially expressed between young and elderly skeletal muscle. Using a correlation based analysis, we show that expression of EIFs and genes from energy metabolism pathways are linked in the meta-analysis data in an age dependent manner.

By analysing the human muscle networks at a high level of detail we generate the hypothesis that EIFs control energy metabolism at the level of transcription in skeletal muscle. To test the hypothesis we chose one of the EIFs most strongly linked to energy metabolism pathways in the correlation

analysis, EIF6 (the gene is hereafter referred to as EIF6 in human, Eif6 in mouse and the protein eIF6), which controls 60s association to the 40s ribosomal pre-initiation complex (PIC) and which is necessary for insulin stimulated translation in MEFs [216]. In this study we have applied multiple omics and bioinformatics approaches to investigate the effect of eIF6 depletion in a heterozygous mice model. Using microarray profiling and MS proteomics we find that depletion of eIF6 controls the expression of a subset of genes and mitochondrial proteins as predicted by the network analysis. This includes many genes related to the function and control of energy metabolism pathways and metabolic homeostasis. Using knowledge-based network analysis tools we examine the possible mechanism of eIF6 regulation of transcription and find that there is a highly significant association between the transcriptional response to eIF6 depletion and treatment with HDAC inhibitors. HDACs are known to control metabolic homeostasis and are differentially expressed in the $Eif6^{+/-}$ mouse, providing an exciting hypothesis that a translation factor may regulate energy metabolism at the transcriptional level through post-translational regulation.

3.2 Methods

3.2.1 Inferring gene-gene correlations using Spearman's rank correlation

In order to better characterise the neighbourhood of each EIF factor we used Spearman's rank correlation. This procedure is similar to a MI-based method (it has the advantage of being a scale free approach able to detect non-linear relationships) but in addition is able to detect the sign of the relationship. To estimate the statistical significance of each correlation we used a permutation approach. Briefly, a p-value was generated for each gene-gene correlation by comparing the correlation value against a large null distribution generated from randomized data. At least 50,000 randomised variables were generated for each comparison. P-values were corrected for multiple testing by calculating the FDR using the Benjamini-Hochberg method [132].

3.2.2 Linear Discriminant Analysis

The ability of expression of EIFs in the human muscle meta-analysis dataset and the Melov et al. dataset to correctly classify young and elderly skeletal muscle was tested using Linear Discriminant Analysis (LDA). First, principle component analysis was performed on the EIF expression data in both datasets. We then used the principle components as a classifier within the LDA algorithm. LDA was run within the R software package using the MASS library.

3.2.3 Gene ontology and pathway enrichment

The online gene ontology tool DAVID was used to detect functional terms enriched (FDR < 10%) within gene lists defined by the correlation analysis in the human meta-analysis data as well as differentially expressed genes and proteins in $Eif6^{+/-}$ skeletal muscle. The online tool Revigo [217] was used to reduce the complexity of Gene Ontology analysis by removing redundant terms. Gene lists ranked by correlation values or differential expression statistic (such as the t-statistic) were tested for enrichment of Gene Ontology terms and KEGG pathways using Gene Set Enrichment Analysis (GSEA). The enrichment of energy metabolism KEGG pathways within genes correlated to EIF gene

expression was tested using a fisher test followed by controlling the FDR at 10% using the Benjamini-Hochberg method [132].

3.2.4 Collection of skeletal muscle

Eif6 heterozygous mice were kindly donated by the lab of Stefano Biffo. These mice express half the normal amount of eIF6 protein in muscle [216]. All animal work has been conducted according to relevant national and international guidelines and approved by the University of Birmingham, Medical School ethics committee. Young (8-12 week) male mice were sacrificed by cervical dislocation and the skeletal muscles were immediately removed, cleaned of any excess fat or connective tissue and either flash frozen in liquid nitrogen or placed in ice-cold PBS supplemented with 10 mM EDTA and 0.05% trypsin for mitochondrial purification. Muscles placed in storage were stored at -80°C until further use.

3.2.5 Transcriptional profiling of $Eif6^{+/-}$ mouse skeletal muscle

Soleus and quadriceps muscles were homogenised in RLT buffer (Qiagen) with added β-mercaptoethanol using a Precellys 24 tissue homogeniser system (Precellys, UK). The tissue lysate was centrifuged at 13,000rpm for 10 minutes and the supernatant removed for RNA extraction. RNA was extracted from the tissue homogenate using RNeasy (Qiagen) columns according to the manufacturer's instructions. Sample purity was assessed by measuring absorbance at 260nm and 280nm using a NanoDrop spectrophotometer, all absorbance ratios were within 1.8-2.0. Cy3 labelled cRNA was generated using the Agilent Low-Input QuickAmp kit according to the manufacturer's instructions. Briefly, 50-100ng of RNA was used as input for the first round of cDNA synthesis, followed by a second step of amplification and Cy3 dye incorporation. 600ng of labelled cRNA was hybridised to Agilent Sureprint G3 Mouse whole genome microarrays. Microarrays were washed and scanned in an Agilent SureScan microarray scanner.

Microarray data was log2 transformed and normalised using quantile normalisation. Differentially expressed genes were detected using Significance Analysis of Microarrays (SAM) [130] with a 5% FDR

cut-off. Probe IDs were linked to gene symbols using the manufacturer's in-house annotation. Where needed, mouse gene names were converted to human homologs using the Mouse Genome Informatics (MGI) database.

3.2.6 Proteomics analysis of mitochondria purified from Eif6$^{+/-}$ skeletal muscle

The isolation of mitochondria was done by Dr Dan Tennant at the University of Birmingham Medical School. The proteomics analysis was done by the proteomics facility at the University of Liverpool Institute for Integrative Biology.

Mitochondria were purified from fresh gastrocnemius muscle of Eif6$^{+/+}$ and Eif6$^{+/-}$ muscle using the protocol described in [218]. Proteomics analysis of the purified mitochondrial was done using a Quadrupole-Orbitrap instrument (QExactive). Raw data was matched against the mouse UniProt database using the Mascot search engine (v2.4.1). The data set was analysed using Progenesis 4.1 LCMS label-free quantification software. Peptide identification was adjusted to a false discovery rate of 1%.

3.2.7 Connectivity Map and Ingenuity analysis

The genes differentially expressed in the Eif6$^{+/-}$ skeletal muscle were analysed using the Ingenuity Pathway Analysis (IPA) application (Palo Alto, www.ingenuity.com) upstream analysis tool.

The Connectivity Map (CM) tool (Broad Institute, www.broadinstitute.org/cmap) holds a collection of thousands of transcriptional profiles (known as signatures) generated from treatment of cell lines with a wide range of drugs and other compounds. CM was used to find transcriptional signatures significantly overlapping with the differentially expressed genes in the Eif6$^{+/-}$ skeletal muscle. The top 1000 most significantly differentially expressed genes in the Eif6$^{+/-}$ muscle were submitted to CM in accordance with the gene set size limit. The top genes were chosen by ranking according to the d-score produced by SAM analysis. The top 1000 genes had a maximum FDR of approximately 2%.

3.3 Results

3.3.1 Correlation analysis links the expression of EIFs to energy metabolism and tissue remodelling

In the previous chapter we identified network modules enriched in oxidative phosphorylation and TCA cycle genes. These modules show an age-specific topology in addition to a change in mRNA levels in elderly muscles. We also described that these were in close proximity of a module enriched with genes encoding for proteins involved in ribosome biogenesis and translation initiation. This raised the interesting hypothesis that the translational machinery may be linked to age-dependent decline in energy metabolism.

We set to address this hypothesis by further characterising the correlation patterns in the neighbourhood (all genes significantly correlated to a given gene) of genes encoding for ribosome biogenesis. We focused on eukaryotic initiation factors as these play a crucial role in ribosomal assembly and recycling and have been shown to play a role in the control of cell growth [219] and extracellular signalling such as hypoxia [220].

We identified 6 EIFs within the network **modules M1, M2** and **M3 (EIF2S2, EIF3H, EIF1, EIF3G, EIF3K, EIF3L)**. 15 EIFs were differentially expressed in elderly muscle in the meta-analysis dataset (8 up-regulated, 7 down-regulated) (**Figure 3.1**). We decided to further investigate the linkage between EIFs and bioenergetics genes in skeletal muscle by developing a higher resolution map and including the sign of the interaction (positive or negative correlation).

This analysis was performed on the full set of 15 differentially expressed EIFs and was at first focused on testing functional enrichment in 4 core energy metabolism pathways (oxidative phosphorylation, TCA cycle, fatty acid metabolism and glycolysis, FDR < 10%) (**Figure 3.1**).

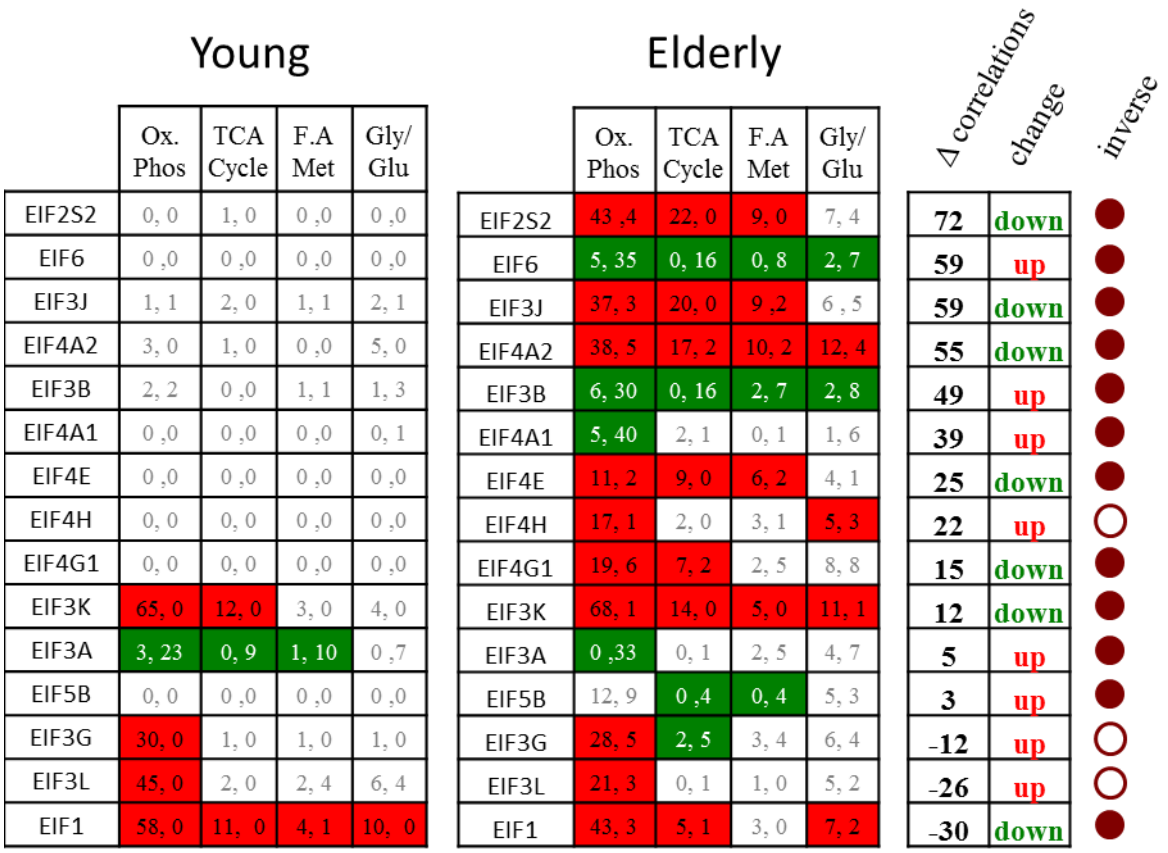

Figure 3.1 – Enrichment of energy metabolism KEGG pathways within genes correlated to expression of eukaryotic initiation factors

This figure shows the number of energy metabolism genes in the correlation neighbourhood (positive correlation, negative correlation) of 15 differentially expressed EIF genes. Enrichment of energy metabolism pathways in negatively correlated genes (green box) and positively correlated genes (red box) has been colour coded. The net total of significant correlations in each age group is calculated and the difference between ages ('Δ correlations') is used to rank each EIF. Our observation that mRNA levels of energy metabolism genes is decreased with age is consistent with the inverse relationship between the change in level of expression of each EIF ('change') and the directionality of the correlation to energy metabolism pathways for 11/15 of the EIFs ('inverse').

The results of this analysis were striking, providing evidence for an age dependent control of energy metabolism by EIFs. In young muscle, significant enrichment of energy metabolism genes was detected in the neighbourhood of only 5 EIFs. However, in elderly muscle the neighbourhood of all 15 EIF genes was enriched with genes from energy metabolism pathways. We ranked the EIFs according to the increase or decrease in the number of significant correlations with age. Overall, the number of significant correlations increased with age, with only 3 EIFs showing an overall decrease.

We previously observed that energy metabolism genes are down-regulated with age. The direction of the change in expression of EIF genes and the correlation to energy metabolism was consistent with this observation for 11/15 EIFs (**Figure 3.1**).

We noticed that one gene in particular, EIF6, had 0 significant correlations with energy metabolism genes in young muscle and ranked number 2 among the genes ranked by changes in correlation (Figure 3.2). We then performed a more in depth analysis of the EIFs using GSEA, a more sensitive functional analysis method. We focused on the top 3 EIFs (EIF2S2, EIF6, and EIF3J). This analysis confirmed that indeed EIF6 expression was not significantly associated to any KEGG pathways in young muscle (**Figure 3.2B**) even at a very permissive FDR (25%), but was associated to 29 pathways in elderly muscle **(Figure 3.2A)**. EIF3J and EIF2S2 were linked to 27 and 30 KEGG pathways respectively in young muscle and 43 and 48 respectively in elderly muscle at this threshold (**appendix 3A**). We mapped the genes from energy metabolism pathways that were correlated to EIF6 expression on to the muscle network (**Figure 3.2C**). This revealed that 21 of the energy metabolism genes within module M3 of the network are linked to EIF6, consistent with the fact that 75% of the connections in M3 are significant only in elderly muscle (see Chapter 2 – Table 2.8).

The KEGG pathways enriched within the correlation neighbourhood of EIF6 in elderly muscle revealed an interesting functional profile in addition to energy metabolism pathways (**Figure 3.2A**). Expression of EIF6 in elderly muscle is negatively correlated to KEGG pathways such as protein export, ubiquitin mediated proteolysis, insulin signalling and Wnt signalling. The inhibition of Wnt signalling by eIF6 has been previously shown in colon cancer cells and mice [221]. Genes positively correlated to EIF6 are enriched in ribosome subunits, cytokine receptor interaction pathways and neuroactive ligand receptor interaction pathways. This observation reveals that EIF6 is linked to additional important functions in ageing muscle.

A

Elderly

KEGG Pathway	NES	FDR q-val
Negative Correlation		
CITRATE_CYCLE_TCA_CYCLE	-3.33	0
OXIDATIVE_PHOSPHORYLATION	-3.03	0
PARKINSONS_DISEASE	-2.81	0
PROPANOATE_METABOLISM	-2.47	0
HUNTINGTONS_DISEASE	-2.47	0
ALZHEIMERS_DISEASE	-2.36	0
PYRUVATE_METABOLISM	-2.28	0.001
MISMATCH_REPAIR	-2.23	0.002
NUCLEOTIDE_EXCISION_REPAIR	-2.13	0.005
PROTEIN_EXPORT	-2.09	0.006
VALINE_LEUCINE_AND_ISOLEUCINE_DEGRADATION	-2.06	0.006
UBIQUITIN_MEDIATED_PROTEOLYSIS	-2.04	0.007
PROTEASOME	-2	0.009
FATTY_ACID_METABOLISM	-1.97	0.011
BUTANOATE_METABOLISM	-1.87	0.024
DNA_REPLICATION	-1.73	0.063
INSULIN_SIGNALING_PATHWAY	-1.64	0.108
SPLICEOSOME	-1.63	0.108
OOCYTE_MEIOSIS	-1.6	0.12
VALINE_LEUCINE_AND_ISOLEUCINE_BIOSYNTHESIS	-1.58	0.137
GLYCOLYSIS_GLUCONEOGENESIS	-1.58	0.131
WNT_SIGNALING_PATHWAY	-1.53	0.161
LONG_TERM_POTENTIATION	-1.52	0.162
PORPHYRIN_AND_CHLOROPHYLL_METABOLISM	-1.5	0.179
ARGININE_AND_PROLINE_METABOLISM	-1.48	0.195
RENAL_CELL_CARCINOMA	-1.47	0.197
Positive Correlation		
RIBOSOME	2.08	0.035
CYTOKINE_CYTOKINE_RECEPTOR_INTERACTION	1.85	0.13
NEUROACTIVE_LIGAND_RECEPTOR_INTERACTION	1.79	0.152

B

Young

KEGG Pathway	NES	FDR q-val
Negative Correlation		
- No Significant Terms-		
Positive Correlation		
- No Significant Terms -		

C

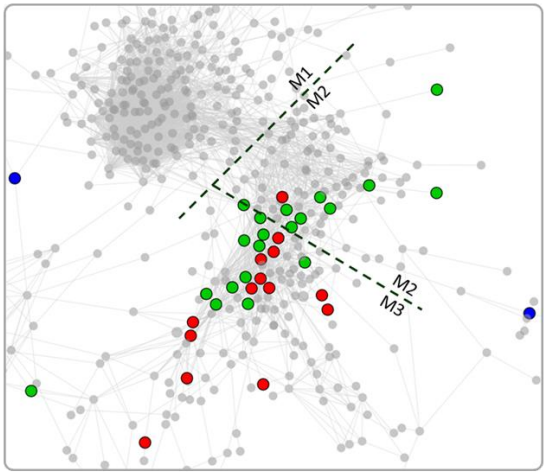

Figure 3.2 – EIF6 is correlated to energy metabolism pathways in an age-dependent manner

Panel A shows KEGG pathways enriched within the neighbourhood of EIF6 in elderly muscle. Panel B shows that no KEGG pathways are enriched within the correlation neighbourhood of EIF6 in young muscle. Panel C shows the energy metabolism genes correlated to EIF6 expression mapped to the central network modules (M1 = 0, M2 = 9, M3 = 21) (red – TCA cycle, green – Ox. Phos., blue – glycolysis).

3.3.2 Eif6 inactivation in mice is consistent with the human muscle biopsies network

The analysis of the human network reveals a link between EIF6 and expression of energy metabolism and cytokine receptor pathway genes in skeletal muscle in an age dependent manner. We chose to validate this prediction using an $Eif6^{+/-}$ heterozygous mouse. Using whole genome microarrays we have identified the transcriptional changes in soleus and quadriceps muscle of young $Eif6^{+/-}$ mice in which expression of eIF6 is reduced by half [216].

eIF6 is involved in ribosomal assembly and therefore its inactivation may affect protein synthesis. Biffo et al. [216] have shown that this is not the case in the haploinsufficient mouse suggesting that in this condition eIF6 is not rate limiting for protein synthesis. They show that the mTOR pathway is not activated in the haploinsufficient mouse.

We could also verify that the morphology (fibre length and diameter) of $Eif6^{+/-}$ skeletal muscles were indistinguishable from wild type animals. Also qPCR comparing the ratio of nuclear DNA to mitochondrial DNA content in $Eif6^{+/-}$ gastrocnemius muscle did not show a significant difference (P = 0.6, data supplied by Dr Tim Pearson, University of Liverpool).

We could identify 1,984 up-regulated and 928 down-regulated genes (5% FDR) in the $Eif6^{+/-}$ soleus muscle (N = 4). Functional analysis reveals many functions enriched within these genes (**Table 3.1**). The most significant enrichment was up-regulation of genes linked to mitochondrial function. This included up-regulation of genes involved in the *TCA cycle*, *mitochondrial transport*, *oxidative phosphorylation*, *mitochondrial ribosome* and *lipid metabolism*. Other functions enriched in up-regulated genes included *contractile fibre parts*, *protein kinase activity*, *apoptosis*, and *regulation of transcription*. The down-regulated genes were not significantly enriched with functional terms, however analysis of the functional groups revealed genes related to cell migration such as Tgfbr1, blood vessel remodelling (integrins), cell adhesion (CD44), chemotaxis (Ccl2, Ccl5, Ccl8, Ccr2), regulation of transcription (Notch1, Hdac4) and cell cycle (Camk2a, Ccng2).

A preliminary analysis of quadriceps muscle (N=2) from $Eif6^{+/-}$ mice showed a similar functional profile. 479 genes were expressed 50% higher on average in the $Eif6^{+/-}$ quadriceps muscle compared to $Eif6^{+/+}$, and were enriched with genes which encode proteins that localise to the *mitochondria, oxidative phosphorylation* components, *translation*, *protein catabolic process* and *contractile fibre* constituents (**Table 3.2**). 288 genes were expressed at least 50% lower in the $Eif6^{+/-}$ quadriceps compared to the $Eif6^{+/+}$. No functional enrichment was found in these genes although similar to the

Up-regulated in Eif6$^{+/-}$ soleus muscle

Category	Term	Count	FDR	Example Genes
CC	Mitochondrion	244	1.4e-22	Ppargc1a, Sod2
KEGG	TCA Cycle	16	1.4e-5	Cs, Sdha, Pck1, Sucla2
BP	Protein serine/threonine kinase activity	67	6.3e-3	Mapks, Rps6ka2, Camk1
BP	Apoptosis	71	2.1e-2	Trp53
BP	Mitochondrial transport	15	6.6e-3	Mtx1, Mtx2, Timm9, Timm10
KEGG	Oxidative Phosphorylation	29	4.3e-3	Cox2, Atp5d, Ndufaf4
CC	Mitochondrial ribosome	11	8.2e-2	Mrps, Mrpl
BP	Lipid metabolism	26	3.0e-2	Hadh, Crat, Acads, Cpt1, Cpt2, Lpl
MF	Transcription cofactor activity	33	2.4e-2	Hdac5, Hdac7
BP	Intracellular protein transport	48	1.6e-2	Ipo7, Ipo13
CC	Contractile fiber part	18	6.9e-2	Myh2, Tpm1, Tpm2
BP	Regulation of transcription from RNA polymerase II promoter	88	2.7e-2	Atf5, Jun, Mef2c, Ppara, Fgf2
BP	Glycerol ether metabolic process	14	2.8e-2	Tnxb. Txn2, Cat
BP	Regulation of cell size	22	8.8e-2	Tgfb1, Tgfb3

Down-regulated in Eif6$^{+/-}$ soleus muscle

Category	Term	Count	FDR	Example Genes
BP	Regulation of transcription, DNA-dependant	92	0.25	Notch1, Esr1, Hdac4, Igf1, Ppargc1b, Rb1
BP	Cell migration	18	0.53	Prkca, Tgfbr1,
BP	Blood Vessel Remodelling	6	0.19	Itga4, Tgfb2, Itgam, Itgb1
CC	Contractile fibre	10	0.58	Drd2
BP	Immune system development	26	0.15	CD28, CD3e, CD8a,, ItgaL
BP	Tissue morphogenesis	22	0.18	Egf
BP	Cell adhesion	36	0.49	CD44
BP	Mitotic cell cycle	18	0.57	Camk2a, ccng2
BP	Hexose metabolic process	16	0.36	Fbp2
BP	Chemotaxis	10	0.59	Ccl2, Ccl5, Ccl8, Prkca, Ccr2

Table 3.1 – Functional analysis of differentially expressed genes in Eif6$^{+/-}$ soleus muscle

soleus they also included genes related to cell cycle and integrin signalling. In summary, a reduction in eIF6 expression results in a transcriptional reprogramming of mouse skeletal muscle characterised by an increase in expression of energy metabolism genes, consistent with the prediction made by the network analysis.

Up-regulated in eIF6 +/- gastrocnemius muscle

Category	Term	Count	FDR
CC	Mitochondrion	79	8.8E-11
BP	Translation	30	6.2E-7
KEGG	Oxidative phosphorylation	16	3.3E-4
BP	Protein catabolic process	29	3.6E-2
CC	Contractile fibre part	9	2.5E-2

Down-regulated in eIF6 +/- gastrocnemius muscle

Category	Term	Count	FDR
BP	Translation	14	0.58
BP	Protein transport	21	0.49
BP	Integrin-mediated signalling pathway	5	0.95
CC	Contractile fibre	5	0.67
BP	Cell cycle	16	0.96

Table 3.2 – Functional analysis of the Eif6$^{+/-}$ gastrocnemius muscle

3.3.3 The transcriptional state of the Eif6 haploinsufficient mouse recapitulates the functional profile of the inferred human EIF6 network neighbourhood

We assessed the accuracy of the predictions made by the correlation analysis in the human meta-analysis data regarding the role of eIF6 in skeletal muscle. To do this we compared the functional profiles of genes correlated to EIF6 expression and differentially expressed genes in the Eif6$^{+/-}$ muscle in human and mouse respectively. A comparison of the gene counts between the functional profiles revealed many functional terms present in both analyses (**Figure 3.3A**). We identified all Gene Ontology terms with a positive gene count in both the correlation and Eif6$^{+/-}$ soleus analysis and submitted them to the semantic similarity tool Revigo [217] to identify key terms. In the case of up-regulation in the Eif6$^{+/-}$ muscle and negative correlation to EIF6 expression this includes terms related to energy metabolism

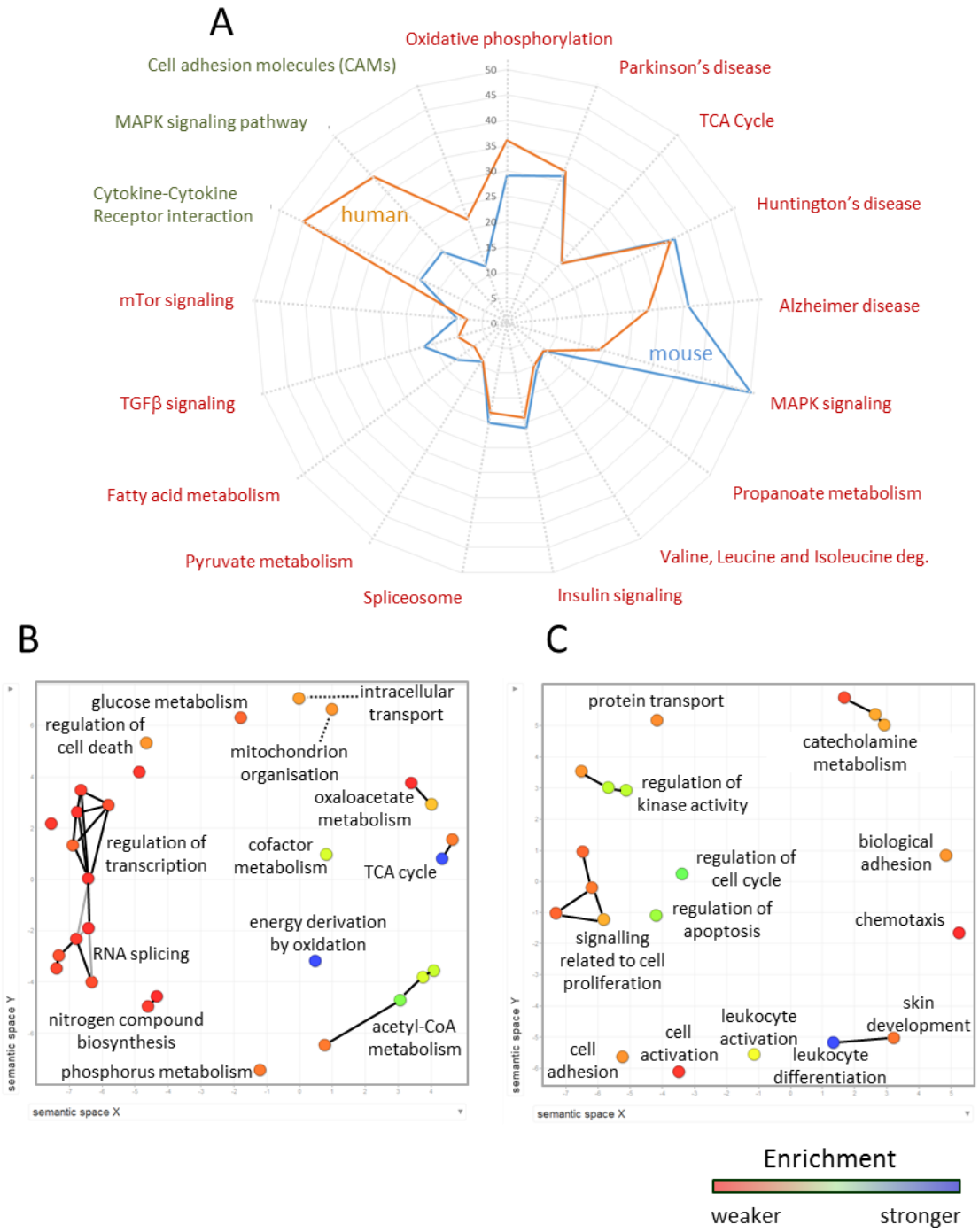

Figure 3.3- Functional similarities between the human EIF6 correlation neighbourhood and the Eif6$^{+/-}$ soleus muscle in mice

Panel A shows the comparison of gene counts for all KEGG pathways identified in the correlation and Eif6$^{+/-}$ muscle analysis. Functions are colour coded according to the change in expression (up – red, down – green) and direction of correlation (negative –red, positive – green). Panel B and C represent the semantic similarity analysis of gene ontology functional terms represented in both the human and mouse analysis.

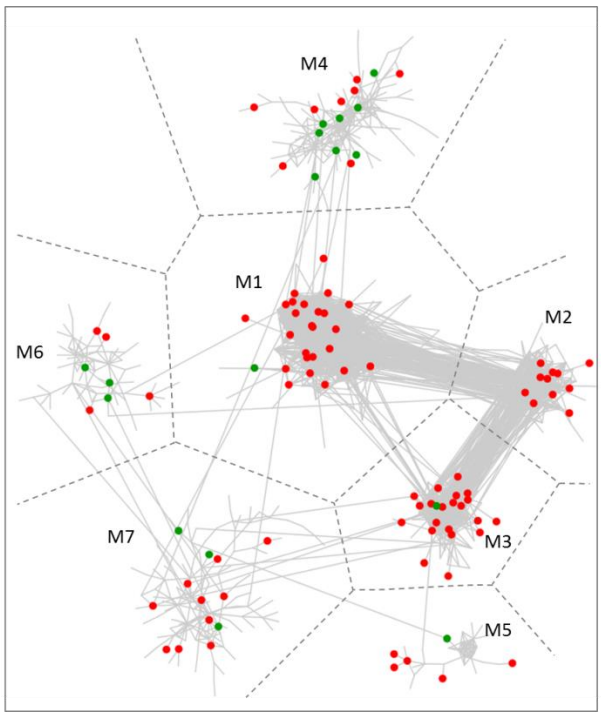

Figure 3.4 – Enrichment of eIF6 regulated genes in the human network modules

This figure shows that module M1 (26 genes), M2 (11 genes) and M3 (22 genes) are enriched with genes differentially expressed in Eif6$^{+/-}$ soleus.

including *TCA cycle*, *energy derivation by oxidation (oxidative phosphorylation)*, *mitochondrial organisation*, *glucose metabolism* and *acetyl-CoA metabolism* (**Figure 3.3B**). On the other hand, genes down-regulated in Eif6$^{+/-}$ muscle and positively correlated to EIF6 expression were associated with terms such as *cell adhesion*, *cell activation* and *regulation of apoptosis* (**Figure 3.3C**). Taken together, this suggests that the predictions made by the human muscle data are recapitulated in the mouse muscle with respect to energy metabolism functions. We identified modules in the human muscle network that were enriched (FDR < 0.01%) with genes differentially expressed in the Eif6$^{+/-}$ soleus. Modules M1 (ribosomes, translation initiation), M2 (oxidative phosphorylation) and M3 (TCA cycle, oxidative phosphorylation) were enriched with genes up-regulated in the Eif6$^{+/-}$ soleus muscle (**Figure 3.4**). However twice as many genes mapped to M3 (22) than M2 (11), suggesting that genes that are highly co-expressed in elderly muscle in an age-dependent manner (module M3) are regulated by eIF6.

3.3.4 Ingenuity Pathway Analysis of the Eif6$^{+/-}$ transcriptional signature

To further investigate the role of eiF6 in controlling transcription in skeletal muscle we used the literature based interaction database Ingenuity (IPA). We analysed the differentially expressed genes from the Eif6$^{+/-}$ soleus muscle using the IPA upstream prediction tool. This identified 39 genes and compounds that are known to interact with genes differentially expressed in the Eif6$^{+/-}$ muscle where the overlap was highly significant ($p < 0.005$) (**Table 3.3**). Amongst these the known targets of insulin receptor (INSR) was the most highly enriched, and the status of insulin receptor is predicted to be activated in the Eif6$^{+/-}$ muscle (**Table 3.3**). 39/47 (83%) of genes with known activation/inhibition by INSR within the IPA network are consistent with activation. The overlap between eIF6 and INSR targets included increased expression of transcriptional factors related to mitochondrial biogenesis and lipid metabolism such as PPARA, NRF1, CPT1B and CPT2 and mitochondrial enzyme subunit genes (**Figure 3.5A**). Interestingly, 6 of the top 10 predicted inhibited factors based on the Eif6$^{+/-}$ upstream analysis are kinase inhibitors, and 4 of these are known to act on kinases within the INSR pathway (U0126, LY294002, PD98059 and Wortmannin target MEK1/2, PI3K, MEK1 and PI3K respectively). Taken together these results suggest an activation of the INSR pathway in the Eif6$^{+/-}$ muscle.

Other effector genes predicted to be activated in the Eif6$^{+/-}$ soleus muscle include PGC-1α. 36/45 (80%) of genes in the IPA network are predicted to be activated (**Figure 3.5B**). PGC-1α is up-regulated in the Eif6$^{+/-}$ soleus (linear fold change = 1.29) and is linked to important genes such as SOD2, CAT, NRF1, PPARA, TXN2, and FASN in the IPA networks (**Figure 3.5B**). Interestingly, the up-regulation of antioxidant enzymes superoxide dismutase 2 (SOD2) and catalase was highlighted by this analysis. Nitric oxide synthase 3 (NOS3/eNOS) is also up-regulated in the Eif6$^{+/-}$ muscle, suggesting a role of eIF6 in controlling oxidative stress. This analysis reveals some of the key regulators of metabolic processes in skeletal muscle that are modulated by eIF6.

Upstream Regulator	Log Ratio	Molecule Type	Predicted Activation State	Activation z-score	p-value of overlap
INSR		kinase	Activated	4.454	2.83E-16
TP53	0.29	transcription regulator	Activated	4.874	3.40E-16
mono-(2-ethylhexyl)phthalate		chemical toxicant	Activated	4.655	7.68E-13
Ins1		other	Activated	4.114	1.01E-11
CREB1		transcription regulator	Activated	3.915	3.09E-11
dexamethasone		chemical drug	Activated	3.699	3.58E-10
methylprednisolone		chemical drug	Activated	2.15	3.78E-10
beta-estradiol		chemical - endogenous mammalian	Activated	3.831	7.34E-10
PPARG		ligand-dependent nuclear receptor	Activated	3.603	2.79E-09
rosiglitazone		chemical drug	Activated	3.878	3.80E-09
PRL		cytokine	Activated	2.319	5.59E-09
PPARGC1A	0.376	transcription regulator	Activated	3.877	6.13E-09
PDGF BB		complex	Activated	4.718	9.85E-09
TGFB1	1.007	growth factor	Activated	2.844	1.97E-08
troglitazone		chemical drug	Activated	2.488	3.60E-08
VEGFA		growth factor	Activated	3.902	1.84E-07
MAPT	0.641	kinase	Activated	2.121	4.57E-07
KLF15	0.423	transcription regulator	Activated	2.691	6.44E-07
U0126		chemical - kinase inhibitor	Inhibited	-3.006	7.28E-07
ESRRA	0.334	ligand-dependent nuclear receptor	Activated	3.132	8.49E-07
EIF2AK3		kinase	Activated	2.389	1.07E-06
LY294002		chemical - kinase inhibitor	Inhibited	-2.404	1.19E-06
CD 437		chemical drug - kinase inhibitor	Inhibited	-4.405	4.71E-06
SB203580		chemical - kinase inhibitor	Inhibited	-3.978	1.70E-05
NRIP1	-0.373	transcription regulator	Inhibited	-2.01	2.87E-05
PD98059		chemical - kinase inhibitor	Inhibited	-3.5	3.66E-05
monocrotaline		chemical toxicant	Inhibited	-2.666	3.90E-05
CD3		complex	Inhibited	-2.734	1.17E-04
wortmannin		chemical - kinase inhibitor	Inhibited	-2.481	2.17E-04
SFTPA1		transporter	Inhibited	-2.65	3.26E-04
CD28	-0.449	transmembrane receptor	Inhibited	-2.456	8.65E-04
BDKRB2		G-protein coupled receptor	Inhibited	-2.04	1.50E-03
vitamin E		chemical drug	Inhibited	-2.197	1.87E-03
DACH1		transcription regulator	Inhibited	-2.795	2.10E-03
PCK1	1.207	kinase	Inhibited	-2.2	2.14E-03
actinomycin D		chemical drug	Inhibited	-2.123	2.36E-03
sirolimus		chemical drug	Inhibited	-2.455	3.95E-03
miR-124-3p (and other miRNAs w/seed AAGGCAC)		mature microRNA	Inhibited	-2.908	4.16E-03
ACOX1		enzyme	Inhibited	-2.611	4.27E-03

Table 3.3 – Ingenuity Pathway Analysis predicts up-stream regulators of eIF6 targets

The change in expression of upstream regulators differentially expressed in the Eif6$^{+/-}$ soleus is represented by the log ratio

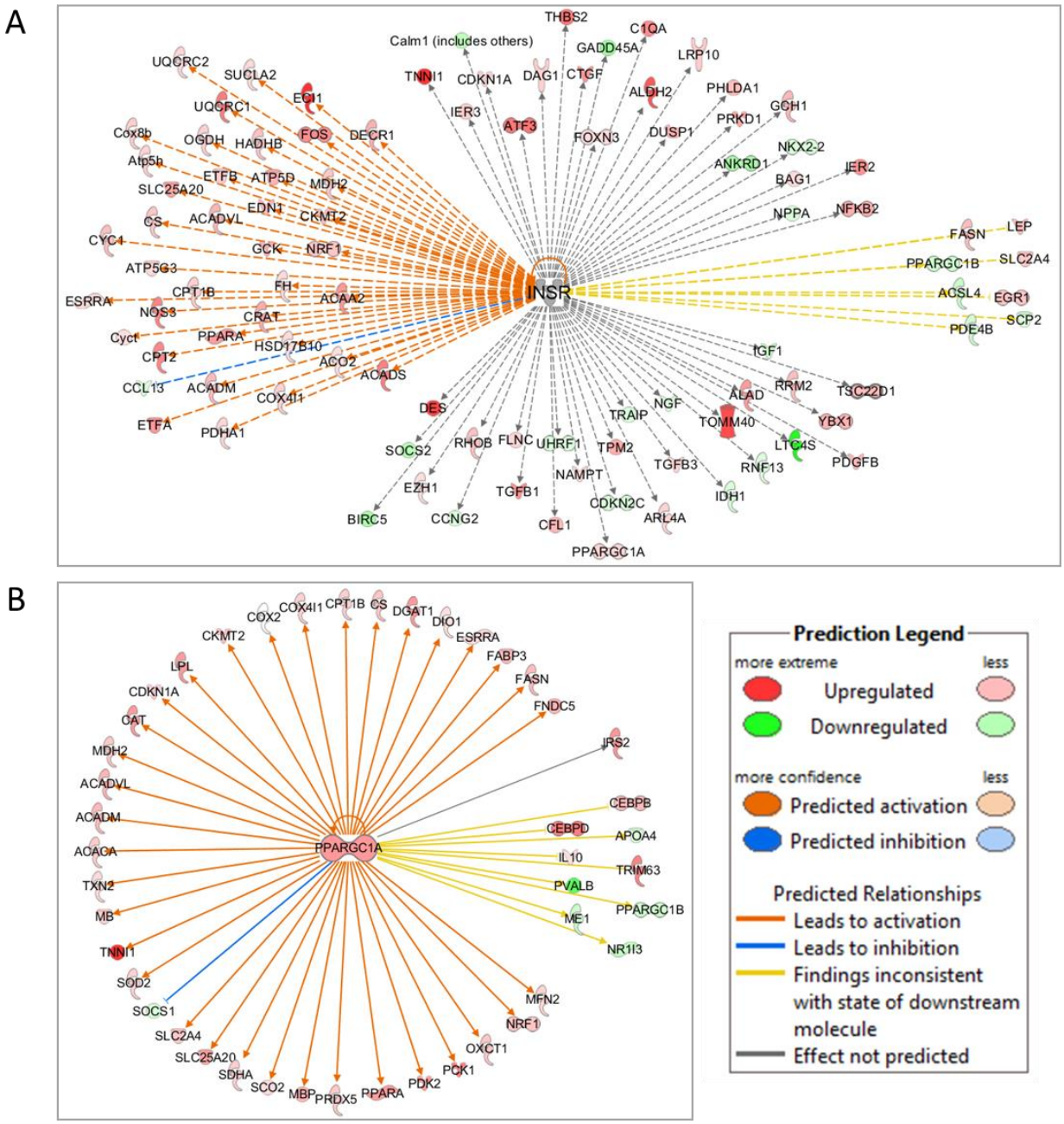

Figure 3.5 – Ingenuity networks showing genes down-stream of INSR and PGC-1α that are differentially expressed in Eif6$^{+/-}$ muscle

Panel A and B show the enrichment of genes downstream of INSR ($p = 2.83e^{-16}$) signalling and PGC-1α ($p = 6.13e^{-9}$) respectively that are differentially expressed in Eif6$^{+/-}$ muscle. Both INSR and PGC-1α signalling is predicted to be activated in Eif6$^{+/-}$ muscle.

3.3.5 Protein expression in Eif6$^{+/-}$ skeletal muscle mitochondria

We have shown that there is differential expression of genes related to mitochondrial function in Eif6$^{+/-}$ muscle. However, mRNA changes are only partially correlated to protein abundance [222]. We have used mass spectrometry to obtain the expression of proteins in purified mitochondria from Eif6$^{+/+}$ and EIf6$^{+/-}$ gastrocnemius muscle of young mice (N = 4). Mitochondria were isolated by Dr Dan Tennant at the University of Birmingham and mass spectrometry experiments were performed by the Liverpool University proteomics facility. We detected 850 proteins at a high confidence (1% FDR), of which 120 proteins were differentially expressed (10% FDR). Principle component analysis (PCA) was able to separate the wild type and heterozygous mice when applied to all detected proteins and differentially expressed proteins (**Figure 3.6A-B**).

We compared the proteins detected in our samples to those in the mouse mitochondrial protein database Mitocarta [223] (www.broadinstitute.org/pubs/MitoCarta) and found a high level of overlap (> 50% for both detected and differentially expressed proteins) (**Figure 3.6C-D**). See **appendix 3B** for the full list of differentially expressed proteins.

We have characterised the differentially expressed proteins using both existing literature to identify individual proteins linked to specific mitochondrial function and functional analysis to provide an overview of the functional classification of the proteins (**Figure 3.7, Table 3.4**). Functional analysis reveals that 72 out of 120 differentially expressed proteins are either known or predicted to associate with the mitochondria (the increase on the experimentally validated Mitocarta database is likely due to predicted functionality within the Gene Ontology database). This includes components of the oxidative phosphorylation pathway, mitochondrial ribosome, and mitochondrial inner membrane. We also find enrichment of cytosolic ribosomal components, proteins associated to the sarcoplasmic reticulum and components of voltage-gated calcium channel complex. A closer inspection of the functions of the differentially expressed proteins (**Figure 3.7**) reveals up-regulation of small molecule transporters such as the calcium uniporter Mcu and the ADP/ATP carrier Slc25a31

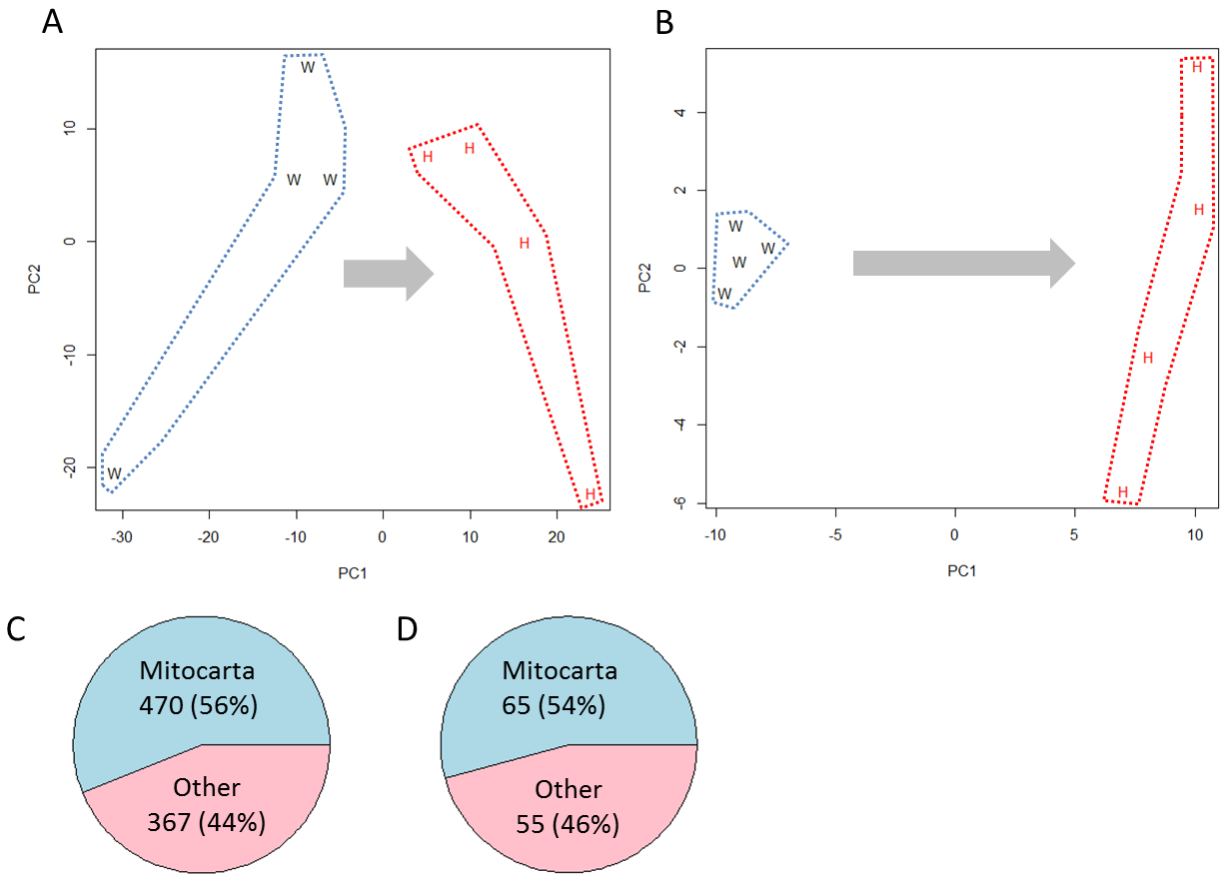

Figure 3.6 – Mitochondrial protein expression separates wild type and heterozygous samples in a PCA

Panel A and B are the results of PCA applied to the protein expression data of all detected proteins (Panel A) and differentially expressed proteins (Panel B). Panel C and D show the overlap between the detected and differentially expressed proteins respectively and the mitochondrial protein database Mitocarta.

(ANT4). We see up-regulation of the translocation factor Pam16 (TIMM16), and down-regulation of Tim9 and Pmpca. Mitochondrial translation factors Taco1, Guf1, Gfm2 and Qrsl1 are down-regulated. Mitochondrial protein complex assembly chaperones Cox20, Cox11, Ndufa11 are down-regulated, while Bcs1l is up-regulated. Proteins related to heme metabolism Cox15, Tmem14c and Cpox are all down-regulated. TCA cycle and oxidative phosphorylation proteins are up-regulated except for Sdhd, MT-Nd4 and Cox15. Eif6 haploinsufficiency therefore regulates the expression of mitochondrial proteins including energy metabolism enzyme subunits. Interestingly this also reveals regulation of mitochondrial ion and protein transport systems and translation factors.

Category	Term	Count	FDR
CC	Mitochondrion	72	2.61E-45
CC	Ribosome	20	2.23E-14
CC	Mitochondrial inner membrane	21	3.87E-12
KEGG	Oxidative phosphorylation	13	1.20E-07
CC	Mitochondrial ribosome	8	3.06E-07
CC	Sarcoplasmic reticulum	7	2.39E-06
CC	Large ribosomal subunit	7	4.96E-06
CC	Small ribosomal subunit	4	0.010842
CC	Voltage-gated calcium channel complex	3	0.039328

Table 3.4 – Functional analysis of differentially expressed proteins

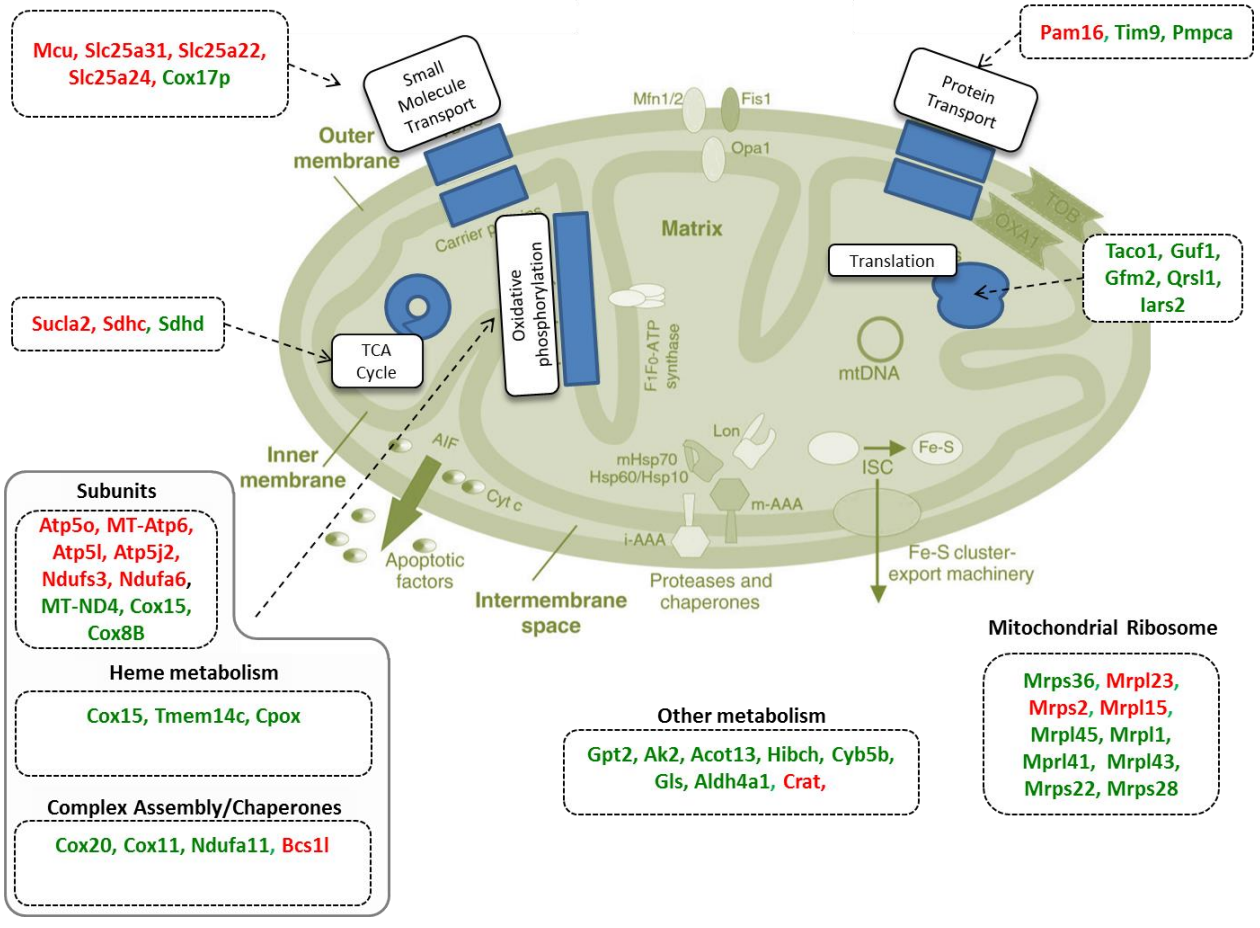

Figure 3.7 – Mapping the differentially expressed proteins to mitochondrial functions.

Up-regulated (red) and down-regulated (green) proteins have been colour coded. The full table of differentially expressed proteins is available in **appendix 3B**. Image adapted from ref [224]

3.3.6 Lysine acetylation is a predicted mechanism of eIF6 control of transcription

We have identified a role of eIF6 in controlling transcription of specific mRNAs. We have used the knowledge base tool Connectivity Map (CM) to investigate potential mechanisms by which eIF6 controls transcription. CM analysis identified 47 transcriptional signatures associated with treatment by a specific compound that had a significant overlap with the $Eif6^{+/-}$ signature ($p < 0.01$) (**Table 3.5**). Where possible we have classified the compounds based on existing literature. Interestingly, we noticed that among the significant signatures were 3 histone deacetylase inhibitors, Scriptaid, Trichostatin A (TSA) and Valproic acid (VPA). Scriptaid is a general histone deacetylase (HDAC) inhibitor known to regulate the expression of genes related to cell cycle and apoptosis [225], two of the functions associated to eIF6 in our analysis. TSA and VPA have been shown to inhibit class 1 and class 2 HDACs [226] [227]. The class 2 HDACs 5 and 7, class 3 sirtuins SIRT4 and SIRT7 are up-regulated in the $Eif6^{+/-}$ soleus microarray data while histone acetyl transferase 1 (HAT1) and HDAC4 are down-regulated. The CM analysis predicts that eIF6 mediated transcriptional control could be acting through lysine deacetylation of proteins.

Compound	Function	Mean Con Score	P-value
irinotecan	inhibits topoisomerase I	0.857	0.00002
benzocaine	inhibits voltage-dependant sodium channels	0.704	0.00004
STOCK1N-35874	-	0.696	0.00445
camptothecin	inhibits topoisomerase I	0.681	0.00086
amantadine	effects dopamine release and uptake	0.664	0.00018
GW-8510	-	0.641	0.0001
daunorubicin	Inhibits progression of topoisomerase II	0.634	0.00062
azacitidine	cytidine analog	0.617	0.00833
penbutolol	Adrinergic blocking agent	0.613	0.00361
biperiden	anticholinergic	0.606	0.00008
lasalocid	anti-parasitic	0.56	0.00195
CP-863187	-	0.54	0.00511
viomycin	antibiotic	0.52	0.004
mebhydrolin	antihistimine	0.519	0.00422
PNU-0251126	-	0.5	0.00511
guanadrel	adringergic blocking agent	0.465	0.00162
isoxicam	anti-inflammatory	0.463	0.00555
Prestwick-692	-	0.446	0.00599
monensin	antibiotic	0.44	0.00113
hycanthone	anti-parasitic	0.413	0.00561
pentoxifylline	phosphodiesterase inhibitor	0.401	0.00937
lisuride	dopamine/serotonin partial agonist	0.376	0.00348
heptaminol	vasoldilator	0.373	0.00515
meteneprost	prostoglandin e2 analogue	0.341	0.00557
thiamphenicol	antibiotic	0.336	0.0029
merbromin	antiseptic	0.304	0.00413
alprostadil	prostaglandin e1, vasodilator	0.29	0.00744
valproic acid	HDAC inhibitor	-0.294	0.00401
wortmannin	PI3K inhibitor	-0.348	0.00545
trichostatin A	HDAC inhibitor	-0.349	0
sirolimus	Rapamycin e.g. mTOR inhibitor	-0.351	0
LY-294002	PI3K inhibitor	-0.388	0
geldanamycin	hsp90 inhibitor	-0.402	0.00112
tanespimycin	hsp90 inhibitor	-0.407	0
alvespimycin	hsp90 inhibitor	-0.42	0.00399
mepyramine	antihistimine	-0.513	0.00999
mefloquine	antimalarial - inhibition of heme synthesis	-0.522	0.00288
amprolium	antiprotozoal	-0.524	0.00681
doxylamine	antihistimine	-0.552	0.00537
hesperidin	Regulates cholesterol	-0.573	0.00772
imipenem	antibiotic	-0.577	0.00121
dequalinium chloride	antiseptic/disinfectant	-0.582	0.00901
procainamide	sodium channel blocker	-0.603	0.00597
molindone	Dopamine blocker	-0.634	0.00058
meptazinol	opiod analgesic	-0.649	0.0001
sulfathiazole	antibacterial - potentially folate synthesis related	-0.662	0.00064
scriptaid	HDAC inhibitor	-0.668	0.00561

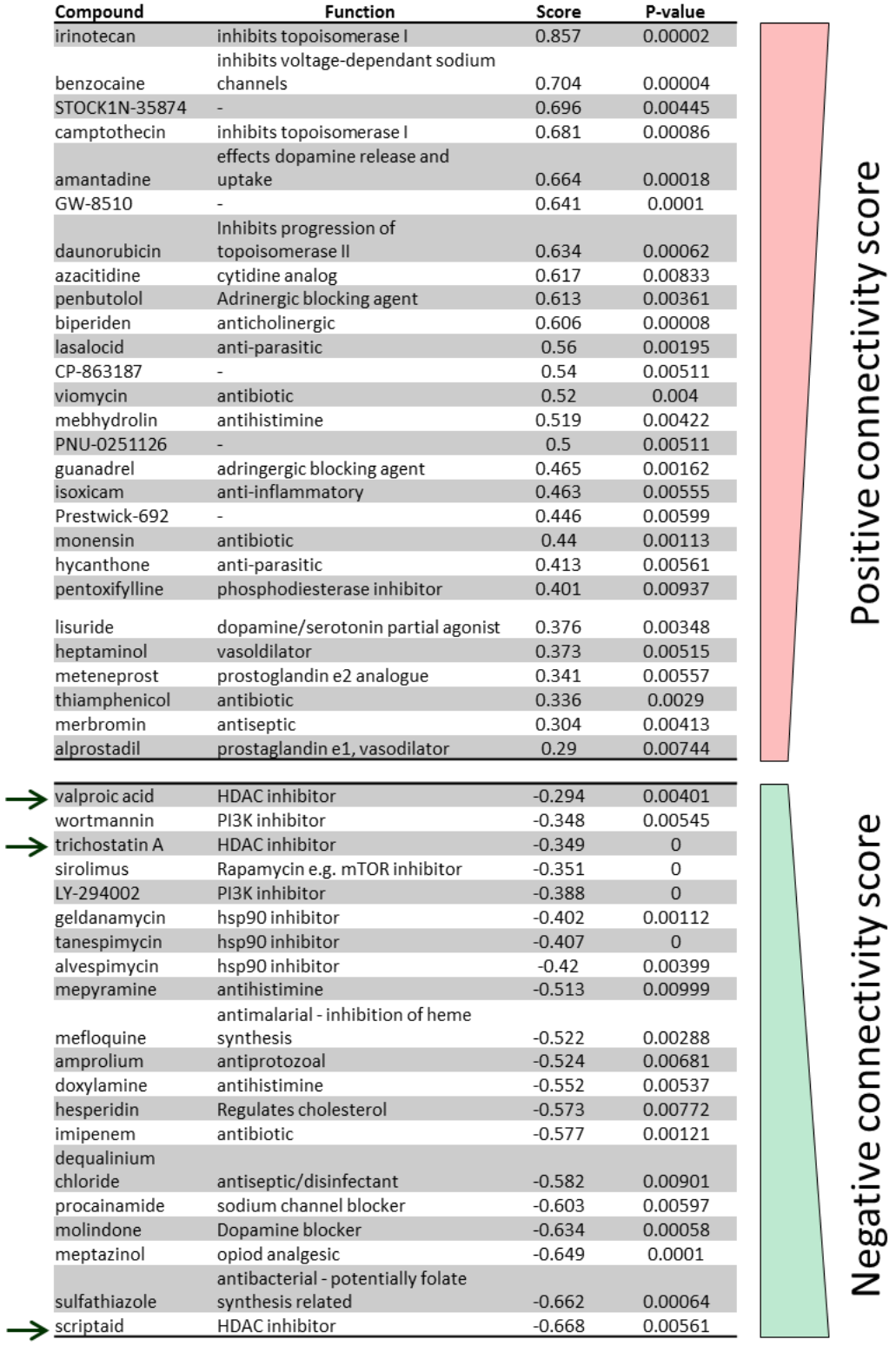

Table 3.5 – Transcriptional signatures with significant overlap to the Eif6$^{+/-}$ signature.

A positive connectivity score represents a similar transcriptional response to treatment with a compound and depletion of Eif6; a negative connectivity score represents an inverse transcriptional response. HDAC inhibitors have been highlighted with arrows.

3.4 Discussion

3.4.1 The role of eukaryotic initiation factors

Eukaryotic initiation factors control translation at the step of ribosome assembly and recycling. Several EIFs have previously been linked to important cellular signalling events. EIF2-α phosphorylation plays a key role in controlling translation during hypoxia [228]. EIF4E is well documented as the target of EIF4E binding proteins which are under the control of the nutrient sensing mTOR signalling pathway and insulin [229] [230]. These mechanisms allow preferential translation of a set of mRNAs, enabling the cell to better adapt to environmental changes. The role of EIF2-α and EIF4E in signalling pathways is linked to their rate limiting role in translation initiation during the formation of the 43S and 48S ribosomal complex respectively and as such they act as downstream targets of signalling pathways. We have identified a subset of EIF genes in human muscle which show both age dependent expression and correlation with energy metabolism genes. We focused on EIF genes that were differentially expressed with age. It is worth noting that in a separate analysis these 15 EIFs obtained an accuracy of 72.5% when used as a classifier in a linear discriminant analysis applied to young and elderly muscle samples from the independent Melov et al. study. This was only 2.5% lower than previous attempts to develop dedicated classifiers of ageing muscle [148]. EIF2-β showed the greatest change in the number of significant correlations with age. Consistent with EIF2-β linkage to energy metabolism genes is the fact that it is regulated by NRF1 [231]. NRF1 controls the expression of genes necessary for mitochondrial metabolism, and is itself induced by PGC-1α. Several subunits of the EIF4F complex, EIF4A1, EIF4A2 and EIF4E also increased correlation with energy metabolism genes with age. These results suggest an age-dependent mechanism linking transcription of translation initiation factors and energy metabolism genes.

3.4.2 Eif6 haploinsufficiency controls expression of energy metabolism genes and proteins

Based on the functional profiling of the network neighbourhood of the most age-specific EIF genes we selected EIF6 to investigate further. eIF6 acts as an anti-association factor by sequestering ribosomal 60s subunits prior to 80s ribosome assembly, thus controlling translation at the step of 40s and 60s binding [232] (**Figure 3.8**, adapted from [233]). Multiple theories outlining the mechanism of eIF6 release from the 60S subunit have been discussed including phosphorylation by RACK1 and Efl1 mediated conformational changes of the 60s subunit, however further evidence is required to confirm these models [232]. The known properties of yeast and mammalian eIF6 are outlined in **Table 3.6** (adapted from [233])**.**

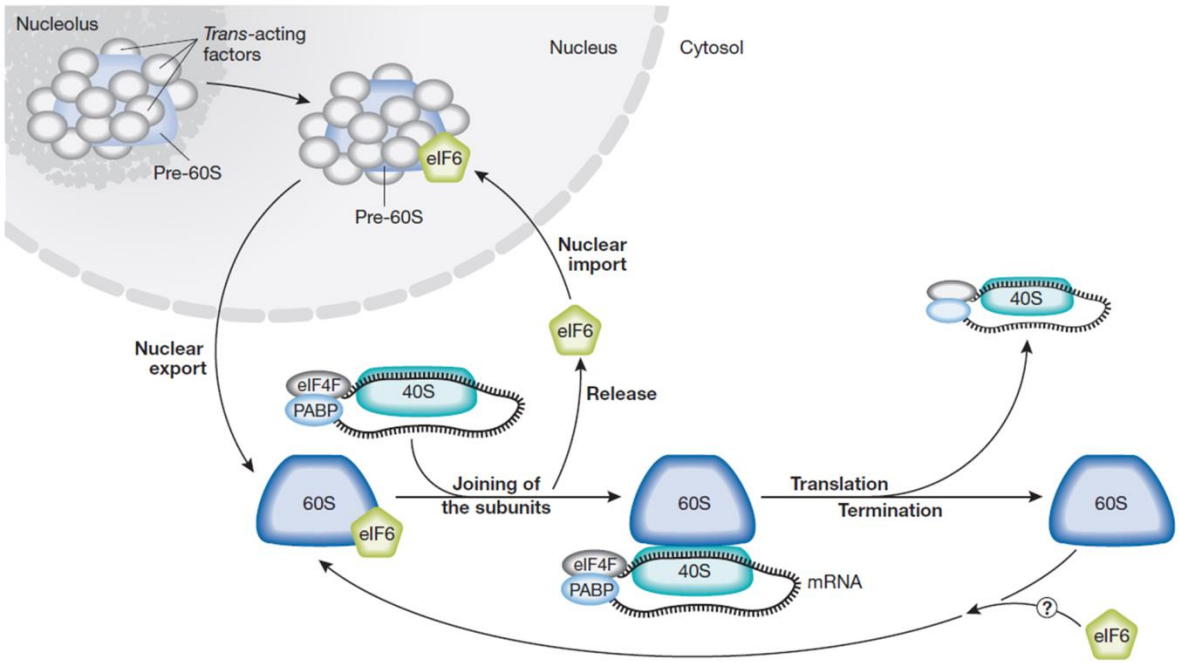

Figure 3.8 – The role if eIF6 in ribosome 80S assembly

eIF6 controls the rate of translation by preventing the association of the 40S and 60S ribosomal subunits prior to translation. Phosphorylation induces eIF6 dissociation from the 60S which is then available for translation. The phosphorylation status of eIF6 controls its localisation. Phosphorylation of eIF6 in the nucleus by casein kinase 1 promotes its export while calcineurin phosphatase promotes the nuclear localisation of eIF6 [234].

Eif6 heterozygous mice are viable and show no visible differences to wild type mice during the first month of life. In adulthood the only biometric differences are a reduction in the weight/body ratio of liver and adipose tissue in $Eif6^{+/-}$ mice [216]. This was associated with decreased cell proliferation and an increased resistance to insulin stimulated translation [216]. $Eif6^{+/-}$ fibroblasts show normal ribosome biogenesis and unaltered basal levels of translation. Both $Eif6^{+/-}$ fibroblasts and hepatocytes are resistant to insulin stimulated translation [233].

Properties	Yeast	Mammalian
Essential	Yes	Yes
Nucleolar localization	Yes	Yes
Cytoplasmic localization	A minor pool	Up to 70%
Function in ribosome biogenesis	Yes, predominant	Likely, not demonstrated
Anti-association activity	Yes	Yes
Role in translation	No	Yes
Expression	Constitutive	Broad variation among cells and tissues
Phosphorylation	Yes, on Ser 174	Yes, on at least Ser 174 and Ser 235

Table 3.6 – Properties of eIF6 in yeast and mammalian systems

We have identified Eif6 as a novel regulator of a set of mRNAs and protein expression in skeletal muscle that is highly enriched in energy metabolism functions. This is a particularly surprising finding considering that eIF6 is not associated with the 40S subunit, and thus should not interfere with the translation of specific mRNAs. This is suggesting that eIF6 has an addition role in control of transcription. Ingenuity network analysis suggests that eIF6 is acting up-stream to repress transcription factors such as PGC-1α, NRF1 and PPARA, and that activation of insulin signalling pathways is a feature of eIF6 depletion. These results are consistent with the link between eIF6 and energy metabolism revealed by the human muscle network. Furthermore, EIF6 is up-regulation in elderly skeletal muscle, consistent with findings that elderly muscle has higher insulin resistance [90] and lower expression of energy metabolism genes.

3.4.3 Depletion of eIF6 produces a signature associated with HDAC inhibitor treatment

Using the online Connectivity Map tool we found that the transcriptional signature following treatment with histone deacetylase inhibitors *in vitro* was significantly overlapping with that of Eif6 haploinsufficiency. Inhibitors of class II HDACs have been linked to improved glucose homeostasis in mouse models of type 2 diabetes [235]. HDACs regulate gene expression by controlling the acetylation of lysine residues on histones. However more recent proteomics analysis has revealed that acetylation status is a key regulator of many diverse proteins [236]. HDACs have been shown to act on lysine residues on proteins as well as histones [237]. Acetylation status has recently been revealed to be an important mechanism of post-translational regulation of metabolic enzymes [238]. This includes enzymes involved in glycolysis, the TCA cycle, fatty acid metabolism and glycogen metabolism [239]. In the past few months, an important study by Still et al. has identified the acetylation sites within the mitochondrial proteome that are regulated during alterations in nutritional status [81], and this has been linked to specific sites of SIRT3 regulation [240]. Expression of a set of five HDACS (HDAC4, 5, & 7, SIRT4 & 7) are up-regulated in $Eif6^{+/-}$ muscle. SIRT4 knock-down in myotubes has been shown to increase fatty acid oxidation, cellular respiration and AMPK activity [241]. HDAC5 inhibition in muscle cells has been shown to increase glucose uptake and insulin activity [242]. On the contrary, expression of other HDACs such as SIRT2 and SIRT3 has been shown to correlate positively with VO2 max in healthy muscle, indicating a positive effect on respiration [174]. In future experiments it will be important to distinguish between specific HDACs activities, as they play contrasting roles. Together, this presents strong motivation for further analysis of the acetylation status of metabolic enzymes in response to eIF6 depletion, as this could represent a key regulatory mechanism linking a translation factor and energy homeostasis.

It is important to note that the data integration process described in chapter two did not distinguish between trained and detrained muscle. However, EIF6 expression was unchanged in the Melov training study which reported up-regulation of many genes involved in oxidative metabolism,

suggesting that physical activity is not a controller of EIF6 expression. In the future, a comparison between young and elderly Eif6$^{+/-}$ and wild type mice will be an important step in deciphering the role of eIF6 in ageing, as the present analysis relies on young mice only. This should be supported by additional clinical evidence.

CHAPTER 4

SIGNALS LINKING EIF6 TO MITOCHONDRIAL FUNCTION, OXIDATIVE STRESS AND SKELETAL MUSCLE REGENERATION

4.1 Introduction

Our analysis has revealed that eIF6 controls a switch in the expression of genes involved in mitochondrial energy metabolism. The model developed from human muscle biopsies (Chapter 2) suggests that this mechanism may be important in ageing individuals, where the expression of this gene increases. Since ageing is a complex process it is unclear what may be regulating the expression of eiF6 in ageing muscles. In this chapter, we focus on identifying stress signals that may regulate Eif6.

We start by examining the effects of oxygen tension in live mice and oxidative stress (generated in cultured myotubes) on Eif6 expression. Hypoxia, a key regulator of mitochondrial respiration [243] and tissue remodelling [244] in skeletal muscle has been previously linked to inhibition of eukaryotic initiation factors such as EIF2α and EIF4F [228] through the unfolded protein response and mTOR kinase respectively. Consistent with these observations, our analysis has revealed that hypoxia is also a potent regulator of Eif6 mRNA expression, which is coupled to a coordinate regulation of many of the genes modulated in the eIF6 depleted muscle. One possible consequence of hypoxia in skeletal muscle is the formation of reactive oxygen species from the electron transport chain, causing oxidative damage and activation of antioxidant, angiogenesis and metabolic signalling pathways such as AMPK activation of PGC-1α [245] and expression of HIF1α [246]. Regulation of Eif6 during hypoxia could be because of a ROS stimulated pathway. We show that Eif6 is regulated in an environment of very high oxidative stress *in vitro*; however this was not coupled to differential expression of genes regulated during depletion of eIF6 in a consistent manner.

The results of our transcriptional profiling of eIF6 depleted muscle revealed differential expression of transcription factors and genes involved in skeletal muscle regeneration and growth, such as NOTCH1 [247], IGF1 [53], FGF2 [248], chemokines [249], cell cycle regulators and cell adhesion molecules. The response to skeletal muscle injury involves the activation, proliferation and differentiation of muscle stem cells (satellite cells) into myotubes, which then fuse to damaged fibres or form new ones. Satellite cells exist under the basal lamina of all muscle fibres in a quiescent state. Recently, inhibitors of mitochondrial activity have been shown to regulate differentiation of satellite cells [250]. Together, these observations lead us to hypothesise that eIF6 plays a role in satellite cell function by controlling transcription within satellite cells. In the second part of this chapter, we investigate the transcriptional state of quiescent, activated and differentiating wild type satellite cells using existing studies, followed by transcriptional profiling of satellite cells from $Eif6^{+/-}$ skeletal muscle in a proliferative state and after induction of differentiation. We show that activation and differentiation in satellite cells involves up and down-regulation of Eif6 expression respectively. The transcriptional state of $Eif6^{+/-}$ satellite cells reveals differential expression of genes related to cell cycle and mitochondrial activity demonstrating that eif6 controls the expression of energy metabolism genes in a cell autonomous manner.

4.2 Methods

4.2.1 Use of existing microarray studies

Six independent studies were used in this analysis. The raw data for each one was downloaded from the NCBI Gene Expression Omnibus (GEO) or provided by the author. The study ID, study title, platform, normalisation method, statistical analysis and experimental conditions of each study are summarised in **table 4.1.**

Study ID	Experiment Title	Conditions	Platform	Normalisation	D.E. Analysis*
GSE9400	Skeletal muscle hypoxia in C57BL mice.	1 week of gradual reduction in O^2 (21% to 10%) followed by 1 week at 10% O^2. Microarray analysis of quadriceps muscle.	Affymetrix MG 430 2.0	RMA (quantile)	SAM (1% FDR)
GSE4330 [247]	Overexpression of PGC-1α in C2C12 myotubes.	Myotubes were infected with adenovirus containing PGC-1α or GFP. Sampling at 0, 24, 48, 72 hours after infection.	Affymetrix U74 Av2	RMA (quantile)	Time-course SAM (10% FDR)
GSE34773 [248]	Skeletal muscle specific PGC-1α knock-out mouse	Microarray profiling of TA muscle	Affymetrix MG 430 2.0	RMA (quantile)	SAM (10% FDR)
GSE3078	Exposure of C2C12 myotubes to H_2O_2.	Myotubes were exposed to 0, 1, 10, 100, 1000μM H_2O_2 for 2 hours.	Affymetrix MG 430A	RMA (quantile)	ANOVA + FDR correction** (10%)
Turan et al. [171]	Comparison of elderly COPD patients vs healthy elderly	Vastus lateralis biopsy and serum protein carbonylation measurements taken from rested patients.	Affymetrix U133 Plus 2.0	RMA (quantile)	SAM (10% FDR)
GSE15155 [252]	Comparison of quiescent and activated satellite cells in mice.	Primary adult satellite cells were isolated and analysed immediately (quiescent) or cultured for 3 days prior to analysis (activated)	Affymetrix U74 Av2	RMA (quantile)	SAM (1% FDR)
GSE10424	Satellite cell differentiation time-course.	Satellite cells were differentiated and collected at 10 time points from 0 to 7 days.	Affymetrix U74 Av2	RMA (quantile)	Time-course SAM (10% FDR)

Table 4.1 – Summary of the studies used in this analysis.

*Method for differential expression analysis. ** Benjamini-Hochberg correction

4.2.2 Additional procedures applied to existing studies

Clustering of the differentially expressed genes in response to H_2O_2 treatment was done using the HOPACH algorithm using the standard parameters (criteria function = median split silhouette (MSS), cluster identification level = MSS, distance matrix = absolute correlation distance). All analysis was performed using the R statistical software package.

To enable us to calculate correlation between physiological measurements and gene expression in the COPD study by Turan et al. the data was transformed into z-scores using the QuantPsych package in the R software. Correlation was calculated using Spearman's rank method. In order to calculate the significance of correlation we used a resampling procedure, as described in chapter 3.2.1.

4.2.3 Eif6$^{+/-}$ satellite cell culture and transcriptional profiling

Young Eif6$^{+/-}$ and wild type mice were sacrificed using cervical dislocation according to the safety and ethical guidelines of the University of Liverpool. Whole hind limb skeletal muscle tissue was dissected. Primary satellite cells were obtained using a pre-plating procedure as described previously [251]. Satellite cells were cultured using DMEM + 20% FCS + 1nM FGFb. Cells were differentiated by switching to differentiation media consisting of DMEM + 2% Horse Serum. All culture media contained antibiotics. Cells were lysed prior to and 24 hours after induction of differentiation by direct addition of RLT buffer (Qiagen) after removal of the media. Each genotype was done in duplicate. RNA was extracted from the cell lysate using RNeasy columns (Qiagen). RNA concentration and purity was assessed using a NanoDrop spectrophotometer, the ratio of 260/280nm was within 1.7-2 for all samples. Amplified cRNA labelled with fluorescent Cy3 dye was generated using the Low-Input Agilent QuickAmp (Agilent, UK) kit as per the manufacturer's instructions. 50ng of labelled cRNA was hybridised to Agilent Mouse G3 Whole Genome microarrays.

Microarrays were scanned using an Agilent SureScan microarray scanner. Raw data was normalised using the Loess method, in which each possible combination of $Eif6^{+/-}$ and $Eif6^{+/+}$ samples were used to calculate fold change ratios. After inspection of the background intensities any probe with a signal intensity of less than 6 across all samples was considered not sufficiently above background and was removed from further analysis. The resulting dataset contains 24,616 probes representing 12,769 unique genes. Differentially expressed genes were detected using a one-sample t-test followed by Benjamini-Hochberg FDR correction with a 10% cut-off. Principle component analysis (PCA) was performed using the R software package.

4.2.4 Functional enrichment analysis

The online gene ontology tool DAVID was used to test for enrichment of functional terms within lists of differentially expressed genes. Terms were deemed significant if the enrichment threshold was less than 10% FDR. Enrichment of transcriptional signatures within network modules was tested using GSEA, as described in chapter 2.2.7.

4.3 Results

4.3.1 Eif6 is up-regulated in mouse hypoxic skeletal muscle

Having demonstrated that eIF6 can induce a coordinated metabolic reprogramming at the gene expression level and that this may be relevant in human muscle ageing we set to identify a micro environmental signal that may be responsible for its transcriptional regulation. We reasoned that elderly individuals show reduced VO2max, a feature that is linked to reduction in muscle oxygenation. Oxygen acts as a potent signalling molecule which controls transcription of hypoxia responsive genes. Hypoxia induces ROS production and acts through the HIF-1α pathway to control transcription of energy metabolism genes [252]. To determine if eIF6 could be a component of the hypoxic response we have analysed a publically available microarray dataset investigating the effect of hypoxia on quadriceps in mice.

Differential expression analysis revealed 3,244 and 3,009 genes up and down-regulated respectively in response to hypoxia (FDR < 1%). Functional analysis (**Table 4.2**) reveals a down-regulation of genes enriched with energy metabolism (*TCA cycle*, *oxidative phosphorylation*, *glycolysis*) and skeletal muscle remodelling (*extracellular matrix*, *collagen*, *muscle tissue development*, *actin cytoskeleton organization*, *regulation of cell adhesion*) functions. Up-regulated genes were enriched in terms related to RNA processing, translation and protein processing (*proteolysis, RNA splicing, ribosomal subunits, translation initiation, protein transport, protein folding, mTOR signalling*). Interestingly, we found that hypoxia stimulates expression of Eif6 by 2.51 fold compared to normoxia (**Figure 4.1A**). In accordance with an increase in expression of Eif6, we found a highly significant overlap between genes down-regulated in response to hypoxia and the genes up-regulated in $Eif6^{+/-}$ muscle (N = 398, 23.8%, $p < 0.001$). Functional analysis of the overlapping genes (**Table 4.3**) revealed enrichment of terms related to energy metabolism (*mitochondrion, TCA cycle, oxidative phosphorylation, fatty acid metabolism*). The expression ratios of these genes in response to hypoxia was consistent with the

change in expression of Eif6 (**Figure 4.1A**). The expression of PGC-1α was stable between normoxic and hypoxic mice (FDR = 41%).

Down-regulated in hypoxia

Term	Category	Count	FDR
CC	Mitochondrion	424	2.80e-59
KEGG	Oxidative phosphorylation	52	1.20e-09
CC	Extracellular matrix	92	2.60e-09
KEGG	TCA Cycle	18	9.30e-06
CC	Sarcoplasmic reticulum	18	6.80e-05
CC	Collagen	13	8.60e-05
BP	Porphyrin metabolic process	14	1.50e-03
BP	Muscle tissue development	40	1.70e-03
CC	Contractile Fibre	30	2.40e-03
MF	Calmondulin binding	31	3.50e-02
BP	Regulation of cell adhesion	27	3.60e-02
KEGG	Glycolysis / Gluconeogenesis	20	4.50e-02
BP	Actin cytoskeleton organization	40	4.80e-02

Up-regulated in hypoxia

Term	Category	Count	FDR
BP	Translation (ribosomes)	126	7.70e-27
BP	RNA processing	146	5.60e-23
BP	Protein transport	173	3.20e-16
BP	Ribosome biogenesis	55	4.90e-16
BP	RNA Splicing	67	5.80e-10
BP	Translation initiation	21	1.90e-06
BP	Chromatin modification	65	4.70e-06
BP	RNA Localisation	28	8.10e-06
BP	Protein folding	39	1.60e-04
BP	Protein transport	32	3.70e-04
BP	Proteolysis	187	3.40e-03
BP	Response to DNA damage stimulus	63	1.10e-02
BP	Programmed cell death	89	8.00e-02
KEGG	mTOR signalling pathway	15	9.10e-02

Table 4.2 – Functional analysis of hypoxic skeletal muscle in mice

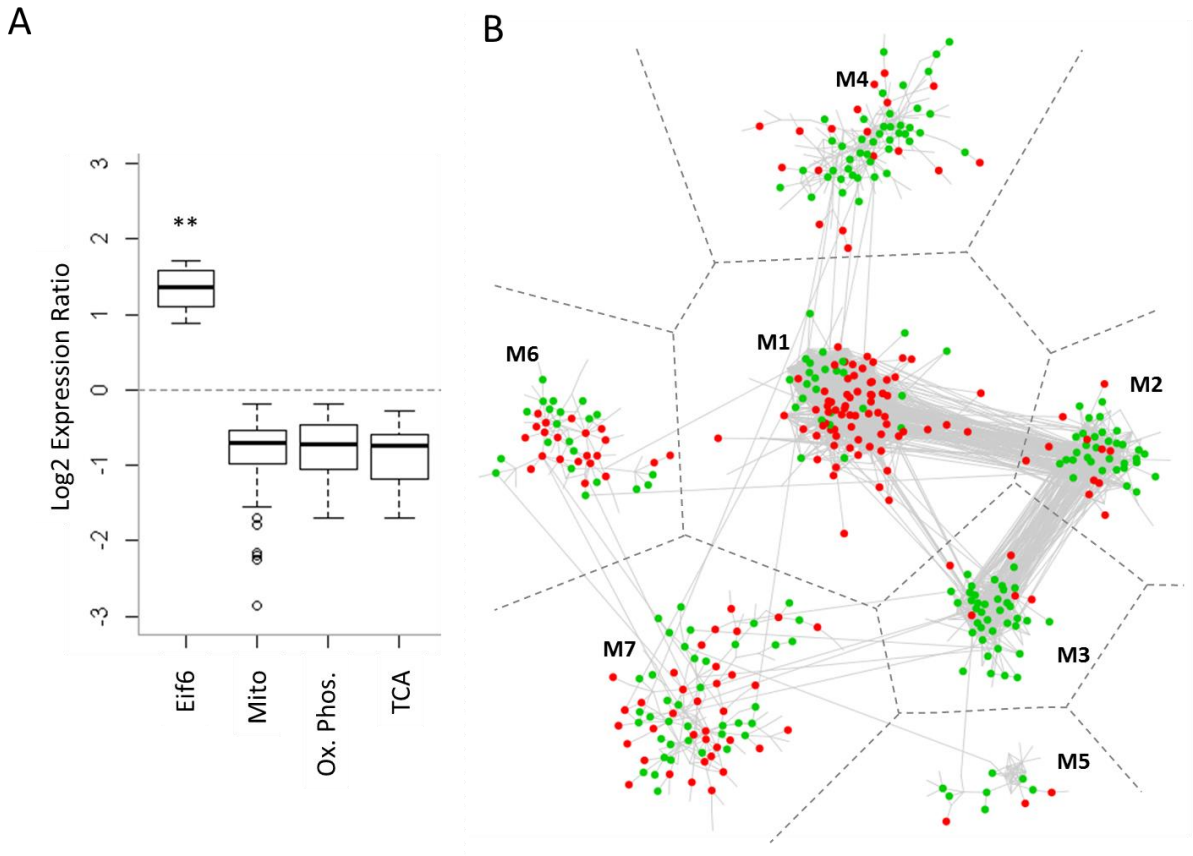

Figure 4.1 – Hypoxia modulates Eif6 expression and targets distinct network modules

Panel A shows the change in expression of Eif6 and putative Eif6 targets in hypoxic muscle. Panel B shows genes modulated by hypoxia mapped to the human muscle network. ** FDR < 1%

Category	Term	Count	FDR
CC	Mitochondrion	104	6.8E-29
KEGG	Oxidative Phosphorylation	22	4.7E-10
KEGG	TCA Cycle	13	5.7E-10
KEGG	Propanoate metabolism	6	9.9E-3
KEGG	Arginine and proline metabolism	7	1.9E-2
BP	Fatty acid metabolic process	13	6.3E-2

Table 4.3 – Functional analysis of genes modulated by hypoxia and Eif6 haploinsufficiency

We mapped the differentially expressed genes to the human muscle network modules and found that a striking 57% (365) of the genes within the network modules are also modulated by hypoxia (**Figure 4.1B**). In accordance with the previously described functional analysis of both the network modules and hypoxic muscle, we found that **module M1** (translation) and **module M2** (Ox Phos.), **M3** (TCA cycle) and **M4** (extracellular matrix remodelling and inflammation) in the network were enriched with up and down-regulated genes respectively ($p < 0.001$).

4.3.2 eIF6 acts up-stream of PGC-1α

Transcription factors such as PGC-1α are known to control expression of genes related to mitochondrial function and mitochondrial biogenesis. In $Eif6^{+/-}$ soleus muscle PGC-1α is up-regulated and Ingenuity network analysis revealed up-regulation of many PGC-1α targets, as shown in the previous chapter. To investigate whether eIF6 is explicitly acting up-stream of PGC-1α to control expression of mitochondrial related genes we analysed two existing microarray studies assessing the transcriptional response to over expression or knock-out of PGC-1α [253] [254]. In muscle specific PGC-1α knock-out mice, the expression of a large subset of 402 genes linked to mitochondrial function is co-ordinately down-regulated, as described in Finley et al. [254]. However in the same study Eif6 expression is comparable to wild type ($p = 0.4455$) (**Figure 4.2A**).

In a study conducted by Calvo et al. [253] the effects of overexpression of PGC-1α in cultured C2C12 cells differentiated into myotubes was investigated. Three days after induction of PGC-1α expression 1165 and 217 up and down-regulated genes respectively were differentially expressed. However, no change in Eif6 expression was seen ($p = 0.4788$). There is a highly significant overlap between the genes up-regulated by PGC-1α overexpression and the genes up-regulated in $Eif6^{+/-}$ soleus muscle (N= 221, 20.1%, p = 1.27e-20), and as expected this overlap is highly enriched with genes related to energy metabolism (*TCA Cycle, oxidative phosphorylation, mitochondrial ribosomes, mitochondrial protein targeting*) (**Table 4.4**). In the human muscle network, **module M2** (ox. phos.) and **module M3** (TCA cycle) were highly enriched with genes up-regulated by PGC-1α (**Figure 4.2B**).

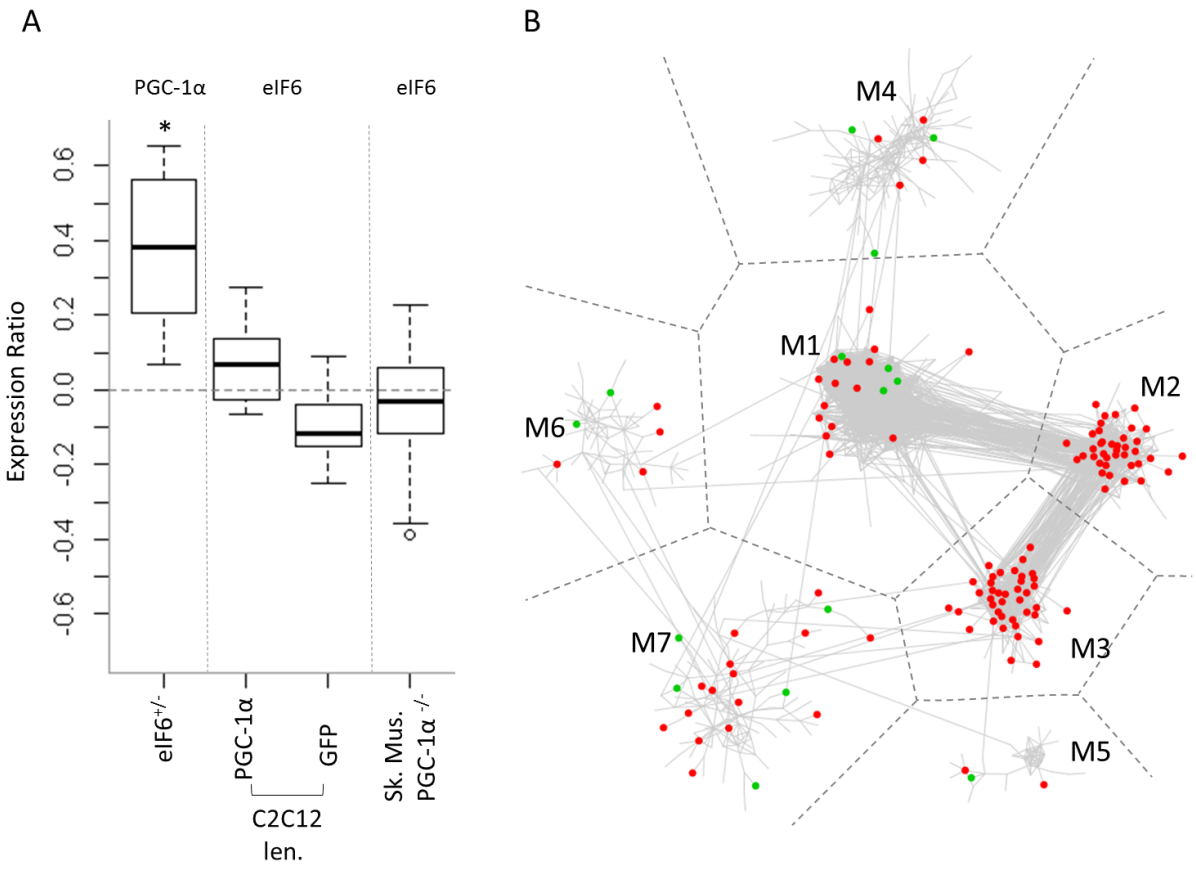

Figure 4.2 – PGC-1α is down-stream of eIF6 and targets module M2 and M3 in the muscle network

Panel A shows differential expression of PGC-1α in Eif6$^{+/-}$ muscle and stable expression of Eif6 in response to lentiviral induced PGC-1α overexpression in myotubes (C2C12) and muscle specific PGC-1α knock-out in mice. Panel B shows enrichment of PGC-1α targets in module M2 and M3 (FDR < 0.01%). * FDR < 5%

Category	Term	Count	FDR
CC	Mitochondrion	103	3.8E-55
KEGG	TCA Cycle	13	2.3E-12
KEGG	Oxidative phosphorylation	19	9.9E-11
KEGG	Valine, leucine and isoleucine degredation	8	1.3E-4
CC	Mitochondrial ribosome	6	2.0E-3
BP	Protein targeting to mitochondrion	5	8.7E-3

Table 4.4 – Functional analysis of the overlap between PGC-1α and Eif6$^{+/-}$ targets

4.3.3 Expression of Eif6 is increased in response to high levels of hydrogen peroxide

The production of reactive oxygen species (ROS) is intrinsic to mitochondrial oxidative metabolism. Damage to proteins caused by ROS builds up as we age. This is thought to be caused by an inability to increase expression of antioxidant proteins. In the Eif6$^{+/-}$ soleus muscle there is increased mRNA expression of genes with antioxidant function such as superoxide dismutase 2 (SOD2) and catalase (CAT), which act in the mitochondria to convert superoxide and hydrogen peroxide to water and oxygen. To determine if expression of Eif6 is regulated by oxidative stress we have analysed an existing microarray dataset in which C2C12 cells were differentiated into myotubes and then exposed to a range of concentrations of hydrogen peroxide. We identified 1,845 differentially expressed genes in response to H_2O_2 treatment (FDR < 5%). Clustering of these genes revealed 4 clusters each representing a distinct transcriptional response to H_2O_2 treatment. Eif6 is significantly up-regulated in response to H_2O_2 treatment (**Figure 4.4**) and is found in cluster 2 (**Figure 4.3**). We have used functional analysis to further characterise each cluster. Cluster 2 represents genes strongly up-regulated in response to high concentrations of H_2O_2 and is enriched with terms such as apoptosis, oxidative phosphorylation, glucose metabolism, response to oxidative stress and cytokine activity. We identified 182 and 76 genes up and down-regulated respectively in the Eif6$^{+/-}$ soleus muscle that were also differentially expressed in response to H_2O_2 treatment. However the overlap was not significant for either (up: $p = 0.2939$, down: $p = 0.26088$), neither was there a clear indication that these genes may respond to H_2O_2 and eIF6 depletion in a similar way. It is worth noting that although expression of Eif6 is significantly increased in response to H_2O_2, the dynamic range across all samples is low (maximum fold change 1.25) compared to the dynamic range across the clinical samples in the muscle meta-analysis dataset (young fold change= 2.39, elderly fold change = 2.58). In conclusion, Eif6 expression is induced by very high concentrations of H_2O_2 in myotubes, but there is no evidence for accompanying regulation of genes differentially expressed in the Eif6$^{+/-}$ muscle.

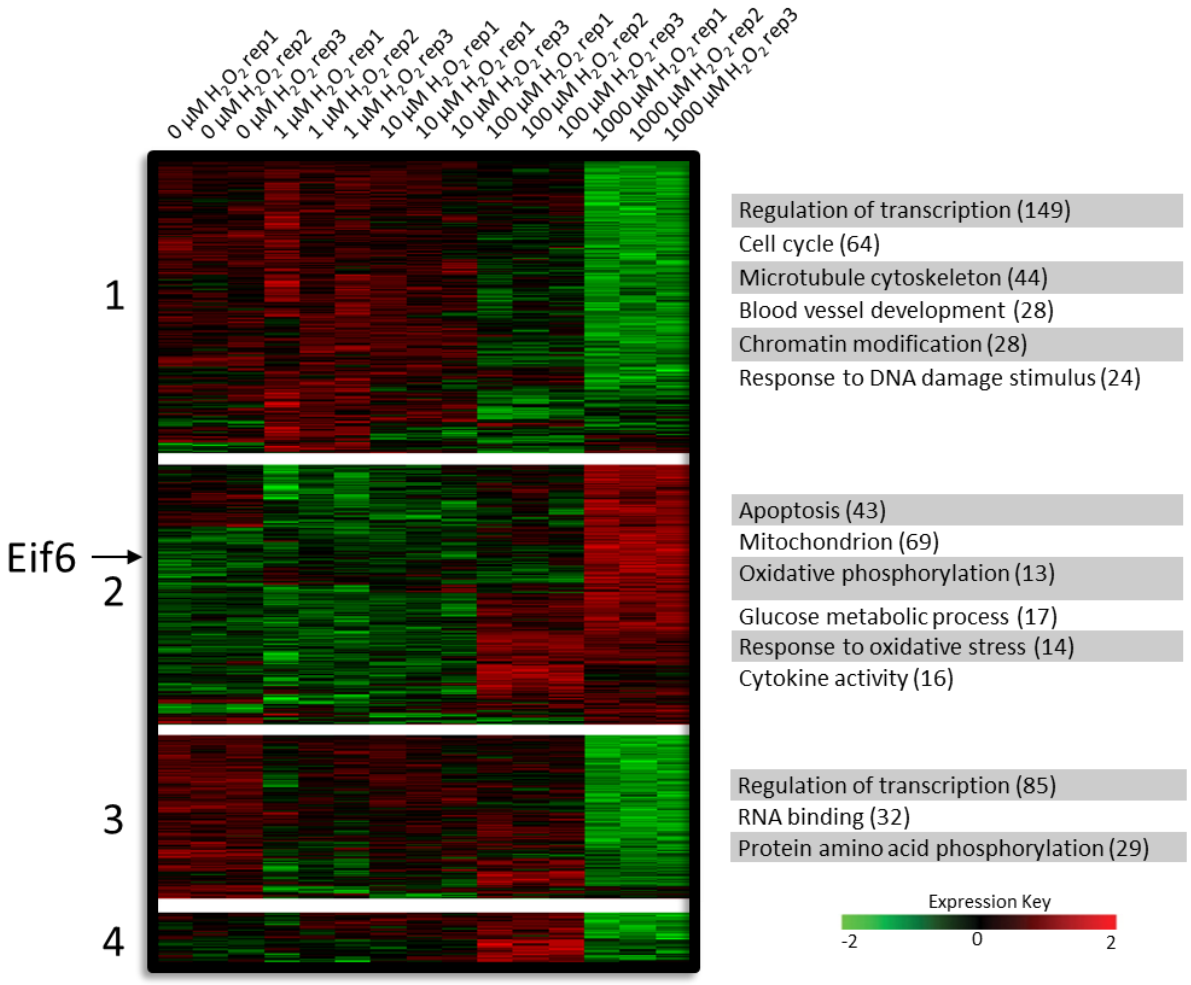

Figure 4.3 – Cluster analysis of genes modulated by H_2O_2

This figure shows the cluster analysis of genes differentially expressed in response to H_2O_2 treatment (FDR < 5%). Functional associated with each cluster were enriched (FDR <10%).

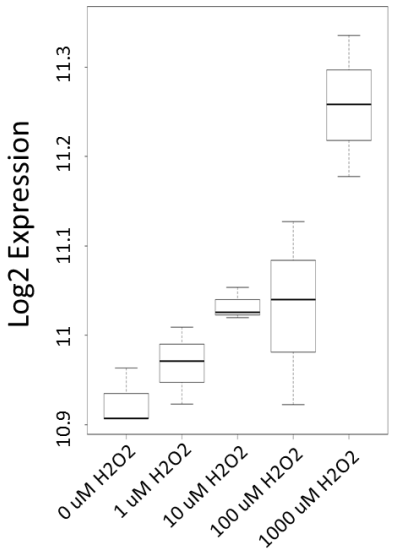

Figure 4.4 – Eif6 expression in response to H_2O_2 treatment
Expression of Eif6 was dose-dependent (ANOVA p = 2.78e-5)

4.3.4 Expression of EIF6 modulates genes linked to an increase in serum protein carbonylation

One consequence of ROS induced damage is irreversible carbonylation of proteins, which can be detected in tissues and serum. Using a clinical study incorporating transcriptional profiling and physiological measurements across 49 individuals, published by Turan et al. [174], we have investigated whether EIF6 expression is predictive of ROS induced protein carbonylation. The study includes COPD patients with normal (n = 14) and low BMI (n = 12) as well as healthy volunteers (n = 23).

We found that EIF6 expression is not correlated to levels of protein carbonylation in muscle or serum from healthy volunteers, or COPD patients. However, 59 genes from mitochondrial energy metabolism pathways (TCA cycle, ox. phos., fatty acid metabolism) such as UQCRC1 (**Figure 4.5C**) and NDUFV1 (**Figure 4.5D**) are negatively correlated to serum protein carbonylation in healthy muscle (FDR < 5%). This is reduced to 18 genes in COPD patients with normal BMI and 0 in COPD patients with low BMI. We found that 26/59 (44%, p = 0.007) of the energy metabolism genes correlated to

serum protein carbonylation in healthy muscle are also up-regulated in the Eif6$^{+/-}$ soleus muscle (**Figure 4.5A**). This number is reduced to 4/14 (28.6%, p = 0.84) in COPD patients with normal BMI (**Figure 4.5B**), and 0% overlap in patients with low BMI. There was some evidence at a nominal p-value threshold that expression of EIF6 was correlated with 55 energy metabolism genes such as ATP5J (**Figure 4.5E**), which is significantly correlated to carbonylation levels (**Figure 4.5F**). However after correction for multiple testing these correlations were non-significant (FDR > 10%).

In summary, genes involved in mitochondrial metabolism are highly correlated to serum protein carbonylation and there is a significant overlap with genes regulated by Eif6 haploinsufficiency. From this we could predict that increased Eif6 expression in elderly muscle could be indicative of increased ROS damage, and individuals with lower Eif6 expression may benefit from increased expression of energy metabolism genes and lower ROS damage.

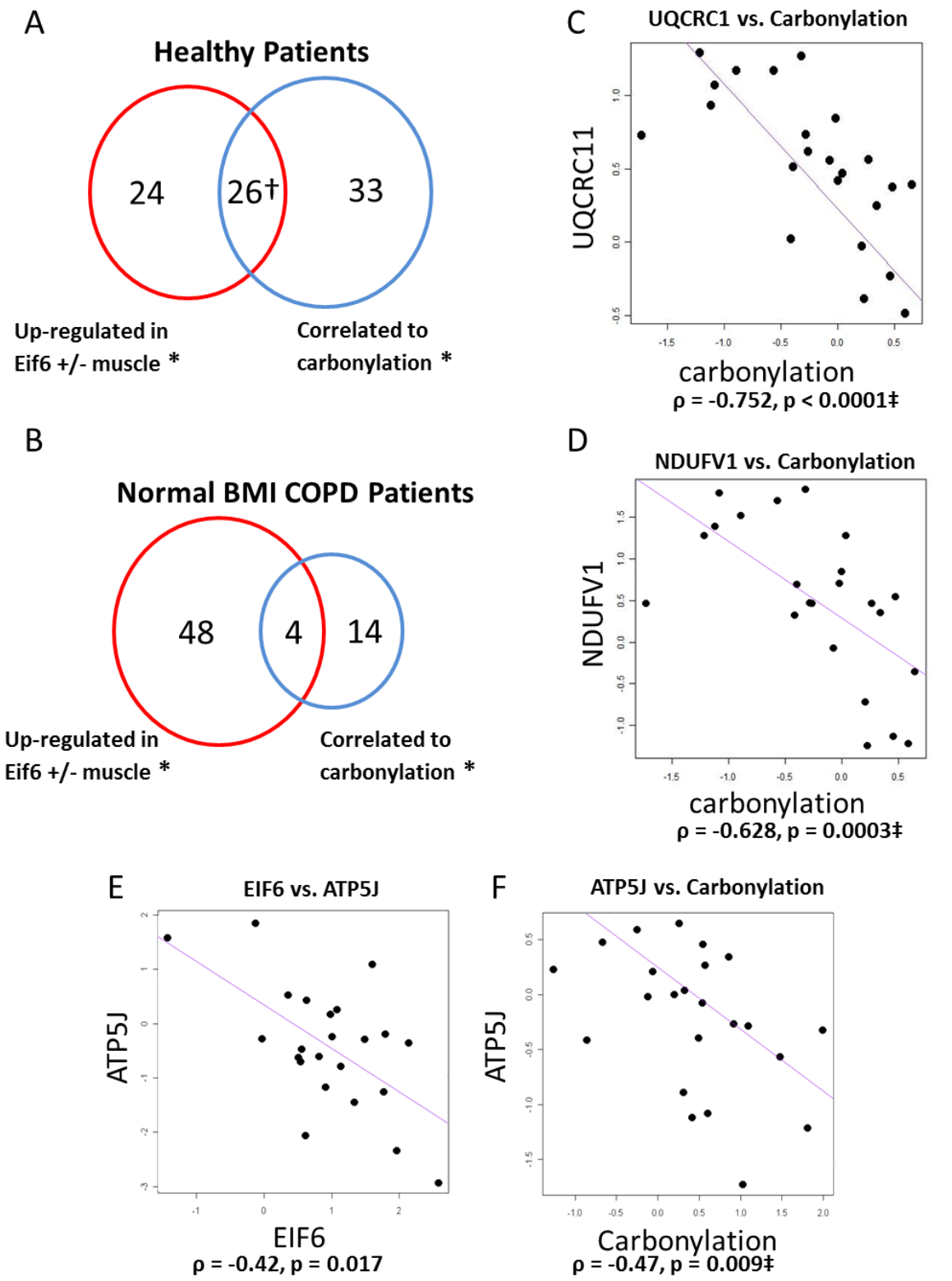

Figure 4.5 – Energy metabolism genes linked to ROS damage are regulated by Eif6 haploinsufficiency

Panel A and B show the overlap of genes up-regulated in Eif6$^{+/-}$ muscle (red) and genes correlated to carbonylation measurements in the clinical data (blue). Panel C and D show scatter plots of oxidative phosphorylation subunit gene expression and carbonylation in healthy muscle. Panel E and F show scatter plots of EIF6 expression and carbonylation in healthy muscle. * Significant at < 5% FDR, ‡ Significant at < 5% FDR. † Significant overlap, p = 0.007.

4.3.5 Eif6 is up-regulated during skeletal muscle satellite cell activation

So far we have focused on the effects of Eif6 haploinsufficiency within a whole muscle environment. However, an important component of muscle biology with implications for muscle growth and regeneration is proliferation and differentiation of skeletal muscle satellite cells (myoblasts). Genes important for satellite cell proliferation and differentiation are differentially expressed in Eif6$^{+/-}$ soleus muscle such as IGF1 [255], and NOTCH1 [247]. Furthermore, eIF6 regulates many genes related to mitochondrial activity, which has recently been shown to regulate myogenic differentiation [256] [257]. We decided to investigate if eIF6 could play a role in satellite cell function. We identified a microarray study available in the GEO database [258] to investigate the transcriptional profile of quiescent and activated satellite cells.

We identified 758 and 620 up and down-regulated genes respectively in activated satellite cells compared to quiescent cells (FDR < 1%). Consistent with re-entry of the satellite cells into the cell cycle, functional analysis (**Table 4.5)** of the up-regulated genes revealed enrichment of terms relating to proliferation and growth (cell cycle, tRNA metabolism, rRNA processing, mRNA transport), metabolism (glutathione metabolism, mitochondrion, protein catabolic process) and nuclear functions (Nucleolus, response to DNA damage stimulus, chromatin modification, DNA packaging). The down-regulated genes are enriched in terms related to tissue remodelling (extracellular matrix, cell adhesion, regulation of inflammatory response, vasculature development) and development (developmental growth, skeletal system development, cell fate commitment).

Interestingly, we found that Eif6 expression is up-regulated in activated satellite cells (fold change = 1.58) (**Figure 4.6A**). Consistent with inverse Eif6 expression, this is accompanied by a significant overlap of genes up-regulated in Eif6$^{+/-}$ soleus muscle and down-regulated in activated satellite cells (373, p = 2.64e-10). We examined the overlapping genes using functional analysis (**Figure 4.6B**). This analysis suggests that eIF6 may play a role in regulating gene expression during the activation of quiescent satellite cells by down-regulating genes related to apoptosis, extracellular matrix processes (including FGFR1, CYR61, and TGFB3) and transcription factors.

Up-regulated in activated satellite cells

Category	Term	Count	FDR
CC	Nucleolus	58	1.10e-23
BP	rRNA processing	25	1.00e-13
BP	Cell cycle	61	1.50e-08
BP	tRNA metabolic process	23	8.70e-08
BP	mRNA transport	15	1.00e-05
BP	Response to DNA damage stimulus	33	1.30e-05
BP	Chromatin modification	28	5.50e-05
KEGG	Glutathione metabolism	12	2.30e-04
CC	Mitochondrion	70	5.80e-04
BP	RNA splicing	23	8.90e-04
BP	Intracellular transport	36	2.40e-03
BP	Protein catabolic process	41	8.90e-03
BP	DNA packaging	13	2.50e-02

Down-regulated in activated satellite cells

Category	Term	Count	FDR
CC	Extracellular matrix	33	2.60e-07
BP	Developmental growth	16	5.60e-04
MF	Transcription factor activity	50	7.00e-04
BP	Cell adhesion	39	2.20e-03
BP	Skeletal system development	24	6.10e-03
BP	Regulation of inflammatory response	10	7.20e-03
BP	Cellular ion homeostasis	22	9.80e-03
BP	Response to hormone stimulus	16	1.80e-02
BP	Cell fate commitment	15	1.80e-02
BP	Endocytosis	16	4.50e-02
BP	Vasculature development	19	4.80e-02
BP	Regulation of MAP kinase activity	10	4.90e-02
BP	Transmission of nerve impulse	17	7.40e-02

Table 4.5 – Functional analysis of differentially expressed genes in activated satellite cells

A

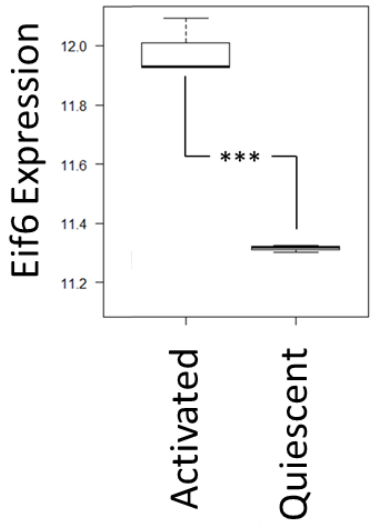

B

Category	Term	Count	FDR
BP	Positive regulation of transcription	26	1.70e-03
BP	Positive regulation of apoptosis	16	1.30e-02
BP	Response to temperature stimulus	7	4.30e-02
CC	Neuron projection	15	6.20e-02

Figure 4.6 – Activation of satellite cells induces expression of Eif6 and genes modulated by Eif6 haploinsufficiency

Panel A shows Eif6 expression is increased in activated (in culture for 72 hours) satellite cells. Panel B shows enrichment of functional terms in genes overlapping between satellite cell activation (down-regulated) and Eif6 haploinsufficiency (up-regulated). *** $p < 0.001$

4.3.6 Eif6 is down-regulated during muscle satellite cell differentiation

The process of satellite cell activation, proliferation and differentiation is a dynamic process involving distinct transcriptional reprogramming at each stage [259] [248]. One of the key properties of muscle regeneration is an overall increase in mitochondrial biogenesis, expression of mitochondria related genes and respiration [260]. In fact, inhibiting mitochondrial function in myoblasts blocks differentiation [256]. We reasoned that Eif6 could be regulated during satellite cell differentiation. We analysed transcriptional profiles of differentiating satellite cells from 0hrs to 7 days.

We utilised a study created by the Ontario Genomics Innovation Centre which is available in the GEO database (GSE10424). We found that 2098 and 1624 genes are up and down-regulated respectively during satellite cell differentiation (FDR < 10%). We used functional analysis to further characterise

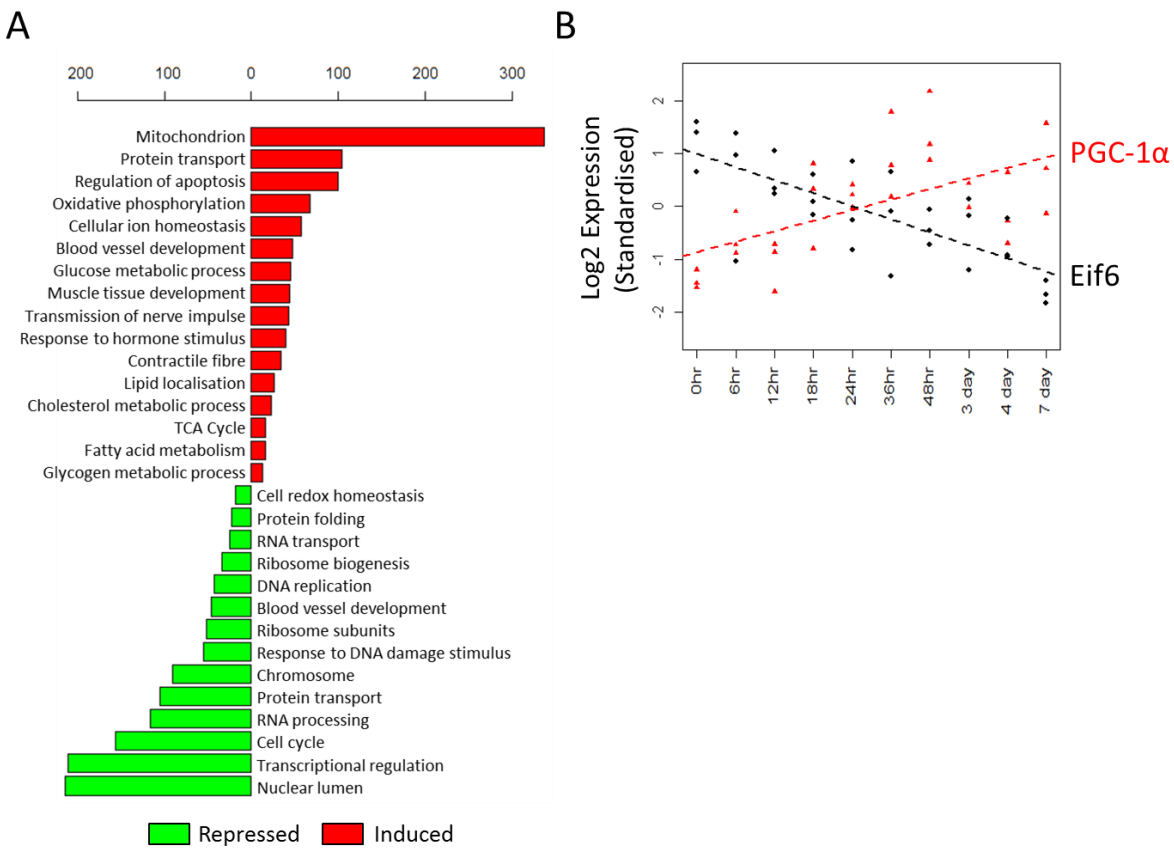

Figure 4.7 – The functional profile of differentiating satellite cells is consistent with the expression of Eif6 and PGC-1α

Panel A shows the functional profile of differentiating satellite cells, ranked by the number of genes in each functional term. Panel B shows the expression profile of Eif6 and PGC-1α during satellite cell differentiation (FDR < 10%).

Category	Term	Count	FDR
CC	Mitochondrion	86	4.0e-21
KEGG	TCA Cycle	12	2.4e-8
KEGG	Oxidative phosphorylation	18	1.9e-6
KEGG	Valine, leucine and isoleucine degredation	8	3.5e-3
CC	Adherens junction	9	2.7e-2
BP	Positive regulation of cell division	6	6.9e-2
KEGG	Fatty acid metabolism	6	7.6e-2
CC	Mitochondrial outer membrane	7	9.2e-2

Table 4.6 – Functional analysis of genes up-regulated during satellite cell differentiation and Eif6 haploinsufficiency

the differentially expressed genes (**Figure 4.7A**). Genes up-regulated during differentiation were enriched with terms related to energy metabolism (*mitochondrion, oxidative phosphorylation, glucose metabolic process, fatty acid metabolism, glycogen metabolic process and lipid localisation*), muscle development (*contractile fibre, muscle tissue development, blood vessel development, transmission of nerve impulse*). The down-regulated genes were enriched with terms relating to cell cycle (*DNA replication, chromosome, cell cycle*), translation (*ribosomal subunits, RNA transport, ribosome biogenesis*), *response to DNA damage stimulus* and *cell redox homeostasis*.

Importantly, we found that expression of Eif6 is down-regulated during the satellite cell differentiation time course (**Figure 4.7B**). This was accompanied by a co-ordinate up-regulation of PGC-1α. This matches our prediction that Eif6 could control energy metabolism genes in differentiating satellite cells. We examined the overlap between genes differentially expressed in the $Eif6^{+/-}$ soleus and during satellite cell differentiation. We found that the only significant overlap ($n = 366$, $p < 0.001$) is between genes up-regulated both in response to eIF6 depletion and during satellite cell differentiation. Functional analysis of the 366 overlapping genes (**Table 4.6**) confirmed that these were enriched with terms related to mitochondrial function (oxidative phosphorylation, TCA cycle, fatty acid metabolism). Also included in the overlap were genes related to adherens junctions and regulation of cell division, which includes the growth factors FIGF (VEGFD), FGF5, PDGFB, TGFB1 and VEGFB.

Expression of Eif6 is increased during satellite cell activation, where it appears to be uncoupled from expression of genes related to mitochondrial function. However during satellite cell differentiation Eif6 expression is decreased, accompanied by a coordinate increase in expression of genes related to mitochondrial function and respiration, which significantly overlap with genes differentially expressed in response to Eif6 haploinsufficiency in whole muscle.

4.3.7 Transcriptional profiling of Eif6$^{+/-}$ primary satellite cells reveals differential expression of energy metabolism genes

We have shown that Eif6 haploinsufficiency causes a significant transcriptional reprogramming in whole muscle. To investigate whether Eif6 haploinsufficiency may cause cell autonomous effects in satellite cells we analysed Eif6$^{+/-}$ and Eif6$^{+/+}$ primary satellite cells during proliferation (0 hours) and after induction of differentiation (24 hours).

We used principle component analysis (PCA) to visually assess the variation between the samples. The wild type and Eif6$^{+/-}$ cell were separated, and there was a similar response to induction of differentiation in both cell types (**Figure 4.8**).

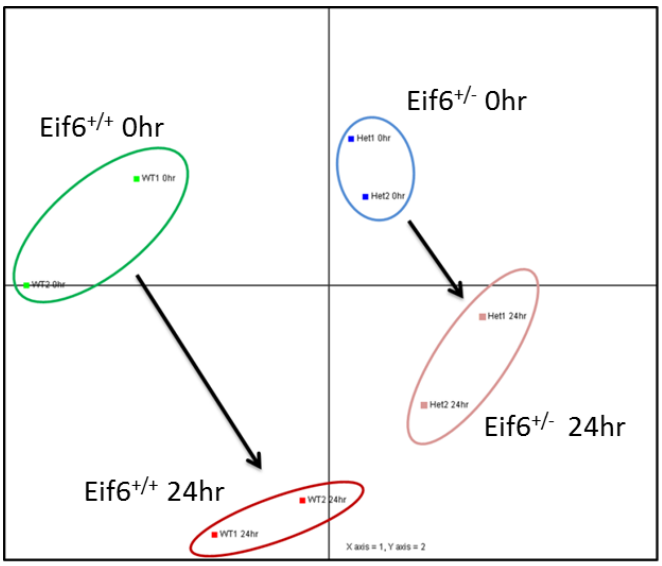

Figure 4.8 – PCA reveals a similar response to induction of differentiation in Eif6$^{+/+}$ and Eif6$^{+/-}$ satellite cells

We identified differentially expressed genes between Eif6$^{+/-}$ and Eif6$^{+/+}$ cells at 0 and 24 hours and between 0 hours and 24 hours in each genotype respectively (FDR < 10%). Eif6 expression was not significantly altered between 0 and 24 hours in either cell type. We found that the largest numbers of differentially expressed genes were between 0 hours and 24 hours regardless of genotype, however

Test	Up-regulated	Down-regulated
eIF6 +/+ 0hr vs eIF6 +/- 0hr	828	668
eIF6 +/+ 24hr vs eIF6 +/- 24hr	1109	1339
eIF6 +/+ 0hr vs eIF6 +/+ 24hr	2678	1976
eIF6 +/- 0hr vs eIF6 +/- 24hr	2111	2004

Table 4.7 – Differentially expressed genes between satellite cells

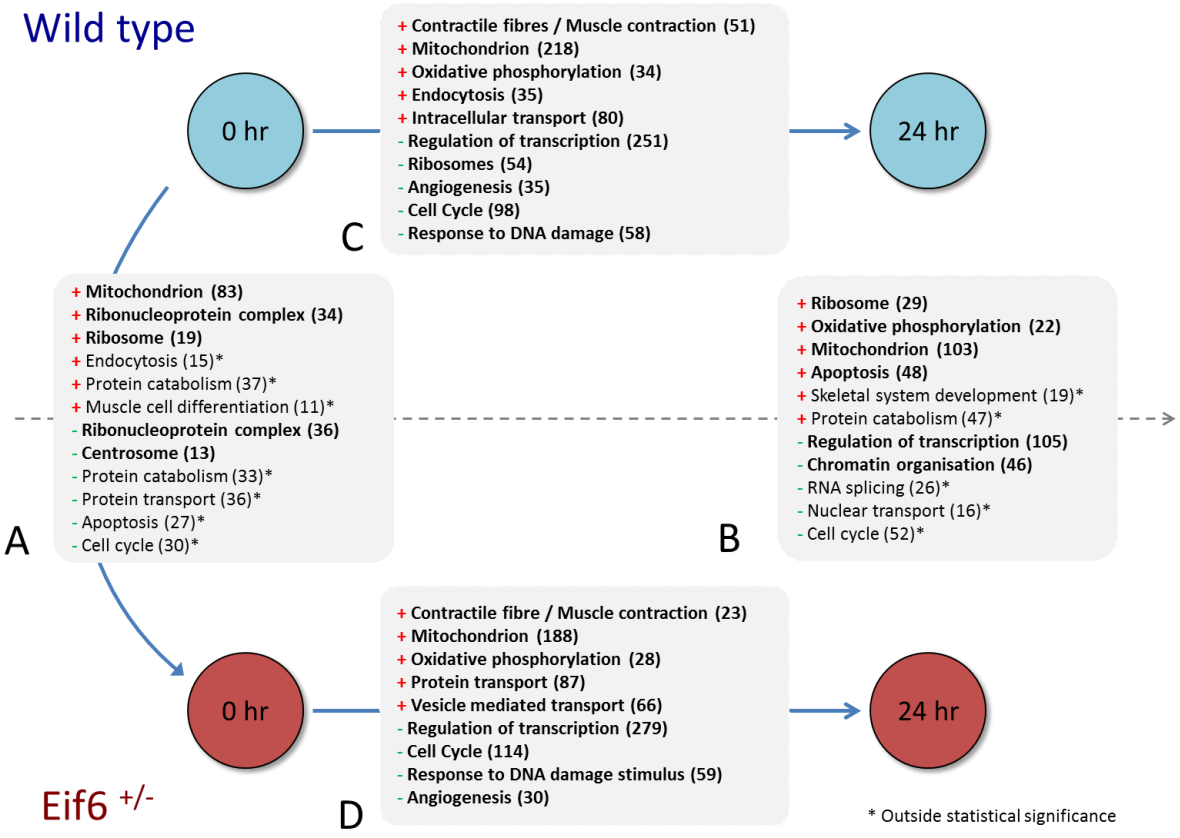

Figure 4.9 – The functional profiles of Eif6$^{+/-}$ satellite cells reveal cell autonomous effects

Box A and B summarise the functional analysis between wild type and Eif6$^{+/-}$ cells at both time points. Box C and D summarise the functional changes between 0hrs and 24hrs in both cell types.

there are a significant number of genes differentially expressed between the Eif6$^{+/+}$ and Eif6$^{+/-}$ cells at both time points (**Table 4.7**). We characterised these differentially expressed genes using functional analysis. This revealed substantial transcriptional reprogramming in both proliferating and differentiating cells. The functional profiles of cells at 0 and 24 hours in both cell types was consistent

with induction of differentiation, with both cell types up-regulating muscle fibre components and mitochondrial genes and down-regulating transcription factors and cell cycle linked genes (**Figure 4.9C-D**).

A comparison of proliferating Eif6$^{+/-}$ and Eif6$^{+/+}$ cells (**Figure 4.9A**) revealed genes related to mitochondrial function, including components of energy metabolism enzymes (Atp5d, Uqcrc2, Ndufs2, Ndufc1), ribosomal subunits and muscle cell differentiation were up-regulated. Interestingly, genes involved in apoptosis and cell cycle were down-regulated. This suggests a potential alteration in proliferative capacity in Eif6$^{+/-}$ satellite cells. Remarkably, functional analysis of the genes differentially expressed at 24 hours in Eif6$^{+/-}$ compared to Eif6$^{+/+}$ cells (**Figure 4.9B**) revealed up-regulation of 22 oxidative phosphorylation enzyme subunits and enrichment of ribosomal subunits and genes associated to mitochondrion, apoptosis and skeletal system development (including Myod1 and myogenin). The down-regulated genes were associated with regulation of transcription (including c-Myc, calcineurin), chromatin organisation, nuclear transport, RNA splicing and cell cycle. We noticed that functional profiles between genotypes at 24 hours have terms in common with the changes seen between 0 and 24 hours (oxidative phosphorylation, mitochondrion, regulation of transcription and cell cycle) (**Figure 4.9C-D**), and that this was specific to the differentiating cells. This suggests that the Eif6$^{+/-}$ cells could have altered differentiation capacity. This is supported by the fact that MyoD and myogenin are up-regulated in Eif6$^{+/-}$ cells compared to Eif6$^{+/+}$ at 24 hours.

4.4 Discussion

4.4.1 Eif6 expression is controlled by hypoxia

The transcriptional profiling of hypoxic skeletal muscle in mice has revealed a co-ordinate down-regulation of genes involved in mitochondrial metabolism, consistent with a decrease in mitochondrial content [252]. Eif6 expression is induced by hypoxia in a manner consistent with our results revealing reprogramming of energy metabolism genes in Eif6 haploinsufficient muscle. The expression of PGC-1α is up-regulated by depletion of eIF6, and we were able to show that eIF6 acts up-stream of PGC-1α in muscle. PGC-1α is activated in response to increased ATP demand, and is induced by exercise and hypoxia [261] [102]. However, in the study we analysed chronic hypoxia failed to module PGC-1α expression. ATP demand in mice kept in chronic hypoxic conditions is likely to be low due to severely decreased activity levels. This suggests that up-regulation of PGC-1α in $Eif6^{+/-}$ muscle could be due to an ATP dependent mechanism. We have shown that eIF6 controls a metabolic reprogramming at the transcriptional and protein level in healthy, unchallenged, young mice. Future experiments investigating the metabolic capacity of muscle from $Eif6^{+/-}$ mice during hypoxia and exercise will be valuable in determining the physiological consequences of Eif6 haploinsufficiency.

Hypoxia is thought to be a cause of ROS formation in skeletal muscle during exercise and disease states such as COPD exacerbations [262]. There is some evidence for ROS mediated expression of Eif6 in myotubes treated with hydrogen peroxide. However this modest change in expression was achieved at a very high concentration of H_2O_2 unlikely to be found in skeletal muscle. We did identify a link between genes regulated by Eif6 haploinsufficiency and serum protein carbonylation, a marker of oxidative stress [61], in a clinical study of healthy, elderly muscle. Energy metabolism genes that are highly negatively correlated to levels of carbonylation are up-regulated in $Eif6^{+/-}$ muscle. This suggests that levels of ROS formation in muscles under-expressing Eif6 could be reduced. This is

supported by the up-regulation of mRNA for anti-oxidant enzymes such as catalase and superoxide dismutase 2 (Sod2) in Eif6$^{+/-}$ muscle.

4.4.2 Eif6 controls gene expression in satellite cells in a cell-autonomous manner

By examining two existing expression profiling studies of satellite cells we revealed that Eif6 expression is increased in activated satellite cells and reduced during differentiation. PGC-1α expression was reduced in line with Eif6 during differentiation. The reason for an up-regulation of Eif6 in activated satellite cells remains unclear. Activation of satellite cells involves re-entry in to the cell cycle and therefore an increase in translation and growth. The increase in expression of Eif6 could facilitate this growth by increasing the availability of mature 60S ribosomal subunits [232] [234].

Analysis of a time-course of satellite cell differentiation revealed a down-regulation of Eif6 in differentiated cells. This was in parallel with an up-regulation of PGC-1α and a significant number of putative eIF6 targets involved in energy metabolism. The analysis of the existing studies led us to hypothesise that eIF6 could play a role in satellite cell differentiation. We generated transcriptional profiles of proliferating and differentiating Eif6 haploinsufficient satellite cells and discovered an extensive transcriptional reprogramming. This was characterised by alterations in mitochondrial genes consistent with the changes seen in the whole muscle. We also found a large number of transcription factors and genes related to cell cycle and apoptosis were altered. This included the myogenic factors myogenin and Myod which were expressed higher in the Eif6$^{+/-}$ cells 24 hours after inducing differentiation. The expression of myogenin is a marker of terminal differentiation in myoblasts and is necessary for the exit of the cell cycle [263]. Higher expression of myogenin was consistent with the functional analysis which revealed down-regulation of 52 cell cycle related genes in Eif6$^{+/-}$ satellite cells. This suggests that Eif6$^{+/-}$ satellite cells may have an increased differentiation capacity.

During myogenic differentiation there is an increase in mitochondrial complex activity, suggesting that the shift from glycolytic metabolism to oxidative phosphorylation occurs during differentiation. A number of studies have highlighted the importance of mitochondrial biogenesis and oxidative phosphorylation during stem cell differentiation [264] [256]. Inhibitors of mitochondrial RNA synthesis, protein synthesis and mtDNA replication have negative effects on myogenesis. A recent study by Jash and Adhya [265] has shown that artificial introduction of the mitochondrial genome into injured muscle increases expression of mitochondrially encoded genes, respiratory capacity and ATP levels while promoting muscle recovery. It also increases differentiation capacity of satellite cells and expression of myogenic factors including myogenin and Myod. We found that expression of c-Myc, which is an important player in preventing the differentiation of myoblasts [266], is significantly lower in differentiating Eif6$^{+/-}$ satellite cells. Seyer et al. have shown that inhibition of mitochondrial activity with chloramphenicol prevents the down-regulation of c-Myc normally associated with satellite cell differentiation [257]. In a follow up study Seyer et al. revealed that inhibition of mitochondrial protein synthesis reduces calcineurin expression [267]. Calcineurin stimulates myoblast differentiation and increases expression of myogenin. The expression of the alpha and beta subunit of calcineurin is higher in Eif6$^{+/-}$ satellite cells compared to wild type 24hours after inducing differentiation. This supports the hypothesis that Eif6$^{+/-}$ satellite cells have an altered differentiation capacity.

CHAPTER 5

MODELLING THE INTERACTION BETWEEN TUMOUR AND STROMA IN AN IN VIVO MODEL OF ANGIOGENESIS

The work presented in this chapter represents a collaborative project between the labs of Francesco Falciani (Liverpool), Roy Bicknell (Birmingham) and Andreas Bikfalvi (CNRS). The Bikfalvi lab completed the in vivo implantation of glioblastomas on the CAM, collected tissue samples, provided the raw microarray data for VEGF treatment of the CAM and provided morphological data (published previously [268]*). Sarah Durant (jointly in Falciani and Bicknell laboratories) completed the microarray expression profiling of the glioblastoma implantation time-course and the cell culture work for the U87 treatments. Rita Gupta in the Falciani lab developed the ODE-based network inference methodology and applied it to the implantation time-course data. Kim Clarke (Falciani lab) performed all the computational analysis described in this chapter, performed the microarray expression profiling analysis of the U87 cytokine and growth factor treatments, validated the ODE-based models and formulated the biological interpretation and hypothesis formulation.*

5.1 Introduction

Angiogenesis is the process by which new blood vessels form from the existing vasculature. This process is vital for a range of processes including wound healing, response to aerobic exercise and tumour development. Tumours are unable to grow larger than 1-2mm^3 [269] without the initiation of angiogenesis to increase oxygen availability.

Angiogenesis is controlled by a complex network of pro and anti-angiogenic factors that regulate the "angiogenic switch" between vascular growth and regression [270]. Despite intensive research efforts the precise mechanism underlying the network of interactions between growth factors, cytokines and extracellular matrix proteins remains only partially understood. Functional genomics technologies have enabled measurements of genes, proteins and metabolites to an unprecedented level of resolution. The application of transcriptomics technologies such as microarrays to the study of angiogenesis has generally been used to investigate the role of a single protein or compound of interest in a model system, primarily endothelium *in vitro* (e.g. VEGF [271], angiopoietin-1 [272], TGF-β [273], BMP6 [274], stem cell factor [275]. More recently, hypothesis generating transcriptomics approaches have successfully identified angiogenesis related expression signatures in a physiological setting such as the chorio-allantoic membrane [276] and tumours [156]. This has revealed novel

biomarkers of tumour status such as insulin-like growth factor receptor and epidermal growth factor receptor [277]. A recent proteomics study [278] addressed the important question of whether blood vessels within tumours exhibit specific protein expression by analysing the entire proteome of micro-dissected capillaries. Despite the challenge of obtaining sufficient material from micro-dissected blood vessels, they were able to identify a protein signature specific for tumour angiogenesis. Other proteomics studies have so far focused on endothelial cells outside of the context of angiogenesis.

However, none of these approaches have truly provided novel mechanistic understanding of this important biological process. In order to address this issue we have applied a reverse engineering approach to a well-established *in vivo* model of angiogenesis, the chicken egg chorio-allantoic membrane (CAM) [279]. The CAM forms the equivalent of the mammalian placenta in eggs of some amniotes.

The CAM is an attractive model to study angiogenesis compared to other existing animal models. Morphological and gene expression data can be obtained easily in a short time frame throughout the development of the vascularised tumour with minimal levels of animal suffering. Glioblastomas implanted on the CAM show many of the hallmarks of the human tumour [268]. We have implanted glioblastoma cells on to the chicken egg CAM, which rapidly form a solid tumour and progressively becomes vascularised during the first week of implantation, as previously described [268] (**Figure 5.1A**). Using whole genome transcriptional profiling and network inference methods we set out to develop a detailed analysis of the changes underlying tumour vascularisation and shed light on the interactions between the tumour and stromal tissue.

We discovered a substantial transcriptional reprogramming in both the tumour and the stroma during the vascularisation of the tumour. We show that genes linked to hallmarks of tumour progression including cell proliferation and angiogenesis are modulated in both the tumour and the stroma. Gene clustering revealed a complex pattern of transcriptional response during the course of the implantation. The analysis of co-expression networks constructed using expression profiles from both the tumour and stroma has shed light on the temporal dynamics of the transcriptional changes

underlying angiogenesis. Furthermore, application of a novel ODE-based network inference method links expression of key growth factors, cytokines and extracellular matrix (ECM) remodelling factors and suggests a central role for IL1α during angiogenesis.

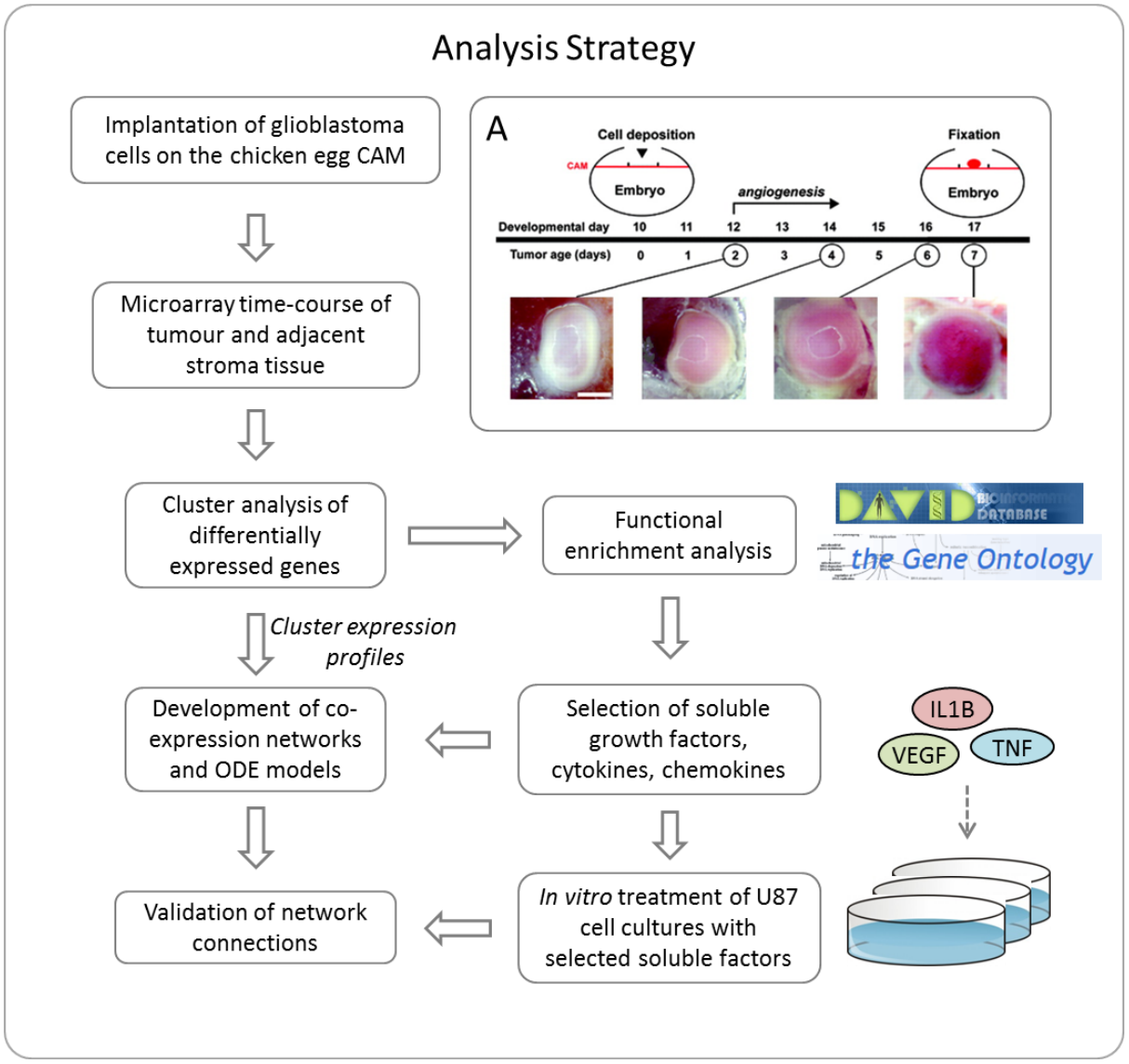

Figure 5.1- Overview of the implantation and analysis strategy

Panel A (inset) shows the progression of implantation (adapted from Bikfalvi et al. [268]). Angiogenesis is visible from 48 hours after implantation. The microarray expression profiling time-course starts at day 10 (pre-implantation), implantation occurs at day 11 and tumours are collected at day 15.

5.2 Methods

5.2.1 Overview of the Analysis Strategy

The analysis strategy is outlined in **Figure 5.1**. Briefly, we have used microarrays to generate transcriptional profiles of tumour and stroma tissue at 10 time points over 5 days following tumour deposition on the chicken egg CAM. We have identified genes differentially expressed in the tumour and the stroma. Cluster analysis has been used to identify groups of differentially expressed genes with similar expression profiles. Expression profiles representative of the behaviour of each cluster have been used to infer correlation based co-expression networks. Simultaneously, functional analysis has informed the selection of 15 differentially expressed genes in the tumour or the stroma consisting of growth factors, cytokines and extracellular remodelling proteins. We have generated transcriptional profiles of tumour cells treated with these factors *in vitro*. These profiles have been used to validate the interactions inferred from the networks.

5.2.2 Cells and Embryos

Fertilised chicken eggs were maintained as previously described [280]. To assess the response of the CAM to VEGF treatment 3µg of $VEGF_{165}$ was deposited on the CAM at developmental day 10 (n = 3). CAM tissue was excised following 24 hours of treatment and snap frozen for RNA extraction and microarray profiling (performed by Martin Hagedorn, University of Bordeaux).

U87 glioblastoma cells were maintained in DMEM, 10% FBS, antibiotics and L-glutamine. U87 cell pellets were deposited on the chicken egg CAM at developmental day 10 as previously described [268]. Tumours were dissected from the CAM and snap frozen every 12 hours following implantation until developmental day 15 (10 time points). Each time point was done in triplicate.

U87 cells were treated with a panel of recombinant growth factors, cytokines and extracellular matrix remodelling proteins. Proteins were dissolved according to the manufacturer's instructions and deposited on the cells to a final concentration of 100ng/ml. This concentration represented a

consensus of the existing literature of cell culture experiments, with the aim of selecting a concentration with high probability of effectiveness. After 24 hours the media was removed and the cells were washed with PBS followed by direct lysis of the cells using RLT buffer (Qiagen, UK). Each treatment was done in triplicate and then pooled for microarray profiling, with the exception of the controls which were profiled in triplicate.

5.2.3 Microarray profiling

RNA was extracted from cells and tissue using RNeasy columns (Qiagen, UK). RNA purity was assessed using a NanoDrop spectrophotometer. RNA was reverse transcribed and the cDNA was labelled with fluorescent Cy3 dye using the Agilent Low-input Quick Amp Kit (Agilent, UK). cRNA was purified using RNeasy columns (Qiagen, UK) and hybridised overnight to Agilent Human 4x44k Whole Genome or Agilent Chicken V1 Whole Genome microarrays according to the manufacturer's protocol. Microarrays were scanned using an Agilent SureScan microarray scanner and processed using Agilent Feature Extraction software.

In order to remove probes from the analysis that could potentially hybridise to both chicken and human cRNA we performed a separate microarray analysis. We created separate pools of RNA from chicken CAM and U87 cells to create chicken and human reference samples. The chicken and human reference RNA was then analysed using both human and chicken whole genome microarrays. RNA extraction, generation of fluorescently labelled cRNA, microarray hybridisation and scanning protocols were identical to those used for the implanted tumour tissue. After subtraction of the background signal, the relative contribution of the human cRNA to the total fluorescence observed for each chicken probe was calculated, and vice versa for the chicken cRNA. Any probe for which the cross-hybridisation of cRNA from the other species resulted in a fluorescent signal > 64 or the relative contribution to the total signal was greater than 15% was removed. 5,272 probes were removed from the chicken data and 9,128 probes were removed from the human data.

5.2.4 Differential expression and cluster analysis

For the tumour implantation time-course the microarray data was log transformed and normalised using quantile normalisation [126]. Differentially expressed genes were identified using 2 steps. Firstly, genes with at least a 2-fold change (linear scale) in expression between time points were selected. Secondly, the Bayesian Estimation of Temporal Regulation (BETR) [131] method was applied to remove noisy genes, using an alpha value (analogous to a p-value) of $1e^{-5}$. This corresponds to a false discovery rate (FDR) < 1% when corrected using the Benjamini-Hochberg method [132].

For the U87 *in vitro* treatments, microarray data was LOESS normalised in order to generate fold change ratios versus the controls. For the VEGF treatment of the CAM the raw data was provided as Affymetrix CEL files. The data was summarised and normalised using the RMA algorithm with a quantile normalisation step. Differentially expressed genes were identified using a one-class T-test followed by Benjamini-Hochberg FDR correction [132] and applying a threshold of 10%.

Functional analysis was done by applying the Gene Set Enrichment Analysis (GSEA) [135] tool to gene lists ranked by fold change values versus the respective controls. Additional functional analysis was done using the online tool DAVID [134]. Terms in the Gene Ontology database with an FDR < 10% were defined as functionally enriched unless otherwise stated.

Genes differentially expressed during the tumour implantation time-course were clustered using the HOPACH algorithm [129]. Clusters containing less than 10 genes were removed from further analysis. The medoid gene of each cluster was chosen as a representative expression profile. In order to increase the number of available data points for network inference the cluster profiles were fitted to 5^{th} degree polynomials using interpolation with a total of 1 data point per hour of the implantation time course (108 hours). Clusters were categorised into distinct time domains according to the amount of time needed for 50% of the total change in expression within the interpolated expression profile of the cluster to occur. The time domains were chosen to represent the first five 12 hour

intervals within the time-course, as we found that all clusters fell within this range. The average expression profile of genes within clusters and with the same functional annotation was calculated by conversion of the expression value to Z scores and averaging. The transcriptional data from the panel of U87 treatments were clustered using a hierarchical clustering as implemented by the *hclust* function in the R software package.

5.2.5 Constructing correlation based co-expression networks

Co-expression networks were generated using spearman correlation between the interpolated cluster expression profiles. In order to integrate our knowledge of the temporal properties of the cluster expression profiles we have introduced a time-delay element to the network, such that two clusters are identified as co-expressed if the expression profiles are highly correlated given a 12-24 hour shift (1 or 2 time domains) of either cluster. A high correlation threshold of 0.9 was chosen to filter insignificant network connections. We then applied a stratified layout to the network such that the time domains were sorted from fast to slow and groups of clusters within the same time domain were within the same strata of the network. We then selected only network connections that were consistent with this hierarchy, such that connections represent a significant correlation between a faster responding cluster and a slower responding cluster. Clusters with similar expression profiles were grouped within the network by applying the HOPACH clustering algorithm to the cluster expression profiles.

5.2.6 Constructing ODE-based networks

The ordinary differential equation (ODE) networks were constructed by Dr Rita Gupta by applying a novel ODE-based network inference method to data selected by Kim Clarke. The inference procedure models networks of directed interactions between genes as ordinary differential equations, as described previously [281]. The method includes a recursive network shrinkage procedure which is able to effectively remove edges that do not contribute to the stability of the network. As such, all connections within the resulting networks are considered significant, as removing them significantly

perturbs the network. However, as this can be a large number of connections that are difficult to interpret we have used a recently developed method [282] to estimate the FDR of each edge and applied a 5% FDR threshold. Consensus networks were generated in each case by taking only edges significant in 4/4 replicated networks.

5.2.7 Validation of the network connections using the *in vitro* treatment expression profiles

The genes encoding for the panel of recombinant proteins used for the *in vitro* U87 treatments are located within gene clusters found in the co-expression network. Gene Set Enrichment Analysis (GSEA) was used to test for enrichment (FDR < 10%) of the gene clusters found down-stream of the network modules containing the recombinant proteins within the transcriptional signature of each treatment. The transcriptional profiles of the U87 cells in response to each treatment were ranked according to fold change versus untreated controls.

5.3 Results

5.3.1 Transcriptional response of normal and tumour tissues in the CAM model

In order to characterise the transcriptional response of normal and tumour cells during development of a vascularised tumour we first developed a bioinformatics pipeline to identify differentially expressed genes, and then simplified the complexity of the transcriptional response in a relatively small number of clusters representing genes with similar expression profiles. Each cluster was assigned to a specific time domain, defined by the time necessary to reach 50% of the range of expression.

We identified 2240 and 2998 genes differentially expressed in the chicken stroma and in the tumour tissue respectively. Cluster analysis identified 26 and 16 gene clusters in the stroma and tumour tissues respectively which were organised into 5 time domains (see methods). Interestingly, we noticed that a much larger proportion of stroma clusters (**Figure 5.2A**, 14 out of 26, 43%) are assigned to the rapid response group (50% of the range reached within 12 hours post-implantation) compared to the tumour clusters (**Figure 5.3A**, 4 out of 16, 15%).

Functional analysis of the clusters from each time domain revealed enrichment of distinct sets of functional terms (**Figure 5.2B, 5.3B**). In the stroma (**Figure 5.2B**), functional enrichment was found in 4/5 of the time domains and represented a diverse set of transcriptional reprogramming that occurs during tumour vascularisation. This was characterised by an early, rapid up-regulation of genes related to stress response and wounding, followed by a down-regulation of genes related to mitochondrial function and cell cycle in the next groups. In the latest time domain functions related to angiogenesis and tissue remodelling are enriched within up-regulated genes.

The functional analysis of the tumour clusters (**Figure 5.3B**) revealed an early up-regulation of genes related to cell cycle and regulation of cell proliferation in the fastest group, followed by a down-

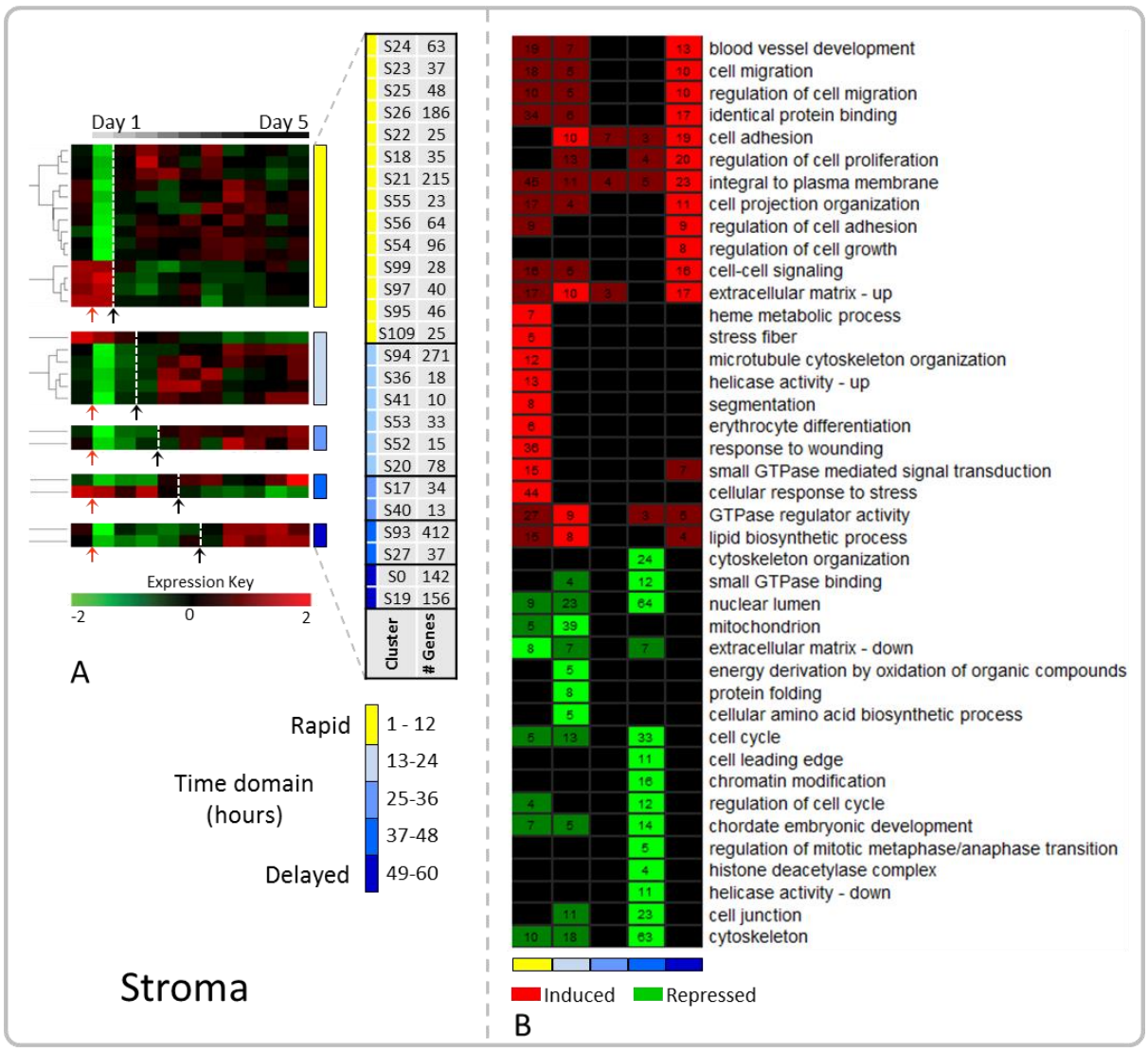

Figure 5.2 – Cluster analysis and functional profiling of the five time domains (stroma)

This figure shows the cluster analysis and functional profiles of the 5 time domains in the stromal tissue. Time domains have been colour coded yellow to blue in panel A and B. **Panel A** shows the cluster expression profiles as a heatmap divided into the 5 time domains. The beginning of the implantation time course (red arrow) and the time domain (black arrow) are marked. Preceding the red arrow is the average expression before implantation. **Panel B** shows the functional profiles of the genes within each time domain represented as the number of genes assigned to each functional term. Significant enrichment (light box, FDR < 10%) is highlighted.

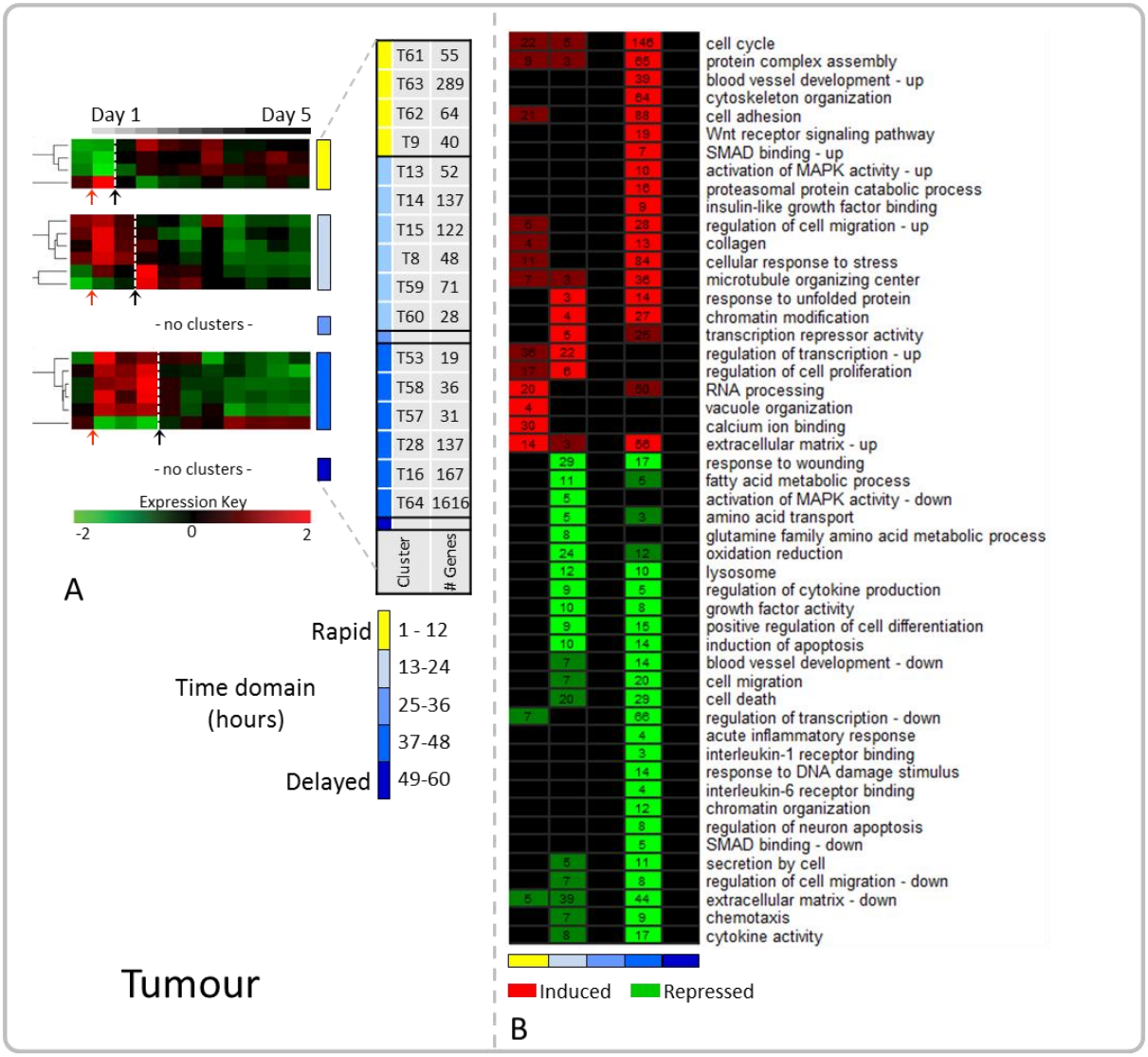

Figure 5.3 – Cluster analysis and functional profiling of the 5 time domains (tumour)

This figure shows the cluster analysis and functional profiles of the 5 time domains in the tumour tissue. Time domains have been colour coded yellow to blue in panel A and B. **Panel A** shows the cluster expression profiles as a heatmap divided into the 5 time domains. The beginning of the implantation time course (red arrow) and the time domain (black arrow) are marked. Preceding the red arrow is the average expression before implantation. **Panel B** shows the functional profiles of the genes within each time domain represented as the number of genes assigned to each functional term. Significant enrichment (light box, FDR < 10%) is highlighted.

regulation of genes related to the response to wounding. Strikingly, the largest transcriptional changes seen in the tumour are found in the 4th response group, representing an alteration in expression of 2006 genes (69% of total differentially expressed genes) centred around 37-48 hours after implantation. The functional profile is consistent with the onset of angiogenesis and escape

from apoptosis observed after tumour implantation [268]. We also find up-regulation of genes related to specific signalling pathways such as SMAD binding, activation of MAPK activity, IGF binding and Wnt receptor signalling. In addition, there is a significant down-regulation of genes related to IL1 receptor binding, IL6 receptor binding and SMAD binding.

5.3.2 Inference of a high-level dynamical model representing stroma-tumour interaction

The results of the expression profiling and functional analysis highlight the complex transcriptional reprogramming that occurs during vascularisation in both stroma and tumour tissues. In order to identify the relationship between the dynamics of the transcriptional response in these two tissues we inferred the underlying structure of a co-expression network representing the relationship between the overall transcriptional activity (defined by the average expression profile of the genes represented in each cluster) of the stroma and tumour gene clusters. This approach inferred a network representing 34 out of 42 of the gene clusters described above. We visualised the 34 clusters connected by 117 directional edges with a hierarchical layout where nodes were positioned within 5 time domains (**Figure 5.4**). We characterised each time domain within the network using functional analysis. The functional profile of each time domain was consistent with the overall analysis shown in **Figure 5.2** & **5.3**, indicating that the clusters contained in the network are the main contributors to the functional profiles. This includes the first time domain which is enriched with genes related to *cellular response to stress*, and *response to wounding* in the stroma and *extracellular matrix* in the tumour. Functions enriched within the second time domain include *cell adhesion* and *mitochondrion* in the stroma and *regulation of transcription* and *induction of apoptosis* in the tumour. Functional terms related to angiogenesis such as *blood vessel development*, *cell adhesion* and *cell migration* are enriched within the 4^{th} and 5^{th} time domains in the tumour and stroma respectively.

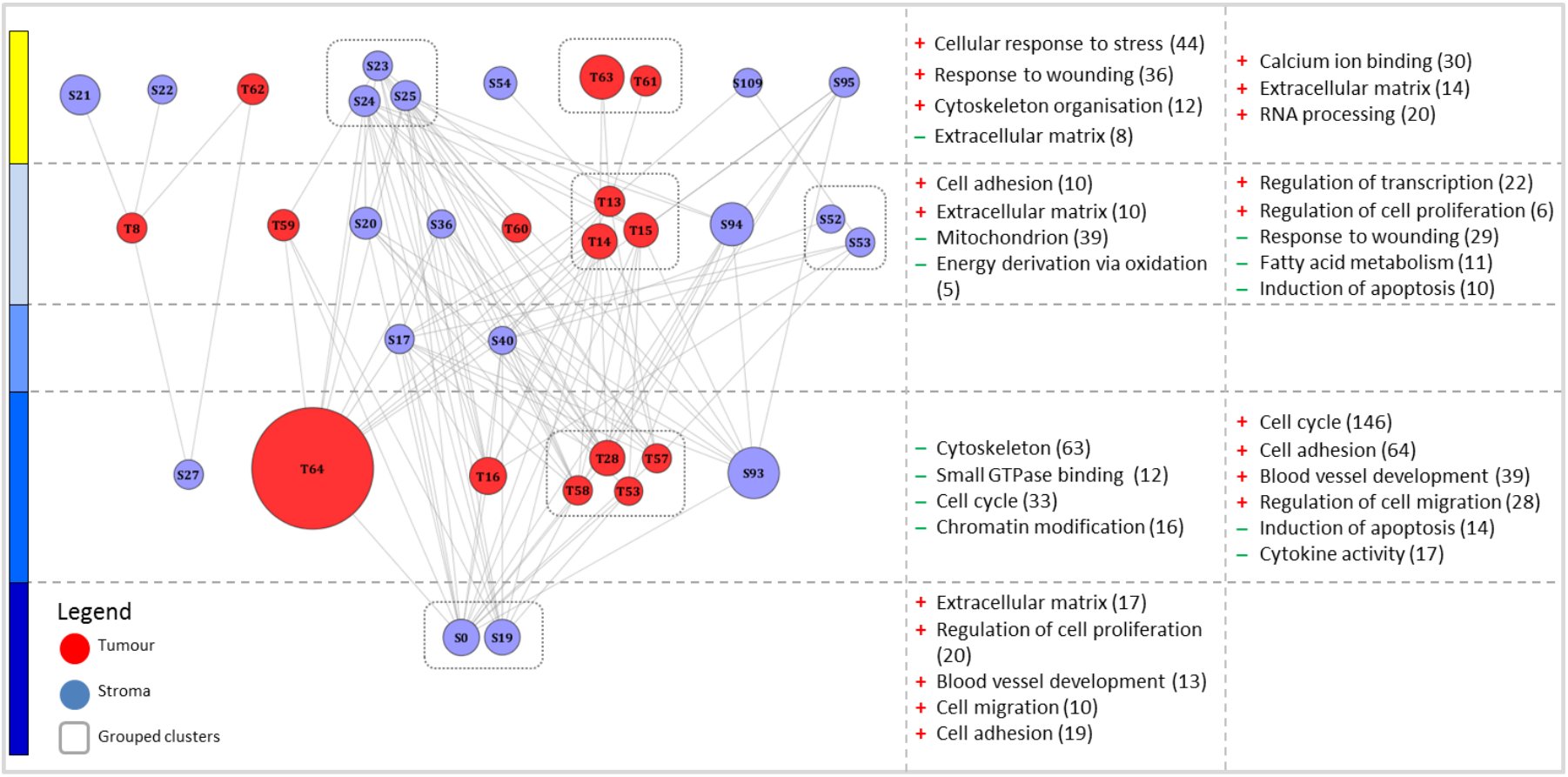

Figure 5.4 – Tumour and stroma co-expression network

This figure shows the structure of the co-expression network organised into the five time domains. Clusters are represented as nodes and edges are significant correlations with a given time delay. A summary of the most significantly enriched functional terms within each time domain is included for the up (+) and down (-) regulated genes. Node size is proportional to the cluster size. Correlation > 0.9 for all edges.

5.3.3 CAM transcriptional response to VEGF is predicted by the high-level dynamical model

The dynamics of expression of tumour VEGFA is cyclic, with a maximum up-regulation at 36 hours post implantation (**Figure 5.5B**). However, in the long term, the expression of VEGFA decreases. Consistent with this expression profile, VEGF is assigned to cluster T59 (**Figure 5.5A**).

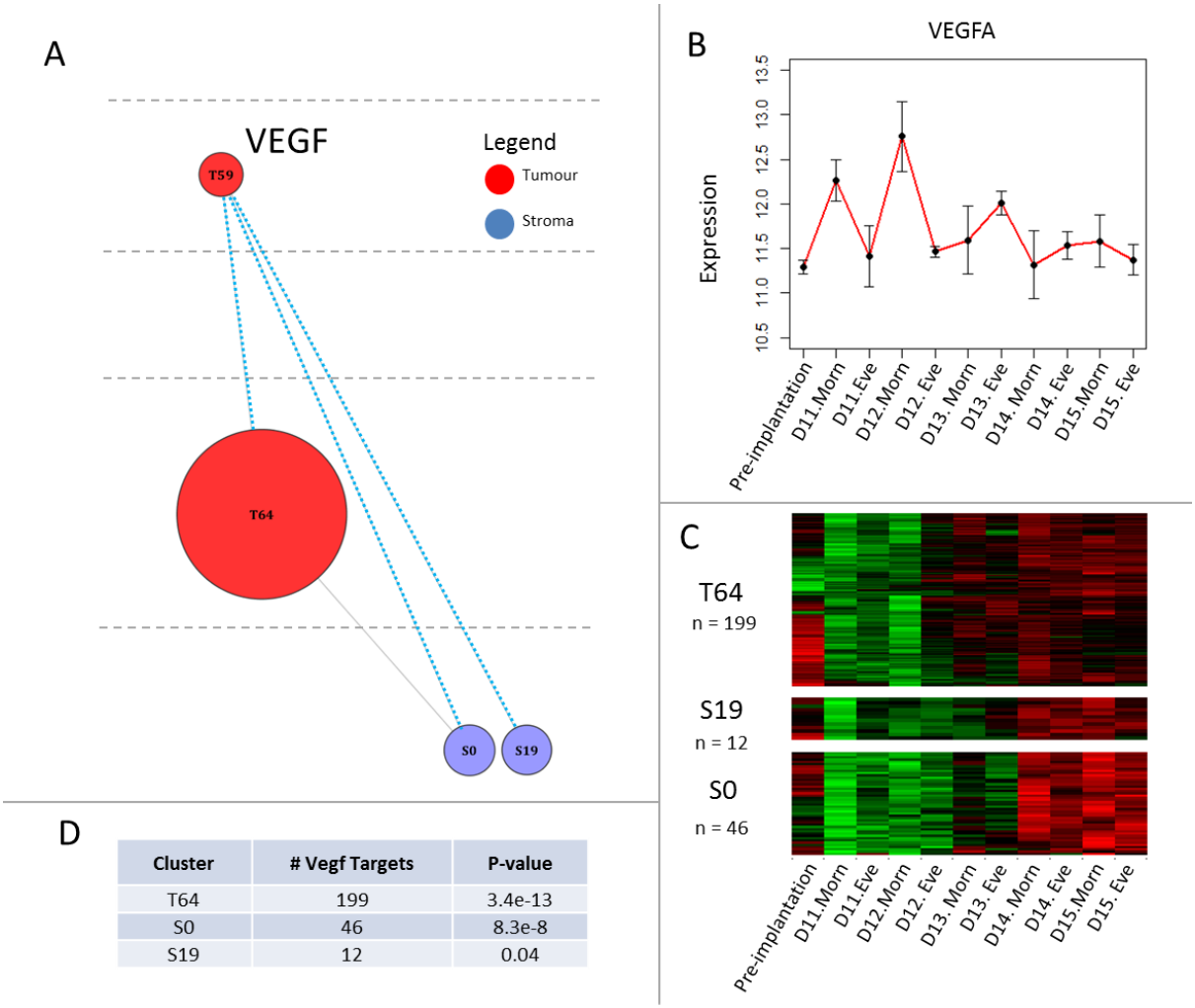

Cluster	# Vegf Targets	P-value
T64	199	3.4e-13
S0	46	8.3e-8
S19	12	0.04

Figure 5.5 – VEGF targets are enriched down-stream of VEGF in the network

Panel A shows the cluster containing VEGFA in the co-expression network and the clusters enriched in VEGF down-stream targets. Panel B shows the modulation of VEGFA expression in the tumour. Panel C is a heatmap representing the expression of VEGFA targets in the clusters down-stream of VEGFA in the co-expression network. Panel D shows the number of VEGF targets in each cluster and the enrichment p-value.

The model we developed suggests that genes responding to an increase in VEGFA would be found in gene clusters downstream of T59, specifically genes in cluster T64, S0 and S19 (**Figure 5.5A**). In order to assess whether this hypothesis was correct, we set to ascertain whether clusters T64, S0 and S19 were enriched of transcriptional targets of VEGF.

Up-regulated in response to VEGF treatment

Category	Term	Count	FDR
BP	cell cycle	126	5.94E-19
BP	DNA replication	42	1.29E-09
BP	blood vessel development	50	2.36E-10
BP	mRNA transport	23	3.36E-06
BP	cytoskeleton organization	57	7.12E-05
BP	negative regulation of transcription	53	0.003342
BP	cell migration	36	0.005902
BP	chromatin modification	34	0.018809
KEGG	ECM-receptor interaction	17	0.007676
CC	extracellular matrix	35	0.088977
BP	cell adhesion	66	0.065774

Down-regulated in response to VEGF treatment

Category	Term	Count	FDR
KEGG	Ribosome	21	1.37E-08
CC	mitochondrion	62	0.011378
CC	NADH dehydrogenase complex	8	0.017099

Table 5.1 – Functional analysis of VEGF responsive genes in the CAM

We could verify that this was indeed the case. By exposing the CAM to recombinant VEGF we could identify 2300 VEGF regulated genes (876 and 1424 down and up-regulated genes respectively). We found that clusters predicted to be downstream VEGF (T6, S0 and S19) were enriched with VEGF responsive genes (**Figure 5.5D, Figure 5.5C**). Functional analysis of the VEGF expression signature revealed up-regulation of terms related to cell cycle, angiogenesis, cell adhesion and extracellular matrix remodelling (**Table 5.1**), a functional profile that was very similar to cluster T64 and S0 (**Table 5.2**). These results validate the model we have developed and suggest that the transcriptional

response of the CAM to tumour cells implantation is indeed only partially dependent on VEGF expression.

S0	142	enzyme linked receptor protein signaling pathway(14), biological adhesion(15), blood vessel development(10), cellular component movement(13), regulation of cell migration(7), cell projection organization(10), regulation of protein kinase activity(10),cell adhesion(15), cell surface receptor signaling pathway(27)
T64	1616	cell cycle(146), biological adhesion(88), DNA recombination(20), metaphase plate congression(7), blood vessel development(39), regulation of cell migration(28), organelle fission(65), actin filament-based process(37), cell cycle process(117), chromosome segregation(26), microtubule-based process(43), cell adhesion(88), cell division(66), response to DNA damage stimulus(63), DNA metabolic process(86), extracellular matrix organization(22), extracellular structure organization(32), calcium-dependent cell-cell adhesion(9),
T28	137	response to extracellular stimulus(10), death(16), regulation of cell death(18), response to wounding(13)

Table 5.2 – Summary of the functional profiles of key clusters

5.3.4 Defining transcriptional signatures of cytokines and growth factors in tumour cells

Having demonstrated that the time-delay co-expression networks can correctly identify the transcriptional targets of VEGF in the CAM, we set out to systematically apply this strategy, focusing on the effects of other secreted factors on tumour cells. We therefore first identified relevant stroma and tumour secreted factors represented within the network modules (**Table 5.3**). We then exposed U87 tumour cells to a selection of these cytokines *in vitro* and performed expression profiling analysis (**Table 5.4**).

Stroma

Gene	Expression	Cluster	U87 treatment	Ligand
CXCL13	down	93	×	
MDK	down	93	×	
PDGFA	down	93	✓ - PDGF-αα	
BMP2	down	94	✓	
TGFB1	down	95	×	
ANGPT2	up	0	×	
PDGFB	up	0	×	
PDGFC	up	0	×	
CCL21	up	19	×	
PDGFD	up	20	×	
CXCL12	up	21	✓	
CXCR7	up	21	R	CXCL12
TNFRSF1A	up	21	R	TNFα
TNFRSF1B	up	22	R	TNFα
FIGF (VEGFD)	up	24	×	
IL15	up	26	✓	

✓- Used for treatment
× - Not treated
R – Receptor for a protein used for treatment

Tumour

Gene	Expression	Cluster	U87 treatment	Ligand
CCL20 (MIP3A)	down	8	✓	
IL1A	down	14	✓	
BMP2	down	15	✓	
CCR1 (MIP5)	down	15	R	CCL15 (MIP5)
CXCL14	down	15	×	
FGF2	down	15	✓	
IL8	down	16	×	
CSF3 (GCSF)	down	28	✓	
IL1B	down	28	✓	
IL6	down	28	✓	
CXCR7	down	8	R	CXCL12
IL6R	down	58	R	IL6
ANGPT2	up	64	×	
CTGF	up	64	×	
CYR61	up	64	×	
HGF	up	64	✓	
ITGAV	up	64	×	
KITLG	up	64	×	
PDGFC	up	64	×	
PDGFRA	up	64	R	PDGF-αα
PDGFRB	up	64	×	
PTN	up	64	×	
TGFB1	up	64	×	
TGFB3	up	64	✓	
BMPR1A	up	64	R	BMP2
VEGFA	up-down	59	✓	

Table 5.3 – Growth factors, cytokines, chemokines and receptors in the stroma and tumour

The 'expression' column provides a summary of the expression change relative to the first time point following implantation.

	# Differentially Expressed Genes				# Enriched Functional Terms					
	5% FDR		10% FDR		NES		FDR		FDR	
Gene	Down	Up	Down	Up	< -1.5	> 1.5	25% lo	25% hi	10% lo	10% hi
BMP2	2961	3016	8862	9186	109	25	66	4	1	4
CXCL12a	241	183	5769	5122	58	28	12	0	5	0
FGFb	805	687	6122	6001	86	55	1	0	1	0
GCSF	999	1190	7082	7943	87	20	5	0	4	0
HGF	118	60	5236	4246	154	42	162	0	23	0
IL15	22	10	3471	3270	32	46	0	0	0	0
IL1a	1972	1669	6641	5783	31	155	0	119	0	49
IL1b	255	467	2792	3326	54	124	1	60	0	38
IL6	1	2	578	721	53	48	13	0	3	0
MIP3a	2395	2587	7970	8581	142	27	141	2	15	0
MIP5	4457	4157	9735	9949	136	24	127	0	19	0
PDGFAA	6	5	3666	3139	62	83	11	1	0	1
TGFB3	4664	4470	9625	9610	69	37	14	0	3	0
TNFa	2351	2327	7395	7534	58	81	2	33	0	23
VEGF	25	41	3221	3054	77	103	6	33	0	14

Table 5.4 – Transcriptional profiling of U87 cells following treatment with 15 soluble factors

NES – Normalised enrichment score, an alternative measure of enrichment provided by GSEA. Lo – down-regulated. Hi – up-regulated

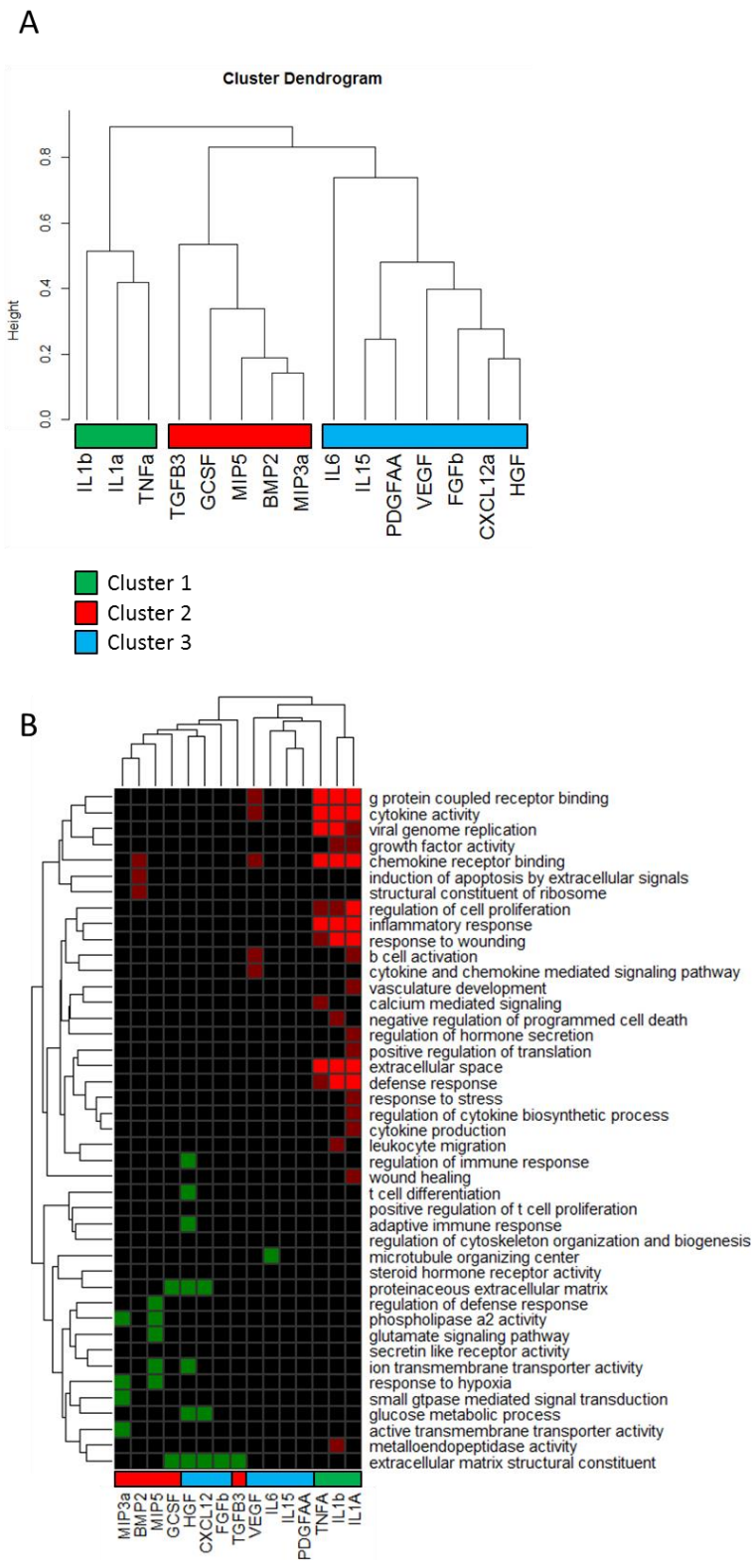

Figure 5.6 – Hierarchical clustering of transcriptional and functional profiles of the U87 treatments

Panel A shows the hierarchical clustering of the entire transcriptional profile of each treatment. Panel B shows the hierarchical clustering of treatments based on GSEA enrichment scores for all functional terms. Terms were enriched at 1% FDR (light boxes) and were selected at a minimum of 10% FDR (dark boxes)

Hierarchical clustering analysis of the expression profiling data identified 3 main clusters of cytokines and growth factors (**Figure 5.6A**). We have characterised each expression profile using functional analysis. The gene level clustering was consistent with a similar hierarchical clustering analysis performed on functional enrichment scores selected at a high level of confidence (FDR < 10%) (**Figure 5.6B**). Both analyses revealed a high similarity in the transcriptional response to the inflammatory cytokines TNFα, IL1β and IL1α (cluster 1 in **Figure 5.6A**). More specifically, the up-regulated genes in response to TNFα, IL1β and IL1α treatment are significantly enriched with terms related to inflammatory response and cell activation (*chemokine receptor binding*, *inflammatory response*, *cytokine activity, cell cycle* and *extracellular space).* In addition to these terms, TNFα treatment induced genes related to calcium mediated signalling. Interestingly, IL1α induced the up-regulation of genes enriched in *response to stress*, *wound healing*, *cytokine production* and *vasculature development*. IL1β induced expression of genes related to *leukocyte migration*, and *negative regulation of programmed cell death*.

Cluster 2 and 3 were primarily characterised by extracellular matrix remodelling factors (FGFb, TGFB3, GCSF, CXCL12, HGF). HGF treatment repressed expression of genes related to glucose metabolic processes, consistent with previous observations that HGF production is linked to high glucose conditions [283]. Both MIP3α (CCL20) and MIP5 (CCL15) treatment decreased the expression of genes related to the response to hypoxia, a process in which both of these chemokines have been shown to play a role [284] [285].

We were puzzled to note each expression profile was either linked to up or down-regulated functional terms. We reasoned that this could be due to the high statistical threshold used for the analysis. Reducing the threshold revealed that the up and down-regulated genes in response to treatment were both enriched with functional terms (**Table 5.4**). We reasoned that this could also explain why the transcriptional signatures linked to VEGF were not enriched in functional terms linked to angiogenesis (e.g. *vasculature development*) (**Figure 5.6B**). VEGF treatment induced genes related to *cytokine and chemokine activity, G protein coupled receptors* and *B-cell activation*. Due to

the importance of VEGF in angiogenesis we examined genes differentially regulated by VEGF using a second functional enrichment tool (DAVID) using a strict selection for differential expression (10% FDR). We found that terms related to angiogenesis were enriched within genes induced and repressed by VEGF (**Table 5.5**), including *inflammatory response, angiogenesis, blood vessel development, wound healing, response to oxygen levels* and *ECM-receptor interaction*. Taken together, this suggests that VEGF treatment of U87 cells does induce a transcriptional signature consistent with extracellular matrix remodelling and induction of angiogenesis by cytokine and chemokine activity.

Up-regulated in response to VEGF treatment *in vitro*

Category	Term	Count	FDR
BP	Negative regulation of apoptosis	26	6.3E-3
BP	Regulation of translation	14	0.013
BP	Regulation of kinase activity	16	0.063
BP	Inflammatory Response	20	0.065
BP	Angiogenesis	12	0.073

Down-regulated in response to VEGF treatment *in vitro*

Category	Term	Count	FDR
BP	Response to oxygen levels	20	4.9E-4
BP	Blood vessel development	24	4.3E-3
BP	Wound healing	22	1.8E-3
KEGG	ECM-receptor interaction	12	0.026
BP	Response to RNA damage stimulus	28	0.027
BP	Collagen metabolic process	7	0.045

Table 5.5 – Functional analysis of genes regulated by VEGF treatment of U87 cells *in vitro*

5.3.5 Validating sub-networks of the co-expression network using the *in vitro* treatments

Next, we set to compare the transcriptional response predicted by our time-course model with the tumour *in vitro* experimentally defined transcriptional signatures. Using the approach pioneered in

the analysis of the response to VEGF treatment on the CAM (see **Figure 5.5**) we could identify 124 cases of gene clusters being enriched with transcriptional targets of secreted factors, as defined by the U87 treatments (see **appendix 5A** for the full table of hits). Of these 124 cases, 13 (10.4%) were matching edges of our high level network model (**Figure 5.7**). Since these connections represent both co-expression *in vivo* and experimentally validated transcriptional regulation in response to treatment *in vitro*, we hypothesized that these connections may represent key events in the development of the vascularised tumour, and therefore examined them in more detail.

We have shown that cluster T64 is highly enriched with genes induced by VEGF treatment of the CAM, and thus we predicted that treatment of U87 cells with VEGF *in vitro* would produce a similar result. Contrary to this prediction, genes down-regulated in response to VEGF treatment of U87 cells were enriched within cluster T64. However, closer examination revealed that this is consistent with the expression of VEGF in the tumour during the CAM time-course. VEGF expression decreases between 36- 48 hours after implantation, consistent with the up-regulation of genes in T64 within the 36-48 hour time domain. Furthermore, two clusters within the same time domain as VEGF, T8 and T14, are highly enriched with genes activated and repressed by VEGF respectively. This is consistent with an activation of VEGF targets coinciding with the transient increase in expression of VEGF in the tumour between 24-36 hours after implantation. In comparison the VEGF treatment of the CAM represents 24 hours of acute VEGF target activation, consistent with the significant enrichment of VEGF targets within cluster T64, S19 and S0. Taken together, this reinforces the role of VEGF signalling, however it also suggests that other factors could play a key role in controlling angiogenesis such as those in cluster T8 and T14.

Cluster T14 contains IL1α and is connected to cluster T64 and T28 in the co-expression networks. Cluster T64 and T28 are enriched with genes repressed and induced by IL1α treatment respectively, consistent with the expression patterns of IL1α, T64 and T28 in the tumour (**Figure 5.7B, Figure 5.7C**). However, this data does not provide knowledge on the very early changes in IL1α expression,

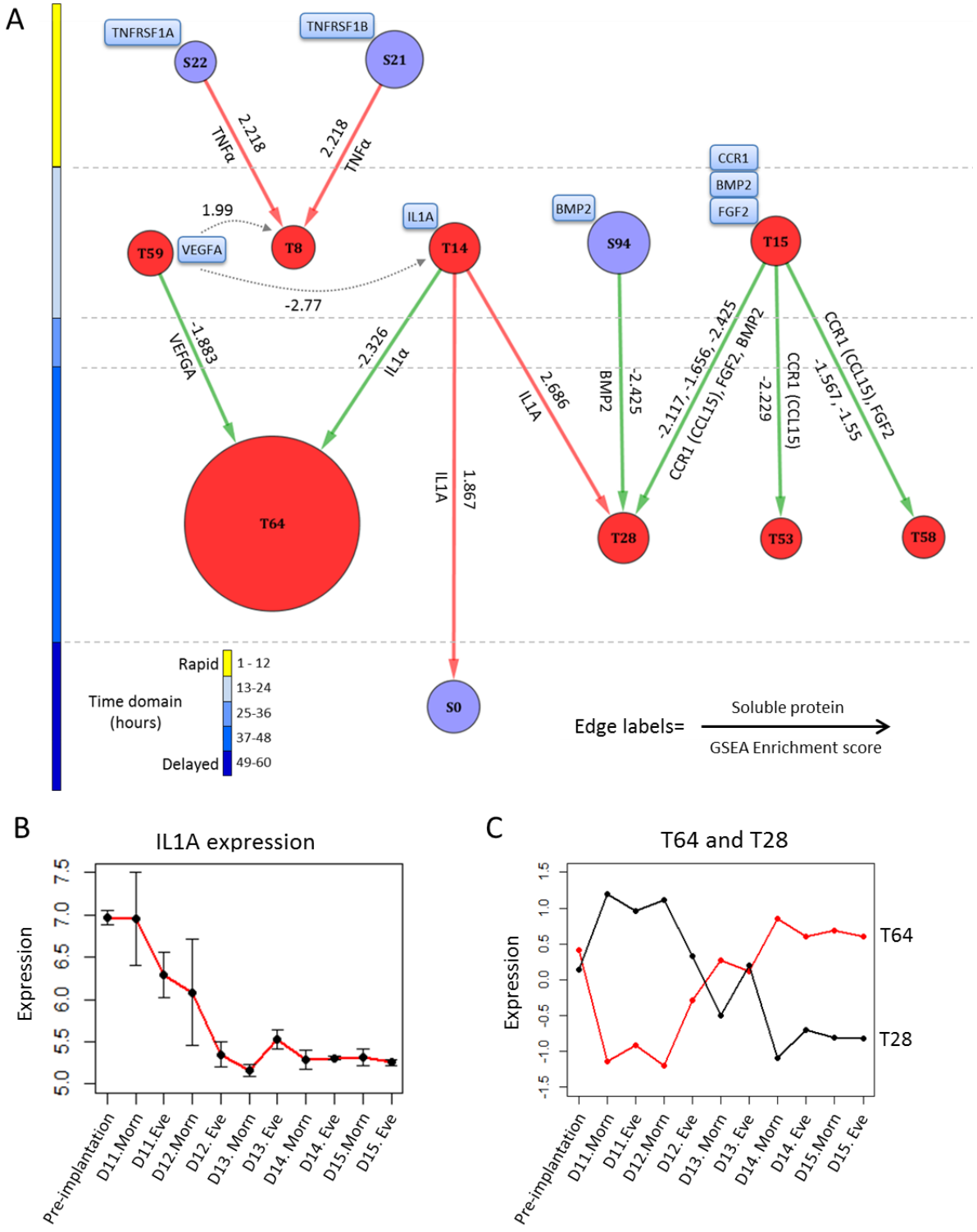

Figure 5.7 – Sub-network of the co-expression network validated by the U87 *in vitro* treatments

The edges in the network in **panel A** represent both co-expression between two clusters and a link between a secreted factor and its target genes, defined by the U87 treatments. The up-stream clusters contain the indicated factors while the down-stream clusters are significantly enriched with genes modulated by treatment with the upstream protein. With the exception of VEGF which is discussed in the text, edges within the same time domain have been removed in order to represent only temporal relationships. **Panel B** and **C** show the expression of IL1α and the medoid expression profile of cluster T64 and T28 respectively.

as the first tumours were sampled after 12 hours of implantation. It is possible that IL1α expression is induced between implantation and the first time point.

Cluster T64 contains 80% of the up-regulated genes in the tumour. Functional analysis of T64 reveals enrichment of terms related to proliferation, extracellular matrix remodelling and angiogenesis. Functional analysis of cluster T28 reveals enrichment of genes related to regulation of cell death and response to wounding (**Table 5.2**). Combined with the analysis of the transcriptional profiles of IL1α and VEGF treatment of U87 cells *in vitro* this analysis presents two hypotheses. Firstly, the transient increase in expression of VEGF and the initial expression of IL1α by the tumour acts as a signalling mechanism to induce pro-inflammatory and pro-angiogenic pathways. Secondly, this expression precedes alterations in expression of a large subset of genes related to cell proliferation, angiogenesis and cell death found in clusters T64 and T28.

5.3.6 High resolution, gene-level dynamical modelling identifies IL1α as a key factor driving tumour implantation in the CAM

Having developed a correlation based co-expression model of tumour expansion and shown that it successfully captures the response of the tumour and stroma to important soluble proteins, we decided to apply a more sophisticated ODE-modelling approach to infer higher resolution (gene level) dynamical models.

We have applied a new ODE-based network inference method, developed by Dr Rita Gupta, to infer connections between secreted factors in the tumour and stroma (**Figure 5.8**). In the first case, we have inferred networks from expression profiles of secreted factors in the tumour and stroma for which we have matching expression profiling data from *in vitro* treatments. The *in vitro* treatment profiles

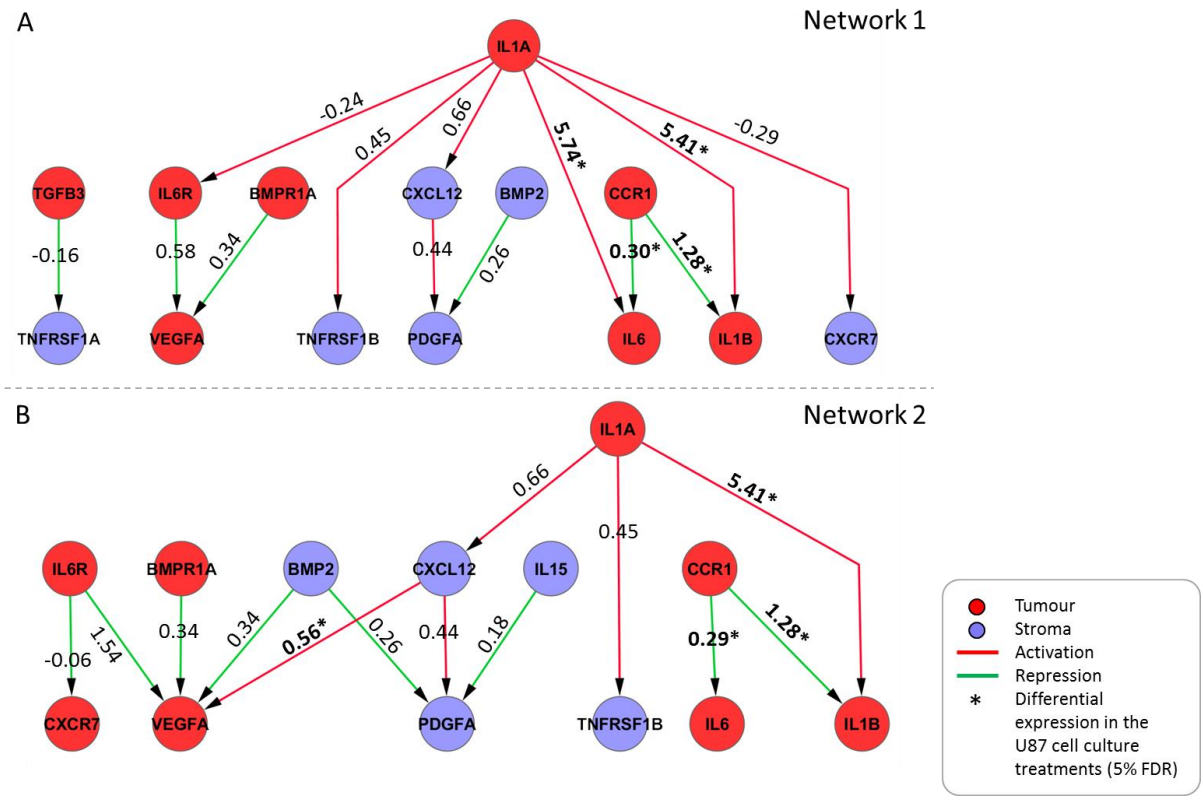

Figure 5.8 – ODE-based networks representing gene level interactions in the tumour and stroma

Panel A is the network constructed with integration of the U87 *in vitro* treatment data into the network inference pipeline. **Panel B** is the network constructed using just the expression profiles from the tumour implantation time-course. Edges are labelled with the log2 fold change of the target gene in response to *in vitro* treatment with the up-stream factor.

have been integrated into the network inference methodology in order to further constrain the network reconstruction (**network 1**). Secondly, a network was generated using the same selection of genes without the integration of the *in vitro* treatment profiles (**network 2**).

While the modelling approach employs a recursive method to identify sparse networks, these are still of difficult biological interpretation as they represent an average of 40% of a fully connected network. We therefore used an additional thresholding procedure developed by Scutari and Nagarajan [282] to further decrease network complexity by selecting only connections which represent a strong interaction. Both networks reinforced the role of IL1α as a hub gene within the network, as it is linked to the expression of IL6, IL6R, TNFRSF1B, CXCL12, IL1β and CXCR7 (**Figure 5.8**). Of these connections, 2 were consistent with the *in vitro* treatments, specifically IL1α induction of

IL1β and IL6 expression, which were both induced by over 32 fold (linear scale) in response to IL1α treatment of U87 cells. This is consistent with the expression changes seen in the CAM implantation time-course, in which IL1α, IL1β and IL6 expression is correlated. In addition, the expression network predicts a role of CXCL12 in inducing expression of VEGF. VEGF expression in U87 cells was up-regulated in response to CXCL12 treatment (fold change 1.47). This interaction is well known, CXCL12 signalling induces VEGF expression at the mRNA level [286] and both act synergistically in response to hypoxia to promote angiogenesis [287]. This interaction may represent a key early signalling event between the tumour and the stroma, as CXCL12 is found within stroma cluster S21 which is induced rapidly in response to implantation.

5.3.7 High resolution dynamical modelling linking soluble factor gene expression to effector functions, confirms IL1α as a key factor driving tumour implantation in the CAM

We reasoned that the expression of soluble factors known to control transcription could be up-stream of effector functions over-represented in the gene clusters. We generated an ODE-based network using gene expression profiles combined with the average expression profiles of genes sets representing biological functions present within gene clusters in the tumour and stroma (**Table 5.6**). Functional terms were aggregated from groups of gene clusters identified with HOPACH (see **Figure 5.4**). The network contained 29 nodes and 43 edges representing 10 biological functions and 19 soluble factors (**Figure 5.9A**). We extracted sub-networks consisting of the network neighbourhood of secreted factors which contained functional terms. We found that IL1α expression was linked to *regulation of cell migration*, *blood vessel development* and *cell adhesio*n (**Figure 5.9B**). We further tested these connections by using GSEA to test for enrichment of the genes comprising the functional terms within the genes regulated by IL1α treatment of U87 cells. We found that genes comprising the *regulation of cell migration* and *blood vessel development* terms were significantly enriched within genes repressed by IL1α treatment. We identified a second sub-network in which

Function	Tissue	Clusters
regulation of transcription	tum	T59
blood vessel development	tum	T64
cell cycle	tum	T64
regulation of cell migration	tum	T64
cell adhesion	tum	S61, 63
blood vessel development	tum	T28, 53, 57, 58
cell migration	tum	T28, 53, 57, 58
regulation of apoptosis	tum	T28, 53, 57, 58
blood vessel development	stroma	S0, 19
regulation of cell migration	stroma	S0, 19
response to stress	stroma	S23, 24, 25
inflammatory response	stroma	S54
cell cycle	stroma	S93

Table 5.6 – Functional terms used in the ODE-networks

TNFRSF1B expression in the stroma was linked to genes involved in the *inflammatory response* (**Figure 5.9D**). GSEA analysis confirmed that the *inflammatory response* gene set was enriched within genes up-regulated in response to TNFα treatment, consistent with expression in the stroma. A third sub-network linking IL6R expression in the tumour to expression of genes related to *regulation of apoptosis* and *cell migration* was identified (**Figure 5.9C**). These connections were also consistent with GSEA analysis which showed that genes making up both these functional groups are activated in response to IL6 treatment. In summary, the genes belonging to effector functions predicted to be downstream of IL1α, TNFα and IL6 were in fact modulated by treatment with the protein.

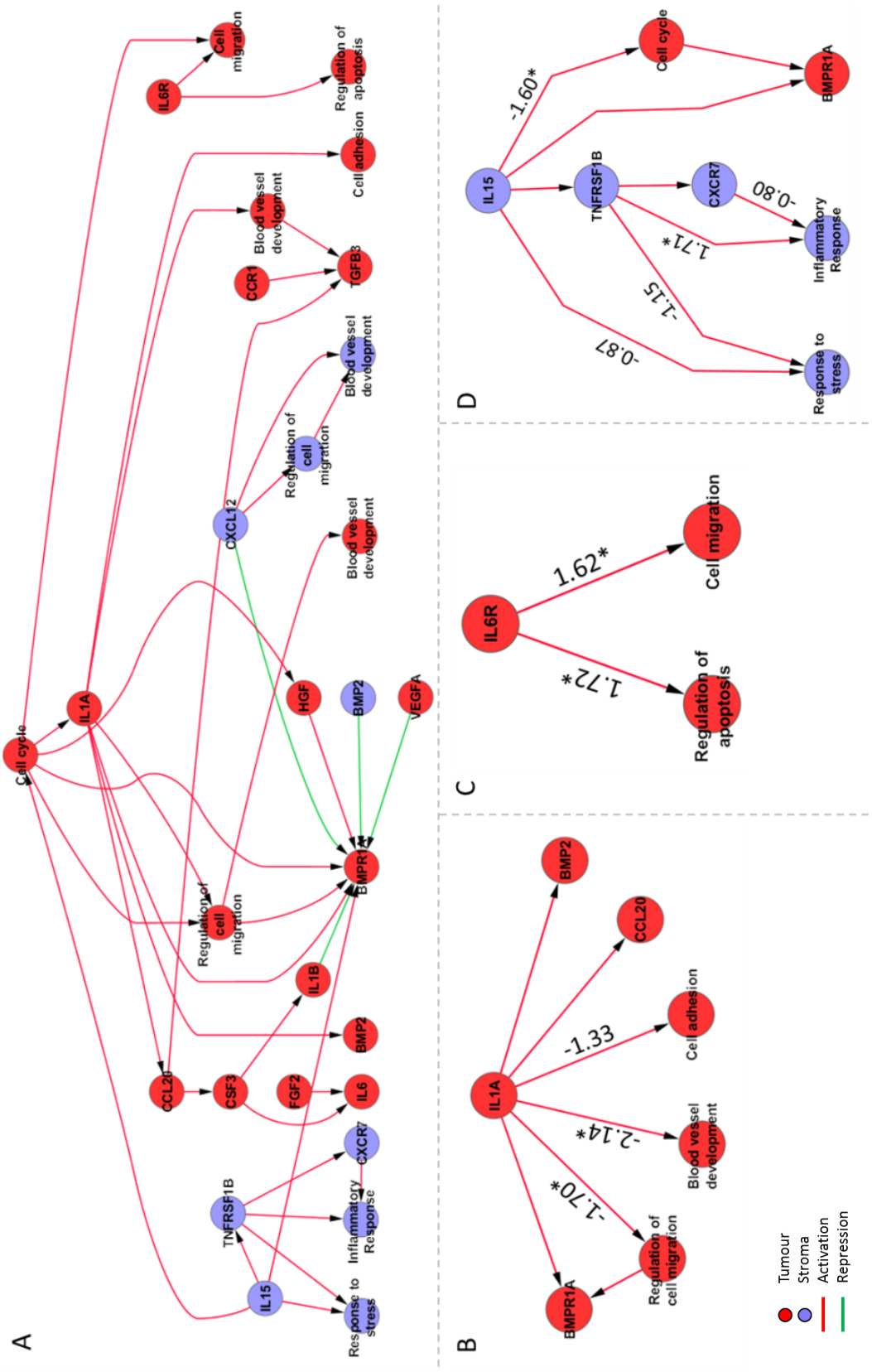

Figure 5.9 – ODE-based networks of soluble factor gene expression and effector functions

Panel A is the entire network organised using a hierarchical layout. Panel B – D are sub-networks of Panel A which link soluble factor expression with effector function. Edge weights indicate GSEA enrichment scores. * Significant enrichment of genes comprising an effector function in the targets of the up-stream soluble factor (FDR < 10%)

5.4 Discussion

We have described the first in-depth gene expression profiling study of a model of angiogenesis in which the state of both the avascular tumour and surrounding stroma has been captured. This has revealed a complex pattern of transcriptional reprogramming during angiogenesis involving differential expression of many growth factors, cytokines, chemokines, and extracellular remodelling factors controlling angiogenesis, cell migration, cell proliferation, apoptosis and other effector functions. Co-expression networks reveal a dynamic hierarchy to these events in which early and delayed changes are linked. Interestingly, the delayed changes appear to be central to the angiogenic process, while the earlier changes appear to represent adaptations to the microenvironment and preceding signalling events. These adaptations may represent key events in the transition from a stable tumour towards the recruitment of the vasculature and tumour growth.

VEGF is perhaps the most well characterised pro-angiogenic factor due to its potent stimulation of both pathological and physiological angiogenesis, as well as the availability of VEGF inhibitors that are effective anti-cancer drugs. Our analysis suggests that VEGF gene expression is not constitutively induced during tumour angiogenesis in the CAM, rather there is a transient increase in expression that precedes the expression of a large number of pro-angiogenic genes. The regulation of VEGFA mRNA stability and translation is complex, with many factors such as stabilising proteins and miRNA targeting able to post-transcriptionally regulate VEGF expression [288]. Further experiments utilising proteomics approaches could provide valuable information allowing the correlation of mRNA expression and protein abundance to be investigated during angiogenesis and glioblastoma development.

5.4.1 The role of IL1α in controlling angiogenesis

One of the key inflammatory cytokines expressed in the tumour is IL1α. IL1α exists as both a precursor and a mature form, however unlike IL1β both forms of IL1α are active. In contrast to IL1β, it appears that IL1α acts primarily through intracellular or juxtracrine signalling pathways, as it is rarely secreted and only in its mature form [289]. IL1α signalling appears to play an important role in a variety of pathologies. IL1α knock-out mice injected with a melanoma cell line show a 50% reduction in vascular growth and microvessel density in matrigel plugs and reduced tumorigenicity compared to wild type mice [290]. In contrast, fibrosarcomas expressing IL1α that were injected into mice have shown reduced tumorigenicity and increased immune response [291]. Consistent with our observations, treatment of cardiac myofibroblasts with recombinant IL1α induces expression of pro-inflammatory markers including IL1β and IL6 [292]. Co-culture of a pancreatic cancer cell line expressing IL1α with fibroblasts induced expression of pro-inflammatory factors, which was reduced when IL1α signalling was blocked [293]. The same study identified a significant link between IL1α gene expression and clinical outcome of pancreatic cancer patients. Importantly, by blocking IL1R signalling one study was able to show how intracellular IL1α pre-cursor is able to cause transcriptional re-programming including induction of pro-inflammatory cytokines in an IL1 receptor independent manner [294].

Our findings reveal IL1α as a hub within networks describing the transcriptional reprogramming that occurs during glioblastoma induced angiogenesis. IL1α is up-stream of effector functions and important secreted factors such as IL6, IL1β and CXCL12. In addition, the co-expression networks place IL1α in the second time domains representing a fast transcriptional response to implantation, up-stream of important effector functions related to angiogenesis and tumour proliferation. This suggests that expression of IL1α may play a key role in controlling angiogenesis in human glioblastoma.

Based on this analysis we propose further experiments to investigate the role of IL1α in glioblastoma development. Using the CAM model we aim to address the questions of whether IL1α signalling in

glioblastoma is necessary for angiogenesis and tumour growth and to shed light on the relative contribution of intracellular and extracellular IL1α signalling. By generating IL1α knock-out glioblastoma cell lines and implanting them on the CAM we will be able to investigate further the role of IL1α.

5.4.2 Angiogenesis in skeletal muscle

Skeletal muscle relies on the efficient and plentiful delivery of oxygen and nutrients via the blood to maintain normal function. In this respect skeletal muscle adapts relatively rapidly to changes in oxygen and nutrient demand by development of additional capillaries. Pro-angiogenic stimuli such as hypoxia, NO release and shear stress activate the angiogenic program [295] [296] by regulating expression of key transcription and growth factors, cytokines and tissue remodelling factors such as VEGF and HIF1A [297], amongst many others.

Recent findings show that muscle regeneration and angiogenesis in response to injury and exercise training is not altered in muscle of elderly individuals [298]. However, in COPD patients versus sedentary controls the angiogenic response to exercise training is blunted [299]. Two hallmarks of COPD exacerbations are hypoxia [300] and inflammation [301] in the muscle, both of which are also important processes controlling angiogenesis. Therefore, it is important to understand how the angiogenic switch is altered in conditions such as COPD, for which very little information exists. We have shown that many growth factors and inflammatory cytokines are differentially expressed during glioblastoma induced angiogenesis, and these factors can be mapped to complex networks. However it is uncertain how applicable this model is to skeletal muscle angiogenesis. Further work will be necessary to build the biological networks underlying skeletal muscle angiogenesis from clinical data, such as identifying the network neighbourhood of IL1α, IL1β and VEGFA, as this represents a significant gap in our current understanding.

CHAPTER 6

CONCLUDING STATEMENT AND FUTURE DIRECTIONS

This thesis has presented the first analysis of transcriptional networks in young and elderly muscle based on a meta-analysis of clinical data. The utilisation of a statistical integration platform to perform the meta-analysis has allowed us to use standard statistical analysis techniques to expand our knowledge of the transcriptional changes between young and elderly muscle. The application of this method to within network inference pipelines is a powerful tool that can extract valuable information form the wealth of data that is currently available.

The network analysis has revealed distinct differences in the underlying structure of networks representing skeletal muscle ageing. We have revealed that energy metabolism genes are both under-expressed and decoupled from sub-networks representing translation and ribosome biogenesis in elderly muscle. These networks represent a valuable resource for investigating the response of skeletal muscle to stressors such as hypoxia, inflammation and exercise. This is highlighted by identifying specific modules within the network that respond to an exercise program in elderly people. This revealed that while core modules representing energy metabolism respond to exercise there is a subset of genes that do not respond to exercise training, and these genes are part of a sub-network highly co-expressed in elderly muscle.

Future interrogation of the networks can shed light on the molecular response to popular intervention strategies to target sarcopenia. In parallel to this, the recent pace of data generation means sufficient data will be available to generate networks specifically from trained and untrained muscle. By comparing these networks across age groups we can further distinguish the effects of ageing from ageing related muscle disuse.

By careful analysis of the network topology and functional profiles of the core modules we identified a link between eukaryotic initiation factors and expression of energy metabolism genes. While

previous work has linked 40S associated eIFs to stress-response pathways such as hypoxia [228] and mTOR signalling [230], very little has been revealed regarding the function of the majority of eIFs outside ribosome assembly. Our analysis suggests that expression of EIF genes is controlled by an age-dependent mechanism coupled to the control of energy metabolism. We validated the network predictions using an Eif6 heterozygous mouse model. Eif6 is one of the most highly age-dependent factors highlighted by the network analysis and is up-regulated in elderly muscle. By using transcriptional profiling and MS proteomics we revealed that $Eif6^{+/-}$ muscle shows a substantial transcriptional reprogramming which is coupled to changes in protein expression in mitochondria. As predicted by the human network the alterations were characterised by increased expression of energy metabolism genes. This represents the first evidence of a 60S associated EIF able to affect global gene expression in muscle tissue.

Future efforts will be directed towards revealing the nature of the metabolic reprogramming within eIF6 haploinsufficient muscle. Recent experiments conducted by the Falciani lab but not covered in this thesis have revealed several intriguing results. Firstly, we have found that in $Eif6^{+/-}$ whole muscle the respiratory control ratio is significantly decreased compared to wild type. This is indicative of mitochondrial dysfunction characterised by a lower capacity for substrate oxidation and reduced ATP turnover. The precise impact of this on ATP availability in the muscle is not yet known. Motivated by the link between eIF6 and serum protein carbonylation levels in clinical data, we have measured ROS generation in $Eif6^{+/-}$ isolated fibres in response to contraction stimulation. This has revealed a striking reduction in ROS generation compared to wild type fibres to the point where stimulated and un-stimulated $Eif6^{+/-}$ fibres are indistinguishable. This suggests an exciting line of enquiry consistent with our analysis of clinical data. Further experiments will be needed to ascertain whether $Eif6^{+/-}$ mice show altered respiratory capacity and ROS generation during exercise, hypoxia and old age, as this could have a significant impact on our use of the Eif6 mouse as a model for metabolic reprogramming.

Protein acetylation has emerged as a key player in the regulation of metabolism in recent years [238]. The transcriptional signature of Eif6 haploinsufficiency was recapitulated by histone deacetylase inhibitors. Recent proteomics analysis has revealed a significant alteration in the acetylome of $Eif6^{+/-}$ muscle. This is characterised by hyperacetylation of NADH dehydrogenase subunits and deacetylation of glycolysis enzymes. Acetylation status regulates both metabolic enzyme abundance and activity, and has divergent effects dependent on the individual enzyme [84]. Future experiments will aim to delineate the effects of acetylation in Eif6 haploinsufficient muscle by assessing the expression and activity of metabolic enzymes.

Eif6 haploinsufficient satellite cells have cell autonomous alterations in transcriptional state. This was characterised by increased expression of energy metabolism genes, an effect that was increased dramatically in differentiating cells. This was accompanied by differential expression of factors known to control myogenic differentiation such as Myod and myogenin. We hypothesise that Eif6 haploinsufficient muscle may show altered regenerative capacity in response to injury. On-going experiments addressing this question include histochemical analysis of an injury model in Eif6+/- and wild type mice as well as characterisation of $Eif6^{+/-}$ satellite cell proliferation and differentiation signalling pathways *in vitro.*

Understanding tissue remodelling processes such as angiogenesis are vital to reducing the impact of age-related diseases such as cancer. The process of angiogenesis has been intensively studied for many years, but the complexity of the process is only recently emerging with the application of systems level analysis [156] [157]. We have constructed the first detailed networks of tumour-stroma expression during angiogenesis based on observational data. By using multiple network inference approaches we are able to predict both high level and gene level interactions between the tumour and stroma. In the future, we will focus on validating the predictions made by the model, such as the central role of IL1α in glioblastoma development, by utilising knock-out cell lines and proteomics alongside classical measures of tumour growth.

APPENDIX

Appendix 3A

KEGG pathway enrichment within the neighbourhood of EIF2S2 (FDR < 25%)

KEGG PATHWAY	NES	FDR q-val
KEGG_PROTEASOME	2.44	0
KEGG_AMINOACYL_TRNA_BIOSYNTHESIS	2.29	0.002
KEGG_PARKINSONS_DISEASE	2.19	0.005
KEGG_OXIDATIVE_PHOSPHORYLATION	2.07	0.014
KEGG_SPLICEOSOME	2.07	0.011
KEGG_RIBOSOME	1.92	0.038
KEGG_HUNTINGTONS_DISEASE	1.89	0.039
KEGG_SELENOAMINO_ACID_METABOLISM	1.8	0.066
KEGG_PYRUVATE_METABOLISM	1.74	0.092
KEGG_RNA_DEGRADATION	1.72	0.092
KEGG_PROTEIN_EXPORT	1.72	0.085
KEGG_GLYOXYLATE_AND_DICARBOXYLATE_METABOLISM	1.65	0.126
KEGG_CITRATE_CYCLE_TCA_CYCLE	1.64	0.129
KEGG_CYSTEINE_AND_METHIONINE_METABOLISM	1.6	0.158
KEGG_NON_HOMOLOGOUS_END_JOINING	1.58	0.166
KEGG_REGULATION_OF_AUTOPHAGY	1.54	0.197
KEGG_ONE_CARBON_POOL_BY_FOLATE	1.5	0.228
KEGG_HISTIDINE_METABOLISM	1.5	0.224

Appendix 3A - Young muscle – positive correlation to EIF2S2

KEGG PATHWAY	NES	FDR q-val
KEGG_ECM_RECEPTOR_INTERACTION	-2.49	0
KEGG_ALLOGRAFT_REJECTION	-2.17	0.007
KEGG_INTESTINAL_IMMUNE_NETWORK_FOR_IGA_PRODUCTION	-2.06	0.021
KEGG_FOCAL_ADHESION	-1.99	0.026
KEGG_GRAFT_VERSUS_HOST_DISEASE	-1.99	0.022
KEGG_CELL_ADHESION_MOLECULES_CAMS	-1.83	0.077
KEGG_GLYCOSAMINOGLYCAN_DEGRADATION	-1.73	0.136
KEGG_SYSTEMIC_LUPUS_ERYTHEMATOSUS	-1.73	0.125
KEGG_MELANOMA	-1.67	0.173
KEGG_AUTOIMMUNE_THYROID_DISEASE	-1.63	0.212
KEGG_LEISHMANIA_INFECTION	-1.62	0.197
KEGG_VIRAL_MYOCARDITIS	-1.58	0.235

Appendix 3A- Young muscle – negative correlation to EIF2S2

KEGG PATHWAY	NES	FDR q-val
KEGG_OXIDATIVE_PHOSPHORYLATION	3.68	0
KEGG_PARKINSONS_DISEASE	3.5	0
KEGG_CITRATE_CYCLE_TCA_CYCLE	3.36	0
KEGG_HUNTINGTONS_DISEASE	3.08	0
KEGG_ALZHEIMERS_DISEASE	3.06	0
KEGG_PYRUVATE_METABOLISM	2.73	0
KEGG_PROPANOATE_METABOLISM	2.69	0
KEGG_VALINE_LEUCINE_AND_ISOLEUCINE_DEGRADATION	2.41	0
KEGG_PROTEASOME	2.11	0.005
KEGG_CYSTEINE_AND_METHIONINE_METABOLISM	2.08	0.006
KEGG_BUTANOATE_METABOLISM	2.06	0.006
KEGG_PROTEIN_EXPORT	2.04	0.007
KEGG_VALINE_LEUCINE_AND_ISOLEUCINE_BIOSYNTHESIS	2.04	0.006
KEGG_PORPHYRIN_AND_CHLOROPHYLL_METABOLISM	1.98	0.01
KEGG_FATTY_ACID_METABOLISM	1.95	0.013
KEGG_GLYOXYLATE_AND_DICARBOXYLATE_METABOLISM	1.93	0.013
KEGG_VIBRIO_CHOLERAE_INFECTION	1.85	0.026
KEGG_PEROXISOME	1.85	0.025
KEGG_ARGININE_AND_PROLINE_METABOLISM	1.78	0.041
KEGG_AMINOACYL_TRNA_BIOSYNTHESIS	1.76	0.045
KEGG_UBIQUITIN_MEDIATED_PROTEOLYSIS	1.75	0.047
KEGG_PATHOGENIC_ESCHERICHIA_COLI_INFECTION	1.7	0.061
KEGG_GLUTATHIONE_METABOLISM	1.65	0.082
KEGG_RENAL_CELL_CARCINOMA	1.63	0.09
KEGG_GLYCOLYSIS_GLUCONEOGENESIS	1.59	0.11
KEGG_PROXIMAL_TUBULE_BICARBONATE_RECLAMATION	1.58	0.116
KEGG_TRYPTOPHAN_METABOLISM	1.55	0.132
KEGG_CARDIAC_MUSCLE_CONTRACTION	1.54	0.138
KEGG_BETA_ALANINE_METABOLISM	1.51	0.155
KEGG_COLORECTAL_CANCER	1.51	0.15
KEGG_PHENYLALANINE_METABOLISM	1.5	0.152
KEGG_GLYCINE_SERINE_AND_THREONINE_METABOLISM	1.5	0.148
KEGG_OOCYTE_MEIOSIS	1.49	0.149
KEGG_INSULIN_SIGNALING_PATHWAY	1.47	0.163
KEGG_NUCLEOTIDE_EXCISION_REPAIR	1.46	0.17
KEGG_RNA_DEGRADATION	1.45	0.179
KEGG_ALANINE_ASPARTATE_AND_GLUTAMATE_METABOLISM	1.43	0.194
KEGG_DNA_REPLICATION	1.41	0.209
KEGG_EPITHELIAL_CELL_SIGNALING_IN_HELICOBACTER_PYLORI_INFECTION	1.38	0.236
KEGG_TYROSINE_METABOLISM	1.38	0.231
KEGG_TERPENOID_BACKBONE_BIOSYNTHESIS	1.36	0.244

Appendix 3A - Elderly muscle – positive correlation to EIF2S2

KEGG_CYTOKINE_CYTOKINE_RECEPTOR_INTERACTION	-2.04	0.044
KEGG_INTESTINAL_IMMUNE_NETWORK_FOR_IGA_PRODUCTION	-1.83	0.179
KEGG_NOTCH_SIGNALING_PATHWAY	-1.81	0.135
KEGG_GLYCOSAMINOGLYCAN_BIOSYNTHESIS_CHONDROITIN_SULFATE	-1.79	0.114
KEGG_NEUROACTIVE_LIGAND_RECEPTOR_INTERACTION	-1.76	0.122
KEGG_ASTHMA	-1.72	0.129
KEGG_GLYCOSAMINOGLYCAN_BIOSYNTHESIS_KERATAN_SULFATE	-1.71	0.12
KEGG_PRIMARY_IMMUNODEFICIENCY	-1.67	0.14

Appendix 3A - Elderly muscle – negative correlation to EIF2S2

KEGG pathway enrichment within the neighbourhood of EIF3J (FDR < 25%)

KEGG PATHWAY	NES	FDR q-val
KEGG_UBIQUITIN_MEDIATED_PROTEOLYSIS	3	0
KEGG_SPLICEOSOME	2.85	0
KEGG_RIBOSOME	2.57	0
KEGG_PROTEASOME	2.53	0
KEGG_PROTEIN_EXPORT	2.42	0
KEGG_AMINOACYL_TRNA_BIOSYNTHESIS	1.89	0.049
KEGG_NUCLEOTIDE_EXCISION_REPAIR	1.68	0.178
KEGG_OOCYTE_MEIOSIS	1.66	0.177

Appendix 3A - Young muscle – positive correlation to EIF3J

KEGG PATHWAY	NES	FDR q-val
KEGG_NEUROACTIVE_LIGAND_RECEPTOR_INTERACTION	-2.37	0.001
KEGG_AUTOIMMUNE_THYROID_DISEASE	-2.24	0.005
KEGG_GRAFT_VERSUS_HOST_DISEASE	-2.12	0.01
KEGG_SULFUR_METABOLISM	-2.03	0.017
KEGG_NITROGEN_METABOLISM	-1.98	0.021
KEGG_CYTOKINE_CYTOKINE_RECEPTOR_INTERACTION	-1.89	0.037
KEGG_ALLOGRAFT_REJECTION	-1.88	0.034
KEGG_TASTE_TRANSDUCTION	-1.82	0.053
KEGG_ASTHMA	-1.81	0.05
KEGG_CELL_ADHESION_MOLECULES_CAMS	-1.77	0.061
KEGG_OLFACTORY_TRANSDUCTION	-1.72	0.082
KEGG_PROXIMAL_TUBULE_BICARBONATE_RECLAMATION	-1.69	0.095
KEGG_TYPE_I_DIABETES_MELLITUS	-1.68	0.094
KEGG_GLYCEROPHOSPHOLIPID_METABOLISM	-1.67	0.099
KEGG_ALPHA_LINOLENIC_ACID_METABOLISM	-1.61	0.138
KEGG_STEROID_HORMONE_BIOSYNTHESIS	-1.59	0.15
KEGG_PRIMARY_IMMUNODEFICIENCY	-1.59	0.146
KEGG_P53_SIGNALING_PATHWAY	-1.58	0.141
KEGG_NATURAL_KILLER_CELL_MEDIATED_CYTOTOXICITY	-1.49	0.246

Appendix 3A - Young muscle – negative correlation to EIF3J

KEGG PATHWAY	NES	FDR q-val
KEGG_CITRATE_CYCLE_TCA_CYCLE	3.31	0
KEGG_OXIDATIVE_PHOSPHORYLATION	3.21	0
KEGG_PARKINSONS_DISEASE	3.17	0
KEGG_HUNTINGTONS_DISEASE	2.72	0
KEGG_PYRUVATE_METABOLISM	2.67	0
KEGG_ALZHEIMERS_DISEASE	2.61	0
KEGG_PROPANOATE_METABOLISM	2.51	0
KEGG_VALINE_LEUCINE_AND_ISOLEUCINE_DEGRADATION	2.49	0
KEGG_UBIQUITIN_MEDIATED_PROTEOLYSIS	2.27	0.001
KEGG_PROTEIN_EXPORT	2.06	0.008
KEGG_VALINE_LEUCINE_AND_ISOLEUCINE_BIOSYNTHESIS	2	0.013
KEGG_BUTANOATE_METABOLISM	1.96	0.016
KEGG_FATTY_ACID_METABOLISM	1.94	0.016
KEGG_CYSTEINE_AND_METHIONINE_METABOLISM	1.93	0.017
KEGG_PEROXISOME	1.91	0.018
KEGG_PROTEASOME	1.8	0.042
KEGG_VIBRIO_CHOLERAE_INFECTION	1.71	0.077
KEGG_CARDIAC_MUSCLE_CONTRACTION	1.7	0.076
KEGG_OOCYTE_MEIOSIS	1.67	0.089
KEGG_ARGININE_AND_PROLINE_METABOLISM	1.65	0.095
KEGG_INSULIN_SIGNALING_PATHWAY	1.65	0.095
KEGG_EPITHELIAL_CELL_SIGNALING_IN_HELICOBACTER_PYLORI_INFECTION	1.65	0.091
KEGG_PORPHYRIN_AND_CHLOROPHYLL_METABOLISM	1.64	0.088
KEGG_GLYCOLYSIS_GLUCONEOGENESIS	1.58	0.124
KEGG_PATHOGENIC_ESCHERICHIA_COLI_INFECTION	1.56	0.139
KEGG_PROXIMAL_TUBULE_BICARBONATE_RECLAMATION	1.54	0.148
KEGG_PHENYLALANINE_METABOLISM	1.54	0.144
KEGG_STARCH_AND_SUCROSE_METABOLISM	1.52	0.153
KEGG_ALANINE_ASPARTATE_AND_GLUTAMATE_METABOLISM	1.51	0.158
KEGG_COLORECTAL_CANCER	1.49	0.168
KEGG_GLYCINE_SERINE_AND_THREONINE_METABOLISM	1.48	0.175
KEGG_ADIPOCYTOKINE_SIGNALING_PATHWAY	1.47	0.184
KEGG_AMYOTROPHIC_LATERAL_SCLEROSIS_ALS	1.43	0.218
KEGG_RENAL_CELL_CARCINOMA	1.42	0.224
KEGG_AXON_GUIDANCE	1.4	0.24
KEGG_TRYPTOPHAN_METABOLISM	1.39	0.24
KEGG_GLUTATHIONE_METABOLISM	1.39	0.242

Appendix 3A - Elderly muscle – positive correlation to EIF3J

KEGG PATHWAY	NES	FDR q-val
KEGG_NOTCH_SIGNALING_PATHWAY	-2.1	0.018
KEGG_RIBOSOME	-1.87	0.1
KEGG_GLYCOSAMINOGLYCAN_BIOSYNTHESIS_CHONDROITIN_SULFATE	-1.85	0.079
KEGG_GLYCOSAMINOGLYCAN_BIOSYNTHESIS_KERATAN_SULFATE	-1.73	0.168
KEGG_GLYCOSPHINGOLIPID_BIOSYNTHESIS_GLOBO_SERIES	-1.73	0.139
KEGG_NEUROACTIVE_LIGAND_RECEPTOR_INTERACTION	-1.71	0.131

Appendix 3A - Elderly muscle – negative correlation to EIF3J

Appendix 3B

Description	Gene Name	log2 Fold Change
Troponin C2, fast	Tnnc2	-3.249
Cytochrome c oxidase, subunit VIIIb	Cox8b	-2.769
Adenylyl cyclase-associated protein 1	Cap1	-2.182
Translation factor Guf1, mitochondrial (Fragment)	Guf1	-2.126
Transmembrane protein 14C	Tmem14c	-2.122
Mitochondrial import inner membrane translocase subunit Tim9 B	Fxc1	-1.918
HIG1 domain family, member 1A	Higd1a	-1.824
Putative uncharacterized protein	Mylpf	-1.703
Troponin T, fast skeletal muscle	Tnnt3	-1.545
28S ribosomal protein S36, mitochondrial	Mrps36	-1.471
MCG129639	Gm6736	-1.330
Cytochrome b5 type B	Cyb5b	-1.308
Coproporphyrinogen-III oxidase, mitochondrial	Cpox	-1.192
Adenylate kinase 2, mitochondrial	Ak2	-0.969
Glutamyl-tRNA(Gln) amidotransferase subunit A, mitochondrial	Qrsl1	-0.965
Cytochrome c oxidase protein 20 homolog	Cox20	-0.932
Abhydrolase domain-containing protein 11	Abhd11	-0.911
NADH-ubiquinone oxidoreductase chain 4	mt-Nd4	-0.841
Thioesterase superfamily member 2	Acot13	-0.811
Succinate dehydrogenase [ubiquinone] cytochrome b small subunit, mitochondrial	Sdhd	-0.790
Ubiquinone biosynthesis protein COQ7 homolog	Coq7	-0.772
Omega-amidase NIT2	Nit2	-0.772
Glutaminase kidney isoform, mitochondrial	Gls	-0.763
Coiled-coil domain-containing protein 58	Ccdc58	-0.737
Deoxyguanosine kinase, isoform CRA_a	Dguok	-0.704
Glutaredoxin 2 (Thioltransferase)	Glrx2	-0.699
28S ribosomal protein S28, mitochondrial	Mrps28	-0.676
Lysophosphatidic acid phosphatase type 6	Acp6	-0.667
28S ribosomal protein S29, mitochondrial	Dap3	-0.661
Translational activator of cytochrome c oxidase 1	Taco1	-0.655
Mitochondrial inner membrane organizing system protein 1	Minos1	-0.641
OCIA domain-containing protein 2	Ociad2	-0.639
Alanine aminotransferase 2	Gpt2	-0.636
Mitochondrial ribosomal protein L45	Mrpl45	-0.635
Protein DJ-1	Park7	-0.620
Cytochrome c oxidase assembly protein COX11, mitochondrial	Cox11	-0.611
MCG5603	Ndufa11	-0.610
MCG130675	2410018M08Rik	-0.602
39S ribosomal protein L43, mitochondrial	Mrpl43	-0.594
Prostamide/prostaglandin F synthase	Fam213b	-0.586
Zinc-binding alcohol dehydrogenase domain-containing protein 2	Zadh2	-0.556
Cytochrome c oxidase assembly protein COX15 homolog	Cox15	-0.495
Cox17p	Cox17	-0.492
Inactive hydroxysteroid dehydrogenase-like protein 1	Hsdl1	-0.484
Isoleucine--tRNA ligase, mitochondrial	Iars2	-0.466
Ribosome-releasing factor 2, mitochondrial	Gfm2	-0.437
Serine protease HTRA2, mitochondrial	Htra2	-0.437
FUN14 domain-containing protein 2	Fundc2	-0.410
Peptidase (Mitochondrial processing) alpha	Pmpca	-0.402
Ornithine aminotransferase, isoform CRA_b	Oat	-0.396
Catechol O-methyltransferase domain-containing protein 1	Comtd1	-0.373
MCG55255	Mrpl41	-0.343
Succinyl-CoA ligase [ADP-forming] subunit beta, mitochondrial	Sucla2	-0.343
Delta-1-pyrroline-5-carboxylate dehydrogenase, mitochondrial	Aldh4a1	-0.338
3-hydroxyisobutyryl-CoA hydrolase, mitochondrial	Hibch	-0.269
28S ribosomal protein S22, mitochondrial	Mrps22	-0.267
39S ribosomal protein L1, mitochondrial	Mrpl1	-0.226
Endonuclease G	Endog	-0.194

Appendix 3B – Down-regulated proteins detected in mitochondrial fraction of Eif6$^{+/-}$ muscle

Description	Gene Name	log2 Fold Change
Calcium channel voltage-dependent alpha 1F subunit	Cacna1f	6.305
Protein Gm5451	Gm5451	5.666
RTN2-C	Rtn2	3.994
Mammalian ependymin-related protein 1	Epdr1	3.946
Carboxypeptidase A3, mast cell	Cpa3	3.930
Histidine rich calcium binding protein, isoform CRA_a	Hrc	3.747
60S ribosomal protein L18 (Fragment)	Rpl18	3.576
Transmembrane protein 109	Tmem109	3.490
Protein Rpl3l	Rpl3l	3.364
Tripeptidyl-peptidase 1	Tpp1	3.298
Trimeric intracellular cation channel type A	Tmem38a	3.223
60S ribosomal protein L18a	Rpl18a	3.150
Prosaposin, isoform CRA_e	Psap	3.043
60S ribosomal protein L13a	Rpl13a	2.988
Cathepsin B	Ctsb	2.979
Peroxisomal multifunctional enzyme type 2	Hsd17b4	2.552
60S ribosomal protein L14	Rpl14	2.541
Ribosomal protein, large, P0	Rplp0	2.416
Sarcoplasmic/endoplasmic reticulum calcium ATPase 1	Atp2a1	2.312
Calcium channel, voltage-dependent, beta 1 subunit	Cacnb1	2.290
Polymerase I and transcript release factor	Ptrf	2.166
MCG1036414	Rpl35a	2.033
AMP deaminase 1	Ampd1	1.918
MCG10168	Rplp1	1.848
Elongation factor 1-alpha	Eef1a2	1.596
Catalase	Cat	1.526
Sodium/potassium-transporting ATPase subunit alpha-2	Atp1a2	1.400
Aspartate-beta-hydroxylase	Asph	1.368
6.8 kDa mitochondrial proteolipid	Mp68	1.259
Basigin	Bsg	1.162
Calsequestrin-1	Casq1	1.144
Voltage-dependent L-type calcium channel subunit alpha-1S (Fragment)	Cacna1s	1.131
Protein Myh15	Myh15	1.107
Synaptophysin-like protein 2 (Fragment)	Sypl2	1.071
RAB1B, member RAS oncogene family, isoform CRA_c	Rab1b	1.065
Calcium-binding mitochondrial carrier protein SCaMC-1	Slc25a24	1.057
Solute carrier family 25 (Mitochondrial carrier; adenine nucleotide translocator), member 31	Slc25a31	1.004
RAS-related C3 botulinum substrate 1, isoform CRA_a	Rac1	0.997
Albumin 1	Alb	0.980
ATP synthase subunit a	mt-Atp6	0.890
Protein Pet112l	Pet112l	0.811
Uncharacterized protein KIAA0564 homolog	Kiaa0564	0.738
28S ribosomal protein S2, mitochondrial	Mrps2	0.703
Obscurin	Obscn	0.677
MCG128338	Mrpl23	0.614
Mitochondrial glutamate carrier 1	Slc25a22	0.604
Succinate dehydrogenase cytochrome b560 subunit, mitochondrial	Sdhc	0.534
Carbonyl reductase [NADPH] 2 (Fragment)	Cbr2	0.521
Coiled-coil domain-containing protein 90B, mitochondrial	Ccdc90b	0.414
39S ribosomal protein L15, mitochondrial	Mrpl15	0.406
NADH dehydrogenase [ubiquinone] iron-sulfur protein 3, mitochondrial	Ndufs3	0.346
Mitochondrial import inner membrane translocase subunit TIM16	Pam16	0.338
ATP synthase subunit g, mitochondrial	Atp5l	0.331
Apolipoprotein O	Apoo	0.310
ATP synthase subunit O, mitochondrial	Atp5o	0.309
Carnitine O-acetyltransferase	Crat	0.296
Protein Gm15118	Gm15118	0.283
ATP synthase subunit f, mitochondrial	Atp5j2	0.278
Acyl carrier protein (Fragment)	Ndufab1	0.273
NADH dehydrogenase [ubiquinone] 1 alpha subcomplex subunit 6	Ndufa6	0.245
Mitochondrial chaperone BCS1	Bcs1l	0.241
Calcium uniporter protein, mitochondrial	Mcu	0.204

Appendix 3B - Up-regulated proteins detected in mitochondrial fraction of Eif6$^{+/-}$ muscle

Appendix 5A

Treatment	Cluster	NES	FDR-q value
BMP2	TUM63	1.808423	0.032104056
	STROMA17	-1.6962	0.03710749
	TUM15	-1.97029	0.001858402
	TUM28	-2.42491	0
	TUM14	-2.61591	0
CXCL12a	TUM63	2.313893	0
	TUM61	2.172523	0
	TUM8	1.612217	0.06708582
	STROMA17	-1.61498	0.074952886
	TUM15	-1.62464	0.0934395
	TUM14	-1.79191	0.026121518
	TUM28	-1.87081	0.016638774
FGFb	TUM63	2.160278	0
	TUM8	2.141246	0
	TUM61	2.009692	0.001490696
	TUM62	1.546353	0.080677815
	TUM13	1.51733	0.08097723
	STROMA27	1.468714	0.09453681
	TUM58	-1.55788	0.07699463
	STROMA20	-1.58065	0.078862056
	STROMA22	-1.58469	0.094521046
	TUM28	-1.65642	0.06858973
	STROMA17	-1.90443	0.010121929
	TUM16	-2.52341	0
GCSF	TUM63	2.089292	0.001989919
	TUM61	1.904912	0.007553245
	TUM16	1.817458	0.01269665
	STROMA22	-1.63677	0.088571936
HGF	TUM63	2.165987	0.000681818
	TUM61	1.905102	0.008719817
	TUM8	1.753197	0.023879273
	STROMA22	-1.56304	0.09796142
	TUM15	-1.64371	0.06484175
	STROMA17	-1.7073	0.048488952
	TUM28	-1.9219	0.009063385
	TUM14	-1.94645	0.014698945
IL15	TUM63	2.220917	0
	TUM61	2.079299	0
	TUM62	1.63574	0.076661795
	STROMA22	-1.59063	0.04944652
	STROMA17	-1.61737	0.049122483
	TUM64	-1.63268	0.04986562
	TUM14	-1.64613	0.05722388
	TUM15	-1.64782	0.08524758
	TUM28	-1.83414	0.02633339
IL1a	TUM28	2.686635	0
	TUM15	2.451045	0
	TUM8	2.380133	0
	TUM61	2.093581	0.001760413
	TUM62	1.975157	0.005195078
	STROMA0	1.866905	0.012209105
	TUM63	1.56317	0.085965015
	TUM13	1.554206	0.080726005
	TUM64	-2.32628	0
IL1b	TUM28	3.052492	0
	TUM15	2.738079	0
	TUM8	2.166225	0.001283345
	STROMA20	-1.61908	0.08682729
	TUM64	-1.76057	0.061991297

Treatment	Cluster	NES	FDR-q value
IL6	TUM63	2.236351	0.072939135
	STROMA25	2.158435	0.04870045
	TUM59	2.098194	0.04149708
	TUM61	2.022475	0.041188
	TUM53	1.906247	0.047498707
	TUM16	1.762103	0.069687195
	STROMA18	1.749685	0.06414143
MIP3A	TUM63	2.841261	0
	TUM61	1.852983	0.015845718
	TUM64	1.636796	0.069634035
	STROMA17	-1.794	0.01238546
	TUM15	-1.92587	0.002741266
	TUM28	-2.29458	0.00047619
	TUM14	-2.64071	0
MIP5	TUM63	2.504441	0
	TUM61	1.850962	0.01199784
	TUM62	1.670246	0.046493586
	STROMA17	-1.51719	0.0880357
	TUM58	-1.56725	0.069494404
	TUM16	-1.80701	0.008770552
	TUM59	-1.89727	0.00528766
	TUM28	-2.11665	0.000737923
	TUM53	-2.22937	0
	TUM14	-2.30332	0
PDGFAA	TUM15	-1.51724	0.08744492
	STROMA40	-1.5376	0.08646353
	STROMA20	-1.57139	0.0810237
	TUM64	-1.60209	0.07710134
	STROMA17	-1.63346	0.079508536
	STROMA22	-1.80246	0.02333146
	TUM14	-1.92802	0.005118062
	TUM28	-2.20409	0
TGFB3	TUM63	1.807826	0.069481514
	TUM58	-1.47986	0.07352676
	STROMA52	-1.49306	0.077183634
	STROMA53	-1.49738	0.08675698
	TUM53	-1.55376	0.06947339
	TUM8	-1.62784	0.04976641
	STROMA22	-1.92446	0.00368571
	TUM28	-2.39513	0
	TUM15	-2.59045	0
TNFa	TUM8	2.218879	0
	TUM28	2.112894	0.002521652
	TUM15	2.014495	0.005805952
	TUM14	-2.2914	0
VEGF	TUM8	1.99592	0.012219415
	TUM63	1.889388	0.014718981
	TUM61	1.813509	0.020207517
	TUM28	1.702719	0.043530066
	TUM15	1.571859	0.09462562
	STROMA55	-1.54881	0.074364156
	STROMA93	-1.68402	0.027171038
	TUM14	-1.87562	0.006511567
	TUM64	-1.88282	0.008298755
	STROMA22	-1.97318	0.007251577
	STROMA17	-2.02152	0.008089055
	TUM14	-2.76678	0

Appendix 5A – This table shows all U87 treatments which resulted in transcriptional signatures that were significantly enriched (FDR < 10%) within modules in the co-expression network.

REFERENCES

[1] J. Morley, A. M. Abbatecola, J. Argiles, V. Baracos, J. Bauer, S. Bhasin, T. Cederholm, A. S. Coats, S. Cummings, W. Evans, K. Fearon, L. Ferrucci, R. Fielding, J. Guralnik, T. Harris, A. Inui, K. Kalantar-Zadeh, B.-A. Kirwan, G. Mantovani, M. Muscaritoli, A. Newman, F. Rossi-Fanelli, G. Rosano, R. Roubenoff, M. Schambelan, G. Sokol, T. Storer, B. Vellas, S. von Haehling, S.-S. Yeh, and S. Anker, "Sarcopenia with limited mobility: an international consensus.," *J. Am. Med. Dir. Assoc.*, vol. 12, no. 6, pp. 403–409, Jul. 2011.

[2] H. C. Kim, M. Mofarrahi, and S. Hussain, "Skeletal muscle dysfunction in patients with chronic obstructive pulmonary disease.," *Int. J. Chron. Obstruct. Pulmon. Dis.*, vol. 3, no. 4, pp. 637–658, 2008.

[3] R. DeFronzo and D. Tripathy, "Skeletal muscle insulin resistance is the primary defect in type 2 diabetes.," *Diabetes Care*, vol. 32 Suppl 2, Nov. 2009.

[4] B. Clark and T. Manini, "Functional consequences of sarcopenia and dynapenia in the elderly.," *Curr. Opin. Clin. Nutr. Metab. Care*, vol. 13, no. 3, pp. 271–276, May 2010.

[5] J. Lee, K. Waak, M. Grosse-Sundrup, F. Xue, J. Lee, D. Chipman, C. Ryan, E. Bittner, U. Schmidt, and M. Eikermann, "Global muscle strength but not grip strength predicts mortality and length of stay in a general population in a surgical intensive care unit.," *Phys. Ther.*, vol. 92, no. 12, pp. 1546–1555, Dec. 2012.

[6] J. Metter, L. Talbot, M. Schrager, and R. Conwit, "Skeletal muscle strength as a predictor of all-cause mortality in healthy men.," *J. Gerontol. A. Biol. Sci. Med. Sci.*, vol. 57, no. 10, Oct. 2002.

[7] D. A. Winter, *Biomechanics and motor control of human movement*. Wiley. com, 2009.

[8] K. C. Darr and E. Schultz, "Exercise-induced satellite cell activation in growing and mature skeletal muscle," *J. Appl. Physiol.*, vol. 63, no. 5, pp. 1816–1821, Nov. 1987.

[9] H. Yin, F. Price, and M. Rudnicki, "Satellite Cells and the Muscle Stem Cell Niche," *Physiol. Rev.*, vol. 93, no. 1, pp. 23–67, Jan. 2013.

[10] A. SANDOW, "Excitation-contraction coupling in muscular response.," *Yale J. Biol. Med.*, vol. 25, no. 3, pp. 176–201, Dec. 1952.

[11] H. Huxley and J. Hanson, "Changes in the Cross-Striations of Muscle during Contraction and Stretch and their Structural Interpretation," *Nature*, vol. 173, no. 4412, pp. 973–976, May 1954.

[12] A. F. Huxley and R. Niedergerke, "Structural Changes in Muscle During Contraction: Interference Microscopy of Living Muscle Fibres," *Nature*, vol. 173, no. 4412, pp. 971–973, May 1954.

[13] R. W. Lymn and E. W. Taylor, "Mechanism of adenosine triphosphate hydrolysis by actomyosin.," *Biochemistry*, vol. 10, no. 25, pp. 4617–4624, Dec. 1971.

[14] A. Termin, R. S. Staron, and D. Pette, “Myosin heavy chain isoforms in histochemically defined fiber types of rat muscle,” *Histochemistry*, vol. 92, no. 6, pp. 453–457, 1989.

[15] B. Essén, E. Jansson, J. Henriksson, A. W. Taylor, and B. Saltin, “Metabolic Characteristics of Fibre Types in Human Skeletal Muscle,” *Acta Physiol. Scand.*, vol. 95, no. 2, pp. 153–165, Oct. 1975.

[16] P. D. Gollnick, B. Sjödin, J. Karlsson, E. Jansson, and B. Saltin, “Human soleus muscle: A comparison of fiber composition and enzyme activities with other leg muscles,” *Pflügers Arch.*, vol. 348, no. 3, pp. 247–255, Apr. 1974.

[17] E. Schultz, M. C. Gibson, and T. Champion, “Satellite cells are mitotically quiescent in mature mouse muscle: an EM and radioautographic study.,” *J. Exp. Zool.*, vol. 206, no. 3, pp. 451–456, Dec. 1978.

[18] C. Collins, I. Olsen, P. Zammit, L. Heslop, A. Petrie, T. Partridge, and J. Morgan, “Stem cell function, self-renewal, and behavioral heterogeneity of cells from the adult muscle satellite cell niche.,” *Cell*, vol. 122, no. 2, pp. 289–301, Jul. 2005.

[19] R. N. Cooper, S. Tajbakhsh, V. Mouly, G. Cossu, M. Buckingham, and G. S. Butler-Browne, “In vivo satellite cell activation via Myf5 and MyoD in regenerating mouse skeletal muscle.,” *J. Cell Sci.*, vol. 112 (Pt 1, no. 17, pp. 2895–2901, Sep. 1999.

[20] M. A. Rudnicki, P. N. Schnegelsberg, R. H. Stead, T. Braun, H. H. Arnold, and R. Jaenisch, “MyoD or Myf-5 is required for the formation of skeletal muscle.,” *Cell*, vol. 75, no. 7, pp. 1351–1359, Dec. 1993.

[21] C. Bjornson, T. Cheung, L. Liu, P. Tripathi, K. Steeper, and T. Rando, “Notch signaling is necessary to maintain quiescence in adult muscle stem cells.,” *Stem Cells*, vol. 30, no. 2, pp. 232–242, Feb. 2012.

[22] C. Holterman and M. Rudnicki, “Molecular regulation of satellite cell function,” *Semin. Cell Dev. Biol.*, vol. 16, no. 4–5, pp. 575–584, Aug. 2005.

[23] Y. Kawabe and M. Rudnicki, “The Role of Satellite Cells and Stem Cells in Muscle Regeneration,” in *Handbook of Growth and Growth Monitoring in Health and Disease*, V. Preedy, Ed. Springer New York, 2012, pp. 1289–1304.

[24] A. Perezruiz, V. Gnocchi, and P. Zammit, “Control of Myf5 activation in adult skeletal myonuclei requires ERK signalling,” *Cell. Signal.*, vol. 19, no. 8, pp. 1671–1680, Aug. 2007.

[25] J. Chakkalakal, K. Jones, A. Basson, and A. Brack, “The aged niche disrupts muscle stem cell quiescence,” *Nature*, vol. 490, no. 7420, pp. 355–360, Oct. 2012.

[26] M. Cree, B. Newcomer, C. Katsanos, M. Sheffield-Moore, D. Chinkes, A. Aarsland, R. Urban, and R. Wolfe, “Intramuscular and Liver Triglycerides Are Increased in the Elderly,” *J. Clin. Endocrinol. Metab.*, vol. 89, no. 8, pp. 3864–3871, Aug. 2004.

[27] B. Goodpaster, L. Thaete, and D. Kelley, “Composition of Skeletal Muscle Evaluated with Computed Tomography,” *Ann. N. Y. Acad. Sci.*, vol. 904, no. 1, pp. 18–24, May 2000.

[28] M. Delmonico, T. Harris, M. Visser, S. Park, M. Conroy, P. Velasquez-Mieyer, R. Boudreau, T. Manini, M. Nevitt, A. Newman, and B. Goodpaster, “Longitudinal study of muscle strength, quality, and adipose tissue infiltration,” *Am. J. Clin. Nutr.*, vol. 90, no. 6, pp. 1579–1585, Dec. 2009.

[29] J. Lexell, C. C. Taylor, and M. Sjöström, “What is the cause of the ageing atrophy? Total number, size and proportion of different fiber types studied in whole vastus lateralis muscle from 15- to 83-year-old men.,” *J. Neurol. Sci.*, vol. 84, no. 2–3, pp. 275–294, Apr. 1988.

[30] J. Lexell, K. Henriksson-Larsén, B. Winblad, and M. Sjöström, “Distribution of different fiber types in human skeletal muscles: Effects of aging studied in whole muscle cross sections,” *Muscle Nerve*, vol. 6, no. 8, pp. 588–595, Oct. 1983.

[31] W. R. Frontera, V. A. Hughes, K. J. Lutz, and W. J. Evans, “A cross-sectional study of muscle strength and mass in 45- to 78-yr-old men and women.,” *J. Appl. Physiol.*, vol. 71, no. 2, pp. 644–650, Aug. 1991.

[32] B. Goodpaster, S. Park, T. Harris, S. Kritchevsky, M. Nevitt, A. Schwartz, E. Simonsick, F. Tylavsky, M. Visser, and A. Newman, “The Loss of Skeletal Muscle Strength, Mass, and Quality in Older Adults: The Health, Aging and Body Composition Study,” *Journals Gerontol. Ser. A Biol. Sci. Med. Sci.*, vol. 61, no. 10, pp. 1059–1064, Oct. 2006.

[33] E. J. Metter, N. Lynch, R. Conwit, R. Lindle, J. Tobin, and B. Hurley, “Muscle quality and age: cross-sectional and longitudinal comparisons.,” *J. Gerontol. A. Biol. Sci. Med. Sci.*, vol. 54, no. 5, May 1999.

[34] R. Baumgartner, K. Koehler, D. Gallagher, L. Romero, S. Heymsfield, R. Ross, P. Garry, and R. Lindeman, “Epidemiology of Sarcopenia among the Elderly in New Mexico,” *Am. J. Epidemiol.*, vol. 147, no. 8, pp. 755–763, Apr. 1998.

[35] K. Short, J. Vittone, M. Bigelow, D. Proctor, and S. Nair, “Age and aerobic exercise training effects on whole body and muscle protein metabolism,” *Am. J. Physiol. - Endocrinol. Metab.*, vol. 286, no. 1, pp. E92–E101, Jan. 2004.

[36] K. Short, J. Vittone, M. Bigelow, D. Proctor, R. Rizza, J. Coenen-Schimke, and S. Nair, “Impact of Aerobic Exercise Training on Age-Related Changes in Insulin Sensitivity and Muscle Oxidative Capacity,” *Diabetes*, vol. 52, no. 8, pp. 1888–1896, Aug. 2003.

[37] J. D. MacDougall, G. C. Elder, D. G. Sale, J. R. Moroz, and J. R. Sutton, “Effects of strength training and immobilization on human muscle fibres.,” *Eur. J. Appl. Physiol. Occup. Physiol.*, vol. 43, no. 1, pp. 25–34, Feb. 1980.

[38] K. E. Yarasheski, J. J. Zachwieja, and D. M. Bier, “Acute effects of resistance exercise on muscle protein synthesis rate in young and elderly men and women.,” *Am. J. Physiol.*, vol. 265, no. 2 Pt 1, Aug. 1993.

[39] S. Welle, C. Thornton, R. Jozefowicz, and M. Statt, “Myofibrillar protein synthesis in young and old men.,” *Am. J. Physiol.*, vol. 264, no. 5 Pt 1, May 1993.

[40] P. Balagopal, O. E. Rooyackers, D. B. Adey, P. A. Ades, and K. S. Nair, “Effects of aging on in vivo synthesis of skeletal muscle myosin heavy-chain and sarcoplasmic protein in humans.,” *Am. J. Physiol.*, vol. 273, no. 4 Pt 1, Oct. 1997.

[41] O. E. Rooyackers, D. B. Adey, P. A. Ades, and K. S. Nair, “Effect of age on in vivo rates of mitochondrial protein synthesis in human skeletal muscle.,” *Proc. Natl. Acad. Sci. U. S. A.*, vol. 93, no. 26, pp. 15364–15369, Dec. 1996.

[42] P. Balagopal, J. Schimke, P. Ades, D. Adey, and S. Nair, “Age effect on transcript levels and synthesis rate of muscle MHC and response to resistance exercise,” *Am. J. Physiol. - Endocrinol. Metab.*, vol. 280, no. 2, pp. E203–E208, Feb. 2001.

[43] D. Cuthbertson, K. Smith, J. Babraj, G. Leese, T. Waddell, P. Atherton, H. Wackerhage, P. Taylor, and M. Rennie, “Anabolic signaling deficits underlie amino acid resistance of wasting, aging muscle,” *FASEB J.*, vol. 19, no. 3, pp. 422–424, Mar. 2005.

[44] C. Katsanos, H. Kobayashi, M. Sheffield-Moore, A. Aarsland, and R. Wolfe, “Aging is associated with diminished accretion of muscle proteins after the ingestion of a small bolus of essential amino acids,” *Am. J. Clin. Nutr.*, vol. 82, no. 5, pp. 1065–1073, Nov. 2005.

[45] R. Koopman and L. J. C. van Loon, “Aging, exercise, and muscle protein metabolism,” *J. Appl. Physiol.*, vol. 106, no. 6, pp. 2040–2048, 2009.

[46] P. Tesch, F. von Walden, T. Gustafsson, R. Linnehan, and T. Trappe, “Skeletal muscle proteolysis in response to short-term unloading in humans,” *J. Appl. Physiol.*, vol. 105, no. 3, pp. 902–906, Sep. 2008.

[47] C. Mendias, J. Gumucio, M. Davis, C. Bromley, C. Davis, and S. Brooks, “Transforming growth factor-beta induces skeletal muscle atrophy and fibrosis through the induction of atrogin-1 and scleraxis,” *Muscle Nerve*, vol. 45, no. 1, pp. 55–59, Jan. 2012.

[48] C. McFarlane, E. Plummer, M. Thomas, A. Hennebry, M. Ashby, N. Ling, H. Smith, M. Sharma, and R. Kambadur, “Myostatin induces cachexia by activating the ubiquitin proteolytic system through an NF-kappaB-independent, FoxO1-dependent mechanism.,” *J. Cell. Physiol.*, vol. 209, no. 2, pp. 501–514, Nov. 2006.

[49] E. Edström, M. Altun, M. Hägglund, and B. Ulfhake, “Atrogin-1/MAFbx and MuRF1 are downregulated in aging-related loss of skeletal muscle.,” *J. Gerontol. A. Biol. Sci. Med. Sci.*, vol. 61, no. 7, pp. 663–674, Jul. 2006.

[50] S. Clavel, A.-S. Coldefy, E. Kurkdjian, J. Salles, I. Margaritis, and B. Derijard, “Atrophy-related ubiquitin ligases, atrogin-1 and MuRF1 are up-regulated in aged rat Tibialis Anterior muscle,” *Mech. Ageing Dev.*, vol. 127, no. 10, pp. 794–801, Oct. 2006.

[51] J. Gumucio and C. Mendias, “Atrogin-1, MuRF-1, and sarcopenia.,” *Endocrine*, vol. 43, no. 1, pp. 12–21, Feb. 2013.

[52] E. Barton-Davis, D. Shoturma, A. Musaro, N. Rosenthal, and L. Sweeney, “Viral mediated expression of insulin-like growth factor I blocks the aging-related loss of skeletal muscle function,” *Proc. Natl. Acad. Sci.*, vol. 95, no. 26, pp. 15603–15607, Dec. 1998.

[53] L. Pelosi, C. Giacinti, C. Nardis, G. Borsellino, E. Rizzuto, C. Nicoletti, F. Wannenes, L. Battistini, N. Rosenthal, M. Molinaro, and A. Musarò, “Local expression of IGF-1 accelerates muscle regeneration by rapidly modulating inflammatory cytokines and chemokines,” *FASEB J.*, vol. 21, no. 7, pp. 1393–1402, May 2007.

[54] R. J. Louard, D. A. Fryburg, R. A. Gelfand, and E. J. Barrett, “Insulin sensitivity of protein and glucose metabolism in human forearm skeletal muscle.,” *J. Clin. Invest.*, vol. 90, no. 6, p. 2348, 1992.

[55] P. L. Greenhaff, L. G. Karagounis, N. Peirce, E. J. Simpson, M. Hazell, R. Layfield, H. Wackerhage, K. Smith, P. Atherton, A. Selby, and M. J. Rennie, “Disassociation between the effects of amino acids and insulin on signaling, ubiquitin ligases, and protein turnover in human muscle,” *Am. J. Physiol. - Endocrinol. Metab.*, vol. 295, no. 3, pp. E595–E604, Sep. 2008.

[56] D. HARMAN, “Aging: a theory based on free radical and radiation chemistry.,” *J. Gerontol.*, vol. 11, no. 3, pp. 298–300, Jul. 1956.

[57] D. Harman, “Free radical theory of aging: effect of free radical reaction inhibitors on the mortality rate of male LAF mice.,” *J. Gerontol.*, vol. 23, no. 4, pp. 476–482, Oct. 1968.

[58] D. Harman, “The biologic clock: the mitochondria?,” *J. Am. Geriatr. Soc.*, vol. 20, no. 4, pp. 145–147, Apr. 1972.

[59] S. Schriner, N. Linford, G. Martin, P. Treuting, C. Ogburn, M. Emond, P. Coskun, W. Ladiges, N. Wolf, H. Van Remmen, D. Wallace, and P. Rabinovitch, “Extension of murine life span by overexpression of catalase targeted to mitochondria.,” *Science*, vol. 308, no. 5730, pp. 1909–1911, Jun. 2005.

[60] T. Nystrom, “Role of oxidative carbonylation in protein quality control and senescence,” *EMBO J.*, vol. 24, no. 7, pp. 1311–1317, Mar. 2005.

[61] E. Barreiro, A. Schols, M. I. Polkey, J. B. Galdiz, H. R. Gosker, E. B. Swallow, C. Coronell, and J. Gea, “Cytokine profile in quadriceps muscles of patients with severe COPD,” *Thorax*, vol. 63, no. 2, pp. 100–107, Feb. 2008.

[62] M. Johnson, M. Robinson, and S. Nair, “Skeletal muscle aging and the mitochondrion,” *Trends Endocrinol. Metab.*, vol. 24, no. 5, pp. 247–256, May 2013.

[63] K. Short, M. Bigelow, J. Kahl, R. Singh, J. Coenen-Schimke, S. Raghavakaimal, and S. Nair, “Decline in skeletal muscle mitochondrial function with aging in humans.,” *Proc. Natl. Acad. Sci. U. S. A.*, vol. 102, no. 15, pp. 5618–5623, Apr. 2005.

[64] K. Conley, S. Jubrias, and P. Esselman, “Oxidative capacity and ageing in human muscle,” *J. Physiol.*, vol. 526, no. 1, pp. 203–210, Jul. 2000.

[65] D. Bota, H. Van Remmen, and K. Davies, “Modulation of Lon protease activity and aconitase turnover during aging and oxidative stress,” *FEBS Lett.*, vol. 532, no. 1–2, pp. 103–106, Dec. 2002.

[66] Y. Matsushima, Y. Goto, and L. Kaguni, “Mitochondrial Lon protease regulates mitochondrial DNA copy number and transcription by selective degradation of mitochondrial transcription factor A (TFAM),” *Proc. Natl. Acad. Sci.*, vol. 107, no. 43, pp. 18410–18415, Oct. 2010.

[67] G. Twig, A. Elorza, A. Molina, H. Mohamed, J. Wikstrom, G. Walzer, L. Stiles, S. Haigh, S. Katz, G. Las, J. Alroy, M. Wu, B. Py, J. Yuan, J. Deeney, B. Corkey, and O. Shirihai, “Fission and selective fusion govern mitochondrial segregation and elimination by autophagy.,” *EMBO J.*, vol. 27, no. 2, pp. 433–446, Jan. 2008.

[68] C. Zhang and A. Cuervo, “Restoration of chaperone-mediated autophagy in aging liver improves cellular maintenance and hepatic function,” *Nat Med*, vol. 14, no. 9, pp. 959–965, Sep. 2008.

[69] J. Wanagat, Z. Cao, P. Pathare, and J. M. Aiken, “Mitochondrial DNA deletion mutations colocalize with segmental electron transport system abnormalities, muscle fiber atrophy, fiber splitting, and oxidative damage in sarcopenia.,” *FASEB J.*, vol. 15, no. 2, pp. 322–332, Feb. 2001.

[70] Z. Wu, P. Puigserver, U. Andersson, C. Zhang, G. Adelmant, V. Mootha, A. Troy, S. Cinti, B. Lowell, R. C. Scarpulla, and B. M. Spiegelman, “Mechanisms controlling mitochondrial biogenesis and respiration through the thermogenic coactivator PGC-1.,” *Cell*, vol. 98, no. 1, pp. 115–124, Jul. 1999.

[71] S. Ghosh, R. Lertwattanarak, N. Lefort, M. Molina-Carrion, J. Joya-Galeana, B. Bowen, J. de J. Garduno-Garcia, M. Abdul-Ghani, A. Richardson, R. DeFronzo, L. Mandarino, H. Van Remmen, and N. Musi, “Reduction in Reactive Oxygen Species Production by Mitochondria From Elderly Subjects With Normal and Impaired Glucose Tolerance,” *Diabetes*, vol. 60, no. 8, pp. 2051–2060, Aug. 2011.

[72] T. Wenz, S. Rossi, R. Rotundo, B. Spiegelman, and C. Moraes, “Increased muscle PGC-1alpha expression protects from sarcopenia and metabolic disease during aging.,” *Proc. Natl. Acad. Sci. U. S. A.*, vol. 106, no. 48, pp. 20405–20410, Dec. 2009.

[73] J. Lin, H. Wu, P. Tarr, C.-Y. Zhang, Z. Wu, O. Boss, L. Michael, P. Puigserver, E. Isotani, E. Olson, B. Lowell, R. Bassel-Duby, and B. Spiegelman, “Transcriptional co-activator PGC-1 alpha drives the formation of slow-twitch muscle fibres.,” *Nature*, vol. 418, no. 6899, pp. 797–801, Aug. 2002.

[74] L. F. Michael, Z. Wu, R. B. Cheatham, P. Puigserver, G. Adelmant, J. J. Lehman, D. P. Kelly, and B. M. Spiegelman, “Restoration of insulin-sensitive glucose transporter (GLUT4) gene expression in muscle cells by the transcriptional coactivator PGC-1.,” *Proc. Natl. Acad. Sci. U. S. A.*, vol. 98, no. 7, pp. 3820–3825, Mar. 2001.

[75] J. Cunningham, J. Rodgers, D. Arlow, F. Vazquez, V. Mootha, and P. Puigserver, "mTOR controls mitochondrial oxidative function through a YY1-PGC-1alpha transcriptional complex.," *Nature*, vol. 450, no. 7170, pp. 736–740, Nov. 2007.

[76] W. W. Winder, B. F. Holmes, D. S. Rubink, E. B. Jensen, M. Chen, and J. O. Holloszy, "Activation of AMP-activated protein kinase increases mitochondrial enzymes in skeletal muscle," *J. Appl. Physiol.*, vol. 88, no. 6, pp. 2219–2226, Jun. 2000.

[77] R. Bergeron, J. M. Ren, K. S. Cadman, I. K. Moore, P. Perret, M. Pypaert, L. H. Young, C. F. Semenkovich, and G. I. Shulman, "Chronic activation of AMP kinase results in NRF-1 activation and mitochondrial biogenesis.," *Am. J. Physiol. Endocrinol. Metab.*, vol. 281, no. 6, Dec. 2001.

[78] H. Zong, J. M. Ren, L. H. Young, M. Pypaert, J. Mu, M. J. Birnbaum, and G. I. Shulman, "AMP kinase is required for mitochondrial biogenesis in skeletal muscle in response to chronic energy deprivation.," *Proc. Natl. Acad. Sci. U. S. A.*, vol. 99, no. 25, pp. 15983–7, Dec. 2002.

[79] R. M. Reznick, H. Zong, J. Li, K. Morino, I. K. Moore, H. J. Yu, Z.-X. Liu, J. Dong, K. J. Mustard, S. A. Hawley, D. Befroy, M. Pypaert, D. G. Hardie, L. H. Young, and G. I. Shulman, "Aging-Associated Reductions in AMP-Activated Protein Kinase Activity and Mitochondrial Biogenesis," *Cell Metab.*, vol. 5, pp. 151–156, 2007.

[80] H.-Y. Lee, C. S. Choi, A. L. Birkenfeld, T. C. Alves, F. R. Jornayvaz, M. J. Jurczak, D. Zhang, D. K. Woo, G. S. Shadel, W. Ladiges, P. S. Rabinovitch, J. H. Santos, K. F. Petersen, V. T. Samuel, and G. I. Shulman, "Targeted expression of catalase to mitochondria prevents age-associated reductions in mitochondrial function and insulin resistance.," *Cell Metab.*, vol. 12, no. 6, pp. 668–74, Dec. 2010.

[81] A. J. Still, B. J. Floyd, A. S. Hebert, C. a Bingman, J. J. Carson, D. R. Gunderson, B. K. Dolan, P. a Grimsrud, K. E. Dittenhafer-Reed, D. S. Stapleton, M. P. Keller, M. S. Westphall, J. M. Denu, A. D. Attie, J. J. Coon, and D. J. Pagliarini, "Quantification of mitochondrial acetylation dynamics highlights prominent sites of metabolic regulation.," *J. Biol. Chem.*, vol. 288, no. 36, pp. 26209–19, Sep. 2013.

[82] M. J. Rardin, J. C. Newman, J. M. Held, M. P. Cusack, D. J. Sorensen, B. Li, B. Schilling, S. D. Mooney, C. R. Kahn, E. Verdin, and B. W. Gibson, "Label-free quantitative proteomics of the lysine acetylome in mitochondria identifies substrates of SIRT3 in metabolic pathways.," *Proc. Natl. Acad. Sci. U. S. A.*, vol. 110, no. 16, pp. 6601–6, Apr. 2013.

[83] C. Cantó, L. Q. Jiang, A. S. Deshmukh, C. Mataki, A. Coste, M. Lagouge, J. R. Zierath, and J. Auwerx, "Interdependence of AMPK and SIRT1 for metabolic adaptation to fasting and exercise in skeletal muscle.," *Cell Metab.*, vol. 11, pp. 213–219, 2010.

[84] Y. Xiong and K. L. Guan, "Mechanistic insights into the regulation of metabolic enzymes by acetylation," *J. Cell Biol.*, vol. 198, pp. 155–164, 2012.

[85] M. Kern, J. a Wells, J. M. Stephens, C. W. Elton, J. E. Friedman, E. B. Tapscott, P. H. Pekala, and G. L. Dohm, "Insulin responsiveness in skeletal muscle is determined by

glucose transporter (Glut4) protein level.," *Biochem. J.*, vol. 270, no. 2, pp. 397–400, Sep. 1990.

[86] C. S. Stump, K. R. Short, M. L. Bigelow, J. M. Schimke, and K. S. Nair, "Effect of insulin on human skeletal muscle mitochondrial ATP production, protein synthesis, and mRNA transcripts.," *Proc. Natl. Acad. Sci. U. S. A.*, vol. 100, no. 13, pp. 7996–8001, Jun. 2003.

[87] J. P. Kirwan, W. M. Kohrt, D. M. Wojta, R. E. Bourey, and J. O. Holloszy, "Endurance exercise training reduces glucose-stimulated insulin levels in 60- to 70-year-old men and women.," *J. Gerontol.*, vol. 48, no. 3, pp. M84–90, May 1993.

[88] G. M. Reaven, N. Chen, C. Hollenbeck, and Y. D. Chen, "Effect of age on glucose tolerance and glucose uptake in healthy individuals.," *J. Am. Geriatr. Soc.*, vol. 37, pp. 735–740, 1989.

[89] C. Yu, Y. Chen, G. W. Cline, D. Zhang, H. Zong, Y. Wang, R. Bergeron, J. K. Kim, S. W. Cushman, G. J. Cooney, B. Atcheson, M. F. White, E. W. Kraegen, and G. I. Shulman, "Mechanism by which fatty acids inhibit insulin activation of insulin receptor substrate-1 (IRS-1)-associated phosphatidylinositol 3-kinase activity in muscle.," *J. Biol. Chem.*, vol. 277, pp. 50230–50236, 2002.

[90] K. F. Petersen, D. Befroy, S. Dufour, J. Dziura, C. Ariyan, D. L. Rothman, L. DiPietro, G. W. Cline, and G. I. Shulman, "Mitochondrial dysfunction in the elderly: possible role in insulin resistance.," *Science*, vol. 300, no. 5622, pp. 1140–2, May 2003.

[91] J. E. Morley, F. E. Kaiser, H. M. Perry, P. Patrick, P. M. Morley, P. M. Stauber, B. Vellas, R. N. Baumgartner, and P. J. Garry, "Longitudinal changes in testosterone, luteinizing hormone, and follicle-stimulating hormone in healthy older men.," *Metab. Clin. Exp.*, vol. 46, pp. 410–413, 1997.

[92] I. Sinha-Hikim, M. Cornford, H. Gaytan, M. L. Lee, and S. Bhasin, "Effects of testosterone supplementation on skeletal muscle fiber hypertrophy and satellite cells in community-dwelling older men.," *J. Clin. Endocrinol. Metab.*, vol. 91, pp. 3024–3033, 2006.

[93] M. Hermann and P. Berger, "Hormonal changes in aging men: a therapeutic indication?," *Exp. Gerontol.*, vol. 36, pp. 1075–1082, 2001.

[94] M. R. Blackman, J. D. Sorkin, T. Münzer, M. F. Bellantoni, J. Busby-Whitehead, T. E. Stevens, J. Jayme, K. G. O'Connor, C. Christmas, J. D. Tobin, K. J. Stewart, E. Cottrell, C. St Clair, K. M. Pabst, and S. M. Harman, "Growth hormone and sex steroid administration in healthy aged women and men: a randomized controlled trial.," 2002.

[95] K. Sakuma and A. Yamaguchi, "Sarcopenia and age-related endocrine function.," *Int. J. Endocrinol.*, vol. 2012, no. Il, p. 127362, Jan. 2012.

[96] D. Tessier, J. Ménard, T. Fülöp, J. Ardilouze, M. Roy, N. Dubuc, M. Dubois, and P. Gauthier, "Effects of aerobic physical exercise in the elderly with type 2 diabetes mellitus.," *Arch. Gerontol. Geriatr.*, vol. 31, pp. 121–132, 2000.

[97] M. a Puhan, H. J. Schünemann, M. Frey, M. Scharplatz, and L. M. Bachmann, "How should COPD patients exercise during respiratory rehabilitation? Comparison of exercise modalities and intensities to treat skeletal muscle dysfunction.," *Thorax*, vol. 60, no. 5, pp. 367–75, May 2005.

[98] D. Mereles, N. Ehlken, S. Kreuscher, S. Ghofrani, M. M. Hoeper, M. Halank, F. J. Meyer, G. Karger, J. Buss, J. Juenger, N. Holzapfel, C. Opitz, J. Winkler, F. F. J. Herth, H. Wilkens, H. a Katus, H. Olschewski, and E. Grünig, "Exercise and respiratory training improve exercise capacity and quality of life in patients with severe chronic pulmonary hypertension.," *Circulation*, vol. 114, no. 14, pp. 1482–9, Oct. 2006.

[99] S. Basaran, F. Guler-Uysal, N. Ergen, G. Seydaoglu, G. Bingol-Karakoç, and D. Ufuk Altintas, "Effects of physical exercise on quality of life, exercise capacity and pulmonary function in children with asthma.," *J. Rehabil. Med. Off. J. UEMS Eur. Board Phys. Rehabil. Med.*, vol. 38, pp. 130–135, 2006.

[100] R. Hambrecht, E. Fiehn, C. Weigl, S. Gielen, C. Hamann, R. Kaiser, J. Yu, V. Adams, J. Niebauer, and G. Schuler, "Regular Physical Exercise Corrects Endothelial Dysfunction and Improves Exercise Capacity in Patients With Chronic Heart Failure," *Circulation*, vol. 98, no. 24, pp. 2709–2715, Dec. 1998.

[101] S. Terada, M. Goto, M. Kato, K. Kawanaka, T. Shimokawa, and I. Tabata, "Effects of low-intensity prolonged exercise on PGC-1 mRNA expression in rat epitrochlearis muscle.," *Biochem. Biophys. Res. Commun.*, vol. 296, no. 2, pp. 350–4, Aug. 2002.

[102] H. Pilegaard, B. Saltin, and P. D. Neufer, "Exercise induces transient transcriptional activation of the PGC-1 gene in human skeletal muscle," *J. Physiol.*, vol. 546, no. 3, pp. 851–858, Jan. 2003.

[103] K. Day, G. Shefer, A. Shearer, and Z. Yablonka-Reuveni, "The depletion of skeletal muscle satellite cells with age is concomitant with reduced capacity of single progenitors to produce reserve progeny," *Dev. Biol.*, vol. 340, pp. 330–343, 2010.

[104] G. Shefer, G. Rauner, Z. Yablonka-Reuveni, and D. Benayahu, "Reduced satellite cell numbers and myogenic capacity in aging can be alleviated by endurance exercise.," *PLoS One*, vol. 5, no. 10, p. e13307, Jan. 2010.

[105] D. J. Kosek, J.-S. Kim, J. K. Petrella, J. M. Cross, and M. M. Bamman, "Efficacy of 3 days/wk resistance training on myofiber hypertrophy and myogenic mechanisms in young vs. older adults.," *J. Appl. Physiol.*, vol. 101, no. 2, pp. 531–44, Aug. 2006.

[106] A. J. Physiol, E. Metab, D. L. Hasten, J. Pak-loduca, K. A. Obert, K. E. Yarasheski, K. L. Hildreth, D. W. Barry, K. L. Moreau, J. Vande Griend, B. Randall, T. Nakamura, P. Wolfe, W. M. Kohrt, J. M. Ruscin, J. Kittelson, M. E. Cress, R. Ballard, R. S. Schwartz, M. J. Toth, M. S. Miller, P. Vanburen, N. G. Bedrin, M. M. Lewinter, A. Ades, B. M. Palmer, C. Castaneda-sceppa, J. He, M. Kawakubo, S. Bhasin, E. F. Binder, E. T. Schroeder, R. Roubenoff, S. P. Azen, F. R. Sattler, G. I. Smith, B. W. Patterson, and B. Mittendorfer, "Resistance exercise acutely increases MHC and mixed muscle protein synthesis rates in 78 − 84 and 23 − 32 yr olds Resistance exercise acutely increases MHC and mixed muscle protein synthesis rates in 78 – 84 and 23 – 32 yr olds," 2013.

[107] N. B. J. Vollaard, D. Constantin-Teodosiu, K. Fredriksson, O. Rooyackers, E. Jansson, P. L. Greenhaff, J. A. Timmons, and C. J. Sundberg, "Systematic analysis of adaptations in aerobic capacity and submaximal energy metabolism provides a unique insight into determinants of human aerobic performance.," *J. Appl. Physiol.*, vol. 106, no. 5, pp. 1479–86, May 2009.

[108] B. E. Phillips, J. P. Williams, T. Gustafsson, C. Bouchard, T. Rankinen, S. Knudsen, K. Smith, J. a Timmons, and P. J. Atherton, "Molecular networks of human muscle adaptation to exercise and age.," *PLoS Genet.*, vol. 9, no. 3, p. e1003389, Mar. 2013.

[109] P. Jaakkola, D. R. Mole, Y. M. Tian, M. I. Wilson, J. Gielbert, S. J. Gaskell, a von Kriegsheim, H. F. Hebestreit, M. Mukherji, C. J. Schofield, P. H. Maxwell, C. W. Pugh, and P. J. Ratcliffe, "Targeting of HIF-alpha to the von Hippel-Lindau ubiquitylation complex by O2-regulated prolyl hydroxylation.," *Science*, vol. 292, no. 5516, pp. 468–72, Apr. 2001.

[110] J. O. A. Forsythe, B. Jiang, N. V Iyer, F. Agani, and S. W. Leung, "Activation of vascular endothelial growth factor gene transcription by hypoxia-inducible factor Activation of Vascular Endothelial Growth Factor Gene Transcription by Hypoxia-Inducible Factor 1," 1996.

[111] H.-P. Gerber, "Differential Transcriptional Regulation of the Two Vascular Endothelial Growth Factor Receptor Genes. Flt-1, BUT NOT Flk-1/KDR, IS UP-REGULATED BY HYPOXIA," *J. Biol. Chem.*, vol. 272, no. 38, pp. 23659–23667, Sep. 1997.

[112] G. Melillo, T. Musso, a Sica, L. S. Taylor, G. W. Cox, and L. Varesio, "A hypoxia-responsive element mediates a novel pathway of activation of the inducible nitric oxide synthase promoter.," *J. Exp. Med.*, vol. 182, no. 6, pp. 1683–93, Dec. 1995.

[113] K. Hirota and G. L. Semenza, "Regulation of angiogenesis by hypoxia-inducible factor 1.," *Crit. Rev. Oncol. Hematol.*, vol. 59, no. 1, pp. 15–26, Jul. 2006.

[114] T. Gustafsson, A. Puntschart, L. Kaijser, E. Jansson, and C. J. Sundberg, "Exercise-induced expression of angiogenesis-related transcription and growth factors in human skeletal muscle.," *Am. J. Physiol.*, vol. 276, pp. H679–H685, 1999.

[115] K. O'Hagan, S. Cocchiglia, A. Zhdanov, M. Tambuwala, E. Cummins, M. Monfared, T. Agbor, J. Garvey, D. Papkovsky, C. Taylor, and B. Allan, "PGC-1α is coupled to HIF-1α-dependent gene expression by increasing mitochondrial oxygen consumption in skeletal muscle cells," *Proc. Natl. Acad. Sci.*, vol. 106, no. 7, pp. 2188–2193, Feb. 2009.

[116] H. Medical, "I s o l a t i o n of a t u m o r f a c t o r r e s p o n s i b l e for angiogenesis* by judah folkman, m.d., ezio merler, p~.d., charles abernathy, m.d., anb gretchen williams," 1971.

[117] K. H. Plate, G. Breier, H. A. Weich, and W. Risau, "Vascular endothelial growth factor is a potential tumour angiogenesis factor in human gliomas in vivo.," *Nature*, vol. 359, pp. 845–848, 1992.

[118] D. Shweiki, M. Neeman, A. Itin, and E. Keshet, "Induction of vascular endothelial growth factor expression by hypoxia and by glucose deficiency in multicell spheroids:

implications for tumor angiogenesis.," *Proc. Natl. Acad. Sci. U. S. A.*, vol. 92, no. 3, pp. 768–772, Jan. 1995.

[119] R. K. Jain, E. di Tomaso, D. G. Duda, J. S. Loeffler, a G. Sorensen, and T. T. Batchelor, "Angiogenesis in brain tumours.," *Nat. Rev. Neurosci.*, vol. 8, no. 8, pp. 610–22, Aug. 2007.

[120] V. Baeriswyl and G. Christofori, "The angiogenic switch in carcinogenesis.," *Semin. Cancer Biol.*, vol. 19, no. 5, pp. 329–37, Oct. 2009.

[121] H. Shen, N. Zamboni, M. Heinonen, and J. Rousu, "Metabolite Identification through Machine Learning— Tackling CASMI Challenge Using FingerID," *Metabolites*, vol. 3, no. 2, pp. 484–505, Jun. 2013.

[122] R. A. Irizarry, B. Hobbs, F. Collin, Y. D. Beazer-Barclay, K. J. Antonellis, U. Scherf, and T. P. Speed, "Exploration, normalization, and summaries of high density oligonucleotide array probe level data.," *Biostat. Oxford Engl.*, vol. 4, pp. 249–264, 2003.

[123] S. D. Pepper, E. K. Saunders, L. E. Edwards, C. L. Wilson, and C. J. Miller, "The utility of MAS5 expression summary and detection call algorithms," *BMC Bioinformatics*, vol. 8, p. 273, 2007.

[124] Z. Wu, R. A. Irizarry, R. Gentleman, F. Martinez-Murillo, and F. Spencer, "A model-based background adjustment for oligonucleotide expression arrays," *J. Am. Stat. Assoc.*, vol. 99, pp. 909–917, 2004.

[125] W. K. Lim, K. Wang, C. Lefebvre, and A. Califano, "Comparative analysis of microarray normalization procedures: effects on reverse engineering gene networks.," *Bioinforma. Oxford Engl.*, vol. 23, pp. i282–8, 2007.

[126] B. M. Bolstad, R. a Irizarry, M. Astrand, and T. P. Speed, "A comparison of normalization methods for high density oligonucleotide array data based on variance and bias.," *Bioinformatics*, vol. 19, no. 2, pp. 185–93, Jan. 2003.

[127] G. K. Smyth and T. Speed, "Normalization of cDNA microarray data.," *Methods San Diego Calif*, vol. 31, pp. 265–273, 2003.

[128] S. Raychaudhuri, J. M. Stuart, and R. B. Altman, "Principal components analysis to summarize microarray experiments: application to sporulation time series.," *Pacific Symp. Biocomput.*, vol. 463, pp. 455–466, 2000.

[129] M. J Van Der Laan, "A new algorithm for hybrid hierarchical clustering with visualization and the bootstrap," *J. Stat. Plan. Inference*, vol. 117, pp. 275–303, 2003.

[130] V. G. Tusher, R. Tibshirani, and G. Chu, "Significance analysis of microarrays applied to the ionizing radiation response.," *Proc. Natl. Acad. Sci. U. S. A.*, vol. 98, pp. 5116–5121, 2001.

[131] M. J. Aryee, J. A. Gutiérrez-Pabello, I. Kramnik, T. Maiti, and J. Quackenbush, "An improved empirical bayes approach to estimating differential gene expression in

microarray time-course data: BETR (Bayesian Estimation of Temporal Regulation),” *BMC Bioinformatics*, vol. 10, p. 409, 2009.

[132] Y. Benjamini and Y. Hochberg, “Controlling the false discovery rate: a practical and powerful approach to multiple testing,” *J. R. Stat. Soc. Ser. B Methodol.*, vol. 57, pp. 289–300, 1995.

[133] M. Ashburner, C. A. Ball, J. A. Blake, D. Botstein, H. Butler, J. M. Cherry, A. P. Davis, K. Dolinski, S. S. Dwight, J. T. Eppig, M. A. Harris, D. P. Hill, L. Issel-Tarver, A. Kasarskis, S. Lewis, J. C. Matese, J. E. Richardson, M. Ringwald, G. M. Rubin, and G. Sherlock, “Gene ontology: tool for the unification of biology. The Gene Ontology Consortium.,” *Nat. Genet.*, vol. 25, pp. 25–29, 2000.

[134] D. W. Huang, B. T. Sherman, and R. A. Lempicki, “Systematic and integrative analysis of large gene lists using DAVID bioinformatics resources.,” *Nat. Protoc.*, vol. 4, pp. 44–57, 2009.

[135] A. Subramanian, P. Tamayo, V. K. Mootha, S. Mukherjee, B. L. Ebert, M. A. Gillette, A. Paulovich, S. L. Pomeroy, T. R. Golub, E. S. Lander, and J. P. Mesirov, “Gene set enrichment analysis: a knowledge-based approach for interpreting genome-wide expression profiles.,” *Proc. Natl. Acad. Sci. U. S. A.*, vol. 102, no. 43, pp. 15545–15550, Oct. 2005.

[136] A. A. Margolin, I. Nemenman, K. Basso, C. Wiggins, G. Stolovitzky, R. D. Favera, and A. Califano, “ARACNE: An Algorithm for the Reconstruction of Gene Regulatory Networks in a Mammalian Cellular Context,” *BMC Bioinformatics*, vol. 7, p. S7, 2006.

[137] A. Margolin, K. Wang, W. Lim, M. Kustagi, I. Nemenman, and A. Califano, “Reverse engineering cellular networks,” *Nat. Protoc.*, vol. 1, no. 2, pp. 662–671, Jun. 2006.

[138] G. Su, A. Kuchinsky, J. H. Morris, D. J. States, and F. Meng, “GLay: community structure analysis of biological networks,” *Bioinformatics*, vol. 26, pp. 3135–3137, 2010.

[139] G. D. Bader and C. W. Hogue, “An automated method for finding molecular complexes in large protein interaction networks,” *BMC Bioinformatics*, vol. 4, no. 1, pp. 1–27, Dec. 2003.

[140] K. Wakita and T. Tsurumi, “Finding Community Structure in Mega-scale Social Networks,” p. 9, Feb. 2007.

[141] P. Shannon, A. Markiel, O. Ozier, N. S. Baliga, J. T. Wang, D. Ramage, N. Amin, B. Schwikowski, and T. Ideker, “Cytoscape: a software environment for integrated models of biomolecular interaction networks.,” *Genome Res.*, vol. 13, pp. 2498–504, 2003.

[142] D. Di Bernardo, M. J. Thompson, T. S. Gardner, S. E. Chobot, E. L. Eastwood, A. P. Wojtovich, S. J. Elliott, S. E. Schaus, and J. J. Collins, “Chemogenomic profiling on a genome-wide scale using reverse-engineered gene networks.,” *Nat. Biotechnol.*, vol. 23, pp. 377–383, 2005.

[143] M. Bansal, G. Della Gatta, and D. Di Bernardo, “Inference of gene regulatory networks and compound mode of action from time course gene expression profiles.,” *Bioinformatics*, vol. 22, pp. 815–822, 2006.

[144] S. Welle, A. I. Brooks, J. M. Delehanty, N. Needler, K. Bhatt, B. Shah, and C. A. Thornton, “Skeletal muscle gene expression profiles in 20-29 year old and 65-71 year old women.,” *Exp. Gerontol.*, vol. 39, pp. 369–377, 2004.

[145] S. Melov, M. Tarnopolsky, K. Beckman, K. Felkey, and A. Hubbard, “Resistance Exercise Reverses Aging in Human Skeletal Muscle,” *PLoS One*, vol. 2, no. 5, p. e465, May 2007.

[146] J. Zahn, R. Sonu, H. Vogel, E. Crane, K. Mazan-Mamczarz, R. Rabkin, R. Davis, K. Becker, A. Owen, and S. Kim, “Transcriptional Profiling of Aging in Human Muscle Reveals a Common Aging Signature,” *PLoS Genet*, vol. 2, no. 7, p. e115, Jul. 2006.

[147] U. Raue, T. Trappe, S. Estrem, H.-R. Qian, L. Helvering, R. Smith, and S. Trappe, “Transcriptome signature of resistance exercise adaptations: mixed muscle and fiber type specific profiles in young and old adults.,” *J. Appl. Physiol.*, vol. 112, no. 10, pp. 1625–1636, May 2012.

[148] P. G. Giresi, E. J. Stevenson, J. Theilhaber, A. Koncarevic, J. Parkington, R. A. Fielding, S. C. Kandarian, G. Paul, and C. Susan, “Identification of a molecular signature of sarcopenia,” pp. 253–263, 2005.

[149] A. M. J. Sanchez, A. Csibi, A. Raibon, K. Cornille, S. Gay, H. Bernardi, and R. Candau, “AMPK promotes skeletal muscle autophagy through activation of forkhead FoxO3a and interaction with Ulk1.,” *J. Cell. Biochem.*, vol. 113, no. 2, pp. 695–710, Feb. 2012.

[150] G. Zhang, B. Jin, and Y.-P. Li, “C/EBPβ mediates tumour-induced ubiquitin ligase atrogin1/MAFbx upregulation and muscle wasting.,” *EMBO J.*, vol. 30, no. 20, pp. 4323–35, Oct. 2011.

[151] A. Abadi, E. I. Glover, R. J. Isfort, S. Raha, A. Safdar, N. Yasuda, J. J. Kaczor, S. Melov, A. Hubbard, X. Qu, S. M. Phillips, and M. Tarnopolsky, “Limb immobilization induces a coordinate down-regulation of mitochondrial and other metabolic pathways in men and women.,” *PLoS One*, vol. 4, no. 8, p. e6518, Jan. 2009.

[152] K. A. Reich, Y.-W. Chen, P. D. Thompson, E. P. Hoffman, and P. M. Clarkson, “Forty-eight hours of unloading and 24 h of reloading lead to changes in global gene expression patterns related to ubiquitination and oxidative stress in humans.,” *J. Appl. Physiol.*, vol. 109, pp. 1404–1415, 2010.

[153] S. Radom-Aizik, S. Hayek, I. Shahar, G. Rechavi, N. Kaminski, and I. Ben-Dov, “Effects of Aerobic Training on Gene Expression in Skeletal Muscle of Elderly Men,” *Med. Sci. Sport. Exerc.*, vol. 37, pp. 1680–1696, 2005.

[154] Y. Wang, J. Winters, and S. Subramaniam, “Functional classification of skeletal muscle networks. I. Normal physiology.,” *J. Appl. Physiol. Bethesda Md 1985*, vol. 113, pp. 1884–901, 2012.

[155] A. Abdollahi, C. Schwager, J. Kleeff, I. Esposito, S. Domhan, P. Peschke, K. Hauser, P. Hahnfeldt, L. Hlatky, J. Debus, J. M. Peters, H. Friess, J. Folkman, and P. E. Huber, "Transcriptional network governing the angiogenic switch in human pancreatic cancer.," *Proc. Natl. Acad. Sci. U. S. A.*, vol. 104, no. 31, pp. 12890–5, Jul. 2007.

[156] M. Anders, M. Fehlker, Q. Wang, C. Wissmann, C. Pilarsky, W. Kemmner, and M. Höcker, "Microarray meta-analysis defines global angiogenesis-related gene expression signatures in human carcinomas," *Mol. Carcinog.*, vol. 52, no. 1, pp. 29–38, Jan. 2013.

[157] L.-H. Chu, C. G. Rivera, A. S. Popel, and J. S. Bader, "Constructing the angiome: a global angiogenesis protein interaction network.," *Physiol. Genomics*, vol. 44, no. 19, pp. 915–924, Oct. 2012.

[158] S. Dodson, V. E. Baracos, A. Jatoi, W. J. Evans, D. Cella, J. T. Dalton, and M. S. Steiner, "Muscle wasting in cancer cachexia: clinical implications, diagnosis, and emerging treatment strategies.," *Annu. Rev. Med.*, vol. 62, pp. 265–79, Jan. 2011.

[159] E. Wouters, E. Creutzberg, and A. Schols, "Systemic effects in COPD.," *Chest*, vol. 121, no. 5 Suppl, May 2002.

[160] K. Hachisuka, Y. Umezu, and H. Ogata, "Disuse muscle atrophy of lower limbs in hemiplegic patients," *Arch. Phys. Med. Rehabil.*, vol. 78, pp. 13–18, 1997.

[161] B. T. Workeneh and W. E. Mitch, "Review of muscle wasting associated with chronic kidney disease 1 – 3," vol. 91, no. April 2009, pp. 1128–1132, 2010.

[162] T. a Scherer, C. M. Spengler, D. Owassapian, E. Imhof, and U. Boutellier, "Respiratory muscle endurance training in chronic obstructive pulmonary disease: impact on exercise capacity, dyspnea, and quality of life.," *Am. J. Respir. Crit. Care Med.*, vol. 162, no. 5, pp. 1709–14, Nov. 2000.

[163] R. Mostert, a Goris, C. Weling-Scheepers, E. F. Wouters, and a M. Schols, "Tissue depletion and health related quality of life in patients with chronic obstructive pulmonary disease.," *Respir. Med.*, vol. 94, no. 9, pp. 859–67, Sep. 2000.

[164] J. Ruiz, X. Sui, F. Lobelo, J. Morrow, A. Jackson, M. Sjöström, and S. Blair, "Association between muscular strength and mortality in men: prospective cohort study," *BMJ*, vol. 337, Jul. 2008.

[165] J. E. Morley, J. M. Argiles, W. J. Evans, S. Bhasin, D. Cella, N. E. P. Deutz, W. Doehner, K. C. H. Fearon, L. Ferrucci, M. K. Hellerstein, K. Kalantar-Zadeh, H. Lochs, N. MacDonald, K. Mulligan, M. Muscaritoli, P. Ponikowski, M. E. Posthauer, F. Rossi Fanelli, M. Schambelan, A. M. W. J. Schols, M. W. Schuster, and S. D. Anker, "Nutritional recommendations for the management of sarcopenia.," *J. Am. Med. Dir. Assoc.*, vol. 11, no. 6, pp. 391–6, Jul. 2010.

[166] T. J. Marcell, "Sarcopenia: causes, consequences, and preventions.," *J. Gerontol. A. Biol. Sci. Med. Sci.*, vol. 58, no. 10, pp. M911–6, Oct. 2003.

[167] G. A. Nader and I. E. Lundberg, “Exercise as an anti-inflammatory intervention to combat inflammatory diseases of muscle.,” *Curr. Opin. Rheumatol.*, vol. 21, pp. 599–603, 2009.

[168] M. Braga, A. P. Sinha Hikim, S. Datta, M. G. Ferrini, D. Brown, E. L. Kovacheva, N. F. Gonzalez-Cadavid, and I. Sinha-Hikim, “Involvement of oxidative stress and caspase 2-mediated intrinsic pathway signaling in age-related increase in muscle cell apoptosis in mice.,” *Apoptosis*, vol. 13, no. 6, pp. 822–32, Jun. 2008.

[169] L. M. Dillon, A. P. Rebelo, and C. T. Moraes, “The role of PGC-1 coactivators in aging skeletal muscle and heart.,” *IUBMB Life*, vol. 64, no. 3, pp. 231–241, Mar. 2012.

[170] P. M. Coen, S. a Jubrias, G. Distefano, F. Amati, D. C. Mackey, N. W. Glynn, T. M. Manini, S. E. Wohlgemuth, C. Leeuwenburgh, S. R. Cummings, A. B. Newman, L. Ferrucci, F. G. S. Toledo, E. Shankland, K. E. Conley, and B. H. Goodpaster, “Skeletal muscle mitochondrial energetics are associated with maximal aerobic capacity and walking speed in older adults.,” *J. Gerontol. A. Biol. Sci. Med. Sci.*, vol. 68, no. 4, pp. 447–55, Apr. 2013.

[171] A. Hiona, A. Sanz, G. Kujoth, R. Pamplona, A. Seo, T. Hofer, S. Someya, T. Miyakawa, C. Nakayama, A. Samhan-Arias, S. Servais, J. Barger, M. Portero-Otín, M. Tanokura, T. Prolla, and C. Leeuwenburgh, “Mitochondrial DNA Mutations Induce Mitochondrial Dysfunction, Apoptosis and Sarcopenia in Skeletal Muscle of Mitochondrial DNA Mutator Mice,” *PLoS One*, vol. 5, no. 7, p. e11468, Jul. 2010.

[172] S. Fulle, F. Protasi, G. Di Tano, T. Pietrangelo, A. Beltramin, S. Boncompagni, L. Vecchiet, and G. Fanò, “The contribution of reactive oxygen species to sarcopenia and muscle ageing,” *Exp. Gerontol.*, vol. 39, no. 1, pp. 17–24, Jan. 2004.

[173] T. Tiganis, “Reactive oxygen species and insulin resistance: the good, the bad and the ugly.,” *Trends Pharmacol. Sci.*, vol. 32, no. 2, pp. 82–9, Feb. 2011.

[174] N. Turan, S. Kalko, A. Stincone, K. Clarke, A. Sabah, K. Howlett, S. J. Curnow, D. a Rodriguez, M. Cascante, L. O’Neill, S. Egginton, J. Roca, and F. Falciani, “A systems biology approach identifies molecular networks defining skeletal muscle abnormalities in chronic obstructive pulmonary disease.,” *PLoS Comput. Biol.*, vol. 7, no. 9, p. e1002129, Sep. 2011.

[175] S. Rome, K. Clément, R. Rabasa-Lhoret, E. Loizon, C. Poitou, G. S. Barsh, J.-P. Riou, M. Laville, and H. Vidal, “Microarray profiling of human skeletal muscle reveals that insulin regulates approximately 800 genes during a hyperinsulinemic clamp.,” *J. Biol. Chem.*, vol. 278, no. 20, pp. 18063–18068, May 2003.

[176] V. K. Mootha, C. M. Lindgren, K.-F. F. Eriksson, A. Subramanian, S. Sihag, J. Lehar, P. Puigserver, E. Carlsson, M. Ridderstrale, E. Laurila, N. Houstis, M. J. Daly, N. Patterson, J. P. Mesirov, T. R. Golub, P. Tamayo, B. Spiegelman, E. S. Lander, J. N. Hirschhorn, D. Altshuler, and L. C. Groop, “PGC-1α-responsive genes involved in oxidative phosphorylation are coordinately downregulated in human diabetes,” *Nat Genet*, vol. 34, no. 3, pp. 267–273, Jul. 2003.

[177] F. H. J. van Tienen, S. F. E. Praet, H. M. de Feyter, N. M. van den Broek, P. J. Lindsey, K. G. C. Schoonderwoerd, I. F. M. de Coo, K. Nicolay, J. J. Prompers, H. J.

M. Smeets, and L. J. C. van Loon, “Physical activity is the key determinant of skeletal muscle mitochondrial function in type 2 diabetes.,” *J. Clin. Endocrinol. Metab.*, vol. 97, no. 9, pp. 3261–9, Sep. 2012.

[178] A. E. Thalacker-Mercer, J. C. Fleet, B. A. Craig, N. S. Carnell, and W. W. Campbell, “Inadequate protein intake affects skeletal muscle transcript profiles in older humans.,” *Am. J. Clin. Nutr.*, vol. 85, no. 5, pp. 1344–52, May 2007.

[179] S. Welle, R. Tawil, and C. a Thornton, “Sex-related differences in gene expression in human skeletal muscle.,” *PLoS One*, vol. 3, no. 1, p. e1385, Jan. 2008.

[180] A. C. Zambon, E. L. McDearmon, N. Salomonis, K. M. Vranizan, K. L. Johansen, D. Adey, J. S. Takahashi, M. Schambelan, and B. R. Conklin, “Time- and exercise-dependent gene regulation in human skeletal muscle.,” *Genome Biol.*, vol. 4, no. 10, p. R61, Jan. 2003.

[181] P. Keller, N. B. J. Vollaard, T. Gustafsson, I. J. Gallagher, C. J. Sundberg, T. Rankinen, S. L. Britton, C. Bouchard, L. G. Koch, and J. A. Timmons, “A transcriptional map of the impact of endurance exercise training on skeletal muscle phenotype.,” *J. Appl. Physiol.*, vol. 110, no. 1, pp. 46–59, Jan. 2011.

[182] I. J. Gallagher, C. Scheele, P. Keller, A. R. Nielsen, J. Remenyi, C. P. Fischer, K. Roder, J. Babraj, C. Wahlestedt, G. Hutvagner, B. K. Pedersen, and J. A. Timmons, “Integration of microRNA changes in vivo identifies novel molecular features of muscle insulin resistance in type 2 diabetes.,” *Genome Med.*, vol. 2, no. 2, p. 9, Jan. 2010.

[183] D. K. Coletta, B. Balas, A. O. Chavez, M. Baig, M. Abdul-Ghani, S. R. Kashyap, F. Folli, D. Tripathy, L. J. Mandarino, J. E. Cornell, R. A. Defronzo, and C. P. Jenkinson, “Effect of acute physiological hyperinsulinemia on gene expression in human skeletal muscle in vivo.,” *Am. J. Physiol. Endocrinol. Metab.*, vol. 294, no. 5, pp. E910–7, May 2008.

[184] X. Wu, A. Patki, C. Lara-Castro, X. Cui, K. Zhang, R. G. Walton, M. V Osier, G. L. Gadbury, D. B. Allison, M. Martin, and W. T. Garvey, “Genes and biochemical pathways in human skeletal muscle affecting resting energy expenditure and fuel partitioning.,” *J. Appl. Physiol.*, vol. 110, no. 3, pp. 746–55, Mar. 2011.

[185] H. Parikh, E. Carlsson, W. A. Chutkow, L. E. Johansson, H. Storgaard, P. Poulsen, R. Saxena, C. Ladd, P. C. Schulze, M. J. Mazzini, C. B. Jensen, A. Krook, M. Björnholm, H. Tornqvist, J. R. Zierath, M. Ridderstråle, D. Altshuler, R. T. Lee, A. Vaag, L. C. Groop, and V. K. Mootha, “TXNIP regulates peripheral glucose metabolism in humans.,” *PLoS Med.*, vol. 4, no. 5, p. e158, May 2007.

[186] D. D. Sears, G. Hsiao, A. Hsiao, J. G. Yu, C. H. Courtney, J. M. Ofrecio, J. Chapman, and S. Subramaniam, “Mechanisms of human insulin resistance and thiazolidinedione-mediated insulin sensitization.,” *Proc. Natl. Acad. Sci. U. S. A.*, vol. 106, no. 44, pp. 18745–50, Nov. 2009.

[187] M. G. Edwards, R. M. Anderson, M. Yuan, C. M. Kendziorski, R. Weindruch, and T. A. Prolla, “Gene expression profiling of aging reveals activation of a p53-mediated transcriptional program,” *BMC Genomics*, vol. 8, p. 80, 2007.

[188] W. E. Johnson, C. Li, and A. Rabinovic, “Adjusting batch effects in microarray expression data using empirical Bayes methods.,” *Biostatistics*, vol. 8, no. 1, pp. 118–27, Jan. 2007.

[189] J. H. Morris, L. Apeltsin, A. M. Newman, J. Baumbach, T. Wittkop, G. Su, G. D. Bader, and T. E. Ferrin, “clusterMaker: a multi-algorithm clustering plugin for Cytoscape.,” *BMC Bioinformatics*, vol. 12, p. 436, 2011.

[190] G. D. Penny, G. F. Kay, S. A. Sheardown, S. Rastan, and N. Brockdorff, “Requirement for Xist in X chromosome inactivation.,” *Nature*, vol. 379, pp. 131–137, 1996.

[191] A. Morrione, “Grb10 adapter protein as regulator of insulin-like growth factor receptor signaling.,” *J. Cell. Physiol.*, vol. 197, pp. 307–311, 2003.

[192] C. Pagiatakis, J. W. Gordon, S. Ehyai, and J. C. McDermott, “A novel RhoA/ROCK-CPI-17-MEF2C signaling pathway regulates vascular smooth muscle cell gene expression.,” *J. Biol. Chem.*, vol. 287, no. 11, pp. 8361–70, Mar. 2012.

[193] T. Yokota, K. Sugawara, K. Ito, R. Takahashi, H. Ariga, and H. Mizusawa, “Down regulation of DJ-1 enhances cell death by oxidative stress, ER stress, and proteasome inhibition,” *Biochem. Biophys. Res. Commun.*, vol. 312, no. 4, pp. 1342–1348, Dec. 2003.

[194] T. Waite and L. Campbell, “Controlling the false discovery rate and increasing statistical power in ecological studies,” *Ecoscience*, vol. 13, no. 4, pp. 439–442, 2006.

[195] H. Y. Chung, M. Cesari, S. Anton, E. Marzetti, S. Giovannini, A. Y. Seo, C. Carter, B. P. Yu, and C. Leeuwenburgh, “Molecular inflammation: underpinnings of aging and age-related diseases.,” *Ageing Res. Rev.*, vol. 8, no. 1, pp. 18–30, Jan. 2009.

[196] S. M. Roth, E. J. Metter, S. Ling, and L. Ferrucci, “Inflammatory factors in age-related muscle wasting.,” *Curr. Opin. Rheumatol.*, vol. 18, pp. 625–630, 2006.

[197] F. H. Van Tienen, P. J. Lindsey, C. J. Van Der Kallen, and H. J. Smeets, “Prolonged Nrf1 overexpression triggers adipocyte inflammation and insulin resistance.,” *J. Cell. Biochem.*, vol. 111, pp. 1575–1585, 2010.

[198] Y. C. Jang, M. S. Lustgarten, Y. Liu, F. L. Muller, A. Bhattacharya, H. Liang, A. B. Salmon, S. V Brooks, L. Larkin, C. R. Hayworth, A. Richardson, and H. Van Remmen, “Increased superoxide in vivo accelerates age-associated muscle atrophy through mitochondrial dysfunction and neuromuscular junction degeneration,” *FASEB J.*, vol. 24, no. 5, pp. 1376–1390, May 2010.

[199] A. G. Ryazanov and B. S. Nefsky, “Protein turnover plays a key role in aging.,” *Mech. Ageing Dev.*, vol. 123, no. 2–3, pp. 207–13, Jan. 2002.

[200] I. Guney, S. Wu, and J. M. Sedivy, “Reduced c-Myc signaling triggers telomere-independent senescence by regulating Bmi-1 and p16(INK4a).,” *Proc. Natl. Acad. Sci. U. S. A.*, vol. 103, no. 10, pp. 3645–50, Mar. 2006.

[201] Per Hydbring and Lars-Gunnar Larsson, “Cdk2: a key regulator of the senescence control function of Myc,” *Aging (Albany. NY).*, vol. 2, no. 4, pp. 244–250, 2010.

[202] Y. Zeng, H.-X. Wang, S.-B. Guo, H. Yang, X.-J. Zeng, Q. Fang, C.-S. Tang, J. Du, and H.-H. Li, "Transcriptional effects of E3 ligase atrogin-1/MAFbx on apoptosis, hypertrophy and inflammation in neonatal rat cardiomyocytes.," *PLoS One*, vol. 8, no. 1, p. e53831, Jan. 2013.

[203] H. S. Thompson, S. P. Scordilis, P. M. Clarkson, and W. a Lohrer, "A single bout of eccentric exercise increases HSP27 and HSC/HSP70 in human skeletal muscle.," *Acta Physiol. Scand.*, vol. 171, no. 2, pp. 187–93, Feb. 2001.

[204] F. Kadi, F. Johansson, R. Johansson, M. Sjöström, and J. Henriksson, "Effects of one bout of endurance exercise on the expression of myogenin in human quadriceps muscle.," *Histochem. Cell Biol.*, vol. 121, no. 4, pp. 329–34, Apr. 2004.

[205] J. Timmons, J. Norrbom, C. Schéele, H. Thonberg, C. Wahlestedt, and P. Tesch, "Expression profiling following local muscle inactivity in humans provides new perspective on diabetes-related genes," *Genomics*, vol. 87, no. 1, pp. 165–172, Jan. 2006.

[206] D. a Hood, "Invited Review: contractile activity-induced mitochondrial biogenesis in skeletal muscle.," *J. Appl. Physiol.*, vol. 90, no. 3, pp. 1137–57, Mar. 2001.

[207] M. R. Deschenes, C. M. Maresh, J. F. Crivello, L. E. Armstrong, W. J. Kraemer, and J. Covault, "The effects of exercise training of different intensities on neuromuscular junction morphology.," *J. Neurocytol.*, vol. 22, no. 8, pp. 603–15, Aug. 1993.

[208] C. Dibble and B. Manning, "Signal integration by mTORC1 coordinates nutrient input with biosynthetic output," *Nat Cell Biol*, vol. 15, no. 6, pp. 555–564, Jun. 2013.

[209] L. Chen, B. Xu, L. Liu, Y. Luo, J. Yin, H. Zhou, W. Chen, T. Shen, X. Han, and S. Huang, "Hydrogen peroxide inhibits mTOR signaling by activation of AMPKalpha leading to apoptosis of neuronal cells.," *Lab. Invest.*, vol. 90, no. 5, pp. 762–73, May 2010.

[210] J. Brugarolas, K. Lei, R. L. Hurley, B. D. Manning, J. H. Reiling, E. Hafen, L. a Witters, L. W. Ellisen, and W. G. Kaelin, "Regulation of mTOR function in response to hypoxia by REDD1 and the TSC1/TSC2 tumor suppressor complex.," *Genes Dev.*, vol. 18, no. 23, pp. 2893–904, Dec. 2004.

[211] S. Johnson, P. Rabinovitch, and M. Kaeberlein, "mTOR is a key modulator of ageing and age-related disease," *Nature*, vol. 493, no. 7432, pp. 338–345, Jan. 2013.

[212] R. Zoncu, A. Efeyan, and D. M. Sabatini, "mTOR: from growth signal integration to cancer, diabetes and ageing.," *Nat. Rev. Mol. Cell Biol.*, vol. 12, no. 1, pp. 21–35, Jan. 2011.

[213] F. B. Favier, F. Costes, A. Defour, R. Bonnefoy, E. Lefai, S. Baugé, A. Peinnequin, H. Benoit, and D. Freyssenet, "Downregulation of Akt/mammalian target of rapamycin pathway in skeletal muscle is associated with increased REDD1 expression in response to chronic hypoxia.," *Am. J. Physiol. Regul. Integr. Comp. Physiol.*, vol. 298, no. 6, pp. R1659–66, Jun. 2010.

[214] T. Yoshida, I. Mett, A. K. Bhunia, J. Bowman, M. Perez, L. Zhang, A. Gandjeva, L. Zhen, U. Chukwueke, T. Mao, A. Richter, E. Brown, H. Ashush, N. Notkin, A. Gelfand, R. K. Thimmulappa, T. Rangasamy, T. Sussan, G. Cosgrove, M. Mouded, S. D. Shapiro, I. Petrache, S. Biswal, E. Feinstein, and R. M. Tuder, "Rtp801 , a suppressor of mTOR signaling , is an essential mediator of cigarette smoke – induced pulmonary injury and emphysema," *Nat. Med.*, no. May, 2010.

[215] M. Laplante and D. M. Sabatini, "An emerging role of mTOR in lipid biosynthesis.," *Curr. Biol.*, vol. 19, no. 22, pp. R1046–52, Dec. 2009.

[216] V. Gandin, A. Miluzio, A. M. Barbieri, A. Beugnet, H. Kiyokawa, P. C. Marchisio, and S. Biffo, "Eukaryotic initiation factor 6 is rate-limiting in translation, growth and transformation.," *Nature*, vol. 455, no. 7213, pp. 684–688, Oct. 2008.

[217] F. Supek, M. Bošnjak, N. Škunca, and T. Šmuc, "REVIGO summarizes and visualizes long lists of gene ontology terms.," *PLoS One*, vol. 6, no. 7, p. e21800, Jan. 2011.

[218] I. Wittig, R. Carrozzo, F. M. Santorelli, and H. Schägger, "Functional assays in high-resolution clear native gels to quantify mitochondrial complexes in human biopsies and cell lines.," *Electrophoresis*, vol. 28, no. 21, pp. 3811–20, Nov. 2007.

[219] D. C. Fingar, S. Salama, C. Tsou, E. Harlow, and J. Blenis, "Mammalian cell size is controlled by mTOR and its downstream targets S6K1 and 4EBP1/eIF4E.," *Genes Dev.*, vol. 16, no. 12, pp. 1472–87, Jun. 2002.

[220] B. G. Wouters and M. Koritzinsky, "Hypoxia signalling through mTOR and the unfolded protein response in cancer.," *Nat. Rev. Cancer*, vol. 8, no. 11, pp. 851–64, Nov. 2008.

[221] Y. Ji, S. Shah, K. Soanes, M. N. Islam, B. Hoxter, S. Biffo, T. Heslip, and S. Byers, "Eukaryotic initiation factor 6 selectively regulates Wnt signaling and beta-catenin protein synthesis.," *Oncogene*, vol. 27, no. 6, pp. 755–762, Jan. 2008.

[222] C. Vogel and E. Marcotte, "Insights into the regulation of protein abundance from proteomic and transcriptomic analyses," *Nat Rev Genet*, vol. 13, no. 4, pp. 227–232, Apr. 2012.

[223] D. J. Pagliarini, S. E. Calvo, B. Chang, S. a Sheth, S. B. Vafai, S.-E. Ong, G. a Walford, C. Sugiana, A. Boneh, W. K. Chen, D. E. Hill, M. Vidal, J. G. Evans, D. R. Thorburn, S. a Carr, and V. K. Mootha, "A mitochondrial protein compendium elucidates complex I disease biology.," *Cell*, vol. 134, no. 1, pp. 112–23, Jul. 2008.

[224] K. S. Dimmer and D. Rapaport, "Proteomic view of mitochondrial function.," *Genome Biol.*, vol. 9, no. 2, p. 209, Jan. 2008.

[225] N. Takai, T. Ueda, M. Nishida, K. Nasu, and H. Narahara, "A novel histone deacetylase inhibitor, Scriptaid, induces growth inhibition, cell cycle arrest and apoptosis in human endometrial cancer and ovarian cancer cells.," *Int. J. Mol. Med.*, vol. 17, no. 2, pp. 323–9, Feb. 2006.

[226] D. Vigushin, S. Ali, P. Pace, and N. Mirsaidi, “Trichostatin A is a histone deacetylase inhibitor with potent antitumor activity against breast cancer in vivo,” *Clin. Cancer …*, pp. 971–976, 2001.

[227] M. Göttlicher, S. Minucci, P. Zhu, O. H. Krämer, a Schimpf, S. Giavara, J. P. Sleeman, F. Lo Coco, C. Nervi, P. G. Pelicci, and T. Heinzel, “Valproic acid defines a novel class of HDAC inhibitors inducing differentiation of transformed cells.,” *EMBO J.*, vol. 20, no. 24, pp. 6969–78, Dec. 2001.

[228] M. Koritzinsky, M. G. Magagnin, T. van den Beucken, R. Seigneuric, K. Savelkouls, J. Dostie, S. Pyronnet, R. J. Kaufman, S. a Weppler, J. W. Voncken, P. Lambin, C. Koumenis, N. Sonenberg, and B. G. Wouters, “Gene expression during acute and prolonged hypoxia is regulated by distinct mechanisms of translational control.,” *EMBO J.*, vol. 25, no. 5, pp. 1114–25, Mar. 2006.

[229] A. Pause, G. J. Belsham, A. C. Gingras, O. Donzé, T. A. Lin, J. C. Lawrence, and N. Sonenberg, “Insulin-dependent stimulation of protein synthesis by phosphorylation of a regulator of 5’-cap function.,” *Nature*, vol. 371, pp. 762–767, 1994.

[230] J. D. Richter and N. Sonenberg, “Regulation of cap-dependent translation by eIF4E inhibitory proteins.,” *Nature*, vol. 433, no. 7025, pp. 477–80, Feb. 2005.

[231] J. A. Chiorini, S. Miyamoto, S. J. Harkin, and B. Safer, “Genomic cloning and characterization of the human eukaryotic initiation factor-2beta promoter,” *J Biol Chem*, vol. 274, no. 7, pp. 4195–4201, 1999.

[232] M. Ceci, C. Gaviraghi, C. Gorrini, L. Sala, N. Offenhäuser, P. C. Marchisio, and S. Biffo, “Release of eIF6 (p27BBP) from the 60S subunit allows 80S ribosome assembly.,” *Nature*, vol. 426, no. 6966, pp. 579–584, Dec. 2003.

[233] A. Miluzio, A. Beugnet, V. Volta, and S. Biffo, “Eukaryotic initiation factor 6 mediates a continuum between 60S ribosome biogenesis and translation.,” *EMBO Rep.*, vol. 10, no. 5, pp. 459–465, May 2009.

[234] A. Biswas, S. Mukherjee, S. Das, D. Shields, C. Wing, and U. Maitra, “Opposing action of casein kinase 1 and calcineurin in nucleo-cytoplasmic shuttling of mammalian translation initiation factor eIF6.,” *J. Biol. Chem.*, vol. 286, no. 4, pp. 3129–3138, Jan. 2011.

[235] M. M. Mihaylova, D. S. Vasquez, K. Ravnskjaer, P.-D. Denechaud, R. T. Yu, J. G. Alvarez, M. Downes, R. M. Evans, M. Montminy, and R. J. Shaw, “Class IIa histone deacetylases are hormone-activated regulators of FOXO and mammalian glucose homeostasis.,” *Cell*, vol. 145, no. 4, pp. 607–21, May 2011.

[236] X.-J. Yang and S. Grégoire, “Metabolism, cytoskeleton and cellular signalling in the grip of protein Nepsilon - and O-acetylation.,” *EMBO Rep.*, vol. 8, no. 6, pp. 556–62, Jun. 2007.

[237] C. Choudhary, C. Kumar, and F. Gnad, “Lysine acetylation targets protein complexes and co-regulates major cellular functions,” *Science (80-.).*, vol. 325, no. August, pp. 834–840, 2009.

[238] Q. Wang, Y. Zhang, C. Yang, H. Xiong, Y. Lin, and J. Yao, "Acetylation of metabolic enzymes coordinates carbon source utilization and metabolic flux," *Science (80-.).*, vol. 327, no. February, 2010.

[239] S. Zhao, W. Xu, W. Jiang, W. Yu, Y. Lin, and T. Zhang, "Regulation of cellular metabolism by protein lysine acetylation," *Science (80-.).*, no. February, pp. 1000–1004, 2010.

[240] A. S. Hebert, K. E. Dittenhafer-Reed, W. Yu, D. J. Bailey, E. S. Selen, M. D. Boersma, J. J. Carson, M. Tonelli, A. J. Balloon, A. J. Higbee, M. S. Westphall, D. J. Pagliarini, T. a Prolla, F. Assadi-Porter, S. Roy, J. M. Denu, and J. J. Coon, "Calorie restriction and SIRT3 trigger global reprogramming of the mitochondrial protein acetylome.," *Mol. Cell*, vol. 49, no. 1, pp. 186–99, Jan. 2013.

[241] N. Nasrin, X. Wu, E. Fortier, Y. Feng, O. C. Bare', S. Chen, X. Ren, Z. Wu, R. S. Streeper, and L. Bordone, "SIRT4 regulates fatty acid oxidation and mitochondrial gene expression in liver and muscle cells.," *J. Biol. Chem.*, vol. 285, no. 42, pp. 31995–2002, Oct. 2010.

[242] S. Raichur, S. Hooi Teh, K. Ohwaki, V. Gaur, Y. Chau Long, M. Hargreaves, S. L. McGee, and J. Kusunoki, "Histone deacetylase 5 regulates glucose uptake and insulin action in muscle cells," *J. Mol. Endocrinol.* , vol. 49 , no. 3 , pp. 203–211, Dec. 2012.

[243] G. Solaini, A. Baracca, G. Lenaz, and G. Sgarbi, "Hypoxia and mitochondrial oxidative metabolism.," *Biochim. Biophys. Acta*, vol. 1797, no. 6–7, pp. 1171–7, 2010.

[244] P. D. Wagner, "Skeletal muscle angiogenesis. A possible role for hypoxia.," in *Hypoxia SE - Advances in Experimental Medicine and Biology*, vol. 502, R. Roach, P. Wagner, and P. Hackett, Eds. Springer US, 2001, pp. 21–38.

[245] P. T. Mungai, G. B. Waypa, A. Jairaman, M. Prakriya, D. Dokic, M. K. Ball, and P. T. Schumacker, "Hypoxia triggers AMPK activation through reactive oxygen species-mediated activation of calcium release-activated calcium channels.," *Mol. Cell. Biol.*, vol. 31, no. 17, pp. 3531–45, Sep. 2011.

[246] S. Bonello, C. Zähringer, R. S. BelAiba, T. Djordjevic, J. Hess, C. Michiels, T. Kietzmann, and A. Görlach, "Reactive oxygen species activate the HIF-1alpha promoter via a functional NFkappaB site.," *Arterioscler. Thromb. Vasc. Biol.*, vol. 27, no. 4, pp. 755–61, Apr. 2007.

[247] I. M. Conboy and T. a Rando, "The regulation of Notch signaling controls satellite cell activation and cell fate determination in postnatal myogenesis.," *Dev. Cell*, vol. 3, no. 3, pp. 397–409, Sep. 2002.

[248] S. B. P. Chargé and M. a Rudnicki, "Cellular and molecular regulation of muscle regeneration.," *Physiol. Rev.*, vol. 84, no. 1, pp. 209–38, Jan. 2004.

[249] C. O. Martinez, M. J. McHale, J. T. Wells, O. Ochoa, J. E. Michalek, L. M. McManus, and P. K. Shireman, "Regulation of skeletal muscle regeneration by CCR2-activating chemokines is directly related to macrophage recruitment.," *Am. J. Physiol. Regul. Integr. Comp. Physiol.*, vol. 299, no. 3, pp. R832–42, Sep. 2010.

[250] A. Wagatsuma and K. Sakuma, “Mitochondria as a potential regulator of myogenesis.,” *ScientificWorldJournal.*, vol. 2013, 2013.

[251] A. Musarò and L. Barberi, “Isolation and Culture of Mouse Satellite Cells,” vol. 633, no. 1, pp. 101–111, 2010.

[252] H. Hoppeler and M. Vogt, “Response of skeletal muscle mitochondria to hypoxia,” *Exp. ...*, 2003.

[253] S. Calvo, M. Jain, X. Xie, S. a Sheth, B. Chang, O. a Goldberger, A. Spinazzola, M. Zeviani, S. a Carr, and V. K. Mootha, “Systematic identification of human mitochondrial disease genes through integrative genomics.,” *Nat. Genet.*, vol. 38, no. 5, pp. 576–82, May 2006.

[254] L. Finley, J. Lee, A. Souza, V. Desquiret-Dumas, K. Bullock, G. Rowe, V. Procaccio, C. Clish, Z. Arany, and M. Haigis, “Skeletal muscle transcriptional coactivator PGC-1α mediates mitochondrial, but not metabolic, changes during calorie restriction,” *Proc. Natl. Acad. Sci.*, vol. 109, no. 8, pp. 2931–2936, Feb. 2012.

[255] a Musarò, K. McCullagh, a Paul, L. Houghton, G. Dobrowolny, M. Molinaro, E. R. Barton, H. L. Sweeney, and N. Rosenthal, “Localized Igf-1 transgene expression sustains hypertrophy and regeneration in senescent skeletal muscle.,” *Nat. Genet.*, vol. 27, no. 2, pp. 195–200, Feb. 2001.

[256] P. Rochard, A. Rodier, F. Casas, I. Cassar-Malek, S. Marchal-Victorion, L. Daury, C. Wrutniak, and G. Cabello, “Mitochondrial Activity Is Involved in the Regulation of Myoblast Differentiation through Myogenin Expression and Activity of Myogenic Factors,” *J. Biol. Chem.*, vol. 275, no. 4, pp. 2733–44, Jan. 2000.

[257] P. Seyer, S. Grandemange, M. Busson, A. Carazo, F. Gamaléri, L. Pessemesse, F. Casas, G. Cabello, and C. Wrutniak-Cabello, “Mitochondrial activity regulates myoblast differentiation by control of c-Myc expression,” *J. Cell. Physiol.*, vol. 207, no. 1, pp. 75–86, Apr. 2006.

[258] G. Pallafacchina, S. François, B. Regnault, B. Czarny, V. Dive, A. Cumano, D. Montarras, and M. Buckingham, “An adult tissue-specific stem cell in its niche: a gene profiling analysis of in vivo quiescent and activated muscle satellite cells.,” *Stem Cell Res.*, vol. 4, no. 2, pp. 77–91, Mar. 2010.

[259] D. D. Cornelison and B. J. Wold, “Single-cell analysis of regulatory gene expression in quiescent and activated mouse skeletal muscle satellite cells.,” *Dev. Biol.*, vol. 191, no. 2, pp. 270–83, Nov. 1997.

[260] A. Wagatsuma, N. Kotake, and S. Yamada, “Muscle regeneration occurs to coincide with mitochondrial biogenesis.,” *Mol. Cell. Biochem.*, vol. 349, no. 1–2, pp. 139–47, Mar. 2011.

[261] J. Norrbom, C. J. Sundberg, H. Ameln, W. E. Kraus, E. Jansson, and T. Gustafsson, “PGC-1alpha mRNA expression is influenced by metabolic perturbation in exercising human skeletal muscle.,” *J. Appl. Physiol.*, vol. 96, no. 1, pp. 189–94, Jan. 2004.

[262] R. C. . Langen, S. . Korn, and E. F. . Wouters, “ROS in the local and systemic pathogenesis of COPD,” *Free Radic. Biol. Med.*, vol. 35, no. 3, pp. 226–235, 2003.

[263] V. Andrés and K. Walsh, “Myogenin expression, cell cycle withdrawal, and phenotypic differentiation are temporally separable events that precede cell fusion upon myogenesis.,” *J. Cell Biol.*, vol. 132, no. 4, pp. 657–666, Feb. 1996.

[264] J. Rehman, “Empowering self-renewal and differentiation: the role of mitochondria in stem cells.,” *J. Mol. Med. (Berl).*, vol. 88, no. 10, pp. 981–6, Oct. 2010.

[265] S. Jash and S. Adhya, “Induction of muscle regeneration by RNA-mediated mitochondrial restoration.,” *FASEB J.*, vol. 26, no. 10, pp. 4187–97, Oct. 2012.

[266] J. H. Miner and B. J. Wold, “c-myc inhibition of MyoD and myogenin-initiated myogenic differentiation.,” *Mol. Cell. Biol.*, vol. 11, no. 5, pp. 2842–51, May 1991.

[267] P. Seyer, S. Grandemange, P. Rochard, M. Busson, L. Pessemesse, F. Casas, G. Cabello, and C. Wrutniak-Cabello, “P43-dependent mitochondrial activity regulates myoblast differentiation and slow myosin isoform expression by control of Calcineurin expression.,” *Exp. Cell Res.*, vol. 317, no. 14, pp. 2059–71, Aug. 2011.

[268] M. Hagedorn, S. Javerzat, D. Gilges, A. Meyre, B. de Lafarge, A. Eichmann, and A. Bikfalvi, “Accessing key steps of human tumor progression in vivo by using an avian embryo model.,” *Proc. Natl. Acad. Sci. U. S. A.*, vol. 102, no. 5, pp. 1643–8, Feb. 2005.

[269] S. R. McDougall, A. R. A. Anderson, and M. A. J. Chaplain, “Mathematical modelling of dynamic adaptive tumour-induced angiogenesis: Clinical implications and therapeutic targeting strategies,” *J. Theor. Biol.*, vol. 241, no. 3, pp. 564–589, 2006.

[270] G. Bergers and L. E. Benjamin, “Tumorigenesis and the angiogenic switch.,” *Nat. Rev. Cancer*, vol. 3, no. 6, pp. 401–10, Jun. 2003.

[271] B. Schweighofer, J. Testori, C. Sturtzel, S. Sattler, H. Mayer, O. Wagner, M. Bilban, and E. Hofer, “The VEGF-induced transcriptional response comprises gene clusters at the crossroad of angiogenesis and inflammation.,” *Thromb. Haemost.*, vol. 102, no. 3, pp. 544–554, Sep. 2009.

[272] S. Fukuhara, K. Sako, T. Minami, K. Noda, H. Z. Kim, T. Kodama, M. Shibuya, N. Takakura, G. Y. Koh, and N. Mochizuki, “Differential function of Tie2 at cell-cell contacts and cell-substratum contacts regulated by angiopoietin-1.,” *Nat. Cell Biol.*, vol. 10, no. 5, pp. 513–526, May 2008.

[273] P. Ranganathan, A. Agrawal, R. Bhushan, A. K. Chavalmane, R. K. R. Kalathur, T. Takahashi, and P. Kondaiah, “Expression profiling of genes regulated by TGF-beta: differential regulation in normal and tumour cells.,” *BMC Genomics*, vol. 8, p. 98, Apr. 2007.

[274] R. Ren, P. C. Charles, C. Zhang, Y. Wu, H. Wang, and C. Patterson, “Gene expression profiles identify a role for cyclooxygenase 2-dependent prostanoid generation in BMP6-induced angiogenic responses.,” *Blood*, vol. 109, no. 7, pp. 2847–2853, Apr. 2007.

[275] L. Sun, A.-M. Hui, Q. Su, A. Vortmeyer, Y. Kotliarov, S. Pastorino, A. Passaniti, J. Menon, J. Walling, R. Bailey, M. Rosenblum, T. Mikkelsen, and H. A. Fine, "Neuronal and glioma-derived stem cell factor induces angiogenesis within the brain.," *Cancer Cell*, vol. 9, no. 4, pp. 287–300, Apr. 2006.

[276] S. Javerzat, M. Franco, J. Herbert, N. Platonova, A.-L. Peille, V. Pantesco, J. De Vos, S. Assou, R. Bicknell, A. Bikfalvi, and M. Hagedorn, "Correlating global gene regulation to angiogenesis in the developing chick extra-embryonic vascular system.," *PLoS One*, vol. 4, no. 11, p. e7856, Jan. 2009.

[277] N. Almog, L. Ma, R. Raychowdhury, C. Schwager, R. Erber, S. Short, L. Hlatky, P. Vajkoczy, P. Huber, J. Folkman, and A. Abdollahi, "Transcriptional Switch of Dormant Tumors to Fast-Growing Angiogenic Phenotype," *Cancer Res.*, vol. 69, no. 3, pp. 836–844, Feb. 2009.

[278] D. A. M. Mustafa, L. J. Dekker, C. Stingl, A. Kremer, M. Stoop, P. A. E. Sillevis Smitt, J. M. Kros, and T. M. Luider, "A proteome comparison between physiological angiogenesis and angiogenesis in glioblastoma.," *Mol. Cell. Proteomics*, vol. 11, no. 6, p. M111.008466, Jun. 2012.

[279] A. C. Tufan and N. L. Satiroglu-Tufan, "The chick embryo chorioallantoic membrane as a model system for the study of tumor angiogenesis, invasion and development of anti-angiogenic agents.," *Curr. Cancer Drug Targets*, vol. 5, pp. 249–266, 2005.

[280] M. Hagedorn, L. Zilberberg, J. Wilting, X. Canron, G. Carrabba, C. Giussani, M. Pluderi, L. Bello, and A. Bikfalvi, "Domain Swapping in a COOH-terminal Fragment of Platelet Factor 4 Generates Potent Angiogenesis Inhibitors," *Cancer Res.*, vol. 62, no. 23, pp. 6884–6890, Dec. 2002.

[281] R. Gupta, A. Stincone, P. Antczak, S. Durant, R. Bicknell, A. Bikfalvi, and F. Falciani, "A computational framework for gene regulatory network inference that combines multiple methods and datasets.," *BMC Syst. Biol.*, vol. 5, p. 52, Jan. 2011.

[282] M. Scutari and R. Nagarajan, "Identifying significant edges in graphical models of molecular networks.," *Artif. Intell. Med.*, vol. 57, no. 3, pp. 207–17, Mar. 2013.

[283] M.-A. Yu, K.-S. Shin, J. H. Kim, Y.-I. Kim, S. S. Chung, S.-H. Park, Y.-L. Kim, and D.-H. Kang, "HGF and BMP-7 ameliorate high glucose-induced epithelial-to-mesenchymal transition of peritoneal mesothelium.," *J. Am. Soc. Nephrol.*, vol. 20, no. 3, pp. 567–81, Mar. 2009.

[284] F. Battaglia, S. Delfino, E. Merello, M. Puppo, R. Piva, L. Varesio, and M. C. Bosco, "Hypoxia transcriptionally induces macrophage-inflammatory protein-3alpha/CCL-20 in primary human mononuclear phagocytes through nuclear factor (NF)-kappaB.," *J. Leukoc. Biol.*, vol. 83, no. 3, pp. 648–62, Mar. 2008.

[285] K. H. Park, T. H. Lee, C. W. Kim, and J. Kim, "Enhancement of CCL15 expression and monocyte adhesion to endothelial cells (ECs) after hypoxia/reoxygenation and induction of ICAM-1 expression by CCL15 via the JAK2/STAT3 pathway in ECs.," *J. Immunol.*, vol. 190, no. 12, pp. 6550–8, Jun. 2013.

[286] Z. Liang, J. Brooks, M. Willard, K. Liang, Y. Yoon, S. Kang, and H. Shim, "CXCR4/CXCL12 axis promotes VEGF-mediated tumor angiogenesis through Akt signaling pathway.," *Biochem. Biophys. Res. Commun.*, vol. 359, no. 3, pp. 716–722, Aug. 2007.

[287] I. Kryczek, A. Lange, P. Mottram, X. Alvarez, P. Cheng, M. Hogan, L. Moons, S. Wei, L. Zou, V. V. Machelon, D. Emilie, M. Terrassa, A. Lackner, T. J. Curiel, P. Carmeliet, and W. Zou, "CXCL12 and vascular endothelial growth factor synergistically induce neoangiogenesis in human ovarian cancers.," *Cancer Res.*, vol. 65, no. 2, pp. 465–472, Jan. 2005.

[288] T. Arcondeguy, E. Lacazette, S. Millevoi, H. Prats, and C. Touriol, "VEGF-A mRNA processing, stability and translation: a paradigm for intricate regulation of gene expression at the post-transcriptional level," *Nucleic Acids Res.*, vol. 41, no. 17, pp. 7997–8010, Jul. 2013.

[289] G. Lonnemann, S. Endres, J. W. Van der Meer, J. G. Cannon, K. M. Koch, and C. A. Dinarello, "Differences in the synthesis and kinetics of release of interleukin 1 alpha, interleukin 1 beta and tumor necrosis factor from human mononuclear cells.," *Eur. J. Immunol.*, vol. 19, no. 9, pp. 1531–1536, Sep. 1989.

[290] E. Voronov, D. Shouval, Y. Krelin, E. Cagnano, D. Benharroch, Y. Iwakura, C. Dinarello, and R. Apte, "IL-1 is required for tumor invasiveness and angiogenesis," *Proc. Natl. Acad. Sci.*, vol. 100, no. 5, pp. 2645–2650, Mar. 2003.

[291] R. Marhaba, I. Nazarenko, D. Knöfler, E. Reich, E. Voronov, M. Vitacolonna, D. Hildebrand, E. Elter, R. N. Apte, and M. Zöller, "Opposing effects of fibrosarcoma cell-derived IL-1 alpha and IL-1 beta on immune response induction.," *Int. J. Cancer*, vol. 123, no. 1, pp. 134–45, Jul. 2008.

[292] N. A. Turner, A. Das, P. Warburton, D. J. O'Regan, S. G. Ball, and K. E. Porter, "Interleukin-1α stimulates proinflammatory cytokine expression in human cardiac myofibroblasts," *Am. J. Physiol. - Hear. Circ. Physiol.*, vol. 297, no. 3, pp. H1117–H1127, Sep. 2009.

[293] V. Tjomsland, A. Spångeus, J. Välilä, P. Sandström, K. Borch, H. Druid, S. Falkmer, U. Falkmer, D. Messmer, and M. Larsson, "Interleukin 1α sustains the expression of inflammatory factors in human pancreatic cancer microenvironment by targeting cancer-associated fibroblasts.," *Neoplasia*, vol. 13, no. 8, pp. 664–75, Aug. 2011.

[294] A. Werman, R. Werman-Venkert, R. White, J.-K. Lee, B. Werman, Y. Krelin, E. Voronov, C. Dinarello, and R. Apte, "The precursor form of IL-1alpha is an intracrine proinflammatory activator of transcription.," *Proc. Natl. Acad. Sci. U. S. A.*, vol. 101, no. 8, pp. 2434–2439, Feb. 2004.

[295] M. Milkiewicz, M. D. Brown, S. Egginton, and O. Hudlicka, "Association between shear stress, angiogenesis, and VEGF in skeletal muscles in vivo.," *Microcirculation*, vol. 8, no. 4, pp. 229–41, Aug. 2001.

[296] O. Baum, L. Da Silva-Azevedo, G. Willerding, A. Wöckel, G. Planitzer, R. Gossrau, A. R. Pries, and A. Zakrzewicz, "Endothelial NOS is main mediator for shear stress-

dependent angiogenesis in skeletal muscle after prazosin administration.," *Am. J. Physiol. Heart Circ. Physiol.*, vol. 287, no. 5, pp. H2300–8, Nov. 2004.

[297] P. Wagner, "The critical role of VEGF in skeletal muscle angiogenesis and blood flow.," *Biochem. Soc. Trans.*, vol. 39, no. 6, pp. 1556–1559, Dec. 2011.

[298] T. P. Gavin, R. S. Ruster, J. A. Carrithers, K. A. Zwetsloot, R. M. Kraus, C. A. Evans, D. J. Knapp, J. L. Drew, J. S. McCartney, J. P. Garry, and R. C. Hickner, "No difference in the skeletal muscle angiogenic response to aerobic exercise training between young and aged men," *J. Physiol.*, vol. 585, no. 1, pp. 231–239, Nov. 2007.

[299] F. Gouzi, C. Préfaut, A. Abdellaoui, E. Roudier, P. de Rigal, N. Molinari, D. Laoudj-Chenivesse, J. Mercier, O. Birot, and M. Hayot, "Blunted muscle angiogenic training-response in COPD patients versus sedentary controls.," *Eur. Respir. J.*, vol. 41, no. 4, pp. 806–14, Apr. 2013.

[300] B. D. Kent, P. D. Mitchell, and W. T. McNicholas, "Hypoxemia in patients with COPD: cause, effects, and disease progression.," *Int. J. Chron. Obstruct. Pulmon. Dis.*, vol. 6, pp. 199–208, Jan. 2011.

[301] M. Montes de Oca, S. H. Torres, J. De Sanctis, A. Mata, N. Hernández, and C. Tálamo, "Skeletal muscle inflammation and nitric oxide in patients with COPD.," *Eur. Respir. J.*, vol. 26, no. 3, pp. 390–7, Sep. 2005.